Under the Influence of Tumor-adjacent Tissue

Dissertation

Anna-Lena Keller

Under the Influence of Tumor-adjacent Tissue:

A 3D Co-culture Model of iPSC-derived Organoids and Patient-derived Microtumors

Dissertation

Anna-Lena Keller

Under the Influence of Tumor-adjacent Tissue: A 3D Co-culture Model of iPSC-derived Organoids and Patient-derived Microtumors

Dissertation

der Mathematisch-Naturwissenschaftlichen Fakultät

der Eberhard Karls Universität Tübingen

zur Erlangung des Grades eines

Doktors der Naturwissenschaften

(Dr. rer. nat.)

vorgelegt von

Anna-Lena Keller M.Sc.

aus Ludwigsburg

Tübingen

2023

Gedruckt mit Genehmigung der Mathematisch-Naturwissenschaftlichen Fakultät der Eberhard Karls Universität Tübingen.

Tag der mündlichen Qualifikation:	08.11.2023
Dekan	Prof. Dr. Thilo Stehle
1. Berichterstatterin:	Prof. Dr. Katja Schenke-Layland
2. Berichterstatter:	Prof. Dr. Ulrich Rothbauer
3. Berichterstatterin:	Prof. Dr. Gabriele Dodt
4. Berichterstatterin:	Prof. Milica Radisic, PhD

Keywords: induced pluripotent stem cells, organoids, breast cancer, patient-derived microtumors, co-culture, extracellular matrix, invasion, fibronectin, metalloproteinase-2

Cover: An abstract kaleidoscope pattern symbolizes the complex composition of the tumor. Differently colored triangles represent individual cells and cell populations with specific phenotypic and molecular characteristics that contribute to tumor heterogeneity.

Printed by: Schwabenprint GmbH, Stuttgart

Colophon: This thesis was typeset with LaTeX, using the `kaobook` class and using the Palatino and Inter typefaces.

To all the brave souls who have ever faced the trials of cancer.

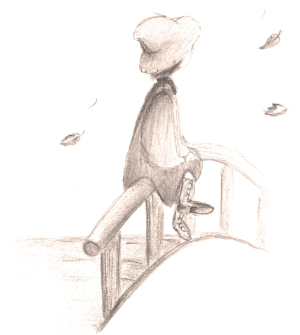

Abstract

Tumor diseases appear to be as individual as the patients themselves - whether solid or leukemic, the “enemy within” exhibits remarkable heterogeneity in morphology, gene and protein expression profiles, epigenetic footprints, cell proliferation kinetics and, as a consequence of these factors, response to therapy. Modern sequencing techniques have confirmed the spatio-temporal heterogeneity of tumors, which is a significant factor in the high recurrence rates that persist in many cancers. As our understanding of the complex dynamics between tumors and their environment continues to grow, there is an urgent need to develop models that can most accurately recapitulate these factors with high similarity and significance to the patient situation. Such models would allow researchers to study the interactions between tumors and their environment in a controlled setting, enabling the discovery of new treatment strategies, particularly with respect to tumor progression and metastasis, and thus of high relevance to patient outcomes. Tumor-adjacent tissue is likely to be the first point of contact with the growing tumor and thus may be a critical determinant of tumor progression. Despite this important fact, it has received little attention.

Therefore, the present work aimed to establish an autologous and allogeneic co-culture system that allows for the investigation of how tumor-adjacent tissue influences tumor growth and invasion with a particular focus on breast cancer, the most common cancer type worldwide. Specifically, we introduce a novel 3D floating matrix co-culture model consisting of two parts: First, iPSC-derived mammary-like organoids (representing the tumor-adjacent mammary epithelium) and second, either breast cancer patient-derived microtumors or breast cancer cell line-derived spheroids.

In a first step, $CD34^+$ hematopoietic stem and progenitor cells were isolated from the peripheral blood of two breast cancer patients diagnosed with an invasive lobular mammary carcinoma. A comprehensive characterization of the newly established iPSC lines confirmed chromosomal stability, expression of endogenous stem cell markers, the loss of exogenous reprogramming factors and their potential to differentiate into the three germ layers: endoderm, mesoderm and ectoderm. Next, the iPSCs were differentiated into mammary-like organoids, which were shown to display important features of the human mammary gland, including the expression of mammary luminal and basal epithelial markers as well as acinar-like structures. Expression of the milk protein, β-casein, was observed under prolactogenic culture conditions.

For the subsequent co-cultivation with the organoids, microtumors were isolated from fresh primary tumor tissue. Microtumors are small fractions of the native tumor and therefore heterogenous in composition, containing not only cancer cells but also immune cell infiltrates, cancer-associated fibroblasts and components of the extracellular matrix. Using histological and protein-based approaches, we confirmed that the isolated microtumors closely resembled the corresponding primary tumor with respect to histological and molecular composition and preserve signaling pathway signatures of their native counterpart. Co-culture data revealed a significant increase in growth and invasiveness of microtumors derived from invasive ductal carcinoma of no special type in the presence of mammary-like organoids. Furthermore, a significant increase in the levels

of the soluble markers fibronectin and metalloproteinase-2, both associated with tumor aggressiveness, invasion and metastasis, was detected in the co-cultures of mammary-like organoids and microtumors/spheroids, compared to the corresponding monocultures. We conclude that tumor-adjacent tissue may "fuel" tumor-progression, probably depending on the stage and the composition of the tumor.

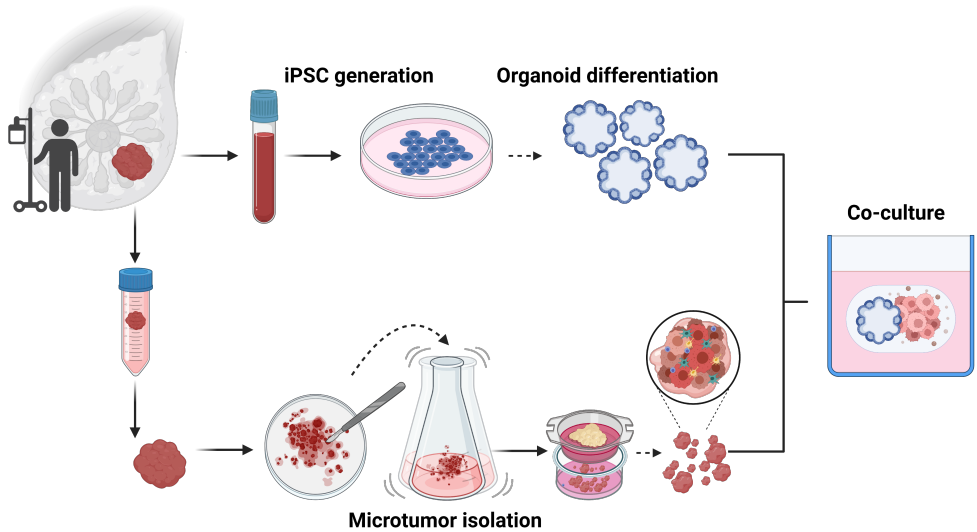

Figure 1: Workflow for the generation of co-cultures from induced pluripotent stem cell-derived mammary-like organoids and patient-derived microtumors.

Zusammenfassung

Tumore scheinen so individuell wie die Patienten selbst zu sein - ob solide oder leukämisch, der "innere Feind" zeigt eine bemerkenswerte Heterogenität in Bezug auf Morphologie, Transkriptionsprofile, epigenetische Fingerabdrücke, Zellproliferationskinetik und - als Folge dieser Faktoren - das Ansprechen auf die Therapie. Moderne Sequenzierungstechniken haben die räumliche und zeitliche Heterogenität von Tumoren bestätigt, die ein wesentlicher Faktor für die hohen Rezidivraten bei vielen Krebsarten ist. Mit zunehmendem Verständnis der komplexen Dynamik zwischen Tumoren und ihrer Umgebung besteht ein dringender Bedarf nach einer Entwicklung von Modellen, die die Situation des Patienten so genau wie möglich nachbilden. Solche Modelle würden es ermöglichen, die Wechselwirkungen zwischen Tumoren und ihrer Umgebung in einer kontrollierten Umgebung zu untersuchen, um neue Behandlungsstrategien zu entdecken und die klinischen Ergebnisse der Patienten zu verbessern. Wenngleich das an den Tumor angrenzende Gewebe der vermutlich erste Kontaktpunkt des wachsenden Tumors ist und daher ein entscheidender Faktor für das Fortschreiten des Tumors darstellt, wurde jedem benachbarten Gewebe bislang wenig Aufmerksamkeit geschenkt.

Ziel dieser Arbeit ist es, ein autologes und allogenes Co-Kultursystem zu etablieren, mit dem untersucht werden kann, wie tumornahes Gewebe das Tumorwachstum und die Tumorinvasion beeinflusst. Hierbei legen wir einen besonderen Fokus auf Brustkrebs, der am häufigsten vorkommende Krebstyp weltweit. Konkret stellen wir ein neuartiges 3D-Matrix-Co-Kulturmodell vor, das aus zwei Teilen besteht: erstens aus iPSC-abgeleiteten Brustdrüsen-ähnlichen Organoiden (die das tumornahe normale bzw. prämaligne Gewebe repräsentieren) und zweitens aus entweder von Brustkrebspatientinnen abgeleiteten Mikrotumoren oder aus Brustkrebszelllinien abgeleiteten Sphäroiden.

In einem ersten Schritt wurden $CD34^+$ hämatopoetische Stamm- und Vorläuferzellen aus dem peripheren Blut zweier Brustkrebspatientinnen mit invasivem lobulärem Mammakarzinom isoliert. Eine umfassende Charakterisierung der neu etablierten iPSC-Linien bestätigte die chromosomale Stabilität, die Expression endogener Stammzellmarker, den Verlust exogener Reprogrammierungsfaktoren und ihr Potenzial zur Differenzierung in die drei Keimblätter: das Endoderm, das Mesoderm und das Ektoderm. Anschließend wurden die iPSCs in Brustdrüsen-ähnliche Organoide differenziert, die wichtige Merkmale der menschlichen Brustdrüse aufweisen, einschließlich des Vorhandenseins von Brustepithel, Myoepithel und azinären Strukturen. Die Expression des Milchproteins β-Casein konnte unter prolaktogenen Kulturbedingungen bestätigt werden.

Für die nachfolgende Co-Kultivierung wurden zudem Mikrotumore aus frischem primärem Tumorgewebe isoliert. Mikrotumore sind kleine Fraktionen des Primärtumors und daher in ihrer Zusammensetzung heterogen. Neben malignen Zellen enthalten sie Immunzell-Infiltrate, Krebs-assoziierte Fibroblasten sowie wichtige Komponenten der Extrazellulären Matrix. Histologische, sowie Protein-basierte Untersuchungen bestätigten, dass die isolierten Mikrotumore in ihrer histologischen und molekularen Zusammensetzung sowie in ihrer Markerexpression eine hohe Ähnlichkeit zu ihrem entsprechenden Primärtumor aufweisen und wichtige Signalwege des

Primärtumors aufrecht erhalten. Die Mikrotumore und Organoide wurden in einem 3D-Matrix-System Co-kultiviert und die daraus resultierenden Daten zeigten eine signifikante Zunahme des Wachstums und der Invasivität von Mikrotumoren des invasiven duktalen Karzinoms ohne speziellen Typ in Gegenwart der Organoiden, was darauf hindeutet, dass tumornahes Gewebe die Tumorprogression “ankurbeln” kann. Darüber hinaus wurde in Co-Kulturen von Brust-ähnlichen Organoiden und Mikrotumoren/ Sphäroiden im Vergleich zu den entsprechenden Mono-Kulturen ein signifikanter Anstieg der löslichen Marker Fibronektin und Metalloproteinase-2 beobachtet, die beide mit Invasion und Metastasierung assoziiert sind. Wir schließen daraus, dass tumornahes Gewebe das Tumorwachstum in Abhängigkeit vom Tumorstadium und der Tumorzusammensetzung beschleunigen kann.

Contents

Abbreviations

Abbreviations used throughout this thesis are arranged alphabetically:

aCGH	Array-based comparative genomic hybridization
BCP	Breast cancer patient
CAF	Cancer-associated fibroblast
CAII	Carbonic anhydrase II
CD	Cluster of differentiation (e.g., CD34)
CiRA	Center for iPS Cell Research and Application
CK	Cytokeratin
CRC	Colorectal cancer
CSC	Cancer stem cells
DCIS	Ductal carcinoma in situ
DTX	Docetaxel
E-Cad	E-Cadherin
EBiSC	European bank for iPSCs
EBNA-1	Epstein-Barr Nuclear Antigen-1
EBV	Eppstein-Barr virus
ECM	Extracellular matrix
EGFR	Epidermal growth factor receptor
EMT	Epithelial-mesenchymal transition
ER	Estrogen receptor
ESC	Embryonic stem cell
FN	Fibronectin
GAG	Glycosaminoglycan
GAPDH	Glyceraldehyde 3-phosphate dehydrogenase
GFR	Growth factor reduced
GSK3β	Glycogen synthase kinase 3-β
H&E	Hematoxylin and Eosin staining
HER2	Human epidermal growth factor receptor 2
HLA	Human leukocyte antigen
HR	Hormone receptor
HSPC	Hematopoietic stem and progenitor cell
ICM	Inner cell mass
IDC-NST	Invasive ductal carcinoma of no special type
IF	Immunofluorecence
IHC	Immunohistochemistry
IL	Interleukin
IlC	Infiltrating immune cell
ILC	Invasive lobular carcinoma
iPSC	Induced pluripotent stem cell

LCIS	Lobular carcinoma in situ
MLO	Mammary-like organoid
MMP	Metalloproteinase
MMR	DNA mismatch repair
MUC2	Mucin 2
MUC5B	Mucin 5B
NK	Natural killer cell
NPHS1	Nephrin
oriP	Origin of plasmid replication
OSKM	Oct4, Sox2, Klf4, c-Myc
PAB	Palbociclib
PAB	Palbociclib
PB	Peripheral blood
PBMC	Peripheral blood mononuclear cell
PCR	Polymerase chain reaction
PDM	Patient-derived microtumor
PG	Proteoglycan
PgR	Progesterone receptor
PODXL	Podocalyxin
pTHrP	Parathyroid hormone
PTX	Paclitaxel
RBC	Red blood cells
ROS	Reactive oxygen species
RT	Reverse transcriptase
STR	Short tandem repeat
TAM (Immune context)	Tumor-associated macrophage
TAM (Appendix F)	Tamoxifen
TDLU	Terminal duct lobular unit
TIL	Tumor infiltrating lymphocytes
TME	Tumor microenvironment
TNBC	Triple negative breast cancer
(F)PTT	(Fresh) primary tumor tissue
(m)EB	(MammoCult™ medium-cultured) embryoid body

List of Figures

List of Tables

List of Publications

Manuscripts accepted for publication

1. **Keller**, **A.-L.**, Binner, A., Schenke-Layland, K., and Schmees, C. (2022). Establishment of Four Induced Pluripotent Stem Cell Lines from CD34+ Hematopoietic Stem and Progenitor Cells from a Patient Diagnosed with an Invasive Lobular Mammary Carcinoma. *Stem Cell Research* **64**, 102902

2. **Keller**, **A.-L.**, Greis, D., Eybe, J., Plöger, S., Weiss, M., Koch, A., Brucker, S. Y., Schenke-Layland, K., and Schmees, C. (2022). Generation and Characterization of Three Induced Pluripotent Stem Cells Lines from an 86-Year Old Female Individual Diagnosed with an Invasive Lobular Mammary Carcinoma. *Stem Cell Research*, 102988

3. **Keller**, **A.-L.**, Binner, A., Breitmeyer, R., Vogel, S., Anderle, N., Rothbauer, U., Schenke-Layland, K., and Schmees, C. (2021). Generation and characterization of the human induced pluripotent stem cell line NMIi010-A from peripheral blood mononuclear cells of a healthy 49–year old male individual. *Stem Cell Research* **54**, 102427

4. Breitmeyer, R., Vogel, S., Heider, J., Hartmann, S.-M., Wüst, R., **Keller**, **A.-L.**, Binner, A., Fitzgerald, J. C., Fallgatter, A. J., and Volkmer, H. (2023). Regulation of synaptic connectivity in schizophrenia spectrum by mutual neuron-microglia interaction. *Communications Biology* **6**, 472

5. Anderle, N., Koch, A., Gierke, B., **Keller**, **A.-L.**, Staebler, A., Hartkopf, A., Brucker, S. Y., Pawlak, M., Schenke-Layland, K., and Schmees, C. (2022). A Platform of Patient-Derived Microtumors Identifies Individual Treatment Responses and Therapeutic Vulnerabilities in Ovarian Cancer. *Cancers* **14**, 2895

6. Walter, B., Canjuga, D., Yüz, S. G., Ghosh, M., Bozko, P., Przystal, J. M., Govindarajan, P., Anderle, N., **Keller**, **A.-L.**, and Tatagiba, M. (2021). Argyrin F Treatment-Induced Vulnerabilities Lead to a Novel Combination Therapy in Experimental Glioma. *Advanced Therapeutics* **4**, 2100078

7. Przystal, J. M., Becker, H., Canjuga, D., Tsiami, F., Anderle,

N., **Keller**, **A.-L.**, Pohl, A., Ries, C. H., Schmittnaegel, M., and Korinetska, N. (2021). Targeting CSF1R alone or in combination with PD1 in experimental glioma. *Cancers* **13**, 2400

8. Holl, M., Becker, L., **Keller**, **A. L.**, Feuerer, N., Marzi, J., Carvajal Berrio, D. A., Jakubowski, P., Neis, F., Pauluschke-Frohlich, J., Brucker, S. Y., Schenke-Layland, K., Kramer, B., and Weiss, M. (2021). Laparoscopic Peritoneal Wash Cytology-Derived Primary Human Mesothelial Cells for In Vitro Cell Culture and Simulation of Human Peritoneum. *Biomedicines* **9**, 176

9. Holl, M., Rasch, M.-L., Becker, L., **Keller**, **A.-L.**, Schultze-Rhonhof, L., Ruoff, F., Templin, M., Keller, S., Neis, F., Keßler, F., Andress, J., Bachmann, C., Krämer, B., Schenke-Layland, K., Brucker, S., Marzi, J., and Weiss, M. (2022). Cell Type-Specific Anti-Adhesion Properties of Peritoneal Cell Treatment with Plasma-Activated Media (PAM). *Biomedicines* **10**, 927

10. Anderle, N., Schäfer-Ruoff, F., Staebler, A., Kersten, N., Koch, A., Önder, C., **Keller**, **A.-L.**, Liebscher, S., Hartkopf, A., Hahn, M., Templin, M., Brucker, S. Y., Schenke-Layland, K., and Schmees, C. (2023). Breast cancer patient-derived microtumors resemble tumor heterogeneity and enable protein-based stratification and functional validation of individualized drug treatment. *Journal of Experimental & Clinical Cancer Research* **42**, 210

Manuscripts submitted for publication

11. **Keller**, **A.-L.**, Anderle, N., Schrenk, M., Greis, D., Binner, A., Visser, D., Göpfert, J., Koch, A., Weiss, M., and Brucker, S. (2023). Co-cultures of iPSC-derived Mammary-like Organoids and Patient-derived Microtumors Model Invasive Behavior of Breast Cancer ex vivo

Table 2: The candidate's contributions to the publications. S = scientific ideas generated by the candidate (in %), D = data generated by the candidate (in %), A = analysis and interpretation by the candidate (in %), P = paper writing by the candidate (in %).

No.	Accepted	No. of authors	Candidate pos.	S	D	A	P
1	yes	4	1	60	75	65	75
2	yes	9	1	60	75	65	75
3	yes	8	1	60	75	65	75
4	yes	10	6	15	10	5	5
5	yes	10	4	20	10	10	5
6	yes	16	9	15	5	5	5
7	yes	16	6	15	10	5	5
8	yes	13	3	20	10	10	10
9	yes	17	4	20	10	10	10
10	yes	14	7	15	10	5	5
11	no	12	1	50	75	75	60

Cancer – a spectrum of diseases

1

1.1 The many faces of the enemy within

Extraordinary laboratory efforts in the field of cancer research over the past decades have allowed us to gain a deeper understanding of tumorigenesis and the serious consequences of somatic aberrations. While early detection of most primary organ-confined malignancies is no longer necessarily a "death sentence", the mortality rates of metastatic cancers remain alarmingly high. (*12*) In fact, during the gradual development of cancer, neoplastic cells can acquire the ability to spread from the primary tumor site to distant parts of the body – a critical and lethal process (*13*).

Tumors are dynamic societies, well adapted for survival (*14*). The concept of cancer as a dynamic disease rather than a molecularly static one emerged from the observation that almost all tumors manage to evade targeted therapeutic intervention, despite the remarkable initial killing effects induced by treatment (*15*). Often described as a "spectrum of diseases", cancers exhibit broadly heterogeneous identities across patients, tumor types, primary and secondary lesions, and within individual tumors (*16*). Germline genetic variation, environmental factors, and/or individual somatic mutation profiles may contribute to "intertumoral heterogeneity", which refers to substantial variability among patients with the same histologic malignancy. "Intratumoral heterogeneity", on the other hand, describes the fact that a single tumor can be extremely diverse in both space and time. (*15*)

Given this immense heterogeneity and the high attrition rate of oncological drug development, the pursuit of a cure for metastatic cancer may seem daunting (*17*, *18*). However, translational research, high-throughput tumor analytical techniques together with multi-omics characterization at high resolution have revolutionized our perspective on cancer treatment from simply considering the anatomical site of the tumor origin towards a personalized approach based on the molecular properties of a tumor. (*18*)

The mechanisms and events that provoke tumor heterogeneity encompass a multitude of parameters such as genetic alterations, epigenetic changes, or the tumor microenvironment (TME), and

are further driven by a complex and individual interplay of both internal and external cues (*15*). Considering the broad complexity of tumor heterogeneity, the reader will be familiarized with the most important of many aspects that contribute to the multifaceted nature of this phenomenon.

1.2 Clonal evolution – survival of the fittest and beyond

"One general law, leading to the advancement of all organic beings, namely, multiply, vary, let the strongest live and the weakest die." (*19*)

More than 150 years ago, Charles R. Darwin published his theory of the "survival of the fittest" in his seminal work "On the Origin of Species" (*19*). His doctrine is still considered the foundation of evolutionary biology, and within this framework the British naturalist paved the way for today's understanding of diversification, somatic selection, and extinction (*20*).

A landmark perspective was provided by the discoverer of the *Philadelphia chromosome*[1], Peter Nowell, who applied Darwin's laws of evolution to cancer (*23*). He described tumor progression as an evolutionary process in which malignant cells develop through an iterative sequence of clonal expansion, genetic diversification, and clonal selection (*24*). In line with Darwin's gradualism, a single cell acquires a series of genetic mutations, which may or may not provide a selective advantage (e.g., through activation of oncogenic pathways and/or inactivation of tumor suppressors), allowing the cell to grow and divide uncontrollably (*15*, *20*, *25*). Over time, further subclones equipped with additional genomic abnormalities and variable fitness may accumulate stepwise. However, the cancer clones must withstand constantly changing selection pressures from their tissue habitat, as they face fierce competition for resources and space (*20*). While the immune cell infiltrate attempts to eradicate the resistant tumor cells, the malignant cells may evolve specific adaptations that allow them to evade both innate and adaptive immune defenses (*26*). As a result, only those cancer clones that are best adapted to their environment – the fittest clones – survive and become dominant, while others may be rendered obsolete and go extinct (*20*).

Indeed, the Darwinian selection process is quite contextual and cannot anticipate possible future changes, so some adaptations may be very advantageous at one time, but as conditions change,

1: The "**philadelphia chromosome**" is a genetic aberration located on chromosome 22. This chromosome is abnormally small due to a reciprocal translocation between chromosome 9 and 22 t(9;22)(q34;q11), resulting in a BCR::ABL fusion gene. This gene encodes a hybrid protein that leads to a constitutively activated tyrosine kinase signaling pathway, causing cells to divide uncontrollably and contributing to the development of certain types of leukemia. (*21*, *22*)

these adaptations may lead the clone down a blind alley until it eventually disappears (*20*).

This phenomenon can be exploited for tumor therapy. The dynamics of cancer clones can be influenced by applying an artificial selection pressure to the malignant cells using standard therapeutic interventions such as drugs or radiation, leading to massive cell death and environmental degradation (*23*). However, it can also unintentionally foster the development of a repertoire of drug-tolerant clones from which therapy-resistant cell populations evolve (*20*). For instance, resistance to anilinoquinazoline (epidermal growth factor receptor (EGFR) inhibitors) can be attributed to a threonine-to-methionine point mutation in EGFR that leads to lung cancer relapse (*27*). In chronic myeloid leukemia, a single amino acid substitution in BCR::ABL renders the fusion protein less sensitive to imatinib (Gleevec) (*28*), while amplification of thymidylate synthase results in resistance to its target 5-fluorouracil in colorectal cancer (*29*). (*30*).

The evolution of distinct subclones leads to a **branched** phylogenetic tree of coexisting molecularly and phenotypically diverse cancer cells and thus, a broad intratumoral heterogeneity (*20*) (**Figure 1.1**A). Genetic studies confirmed a non-linear, branched evolution in a variety of tumor types, including pancreatic cancer (*31*), breast cancer (*32*), chronic lymphocytic leukemia (*33*), or childhood acute lymphoblastic leukemia (*34*).

Despite Nowell's advanced idea of a branched tumor evolution, his concept was widely overlooked (*20*). The traditional view of tumor evolution was **linear**, with a single clone of cancer cells acquiring genetic alterations over time, resulting in a new distinct genetic profile with such a powerful growth advantage that this clone outcompetes the ancestral one (*15*, *20*). In other words, driver mutations give the host cells such a selective advantage that they displace all former clones through selective sweeps (*25*, *35*). As a result, the tumor would consist of clonally identical cells, while the corresponding phylogenetic tree would contain a dominant clone accompanied by rare intermediates that survived the previous selective sweeps (**Figure 1.1**B). However, there is little evidence to support the linear evolutionary mode, as these studies did not incorporate genome-wide markers and may have missed heterogeneous mutations that distinguish different clones. (*35*)

Of note, Darwin's model is not sufficient to entirely explain tumor evolution. Non-Darwinian mechanisms were identified as

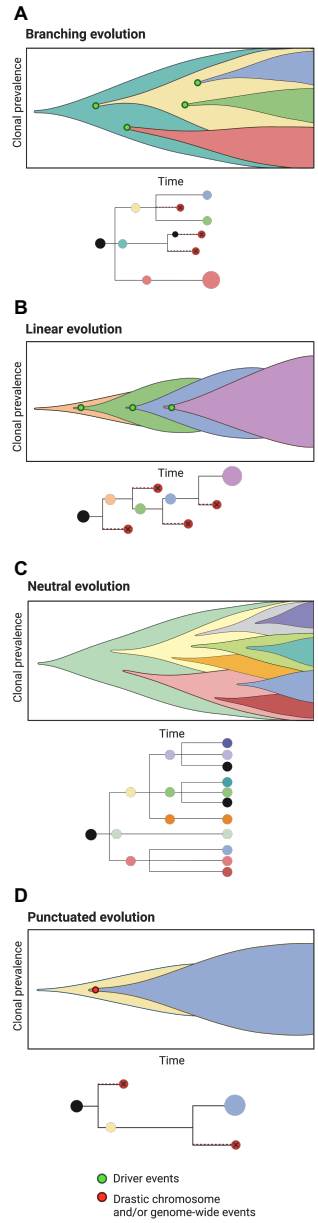

Figure 1.1: Tumor evolution models. A. Branched evolution. **B.** Linear evolution. **C.** Neutral evolution. **D.** Punctuated evolution described by Muller plots showing the clonal prevalence over time and by phylogenetic trees. Different colors represent different clones. Figure adapted and modified from Vendramin et al. (*20*)

important characteristics of tumor evolution. Modern techniques such as bulk and/or single-cell DNA sequencing combined with fast deep learning solutions allow the identification of other tumor evolutionary trajectories and the generation of the most likely tumor phylogeny. (*36*, *37*) This information is highly valuable for further downstream analysis, clinical forecasting and therapeutic decision making (*37*, *38*).

One of the evolutionary models that goes beyond Darwin's theory is the idea of **neutral evolution**, which states that the accumulation of random mutations over the lifetime of a tumor leads to high intratumoral heterogeneity. According to this theory, heterogeneity is by-product of cancer progression rather than an active driving force. It lacks the idea of selective advantage or fitness changes, resulting in a highly divergent phylogenetic tree. (*35*) Some tumors harbor numerous passenger mutations, which account for the vast intratumoral heterogeneity (*39*) (**Figure 1.1**C). This was shown, for instance, by Ling and colleagues, who analyzed nearly 300 regions within a hepatocellular carcinoma using either whole-exome sequencing or genotyping and detected more than 100 million mutations in the coding region with no particular selection for any clone – a number that cannot be explained by a Darwinian selection procedure (*40*).

The linear, branched and neutral model assume that a tumor acquires mutations in a sequential and gradual manner over time. However, evidence exists that long periods of a gradual mutational equilibrium can be interrupted by an outburst of multiple aberrations across the genome as a consequence of certain catastrophic events such as chromosomal instability (*41*), chromosomal rearrangements via breakage-fusion-bridge cycles (*42*) or chromothripsis[2](*44*). Thus, contrary to Darwin's theory, cancer cells may undergo "saltatory jumps" that could, on the one hand, allow the tumors to potentially achieve a better fitness than it would be possible through the gradual accumulation of alterations or, on the other hand, could lead to detrimental results. (*20*)

2: **Chromothripsis** is a genetic condition that involves extensive fragmentation of chromosomes and subsequent reassembly in a different order and is associated with oscillating copy number abnormalities (*43*).

An example of this **punctuated evolution** was given by sequencing results from a number of prostate cancers, which showed that multiple DNA translocations and deletions occurred independently in a devastating process called chromoplexy[3] (*45*).

3: **Chromoplexy** refers to a class of chained DNA rearrangement events in which genetic material is exchanged between chromosomes, resulting in the formation of new chromosomal structures and the loss of multiple copies (*43*).

In addition, sequencing data from triple-negative breast cancer (TNBC) patients challenged the concept of gradual evolution, as the investigators detected a few major subpopulations of clonal

cells within the breast carcinomas, as well as a smaller subpopulation of non-clonal cells showing loss of entire chromosomes or chromosome arms or with metastable or pseudodiploid properties. These alterations must have been acquired in short, punctuated events during early stages of tumor development, with subsequent stable clonal expansions (**Figure 1.1**D). (*46*)

1.3 Genomic instability

Nature has provided us with a toolkit of "emergency mechanisms" that control the precise execution of cell divisions, repair unwanted genetic alterations or patrol our bodies to eliminate abnormal cells (*47*).

However, internal factors including oxidative stress, DNA replication or repair errors, and the exposure to external genotoxic agents such as tobacco smoke or asbestos[4] can induce copy number variations of specific loci, large chromosome segments, or even whole genomes, leading to the bypassing or loss of function of these emergency mechanisms. (*15*, *41*, *47*) What's more, as we age, DNA repair becomes less efficient and more prone to error. The result is an accumulation of DNA damage and mutations, accelerating the process of age-related physiological decline (*49*).

Genomic instability and aneuploidy, an abnormal karyotype, may be the consequences (*46*). There are several major mechanisms involved in genomic instability. For instance, abnormal bases and nucleotides, such as deaminated cytosines or pyrimidine dimers induced by UV-light are normally excised and repaired(*50*). However, germline mutations in components involved in the corresponding repair mechanisms predispose a person to skin cancer (*51*). Furthermore, a defect in the DNA mismatch repair (MMR) mechanism, such as loss of function of MSH2 and MLH1 genes, which are required for MMR, can lead to hypermutation and microsatellite instability, ultimately driving oncogenic transformation (*15*, *50*). MMR deficiency that leads to microsatellite instability has been observed in several types of cancer, most frequently in colorectal cancers (CRC) (*50*, *52*). In contrast, defects in homologous recombination are more often detected in ovarian and breast tumors (*50*). Genomic instability creates a wide range of genetic alterations, giving rise to distinct subclones within a tumor. These subclones can exhibit varied treatment responses, cell behaviors, gene expressions and promote tumor evolution

4: **Why is asbestos so harmful?** Asbestos, a silicate mineral composed of bundles of fibers, exists naturally in the environment. It was widely used in industry because of its low electrical and thermal conductivity and relative resistance to chemical degradation. However, when inhaled, these fibers reach the alveoli and trigger inflammatory responses. Macrophages attempt to engulf the fibers, but when the fibers are larger than 5 µm, their geometry prevents successful phagocytosis. Consequently, the fibers persist in the lung and activate the NLRP3 inflammasome, resulting in the maturation of IL-1β and ultimately chronic inflammation, which has multiple effects on carcinogenesis. (*48*)

and thus, are a major contributor to cancer heterogeneity (*50*, *53*).

1.4 Cancer stem cells

In addition to the large number of differentiated malignant and non-malignant cells that make up the tumor ecosystem, a rare but potent subpopulation was identified within most tumors and represents a major challenge to cancer therapy. This cellular fraction is referred to as cancer stem cells (CSCs), reflecting their stem cell-like properties, including self-renewal, differentiation, dedifferentiation, transdifferentiation, quiescence, and symmetric/asymmetric cell division. (*54*)

According to the CSC theory, intratumoral heterogeneity is established by a differentiation hierarchy resulting in a broad set of very distinct cell types present within the tumor (*55*). In this way, the small fraction of CSCs maintains tumor progression through the production of new stem cells and differentiation into a mass of specialized non-CSCs (*56*). It is noteworthy that terminally differentiated cells can dedifferentiate and acquire CSC features under certain conditions, and thus the cellular hierarchy is not a one-way street, but can be dynamic and reversible (*55*). CSCs can not only promote and sustain tumor onset, expansion, metastasis and disease relapse, but are also resistant to conventional cancer therapies (*54*, *57*–*59*).

If a therapeutic agent succeeds in eliminating all non-CSCs, the tumor may shrink or disappear, but the remaining CSCs evade the intervention and are responsible for tumor regrowth (*60*). After their initial discovery in human acute myeloid leukemia, CSCs could be harvested from most malignancies of hematopoietic origin and solid tumors, e.g., breast (*61*–*63*), ovarian (*57*, *64*, *65*), colon (*66*–*69*), brain (*70*, *71*), liver (*72*–*74*) or pancreatic (*75*–*77*) cancers (*58*). A large number of CSC surface markers have been identified, most of which are well known from embryonic or adult stem cell surfaces (*78*). One such marker is cluster of differentiation (CD) 44, a class I transmembrane glycoprotein associated with the modulation of mesenchymal-like processes such as cell adhesion, invasion, and migration (*54*, *79*). Indeed, Al-Hajj and colleagues observed that a fractioned $CD44^+/CD24^-$ subpopulation from breast cancer patients harbored a 100-fold greater tumorigenic capacity compared to the unsorted cells after transplantation into immunodeficient mice (*54*, *61*).

Due to their high differentiation potential, CSCs play a significant role in cancer heterogeneity. For example, CSCs have been found to generate neurons that synapse with innervating fibers. Tissue innervation is an important event regulating organogenesis, homeostasis, cellular plasticity or response to injury. (*69*) However, the crosstalk between cancer and neural cells is associated with a poor clinical outcome (*69*, *80*, *81*). It has been shown that a fraction of CSCs isolated from colorectal and gastric cancer patients are capable of generating sympathetic and parasympathetic neurons, which are involved in tumor neurogenesis and tumor growth (*80*).

However, the CSC model has been met with strong skepticism because the gold standard for identifying CSCs involves dissociating the tumor into a single-cell suspension before transplanting the CSCs into immunocompromised mice. This procedure disrupts the natural tumor environment and exposes the CSCs to a new host environment, which may influence their behavior. (*55*)

1.5 Cell plasticty

While cellular plasticity is an important feature for tissue homeostasis and damage repair, it also allows cancer cells to rapidly undergo fundamental changes in the cell's biological properties as a result of reversible and dynamic epigenetic and transcriptional alterations (*20*). A prominent example of cell plasticity is epithelial-mesenchymal transition (EMT), a fundamental process in cancer metastasis. During EMT, epithelial cells lose their cell-cell adhesion, dedifferentiate and acquire mesenchymal, migratory characteristics. (*82*, *83*)

1.6 The TME and its contribution to the hallmarks of cancer

Douglas Hanahan and Bob Weinberg defined a set of characteristics, referred to as the "hallmarks of cancer" that are common to most types of cancers (*13*, *84*, *85*). These hallmarks describe the various features tumors can acquire during progression. The successive acquisition of the hallmarks allows cancer cells to bypass natural protective functions that prevent the unauthorized proliferation of outlaw cells in higher organisms (*17*).

The hallmarks of cancer are: sustaining proliferative signaling, evading growth suppressors, avoiding immune destruction, enabling replicative immortality, tumor-promoting inflammation, activating invasion and metastasis, inducing angiogenesis, genome instability and mutation, resisting cell death, deregulating cellular energetics (*13*, *84*).

As the reader is without doubt very familiar with the hallmarks of cancer, it might not be necessary to discuss them in detail. Instead, a selection of hallmarks will be examined from a different perspective by viewing them through the lens of the TME.

While new tools and techniques such as whole genome sequencing or epigenetic and transcriptional profiling expanded our knowledge of the driving forces of malignant transformation, the massive amount of information challenged us to distill the data into a clear understanding of key cellular events that can be translated into more effective and targeted therapies (*17*). Today, we are well aware of the fact that neoplastic cells alone do not manifest the disease but need the help of the members of the TME, a highly heterogenous and dynamic habitat, which contributes to the establishment of the cancer hallmarks (*17*, *20*). Rather than being a silent witness, the TME plays an active role in the disease progression (*86*). As malignant cells face constant stochastic and dynamic changes in their environment, they also progressively remodel the TME to their own advantage (*11*). In addition to neoplastic cells, the TME is composed of numerous recruited and tissue-resident cells and components, including immune cells, pericytes, fibroblasts, tumor vasculature or extracellular matrix (ECM), which exchange soluble factors and secreted vesicles with the cancer cells (*87*). In this way, the two candidates – the cancer cells and the TME – are in a constant dialog and mutually influence each other (*88*).

1.6.1 Cancer-associated fibroblasts

Fibroblasts are a predominant cellular component of the normal stroma and play a critical role in wound healing and tissue repair (*89*). However, the processes associated with wound healing can be hijacked by a tumor. In fact, it can masquerade as injured tissue and recruit resources from the host to promote its own growth and survival, ultimately behaving like a wound that never fully heals (*90*). During tumorigenesis, normal fibroblasts can be misdirected and educated to become cancer-associated fibroblasts

(CAFs), which are phenotypically and functionally distinct from their normal counterparts (*91*). However, multiple other cell types, including bone marrow-derived cells (*92*) or trans-differentiated pericytes (*93*) can also give rise to CAFs, so CAFs are considered to be a cellular state rather than an actual cell type (*93*). They can secrete various growth factors, including HGF, FGF, IGF1 or SDF-1/CXCL12 as well as various pro-inflammatory signals, which drive cancer cell proliferation, act as survival signals or lead to the recruitment and activation of infiltrating immune cells (IICs) (*17*, *94*). Through their expression of proangiogenic signaling proteins such as VEGF, FGFs or IL-8/CXCL8, CAFs can mediate angiogenesis (*95*).

Furthermore, CAFs can secrete ECM proteins, including periostin, fibronectin (FN) and collagen 1, which sequester pro-angiogenic factors and may shield nearby tumor cells from targeted kinase inhibitors and immunotherapies (*96*). CAFs can be also linked to the hallmark "deregulating cellular energetics". Cancer cells are capable of releasing reactive oxygen species (ROS) that induce CAFs to undergo a metabolic shift towards aerobic glycolysis (*97*). This results in a CAF-mediated increase in lactate and pyruvate, which can in turn fuel cancer cell proliferation (*97*, *98*). L-lactic acid also reduces environmental pH, impairs T-cell glycolysis and effector T-cell function, decreases dendritic cell activation, can recruit and induce regulatory T-cells or TAMs, and is thus a key mediator of tumor-induced immunosuppression (*99*, *100*). Moreover, it was demonstrated that the progression from normal/benign breast hyperplasia to ductal carcinoma in situ (DCIS) to invasive ductal carcinoma (IDC) can be fueled by the receptor pair HGF (from fibroblasts or endothelial cells) and c-Met (from malignant cells) (*91*, *101*, *102*).

1.6.2 Infiltrating immune cells

Infiltrating immune cells (IICs) gained a lot of attention due to their key role in tumorigenesis. IICs provide mitogenic cues that stimulate tumor cell proliferation through a variety of growth factors or cytokines, including EGF, TGF-b, TNF-a, FGFs, interleukins (ILs), chemokines, histamines and heparins. Furthermore, IICs mediate ECM degradation through the secretion of proteolytic enzymes (e.g., metallo-, serine- and cysteine proteases), which in turn releases matrix-bound growth factors that enable sustained proliferative signaling. (*103*, *104*)

When cells are part of an organized epithelium, as it is the case under normal circumstances, the adherent cells receive survival signals through homo- and heterotypic adhesion molecules, which is critical for homeostasis and integrity. If those cells detach from their cellular network and thus, lose adhesion, they are destined to undergo programmed cell death. (*105*) However, cancer cells can resist cell death by escaping the dependence on survival signals (*17*). This can be mediated by IICs, which bind to the cancerous cells and maintain the adhesion-related survival signals, even when the tumor cell detaches (e.g., during invasion and metastasis) (*17*). For example, tumor-associated macrophages (TAMs) can bind to breast cancer cells via the α-4 integrin/VCAM-1 receptor pair. This clustering activates a mediator of receptor tyrosine signaling, Ezrin, which triggers PI3K/AKT signaling and eventually inhibits apoptosis of the breast cancer cells (*106*).

In fact, the tumor's "immune footprint" is a critical but complex determinant of therapeutic response and overall clinical outcome (*107*). While certain players, such as M2 macrophages and $FoxP3^+$ regulatory T-cells, can promote cancer growth, tumor-infiltrating M1 macrophages, stromal $CD4^+$ T-cells in proximity to $CD8^+$ cytotoxic T-cells, and the presence of dendritic cells within tertiary lymphoid structures[5] have been shown to suppress tumor growth (*109*). However, studies have shown that therapeutic interventions can exert an unfortunate impact on the tumor immune response. For instance, exposure of various cancer cell types to clinically relevant doses of radiation results in resistance to natural killer (NK) cell cytotoxicity, primarily due to radiation-induced resistance to perforin (*110*).

5: **Tertiary lymphoid structures** are organized clusters of immune cells that develop postnatally in non-lymphoid tissues at sites of chronic inflammation, such as in autoimmune diseases or cancer (*108*).

1.6.3 Vasculature

The majority of blood vessels in healthy adult tissue are quiescent, with few exceptions (*17*). In the context of cancer, they represent a major modulator for tumor growth by "feeding" the tumor with nutrients and oxygen (*111*). From a historic point of view, lesional de novo vascularization was believed to be regulated by cancer cells secreting pro-angiogenic factors, which is indeed one mechanism but not the only one. TME stromal cells play a critical role in the induction of angiogenesis and resistance to cell death. (*17*)

For example, TAMs can stimulate tumor angiogenesis by secreting VEGF-A and furthermore enable the access to ECM-sequestered

VEGF-A by producing the proangiogenic matrix metalloproteinase (MMP)-9 (*103*, *104*). In addition, the recruited blood vessels allow the cancer cells to travel through the bloodstream to distant parts of the body, enabling invasion and metastasis (*13*, *17*).

1.6.4 Extracellular matrix

Another important, albeit non-cellular, contributor to cancer progression is the ECM. Composed of a pleiotropic meshwork of diverse crosslinked macromolecules and proteins, the ECM acts as an orchestrated regulator of tissue integrity and homeostasis, providing protection, structure, and rigidity. Its composition and topography differ from organ to organ and tissue to tissue, reflecting the specific functions and needs of each. (*11*, *112*)

The predominant components of the ECM comprise fibrous (glyco-)proteins such as collagen, FN, laminin and elastin; proteoglycans; hyaluronan; or non-structural regulators such as tenascin, fibulins, osteopontin or thrombospondins (*112*, *113*). Biochemical and molecular cues present in the ECM, such as sequestered cytokines or growth factors, are perceived by cells and translated into downstream cellular responses, and thus, are in a continuous biochemical and biophysical dialog with the neighboring cells (*114*, *115*).

During tumor progression, the evolving cancer tips the balance of ECM synthesis and degradation in its advantageous direction. This can be mediated via increased MMP expression, a large family of structurally related, zinc-dependent endopeptidases. (*116*) Under pathogenic conditions, the endopeptidase activity of MMPs can extensively degrade ECM components thereby facilitating tumor invasion and metastasis and the release of matrix-bound biochemical cues that promote tumor progression (*117*) (**Figure 1.2**).

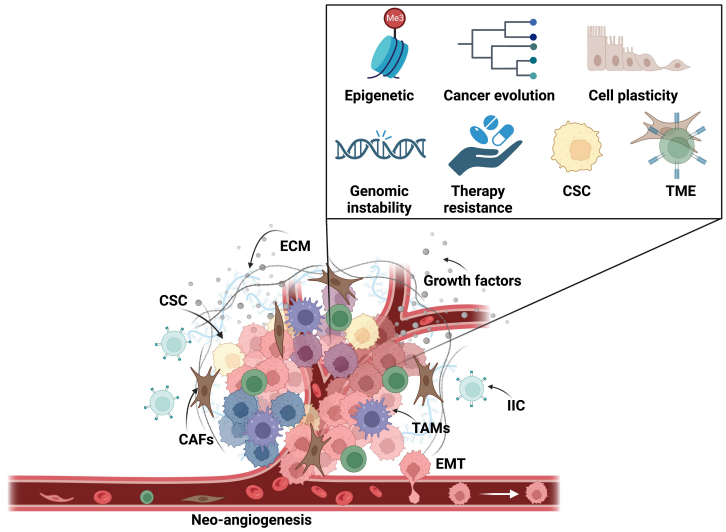

Figure 1.2: Contributors to tumor heterogeneity. A tumor is a heterogeneous composition of numerous (maligant) cell populations and molecular entities that undergo dynamic spatiotemporal changes. Major determinants of cancer heterogeneity include epigenetic alterations, molecularly and phenotypically diverse cancer clones (cancer evolution), cell plasticity (e.g., EMT involved in invasion and metastasis), genomic instability (e.g., defects in DNA repair mechanisms), therapy (artificial selection pressure can lead to more resistant clones), CSC and the complex TME (including IICs, ECM and its bound growth factors, CAFs, TAMs or the induction of neoangiogenesis).

1.7 Breast cancer: an example of a highly diverse malignancy

Breast cancer represents a highly heterogeneous collection of malignancies and accounts for a significant proportion of cancer-related morbidity and mortality worldwide (*118*, *119*). Promoting a healthy lifestyle holds great promise for reducing the risk of breast cancer, as approximately 20% of breast cancers are due to modifiable factors such as physical inactivity, alcohol consumption, smoking or obesity (*120*, *121*). In addition, lack of breastfeeding and early onset of menarche are associated with an increased risk of breast cancer, whereas full-term pregnancy at a younger age and an increased number of births correlate with a decreased likelihood of (hormone receptor (HR)-positive) developing mammary carcinoma(*120*, *122*–*125*), the latter possibly due to a persistent decreased number of breast epithelial stem or multipotent progenitor cells (providing fewer targets for oncogenic transformation) (*120*, *126*).

Another risk factor for breast cancer is the genetic predisposition. It is estimated that approximately 10% of breast cancers are associated with a family history, which can be determined with models such as the "family history score" (*120*, *127*). For example, mutations in the BRCA1 and BRCA2 tumor suppressor genes, whose proteins are involved in DNA repair, are inherited in an autosomal dominant manner, with a 72% (BRCA1) and 69%

(BRCA2) chance of developing breast cancer by the age of 80 (*120*, *128*).

Despite affecting the same anatomic region, the causes of breast cancer are diverse and result in many subtypes with different pathologic features and clinical outcomes (*129*). Breast cancers typically arise in the mammary epithelium and are classified as adenocarcinomas. If the breast carcinoma exhibits distinct cytological and architectural characteristics consistently associated with certain clinical presentations and outcomes, the cancer belongs to the group of "histological special types", which represent up to 25% of all invasive breast cancers and include multiple breast cancer types, including invasive lobular carcinoma (ILC), mucinous or tubular mamma carcinomas. (*130*)

However, most breast cancers belong to the group of "invasive ductal carcinoma of no special type" (IDC-NST), as their histological features do not justify their classification as one of the special tumors (*129*).

Furthermore, breast cancers can be classified as carcinoma in situ or invasive carcinoma. Carcinoma in situ is an early stage of cancer and is considered non-invasive or pre-invasive because the abnormal cells have not (yet) invaded the surrounding breast tissue. If left untreated, carcinoma in situ may (but does not necessarily) develop into invasive cancer. Carcinoma in situ can be further divided into DCIS, which is confined to the milk ducts, and lobular carcinoma in situ (LCIS), which is confined to the lobules (the milk-producing glands). The invasive counterparts of these conditions are the IDC-NST and the ILC. Invasive carcinomas are characterized by their ability to invade the surrounding tissue, which is a crucial step in the development of metastatic processes through the blood or lymphatic systems (**Figure 1.3**A). (*129*, *130*)

Although the histologic type provides important information, its clinical relevance is limited. On the contrary, the molecular pattern of the breast tumor is crucial for making treatment decisions in a clinical setting (**Figure 1.3**B). In addition, in order to assess the potential response to chemotherapy, genetic information about a tumor is of great value. Genetic tests, such as MammaPrint and Oncotype DX[6], play a crucial role in determining the suitability of chemotherapy for individual patients (*133*) .

Luminal A-like tumors are identified by strong estrogen receptor (ER) and/or progesterone receptor (PgR) expression, lack human epidermal growth factor receptor 2 (HER2) expression, show low proliferation rates (Ki-67 low), are associated with a favorable

6: **MammaPrint** is a commercially available microarray-based multigene profiling test designed for personalized treatment of both ER^+ and ER^- breast cancer patients. MammaPrint evaluates the activity of 70 genes in early-stage breast cancer and calculates a tumor recurrence score to predict whether a patient will benefit from chemotherapy. Information about the tumor's gene signature helps distinguish the subset of patients with a low risk of distant metastasis from those who will be affected by metastasis in the first 5 years after surgery. The MammaPrint gene expression signature includes proteins associated with key cancer hallmarks, broadly covering proliferation, resistance to apoptosis, invasion and dissemination. Another example of a successful genomic test is **Oncotype DX**, which is used to predict the risk of relapse in patients diagnosed with ER^+ breast cancer. It measures 16 markers and 5 control genes and uses the data to classify patients into different risk groups. High-risk patients are more likely to profit from adjuvant chemotherapy, while low-risk patients are recommended to avoid chemotherapeutic intervention. (*131*–*133*).

prognosis, and often respond to hormone therapy. *Luminal B*-like tumors show ER expression but are not (or at least to a lower extent) positive for PgR, while HER2 may be present (luminal B-like HER2$^+$) or absent (luminal B-like HER2$^-$). This type shows high proliferation rates (Ki-67 high).

HER2-enriched, non-luminal tumors are HER2-positive, are characterized by low or absent ER and PgR expression and have a high Ki-67 score. This tumor type is aggressive but generally responsive to targeted therapies.

A rather poor prognosis is associated with the highly aggressive *TNBC*, which lacks HR expression (ER, PgR, HER2) and has a high proliferation index. (*130*, *134*–*136*)

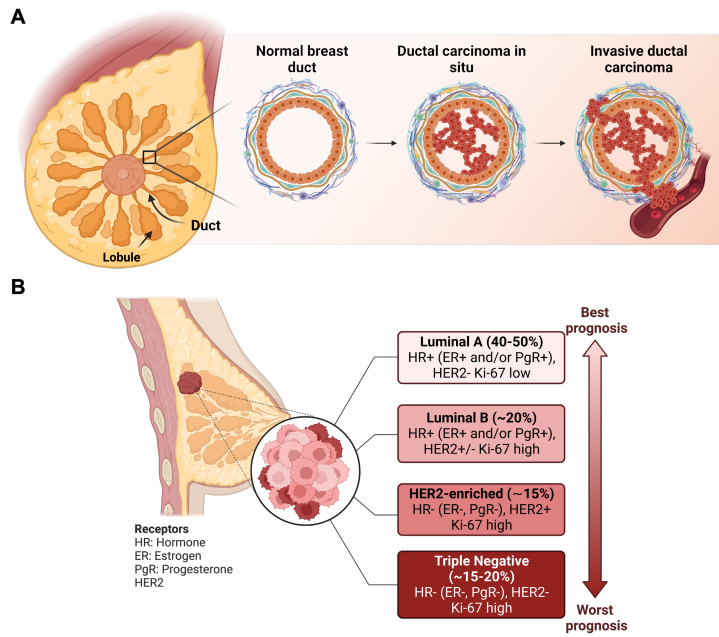

Figure 1.3: Subtypes and anatomy of breast cancer. A. Left: Schematic view of female breast anatomy depicting the collecting ducts and lobules. Right: Schematic cross-sections of a normal mammary duct, DCIS (accumulation of abnormal cells in the lumen of the duct without invasion of the epithelial basement membrane into the adjacent stroma), and IDC (invasion into the surrounding stroma and metastasis). **B.** Schematic representation of the breast cancer molecular subtypes based on the expression of HR, the receptor tyrosine kinase HER2 and the proliferation marker Ki-67. The following subtypes are listed in descending order of prognosis: Luminal A, Luminal B, HER2-enriched, TNBC.

The power of pluripotency 2

2.1 From the zygote to the living organism

The human body is made up of trillions of cells that are spatially organized and exert a plethora of functional states (*137*).

With advancements in bulk sequencing and single-cell analysis, researchers have been able to identify cellular genomic expression patterns and genetic features with high precision, providing insights into the cellular distribution and developmental trajectories across our organs (*138*). Although it is estimated that the human body consist of over 200 highly specialized cell types, all cells can be traced back to a unicellular, diploid progenitor: the zygote (*139*).

The zygote is formed at the earliest stage of human development when a sperm successfully enters an ovum. This event is followed by a turbulent period of rapid cell division known as cleavage, during which the zygote divides several times without significant overall growth. (*141*) Once the resulting cell sphere has reached a stage of 16 totipotent cells, the cell mass is referred to as morula. Totipotent cells harbor the capacity to give rise to all embryonic – and extra-embryonic cells and therefore display the greatest differentiation potential. (*142*, *143*)

Through the process of compaction, the outer cell layer of the morula is tightly bound together by the formation of gap junctions and desmosomes, giving rise to the trophoblast. The trophoblast actively transports sodium ions and water, leading to the formation of a cavity within the morula, which eventually gives rise to a hollow ball of cells called the blastocyst. The outer cells of the blastocyst develop into the first extraembryonic tissue, the trophectoderm, which plays an important role in implantation by attaching to the uterine epithelium and invading into the endometrium. (*143*, *144*)

The cells trapped inside the blastocyst represent the pluripotent inner cell mass (ICM). The ICM begins to differentiate into the epiblast and the hypoblast. While the hypoblast develops into the yolk-sac and later the chorion, the epiblast gives rise to all

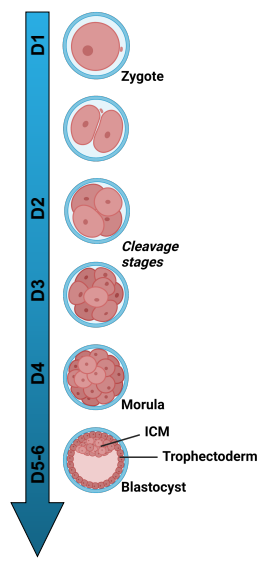

Figure 2.1: From the zygote to the blastocyst. During eary human development, the zygote undergoes several cleavage divisions within the first 5 days (D) after fertilization. Around day 5, the blastocyst is formed and contains the both the ICM (giving rise to all embryonic tissues) and the trophectoderm (that develops into extra-embryonic tissues). Figure partially adapted from Popovic et al. (*140*).

the three germ layers, the ectoderm, the mesoderm and the endoderm during gastrulation (*143*). Gastrulation is followed by organogenesis, in which the three germ layers give rise to the entire organ system of the new individual (*145*) (**Figure 2.1**).

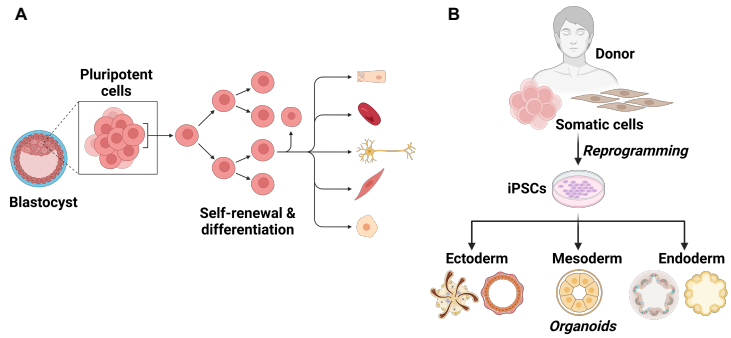

Figure 2.2: (Induced) pluripotent stem cells have the potential to differentiate into various cell types of all the three germ layers. A. Pluripotent stem cells can self-renew and differentiate into all embryonic tissues and cell types (*146*) **B.** iPSCs can be generated from donor-derived somatic cells (such as $CD34^+$ hematopoietic stem and progenitor cells or fibroblasts) and further differentiated into various organoid types representing all three germ layers.

2.2 Pluripotency in research

In the late 1990s, Dr. James Thomson and colleagues at the University of Wisconsin-Madison, successfully isolated embryonic stem cells (ESCs) from a human blastocyst (*147*). Due to their pluripotent nature, ESCs have the ability to proliferate indefinitely and give rise to all cell types and thus, opened promising research applications (*148*) (**Figure 2.2**A). However, the use of ESCs has triggered a multifaceted ethical debate, encompassing a range of moral, cultural and societal issues (*149*). In 2006, a powerful alternative was provided by a team of scientists led by Shin'ya Yamanaka, who made the groundbreaking discovery that terminally differentiated murine cells can be converted back into a pluripotent state by overexpressing a quartet of reprogramming factors: Oct4, Sox2, Klf4 and c-Myc (OSKM / Yamanaka-factors) (*150*). They called these new candidates "induced pluripotent stem cells" or "iPSCs". Only one year later, the successful generation of iPSCs from adult human fibroblasts was demonstrated by several groups, including Yamanaka's (*151*, *152*) (**Figure 2.2**B).

Albeit iPSCs are artificially generated cells and do not naturally exist in the human body, they show remarkable molecular and functional resemblance to ESCs, including cellular morphology, expression of pluripotency markers, similar gene expression profiles, the ability to differentiate into the three germ layers and the capacity to self-renew (*153*, *154*). This advance set off a race of

breathtaking pace: Numerous studies have applied iPSC technology to developmental biology, in vitro disease modeling, drug screening or toxicity studies and have shown great promise in cell and gene therapy to substitute damaged, non-functional, degenerated, or lost tissues (*155*). A very valuable aspect of iPSC technology is the possibility of autologous transplantation, which avoids the risks and complications associated with immune rejection (*156*, *157*). Combined with rapid advances in precision DNA editing, iPSCs offer the possibility of individualized cell-based autologous therapies for a wide range of diseases (*158*). In this scenario, disease-causing mutations could be accurately corrected in a patient's own iPSC line resulting in a tailored, specific clinical treatment. One of the first clinical trials was undertaken in Japan in 2014, where iPSC-derived retinal pigment epithelium sheets were used for the treatment of neovascular age-related macular degeneration. (*159*)

However, the main difficulty associated with autologous transplantation is the fact that the entire labor-intensive and costly process of clinical-grade iPSC generation, characterization and any subsequent necessary interventions must be carried out for each patient individually (*156*). To overcome these obstacles, an alternative approach was in demand. Scientists at the Center for iPS Cell Research and Application (CiRA) at Kyoto University and the CiRA Foundation in Japan therefore set out to generate a clinical-grade iPSC haplobank from donors homozygous for human leukocyte antigen (HLA)-A, HLA-B and HLA-DR alleles – the major determinants of transplant rejection – to match as many people in Japan as possible. To date, the haplobank covers 40% of the Japanese population with a low risk of immune rejection and already found application in more than 10 clinical trials. (*160*)

2.3 Generation of iPSCs

2.3.1 Donor material collection

Skin dermal fibroblasts are still the most widely used source for iPSC generation, given their commercial availability, simple handling, and inexpensive cell culture media (*154*). However, isolation of these cells requires a skin biopsy, which is an invasive surgical procedure. (*161*) It takes weeks to expand the fibroblasts to the appropriate cell count and the reprogramming efficiency is generally low in older donors. Fibroblast isolation may not be

appropriate in children or patients with abnormal wound healing, skin diseases or coagulation disorders. Furthermore, permanent exposure to stressors such as UV radiation puts them at risk of accumulating point mutations that are perpetuated in the iPSCs. (*154*) As a result of these drawbacks, much research effort has been invested to find alternative cell sources, and this has proven fruitful: Numerous publications describe the successful generation of iPSCs from various cell types including keratinocytes (*162*), T- and B-lymphocytes (*163*, *164*), mesenchymal stem cells from adipose tissue (*165*), mesenchymal-like stem/progenitor cells from dental tissue (*166*), renal epithelial cells from urine (*167*, *168*), hepatocytes (*169*), amniotic fluid stem cells (*170*) or hematopoietic stem/progenitor cells (*1*–*3*, *136*, *154*). Indeed, most – if not all – somatic cells have the potential to be dedifferentiated into iPSCs, albeit with variable reprogramming efficiencies and kinetics (*154*, *171*). For this reason, it is desirable to find types of cells that fulfil the following requirements:

1. isolation through minimal invasive procedures,
2. rapidly expandable,
3. widespread presence in the tissue,
4. minimized risk of chromosomal aberrations or point mutations due to the lack of exposure to environmental mutagens,
5. high reprogramming efficiency and fast kinetics and
6. ability to be sourced from donors of all genders, ages and health conditions (*154*).

Mononuclear cells derived from peripheral blood (PB) are a popular source for reprogramming, as they match more closely the epigenetic profiles and gene expression patterns of ECSs and iPSCs than age-matched fibroblasts (*172*). Blood itself is a heterogeneous composition of different cell types, with an abundance of erythrocytes and platelets – enucleated cells not suitable for reprogramming. Therefore, these non-reprogrammable cells must first be separated from the total cell fraction. This can be achieved by density gradient centrifugation, which retains peripheral blood mononuclear cells (PBMCs) (*173*).

Lymphocytes represent a large fraction of the PBMC population and the successful reprogramming of terminally differentiated T- and B-cells has been demonstrated (*164*, *174*). However, they are subject to somatic V(D)J DNA rearrangements of the T-cell receptor and immunoglobulin loci, respectively, and the impact of these rearrangements on iPSCs and their downstream cell lineages remains unresolved (*161*, *172*). There is also evidence that reprogrammed T-cells have the potential to spontaneously induce

T-cell lymphomas in mice, limiting their therapeutic potential (*175*). An alternative, attractive but relatively rare (<0.1%) cell source is $CD34^+$ hematopoietic stem and progenitor cells (HSPCs) as they are amenable to reprogramming and lack detectable gene rearrangements (*161*). In addition, less than 10 mL of whole blood is already sufficient for the generation of multiple iPSC colonies (*161*, *176*). In the present work, this cell type was used to generate iPSCs form a healthy donor and breast-cancer patients.

2.3.2 Reprogramming strategies

Multiple dedifferentiation strategies have been established to generate iPSCs which meet (dependent on the application) the desired safety and quality criteria. These methods can be divided into four subcategories: genome integrative or non-integrative vehicles delivered by either viral or non-viral techniques (*177*, *178*). Integrative techniques have raised concerns about oncogenic transformation or disruption of host suppressor gene expression, particularly if the insertion happens in an open reading frame or alters the expression of nearby oncogenes (*179*). Therefore, non-integrating methods for the generation of exogenous DNA-free iPSCs have been developed and comprise various delivery vehicles such as mRNAs (*180*), miRNAs (*181*), transposons (*182*, *183*), proteins (*184*), minicircles (*185*), antibodies (*186*), Sendai virus (*187*) and Adenovirus (*188*) or episomal vectors (*189*).

Episomal vector-based reprogramming

Compared to other DNA-based reprogramming methods, such as conventional plasmids or minicircle vectors, which require multiple transfections because of their inability to replicate in mammalian cells, episomal vectors offer several advantages. These include long-term stable expression with a single transfection, safety, cost-effectiveness, and the ability to remain extra-chromosomal, thus avoiding regulatory constraints and disruptions of important genomic regions of the host cell. Moreover, episomes are lost at a rate of approximately 5% per cell cycle, which facilitates the removal of exogenously introduced vectors from the generated iPSCs without any external manipulation. Unlike chromosome-integrating plasmids, episomal vectors often achieve higher transfection efficiencies. (*179*, *190*)

Episomal vectors based on elements of Eppstein-Barr virus (EBV), a human gamma herpesvirus, have become very popular for iPSC generation. These plasmids carry the origin of plasmid replication (oriP) and the EBV nuclear antigen-1 (EBNA-1). EBNA-1 encodes a protein that gets expressed from its viral promoter after transduction into somatic cells. (*190*, *191*) Subsequently, the C-terminal domain of EBNA-1 binds to oriP, while the N-terminal domain of EBNA-1 tethers the episomal DNA to the chromosome, allowing the vectors to replicate extra-chromosomally during each cell cycle (*190*, *191*).

2.4 Organoids – self-organizing tissue replicas in a dish

During tissue development, cells undergo a meticulously orchestrated series of movements that are directed by gradients of far-reaching signaling molecules and physical forces from neighboring cells. In fact, close attachment to neighboring cells results in push-pull interactions that initiate internal biochemical rearrangements. As a result, cells can asymmetrically apply further forces on their neighboring cells, creating a positive feedback loop that ensures that cells throughout the organ achieve the proper shape and size. (*192*)

Recapitulation of these complex physical and biochemical interactions in vitro is rather limited compared to their in vivo counterparts. However, organoid technology is a rapidly advancing field that holds great promise for expanding our understanding of human (developmental) biology and disease in a more physiologically relevant context than traditional 2D cell culture (*193*). These "mini-organs" are typically generated by culturing stem cells under well-defined conditions that mimic the microenvironment of the tissue of interest at the micrometer to millimeter scale. (*194*) Within this environment, stem cells can differentiate into multiple cell types and self-organize without external guidance into a complex structure that resembles the native tissue or organ (*195*).

The term "organoid" originally stemmed from classical developmental biology, where organogenesis was studied by cell dissociation and reaggregation experiments (*196*). However, as with any term that embraces a popular concept or idea, the meaning of "organoids" began to blur and became an umbrella word for a

wide range of in vitro and in vivo cellular models (*14*). Thus, a clear definition of "organoids" was required. Madeline Lancaster and Jürgen Knoblich provided a widely accepted definition, describing an organoid as *"a collection of organ-specific cell types that develops from stem cells or organ progenitors and self-organizes through cell sorting and spatially restricted lineage commitment in a manner similar to in vivo"* (*197*).

Therefore, an organoid must resemble the native tissue or organ by fulfilling the following criteria:

1. it must encompass more than one cell type of the corresponding organ,
2. recapitulate some organ-specific functions (e.g., contraction, filtration, excretion) and
3. exhibit cellular organization similar to the natural counterpart (*197*).

Self-organization, or in other words the ability of cells to organize themselves into higher order, is a fundamental process in biology but deciphering the underlying mechanisms of self-organizing systems' inherent non-linearity is a challenging task (*198*).

One key mechanism that drives self-organization is cell sorting, a process, in which different cell types with distinct adhesive properties segregate and move into different regions and thus, achieve the most thermodynamically stable arrangement (*197*). The physical interactions between different cells are mediated by the differential expression of variable cell adhesion molecules, cortical tension and/or cell motility and contractility (*195*, *197*).

The process of tissue morphogenesis is further mediated by spatially restricted cell-fate decisions. As the progenitor cells differentiate into more mature cells, they are pushed into a more superficial position due to the spatial limitations of the tissue or the orientation of division, which further supports their differentiation. The progeny may continue to undergo cell division, further differentiation and dislocation (*197*) (**Figure 2.3**).

Of note, the exogenous signals in the culture medium determine the specific developmental trajectories (driving them into "brain", "kidney" or "intestine"), but differentiation into organ-specific cell types in a defined spatial arrangement is a consequence of self-organization (*198*). While in vivo development is highly reproducible, each in vitro made organoid represents a unique and heterogeneous collection of cells, and no two organoids are exactly alike. Organoids vary considerably in terms of their

relative position of certain tissue domains, which can be attributed to the fact that, unlike the developing in vivo organ, organoids lack dorsal-ventral and anterior-posterior axis formation. (*197*, *198*) This fact needs to be considered when organoids are used in specific experimental setups.

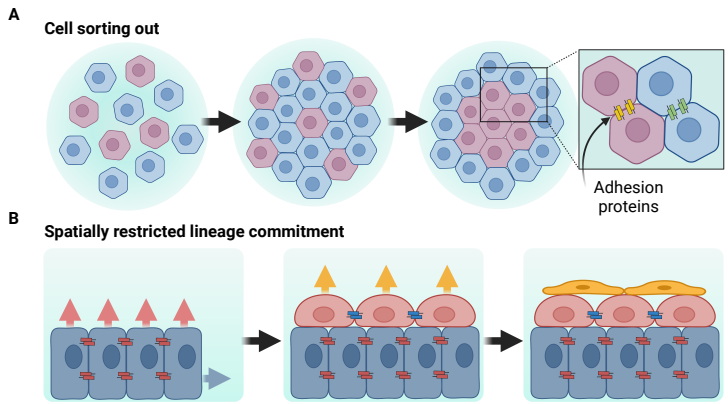

Figure 2.3: Key mechanisms of self-organization. A. Cell sorting out, a process in which cells migrate to different domains based on varying adhesion properties. **B.** Spatially restricted lineage commitment, where progenitor cells (blue) give rise to more differentiated cells (red) that are displaced into a more superficial position due to spatial constraints or division orientation. The new position fosters their differentiation, and they give rise to even more differentiated cells (yellow) that are further dislocated. Figure adapted from Lancaster and Knoblich (*197*).

2.5 Organoid culture and application

The innovative methodology of growing miniature three-dimensional organotypic structures from stem and progenitor cells in a laboratory setting paved the way for groundbreaking discoveries. Under well-chosen conditions, adult stem cells can be induced in vitro to reconstitute a scaled-down version of the organ in which they once inhabited (*199*). The group led by Hans Clevers made the observation that $Lgr5^{+}$ stem cells can be used to grow into crypt-villus intestinal organoids that contain all cell types of the intestinal epithelium (*200*). These findings have been extended to other tissues including liver (*201*), pancreas (*202*), fallopian tube (*203*), prostate (*204*) or stomach (*205*). However, adult stem cell tissue derived organoids require tissue and biopsies, which comes along with invasive surgical procedures (*199*). Their potential for genome editing is restricted and their differentiation potential is limited but the protocols for the organoid generation are relatively simple (*206*).

To circumvent these obstacles, protocols have been established that describe the generation of organoids from iPSCs. While they harbor a high potential for genome editing and can be obtained via a minimal procedure, the protocols for iPSC-derived organoid generation require multiple steps and are rather complex.

Furthermore, in contrast to adult stem cell-derived organoids, iPSC-based systems harbor the potential to direct the iPSCs to any organ-specific differentiation, allowing e.g., for a co-culture of two organoid types from one donor. (*206*)

One of the best-known types of iPSC-derived organoids are cerebral organoids, colloquially known as "mini-brains", developed by M. Lancaster and J. Knoblich in 2013 (*207*). The cerebral organoids self-organize in a manner reminiscent of the early stages of the developing human brain, encompassing several discrete but interdependent brain regions, including a cerebral cortex with progenitor populations that organize and produce mature cortical neuron subtypes. In addition, the organoids showed a progenitor zone organization with abundant outer radial glia stem cells, a feature also seen in human cortical development (*208*). Finally, the patient iPSC-derived brain organoids were used to model CDK5RAP2-dependent microencephaly and observed premature neuronal differentiation in patient organoids (*207*).

After this breakthrough observation, the past decades of intense organoid research witnessed the appearance of protocols describing the generation of numerous organoid types including but not limited to brain (*209*–*211*), retina (*212*–*214*), gut (*215*–*218*), kidney (*219*–*221*), liver (*218*, *222*–*225*), stomach (*226*, *227*), pancreas (*228*, *229*) or mammary gland (*11*, *230*, *231*).

Undoubtedly, tremendous progress has been made in the field of organoids, and yet organoid research is still in its infancy, striving to reveal the full potential of organoids to decipher a wide range of biological mechanisms.

3 Objectives

The primary objective of the present thesis is the establishment of a 3D co-culture model system, which allows to investigate tumor-TME interactions and the influence of tumor-adjacent mammary epithelium on breast tumor growth and invasiveness in both autologous and allogeneic settings.

To achieve this, the first step will involve the generation of iPSCs from PB of two breast cancer patients, followed by a comprehensive characterization of the iPSC clones to ensure their high quality. In a next step, we will differentiate the patient-derived iPSCs into mammary-like organoids (MLOs) and demonstrate their functionality by proving expression of luminal and basal epithelial markers, as well as milk protein (β-casein) expression upon hormonal stimulation.

We will combine the MLOS (that function as model for tumor-adjacent mammary epithelial tissue) with patient-derived microtumors (PDMs) in a 3D flaoting co-culture setup. The PDMs will be isolated from fresh primary tumor tissues from cancer treatment-naïve breast cancer patients, including but not limited to the patients who donated blood for the iPSC generation. Subsequently, the microtumors will be embedded in 3D Matrigel-collagen droplets to investigate the influence of ECM on PDM invasiveness.

Ultimately, we will co-culture the tumor models with MLOs to investigate the effect of tumor-adjacent mammary epithelial tissue on tumor growth and invasiveness for 10 days. To compare the in vitro behavior of established breast cancer models, co-culture experiments will also be conducted using spheroids from the highly invasive breast cancer cell line MDA-MB-231 and the poorly invasive breast cancer cell line MCF-7.

Using bead-based immunoassay, we aim at the identification of markers that may be associated with increased tumor growth and invasiveness in the co-culture system. Furthermore, we will perform an in-depth characterization of a broad set of breast microtumors. The histological and molecular composition and characteristics of the microtumors will be assessed using histological and protein-based approaches to confirm the positive correlation between microtumors and their corresponding native tumor.

This thesis aims to not only emphasize the importance of tumor-adjacent tissue in cancer progression but also highlights the significant variability within tumors of the same anatomical region. Our model system has the potential to serve as new platform for investigating tumor invasion-related processes and studying treatment approaches targeting these processes.

Results I

Generation and characterization of CD34$^+$-derived iPSCs from two breast cancer patients and one healthy donor

4

The contents of this chapter are based on

Keller, A.-L., Binner, A., Schenke-Layland, K., and Schmees, C. (2022). Establishment of Four Induced Pluripotent Stem Cell Lines from CD34+ Hematopoietic Stem and Progenitor Cells from a Patient Diagnosed with an Invasive Lobular Mammary Carcinoma. *Stem Cell Research* **64**, 102902

Keller, A.-L., Greis, D., Eybe, J., Plöger, S., Weiss, M., Koch, A., Brucker, S. Y., Schenke-Layland, K., and Schmees, C. (2022). Generation and Characterization of Three Induced Pluripotent Stem Cells Lines from an 86-Year Old Female Individual Diagnosed with an Invasive Lobular Mammary Carcinoma. *Stem Cell Research*, 102988

Keller, A.-L., Binner, A., Breitmeyer, R., Vogel, S., Anderle, N., Rothbauer, U., Schenke-Layland, K., and Schmees, C. (2021). Generation and characterization of the human induced pluripotent stem cell line NMIi010-A from peripheral blood mononuclear cells of a healthy 49–year old male individual. *Stem Cell Research* **54**, 102427

4.1 Highlights

- CD34$^+$ cells are isolated from peripheral blood of one healthy donor and two treatment-naïve breast cancer patients diagnosed with invasive lobular carcinomas, and subsequently reprogrammed to a pluripotent state.
- Comprehensive characterization confirmed genomic stability, normal morphology, endogenous expression of stem cell markers, loss of reprogramming factors, absence of mycoplasma contamination, trilineage differentiation potential and correct identity of all induced pluripotent stem cell clones.

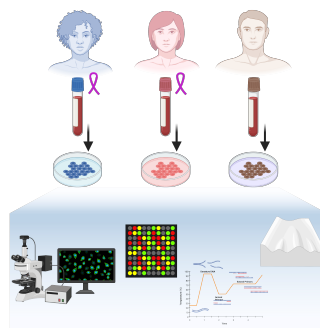

4.2 Background

Following the revolutionary discovery that adult somatic cells can be reprogrammed into a pluripotent state, there has been increasing interest in exploiting the full potential of iPSCs. In

vitro, iPSCs have the remarkable ability to both self-renew and differentiate into any cell type from the three germ layers (*146*). This versatility makes iPSCs invaluable for organoid development and promising for many research applications. Despite recent advances in iPSC reprogramming protocols, the quality of iPSC lines can vary widely, affecting their differentiation potential (*233*, *234*). Therefore, conducting a comprehensive characterization is essential to ensure the reliability and reproducibility of downstream iPSC-based applications.

One significant concern associated with iPSC generation is the maintenance of genomic integrity. In addition, the characterization process typically includes several key assessments, such as evaluating normal morphology, examining the expression of endogenous stem cell markers, verifying the loss of exogenously introduced reprogramming vectors, evaluating their potential to differentiate into the three germ layers, performing single tandem repeat (STR) analysis, and detecting the absence of mycoplasma contamination (*235*). This chapter outlines the successful generation of iPSCs from $CD34^+$ HSPCs, followed by an in-depth characterization of the iPSC clones.

The first step towards this goal was the establishment of a reprogramming protocol (**Figure 4.1**). Our initial success was demonstrated using $CD34^+$ HSPCs obtained from PB of a healthy male donor (**Appendix D**). However, the protocol was based on a home-brewed media and lacked an initial $CD34^+$ HSPC enrichment step, which could have contributed to the poor reprogramming efficiency we observed. Therefore, we continued subsequent reprogrammings using pre-prepared media, which are less susceptible to batch-to-batch variability and included a $CD34^+$ HSPC enrichment step prior to PBMC isolation. These modifications resulted in a significant improvement in reprogramming efficiency. While the initial protocol required 50 mL PB and resulted in three high-quality iPSC clones, the modified protocol required only 5-9 mL PB and produced up to 12 high-quality clones. We used the modified protocol to reprogram $CD34^+$ HSPCs obtained from two breast cancer patients (**Appendix B**, **Appendix C**).

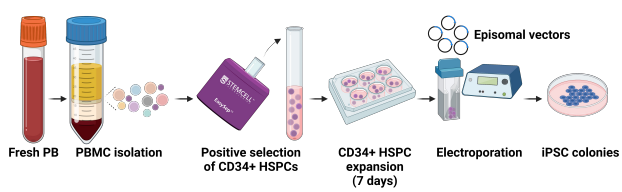

Figure 4.1: Schematic workflow for the generation of iPSCs. PBMCs were isolated from fresh whole blood. $CD34^+$ HSPCs were purified by positive selection and cultured for 7 days. Electroporation was used to introduce episomal vectors. Arising iPSC colonies were individually selected and expanded.

4.3 Generation of the iPSC line NMIi010-A based on the initial reprogramming protocol

50 mL of PB was collected from a healthy male donor (**Appendix D**) and immediately processed for PBMC isolation by density gradient centrifugation using Lymphoprep™ density gradient medium and SepMate™-50 tubes. After mononuclear cell isolation, $CD34^+$ HSPCs were positively selected and expanded in a $CD34^+$ expansion medium based on StemPro™-34 SFM medium, supplemented with GlutaMAX™, SCF, IL-3, GM-CSF. This step was necessary to increase the number of $CD34^+$ cells to be sufficient for reprogramming (approximately 10^6 cells), due to their naturally low abundance in PB (*161*). After 7 days, the composition of the expanded cells was determined by flow cytometry. The data indicated, that a total of 99.8% of the cell fraction was positive for CD45, which is expressed on the plasma membrane of all hematopoietic cells except erythrocytes and platelets (*236*), while 99.7% of the total cell population were CD34 positive. Only a small fraction of 12.3% was composed of T-cells, (activated) monocytes/macrophages, neutrophils and eosinophils, natural killer (NK) cells and B-cells, as indicated by the expression of CD3, CD14, CD16, CD19, CD20 and CD56, respectively (**Figure 4.2**).

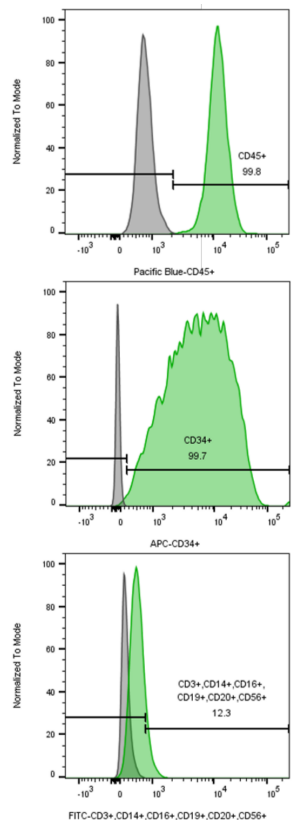

Figure 4.2: Expression of cell surface markers in the expanded cell fraction on day 7. Top: 99.8% of the examined cell population displayed positive expression of CD45, a cell surface marker present on all hematopoietic cells except erythrocytes and platelets. Middle: $CD34^+$ expression, the markers for HSPCs, was detected in 99.7% of the cell population. Bottom: A subset of cells comprising 12.3% showed positive expression for CD3 (T-cells), CD14 (monocytes/-macrophages, with lower levels on neutrophils and eosinophils), CD16 (NK-cells, activated monocytes/-macrophages, and neutrophils), CD19 and CD20 (B-cells), and CD56 (NK-cells). Flow cytometry data were acquired using the BD LSRFortessa™ Cell Analyzer (BD Biosciences) and analyzed using FlowJo v10 software (FlowJo LLC).

Upon reaching the desired cell count, the cells were transfected with episomal vectors. In the present study, we used an optimized set of five episomal vectors, designed by Dr. Okita at CiRA, Kyoto. The vector set consisted of pCE-hOCT3/4 encoding Oct4, pCE-hSK encoding both Sox2 and Klf4, pCE-hUL encoding c-Myc and Lin28, pCE-mP53DD encoding mp53DD, and pCXB-EBNA1 encoding EBNA-1 (Epi5™ episomal vectors). The transfected cells were then plated on a hESC-qualified Matrigel-coated well plate in complete StemPro™-34 SFM medium. On day 1 post-electroporation, the medium was changed to N2B27 medium, based on DMEM/F-12 with HEPES, and supplemented with N2, B27, MEM non-essential amino acid solution, GlutaMAX™, β-mercaptoethanol, and FGF-β. On day 9, the medium was switched to mTeSR™ Plus iPSC medium. Cells were monitored until first iPSC colonies appear (around day 21 post-transfection) (**Figure 4.3**). Individual iPSC clones were manually picked and transferred to a fresh Matrigel-coated plate. The iPSCs were then cultured in mTeSR™ Plus iPSC medium.

4.4 Generation of iPSCs from HSPCs obtained from PB of two breast cancer patients

5 - 9 mL of PB was collected from two treatment-naïve breast cancer patients diagnosed with ILC at the University Hospital of Tübingen, Germany (**Appendix B**,**Appendix C**). Upon sample receipt, a human hematopoietic progenitor cell enrichment cocktail was added to the blood sample. The cocktail was designed to target non-progenitor cell populations via tetrameric antibody complexes recognizing CD2, CD3, CD14, CD16, CD19, CD24, CD56, CD61, CD66b and glycophorin A on red blood cells (RBC) for depletion. Following the enrichment step, the lineage-committed cells and RBCs were separated from the pre-enriched progenitors via density gradient centrifugation. The $CD34^+$ HSPCs were then purified through positive selection. Subsequently, the cells were transferred to a $CD34^+$ expansion medium supplemented with a defined set of cytokines and growth factors, including Flt3L, SCF, IL-3, IL-6 and TPO. Cells were cultured for up to 7 days. For the transfection step, the cells were combined with the Epi5™ episomal vector mixture, as described above. After electroporation, the cells were resuspended in $CD34^+$ expansion medium and transferred to a well plate coated with hESC-qualified Matrigel. The cells were initially cultured in $CD34^+$ expansion medium until day 3 post-electroporation and then switched to ReproTesR™ until the first iPSC colonies appeared.

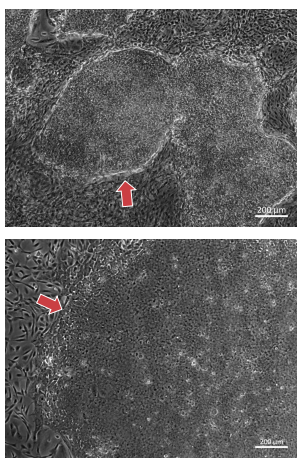

Figure 4.3: Putative iPSC colonies emerge from the monolayer of non-reprogrammed cells. At approximately day 21 post-electroporation, putative iPSC colonies (red arrow) emerge and are clearly distinguishable from the surrounding cells. Scale bars: 200 µm

4.5 iPSC characterization

Stringent functional and molecular assays are essential to evaluate the pluripotency potential of a newly generated iPSC line. During reprogramming, putative iPSC colonies appeared between a densely packed monolayer of non-reprogrammed cells and exhibited a characteristic cell and colony morphology that distinguishes them from other cells in the same culture (**Figure 4.3**). iPSC colonies were compact and grew large with defined borders and a cobblestone-like appearance. The cells within the colonies were small, exhibiting a prominent nucleus and a small cytoplasm (**Appendix B** Fig. 1D, **Appendix C** Fig. 1B, **Appendix D** Fig. 1A). Monitoring the morphology of iPSC cultures provides important information about the culture status, such as the homogeneity of

their undifferentiation status and the number of spontaneously differentiated cells (*233*).

Since iPSCs tend to acquire chromosomal aberrations not only during the reprogramming process, but also after prolonged cell culture, we examined the iPSC clones for their genomic integrity, which can severely affect the differentiation potential and lead to reduced reliability and reproducibility of experiments (*237*). It was described that chromosomal aberrations predominantly occur with higher frequency in the chromosomes 1q, 4p, 8q, 10p, 12p, 18q, 10q, and Xp (*237*). Array-based comparative genomic hybridization (aCGH) is a cytogenetic technique that allows for the analysis of copy number variations in the sample of interest compared to a reference sample. Its high-resolution, genome-wide detection of numerical chromosomal abnormalities and unbalanced structural alterations and the fact that it has a fast turn-around time as no fresh sample (dividing cells) is needed, makes it an attractive alternative to karyotyping. Of note, aCGH is limited by the fact that it cannot detect balanced rearrangements like translocations and inversions, and small mosaicism. (*237*, *238*)

In the present work, aCGH was carried out at the Institute for Clinical Genetics, Klinikum Stuttgart, Germany. Sample DNA (isolated and purified from iPSC pellets) and a reference genome were labelled with different fluorescent dyes and hybridized on the microarray. Each spot on the microarray indicated a certain fluorescent signal intensity, which served as a relative measure of the sample DNA bound to the DNA sequence on that certain spot. The relative abundance of sample and reference DNA were reflected by the ratio of the intensities of the fluorophores on each spot (*239*). The aCGH data confirmed the genomic integrity of all iPSC lines as no copy number variation was detected in any of the iPSC clones (**Appendix B** Fig. 1C; **Appendix C** Fig. 1C; **Appendix D** Fig. 1E).

Furthermore, the iPSCs were examined for endogenous expression of a defined set of undifferentiation markers by immunofluorescence (IF) staining, reverse transcriptase (RT) polymerase chain reaction (PCR) and flow cytometry, respectively. All iPSC clones showed positive expressions of a set of undifferentiation markers, including Oct4, Nanog, Sox2, DNMT3, c-Myc, TRA-1-81, and TRA-1-60 (**Appendix B** Fig. 1A,B,E; **Appendix C** Fig. 1A,E,F; **Appendix D** Fig. 1B,C,D; **Figure 4.4**). Additionally, we demonstrated that exogenously introduced reprogramming vectors were depleted before the iPSCs were used for further experiments.

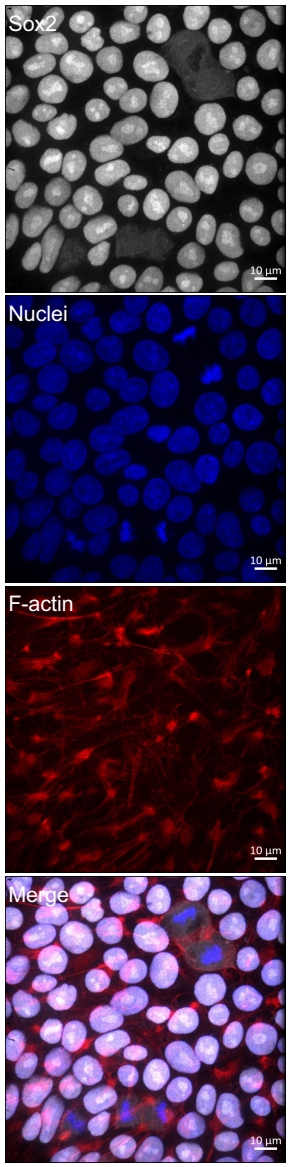

Figure 4.4: iPSC colonies express Sox2. Example of Sox2-expressing iPSCs. Counterstaining: DAPI and Phalloidin. Captured at a magnification of 64x with a Zeiss CellObserver Z1 (Carl Zeiss). Scale bars: 10 µm

For this purpose, total iPSC RNA was isolated and transcribed into cDNA using MuLV reverse transcriptase. PCR confirmed the loss of the reprogramming vectors (indicated by the absence of the EBNA-1 gelband). The housekeeping gene glyceraldehyde 3-phosphate dehydrogenase (GAPDH) and a reprogramming plasmid mixture were included as positive controls (**Appendix B** Fig. 1B; **Appendix C** Fig. 1F; **Appendix D** Fig. 1D).

The remarkable potential of iPSCs to differentiate into cells from any of the three germ layers is one of the major advantages of iPSCs and an important prerequisite for their successful generation (*233*). A straightforward way to drive iPSCs into the germ layers is offered by commercial differentiation kits, which allow for rapid, parallel and reproducible differentiation. IF staining confirmed the expression of certain transcription factors specific to the individual germ layers. Ectodermal differentiation was shown by a positive Pax6 expression, while mesodermal differentiation was demonstrated by Brachyury expression. The successful differentiation into the endoderm was confirmed by a positive expression of Sox17 (**Appendix B** Fig. 1F; **Appendix C** Fig. 1D; **Appendix D** Fig. 1F).

Short tandem repeats are repeated DNA-sequences that comprise approximately 3% of the human genome, but the number of repeat units varies greatly from one individual to the next. Therefore, STR analysis provides a high degree of discrimination, making it an invaluable tool for identification applications. (*240*) To exclude a mix up between the iPSC samples, STR analysis was performed at the Institute for Pathology, Klinikum Stuttgart. A 100% allele match at different loci was confirmed between parental cells and derived iPSCs, while the individual clones from different donors were clearly distinguishable. Thus, the correct identity of the iPSC clones was confirmed (data can be found in the journal's archive).

On a regular base, the cell culture was monitored for the absence of a potential mycoplasma contamination. To this end, the cell culture supernatant was collected and examined by conventional, endpoint PCR. The PCR detects the highly conserved 16S rRNA coding region in the mycoplasma genome (*241*). Internal amplification controls were added (supplemental information of **Appendix B**, **Appendix C** and **Appendix D**).

It is worth mentioning that additional data related to the characterization of iPSCs, such as the expression of additional ecto-, meso- and endodermal markers, were experimentally confirmed.

However, these data were not included in the corresponding publications due to space limitations. If readers are interested in accessing these data, they are kindly directed to the *hPSCreg* database, a global registry for human iPSC lines, by scanning the QR codes or by opening the weblinks provided in **Appendix A**. Characterization data can be found under the respective "Characterization" category. The database also contains information on culture conditions, derivation and ethics.

4.6 Conclusion

We described the successful generation and comprehensive characterization of 8 iPSC lines to ensure the use of high quality iPSCs as the basis for subsequent organoid generation. The genomic integrity of all clones was confirmed by aCGH, and the expression of endogenous undifferentiation markers was demonstrated by flow cytometry, IF staining and RT-PCR. Loss of exogenously introduced episomal reprogramming vectors was confirmed and successful in vitro differentiation into all three germ layers was demonstrated. Furthermore, all iPSC clones showed normal iPSC morphology and no mycoplasma contamination was detected. Finally, STR analysis confirmed the correct identity of the iPSC clones.

It is worth noting that the characterization methods were primarily established using iPSCs generated from the $CD34^+$ cells HSPCs of the healthy donor (**Appendix D**). However, these iPSCs will not be used in the co-culture system involving microtumors or breast cancer cell line-derived spheroids. Instead, they were utilized to further establish the differentiation protocols for the generation of kidney and colon organoids (see **Outlook**).

Results II

Co-cultures of iPSC-derived Mammary-like organoids and patient-derived microtumors model invasive behavior of breast cancer ex vivo

5

The contents of this chapter are based on

Keller, A.-L., Anderle, N., Schrenk, M., Greis, D., Binner, A., Visser, D., Göpfert, J., Koch, A., Weiss, M., and Brucker, S. (2023). Co-cultures of iPSC-derived Mammary-like Organoids and Patient-derived Microtumors Model Invasive Behavior of Breast Cancer ex vivo

5.1 Highlights

- Generation of induced pluripotent stem cell-derived mammary-like organoids that express luminal and basal markers of the mammary gland as well as milk protein upon hormonal stimulation.
- Isolation of breast microtumors from fresh primary tumor tissue of three cancer treatment-naïve patients.
- Tumor-adjacent mammary epithelial tissue (mammary-like organoids) enhances breast cancer growth and invasion.
- Invasion and metastasis-related markers (fibronectin and metalloproteinase-2) are upregulated in co-cultures of breast cancer spheres and mammary-like organoids.

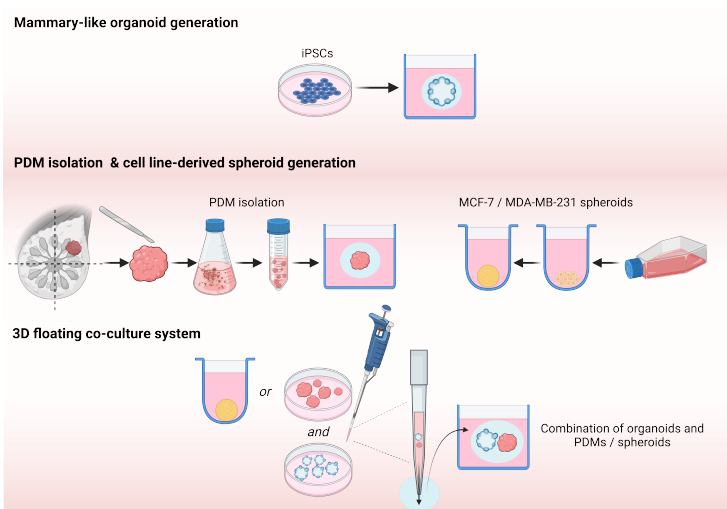

5.2 Background

The female breast consists of a highly branched ductal-lobular network and is surrounded by subcutaneous adipose tissue and collagenous interstitial stroma. The ductal system converges cylindrically from the mammary papilla and terminates in the lobules, collectively referred to as the terminal duct lobular unit (TDLU) (**Figure 1.3**A). (*242*)

These units contain clusters of acini where milk is produced and stored in response to hormonal signals (*242*). The collecting ducts and lobules are composed of two epithelial cell layers: the inner part is formed by a polarized luminal epithelium, while the outer layer is defined by the myoepithelium (*243*). In addition, a laminin-rich basement membrane surrounds the myoepithelial cells and separates the stroma from the ducts (*242*). In its role as a natural paracrine tumor suppressor, the myoepithelium is known to act as a guardian of tissue integrity (*244*). It functions as a "fence", preventing pre-invasive in situ carcinomas that arise and accumulate in the luminal epithelium from spreading (*245*). However, as the disease progresses, malignant cells may become invasive and break through their "natural fence" to conquer the surrounding tissue, an absolute prerequisite for breast tumor invasion and metastasis (*246*).

Indeed, breast cancer is a complex disease involving intricate interactions between malignant cells, normal and non-neoplastic cells, and the various components of the surrounding stroma. In order to identify the mechanisms that drive cancer progression, a comprehensive understanding of these interactions is critical. For instance, the interaction between breast cancer cells and adipocytes has been shown to promote tumor progression through the secretion of various inflammatory factors, MMPs, cytokines, and growth factors that stimulate programs for EMT. (*247*–*249*)

While the interplay between cancer cells and stromal components has been extensively studied, less attention has been paid to tumor-adjacent mammary epithelial cells, which are likely the first point of interaction during tumorigenesis and are in direct physical contact with the growing tumor. Direct cellular contact can determine whether a cell undergoes cell death, becomes quiescent or develops into a clinically-relevant tumor, and is therefore a critical factor for the course of the disease (*250*). Indeed, previous work has demonstrated that cancer-adjacent normal and/or benign mammary epithelial cells can promote breast cancer proliferation

and progression (*250*–*252*). However, these studies have predominantly been performed in two-dimensional culture conditions and/or with cancer cell lines that do not recapitulate the complex architecture and composition of tumors.

In the present work, we aimed to investigate the influence of tumor-adjacent mammary epithelial cells on breast tumor growth and invasion. To achieve this, we developed a 3D co-culture system using autologous and allogeneic interactions. This system involved iPSC-derived MLOs representing the tumor-adjacent mammary epithelium, along with either PDMs isolated from fresh primary breast cancer tissue or 3D spheroids derived from breast cancer cell lines.

First, we differentiated iPSCs into MLOs, expressing both luminal and basal mammary markers. The functionality of these organoids was confirmed by inducing milk protein expression upon hormonal stimulation. Next, we isolated PDMs from three different breast cancer patients and studied their behavior in a 3D ECM. Finally, we combined the MLOs with either the PDMs or 3D spheroids derived from highly metastatic and non-metastatic breast cancer cell lines and observed changes in the growth and invasiveness of the respective cancer models in the presence or absence of MLOs. Using bead-based immunoassays, we identified two markers associated with invasion and metastasis, MMP2 (*253*) and FN (*254*), that were upregulated in the co-cultures (*253*, *254*). Our findings emphasize the potential significance of the tumor-adjacent mammary epithelium in relation to tumor growth, invasion, and processes associated with metastatic progression (*11*) .

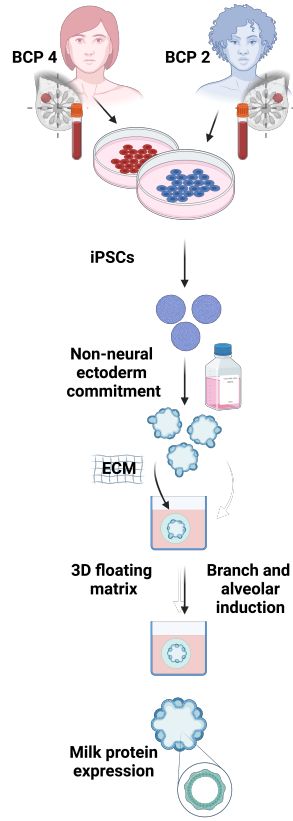

Figure 5.1: Schematic workflow for the generation of iPSC-derived mammary-like organoids (MLOs). Single-cell iPSCs are formed into MammoCult™ medium-cultured embryoid bodies (mEBs) and maintained in complete MammoCult™ medium for 10 days. At day 10, the mEBs are transferred into a 3D Matrigel-collagen mixed gel floating matrix suspended in EpiCult™-B human medium supplemented with pTHrP for 5 days. From day 15 to day 35, the medium is supplemented with hydrocortisone, insulin, FGF10 and HGF to induce branching and alveolar induction. Milk protein expression is induced by prolactogenic medium for additional 5 days.

5.3 Generation of iPSC-derived MLOs

Our first goal was the generation of functional MLOs. To achieve this, we followed a two-step protocol originally established by Ying Qu and colleagues (*230*) (**Figure 5.1**; **Appendix E** Fig.1A).

First, we induced mammary differentiation in vitro by generating 3D cell aggregates called embryoid bodies (EBs). To form EBs, we dissociated the iPSCs from their neighboring cells and from their underlying matrix (Matrigel) and plated a defined number of single cell iPSCs on anti-adhesive substrates pretreated with a surfactant solution to reduce surface tension and prevent cell adhesion. However, the dissociation of the iPSC colonies could

cause the cells to undergo anoikis due to the lack of cell-cell interactions and ECM (*255*). To prevent cell death, a RHO/ROCK signaling inhibitor was added to the single cell suspension (*256*). The EBs were cultured in complete MammoCult™ medium, which enriches mammary epithelial progenitor cells within the cell aggregates. The resulting EBs are referred to as MammoCult™ medium cultured embryoid bodies (mEBs) to highlight their active differentiation into the non-neural ectodermal lineage (*11*).

Studies have indicated that the neural lineage is the "default" differentiation pathway for iPSCs (*257*). Therefore, we first validated the successful enrichment of cells associated with the non-neural ectoderm. We cultured both mEBs and control EBs (the latter incubated in regular iPSC maintenance medium) in their respective media for 10 days. The cell aggregates were then analyzed by whole-mount IF staining to examine the expression of the non-neural markers AP2γ and cytokeratin (CK) 18, as well as the stem cell marker Sox2 (**Figure 5.2**) The analysis revealed a significant increase in AP2γ and CK18 expression in mEBs compared to EBs, indicating the upregulation of markers linked to mammary differentiation. In contrast, EBs exhibited significantly higher Sox2 expression compared to mEBs, indicating the downregulation of undifferentiation markers in the lineage committed mEBs (**Appendix E** Fig.1B). These results demonstrate the successful differentiation of iPSCs toward the non-neural lineage.

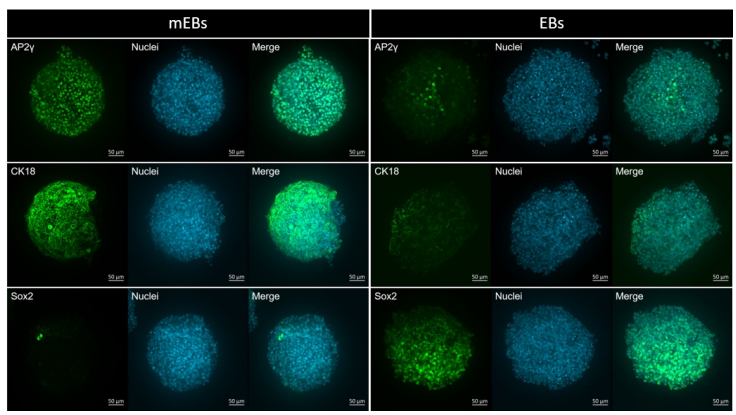

Figure 5.2: Whole mount immunofluorescnce staining of day 10 mEBs and EBs. On day 10, EBs (cultured in stem cell maintenance medium) and mEBs (cultured in differentiation medium) were prepared for whole mount IF staining with AP2γ, CK18 and Sox2. Nuclear counterstaining: DAPI. Scale bars: 50 µm.

On day 10, the mEBs were placed at the center of a liquid Matrigel-collagen droplet, which resembles the approximate stiffness as in a normal mammary gland (~170 Pa) (*230*, *258*). After solidification, the matrix droplet was transferred to complete EpiCult™-B human medium supplemented with parathyroid hormone (pTHrP), resulting in a 3D floating matrix system (*11*).

After 5 days, media conditions were changed to complete EpiCult™-B human medium supplemented with hydrocortisone, insulin, HGF and FGF10 until day 35 for mammary cell specification and branch and alveolar induction. To demonstrate functionality, day 35 MLOs were incubated in prolactogenic medium for 5 days to induce milk protein expression (*11*). β-casein is the predominant protein contributing to the peptidome of human milk (*259*). We observed β-casein in the lumen of the potential acinar structures of the MLOs via whole mount IF staining (**Appendix E** Fig.1C). Furthermore, MLOs were stained positive for the luminal epithelial markers CK8, CK18 and EpCAM, as well as for the expression of the basal epithelial markers CK14 and p63 (**Appendix E** Fig.1C). At day 35, the overall viability of the organoids was assessed. Data analysis revealed an overall mean viability of approximately 88% (**Appendix E** Fig.1E).

In summary, we successfully differentiated breast cancer patient-derived iPSCs into functional MLOs for subsequent co-culture with autologous and allogeneic PDMs or breast cancer cell line derived spheroids.

5.4 Isolation of breast cancer PDMS

We previously described the isolation of ovarian and glioma microtumors from fresh primary tumor tissue (FPTT) (*5*–*7*), and confirmed that the histopathologic features of the PDMs were comparable to those of the primary tumor tissue (*5*). Building on this knowledge, we isolated PDMs from primary breast cancer lesions. In scope of the present study, we obtained FPTTs from 3 cancer treatment-naïve breast cancer patients (BCPs) after completion of histopathological examination at the University Hospital Tübingen. Upon tissue receipt, the tumors were mechanically dissected into small fractions (1-2mm) and enzymatically digested overnight with gentle shaking. Between 200 and 4500 PDMs were retained after filtration, depending on the size and composition of the FPTT (**Figure 5.3**; **Appendix E** Fig.A2).

BCP1 had been diagnosed with IDC-NST, BCP2 with ILC, and BCP3 with mucinous ductal carcinoma (**Table 5.1**; **Appendix E** Table1). All tumors were of the luminal type, as indicated by HR expression and absence of HER2. It was found that BCP1 exhibited the highest tumor proliferation rate (Ki-67 = 21%), while BCP2 and BCP3 showed Ki-67 scores of 10% and 5-10%, respectively. The TNM classification, which describes tumor size (T), involvement

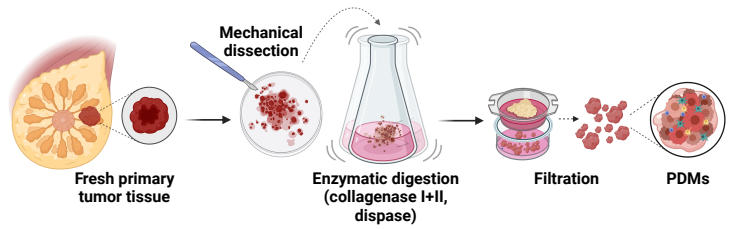

Figure 5.3: Workflow for the isolation of PDMs from FPTT. Upon sample arrival, the FPTT is mechanically dissected into 1-2 mm pieces and subsequently enzymatically digested overnight using Liberase™, an enzyme mixture consisting of collagenase I+II and dispase. PDMs are retained by filtration. Figure adapted and modified from Anderle et al. (*5*)

of regional lymph nodes (N), and presence of distant metastases, revealed that both BCP1 and BCP2 had developed T3 breast tumors, indicating a tumor size over 5 cm. BCP3's tumor was classified as T2, indicating a size of 2–5 cm. BCP1 showed the highest regional lymph node involvement, with 7+ invaded lymph nodes (N3). BCP2 had 1-3 invaded lymph nodes (N1), while BCP3 had no detected spread to regional lymph nodes (N0). Lymphatic pathway invasion (L), perineural tissue invasion (Pn), and venous structure invasion were also examined. Metastases and venous structure invasion were not detected. BCP1 showed invasion to the lymphatic pathways, whereas BCP2 exhibited perineural invasion. Overall, BCP1 represents the most advanced tumor tested.

Table 5.1: Overview of the anonymized patient cohort. Breast cancer patient (BCP1) was diagnosed with IDC-NST, BCP2 with ILC and BCP3 with a mucinous (Muc) ductal carcinoma. H.=histological type, T.=tumor size, N.=involvement of regional lymph nodes, L.=lymphatic pathway invasion, Pn.=perineural tissue invasion. Metastases and venous structure invasion were not detected in any of the patients.

Patient	PDMs	iPSCs	H	ER	PgR	HER2	T	N	L	Pn	Ki-67 (%)
BCP1	yes	no	IDC-NST	+	+	-	3	3a	1	0	21
BCP2	yes	yes	ILC	+	+	-	3	1a	0	1	10
BCP3	yes	no	Duc;Muc	+	+	-	2	0	0	0	5-10

Notably, we also received a blood sample from BCP2, which we used to isolate $CD34^+$ HSPCs for the subsequent iPSC generation (**Appendix C**). Consequently, BCP2 PDMs were co-cultured with BCP2-iPSC-derived MLOs, creating an autologous co-culture system. The other co-culture systems remained allogeneic.

To compare the PDMs' performance and in vitro behavior with widely used breast cancer model systems, we generated spheroids from the highly invasive MDA-MB-231 and the poorly invasive MCF-7 breast cancer cell lines (*260*). These spheroids derived from both cell lines, together with the PDMs, are hereafter collectively referred to as "breast cancer spheres". After their generation, the breast cancer spheres were cultured in suspension without the

presence of ECM (**Appendix E** Fig. 3A). However, solid tumors in patients are subject to continuous dynamic influences from the surrounding connective tissue and ECM. Therefore, we aimed to explore the effect of ECM on the morphology and behavior of breast cancer spheres by embedding them in Matrigel-collagen droplets using the same Matrigel:collagen concentrations and ratios as for MLO generation (**Appendix E** Fig. 3C). By following the same protocol used for MLOs, we ensured a consistent approach to studying the behavior of breast cancer spheres and subsequent co-cultures.

All breast cancer spheres retained a circular phenotype without exhibiting protrusions or invasive morphologies in suspension culture (**Appendix E** Fig. 3A). However, a notable observation was that BCP-1 PDMs acquired a highly invasive phenotype as early as 3 days in floating ECM. Of note, MDA-MB-231 spheroids also showed a similar tendency towards an invasive phenotype, although less pronounced. PDMs from BCP2 and BCP3, as well as MCF-7 spheroids maintained a circular, non-invasive phenotype throughout the 10 days (**Appendix E** Fig. 3B,C). We also assessed the viability of the breast cancer spheres after 10 days of culture to ensure that the observed differences in behavior were not due to a toxic effect of the matrix. However, no significant difference was observed between the tested models, with an overall high cell viability (**Appendix E** Fig. 3E).

The data indicate that PDMs derived from BCP1 exhibit significantly increased invasiveness when cultured in ECM compared to PDMs from the other two patients. Notably, BCP1 had been derived from the FPTT with the most advanced cancer stage among the three patients. The influence of ECM on invasive behavior was also observed, albeit to a lesser extent, in MDA-MB-231-derived spheroids, which are known for their invasive characteristics. In contrast, the poorly invasive MCF-7 spheroids exhibited a behavior similar to that of BCP2 and BCP3. These findings underline the critical role of the ECM in in vitro systems, particularly in influencing the invasiveness of breast cancer cells.

5.5 Co-culture of breast cancer spheres and early MLOs

To study the potential influence of tumor-adjacent mammary epithelial tissue on tumor growth and invasiveness, we performed

co-culture experiments using a single organoid and a single breast cancer sphere placed in close proximity within a matrix droplet. Over a period of 10 days, we monitored the growth and invasiveness of each cancer model. In particular, we observed that the organoid and the corresponding breast cancer sphere migrated towards each other, eventually forming a compact two-component structure. In particular, BCP1 PDMs showed spindle-like growth towards the MLOs as early as day 3 of co-culture (**Appendix E** Fig. 4C, *d3-20x, blue arrow*).

Next, we evaluated the growth (measured by size increase) and the invasiveness (determined by circularity reduction) of the breast cancer spheres cultured alone or in co-culture with MLOs. In the case of BCP1 PDMs, co-culture with MLOs resulted in a significant increase in both size (area fold change) and invasiveness compared to monoculture conditions without MLOs (**Appendix E** Fig. 4A,B). Similarly, MDA-MB-231 spheroids co-cultured with MLOs showed a trend toward increased invasiveness and size compared to the corresponding MDA-MB-231 spheroid monoculture, although to a lesser extent than BCP1. The breast cancer spheroids, which previously maintained a circular, non-invasive phenotype, also appeared to be unaffected by the presence of MLOs. They did not demonstrate significant size increase or adopt an invasive phenotype upon co-culture. These observations suggest that the presence of tumor-adjacent mammary epithelium may promote tumor growth and invasiveness, but probably only in tumors that have reached a certain progression threshold and/or exhibit an activated pro-invasive/pro-metastatic gene expression profile.

Our next objective was to investigate the potential upregulation of invasion- and metastasis-associated markers in the respective co-cultures using bead-based immunoassays. We found that FN and MMP2, both known as breast cancer markers associated with tumor aggressiveness, invasion and metastasis (*253*, *254*), were significantly upregulated in all co-cultures involving BCP1, BCP2, BCP3, and MDA-MB-231, but not in the case of MCF-7, by day 10 compared to monocultured MLOs and breast cancer spheres **Appendix E** Fig. 4D,E). Notably, the co-culture of BCP1 PDMs and MLOs exhibited the highest level of soluble FN among all co-cultures. Additionally, MMP2 levels were significantly higher in the BCP1 + MLO co-culture compared to other co-cultures, except for the highly invasive MDA-MB-231 co-culture.

Taken together, these findings demonstrate that tumor-adjacent mammary epithelium plays a supportive role in promoting tumor growth. This supportive effect is likely attributed, at least in part,

to the activation of invasion and metastasis-related markers such as MMP2 and FN in breast cancer. Importantly, this mechanism is most likely not limited to MMP2 and FN but encompasses additional factors that remain to be elucidated.

5.6 Conclusion

In the present study, we have introduced a novel 3D co-culture platform incorporating breast cancer spheres and MLOs, representing tumor-adjacent mammary epithelial tissue. These breast cancer spheres consisted of either primary tumor-derived microtumors, encompassing the heterogeneous histologic and molecular characteristics of breast carcinomas (see **Appendix F**), or spheroids derived from well-established breast cancer cell lines.

Our results highlight the importance of incorporating the ECM in in vitro studies, as it can potentially enhance tumor invasiveness, likely influenced by the tumor composition and stage. Furthermore, the presence of tumor-adjacent mammary epithelial tissue amplifies this effect, as we demonstrated its ability to potentiate tumor growth and invasiveness. We identified well-known markers, FN and MMP2, asssociated with breast cancer invasion, metastasis and poor clinical outcome (*253*, *254*), which were upregulated especially in the co-cultures of MLOs and the highly invasive breast cancer spheres compared to respective monocultures.

In our setup, the autologous conditions (BCP2 PDMS with MLOs) did not significantly affect tumor size, invasiveness, or marker upregulation when compared to the allogeneic setups. However, this optionally autologous experimental setup provides a valuable platform for future studies focusing on the addition of tumor-infiltrating lymphocytes (TILs), where HLA matching would be advantageous.

Results III

PDMs resemble tumor heterogeneity and enable individualized drug treatment

6

The contents of this chapter are based on

Anderle, N., Schäfer-Ruoff, F., Staebler, A., Kersten, N., Koch, A., Önder, C., **Keller, A.-L.**, Liebscher, S., Hartkopf, A., Hahn, M., Templin, M., Brucker, S. Y., Schenke-Layland, K., and Schmees, C. (2023). Breast cancer patient-derived microtumors resemble tumor heterogeneity and enable protein-based stratification and functional validation of individualized drug treatment. *Journal of Experimental & Clinical Cancer Research* **42**, 210

6.1 Highlights

- Patient-derived microtumors were isolated from fresh primary tumor tissue with high cell viability.
- The microtumors closely resemble features of the corresponding primary tumor tissue, including histotypes, extracellular matrix components, protein expression or signaling pathway activity.
- Triple negative breast cancer microtumors show remarkable features in oncogenic pathways, associated with disease relaspe.
- Identification of defined protein panels associated with treatment response or resistance.

6.2 Background

As any other biological system, cancer is robust and reacts on external selection pressures with intrinsic error corrections or by rewiring certain signals to restore homeostasis, which renders therapeutic intervention not as effective as hoped (*20*). It must be acknowledged that cancer progression and therapy resistance is the result of a complex interplay between heterogenous neoplastic cell populations and their "soldiers", namely those components of the TME that help cancer cells to survive (*17*). A reliable cancer model must therefore incorporate key features of the native tumor and, simultaneously, must bridge the gap between experimental tractability and physiological relevance.

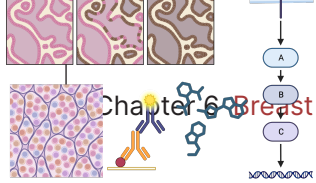

While data from genomic, transcriptomic, and proteomic studies have expanded our knowledge of cancer, they cannot be directly translated into better treatments (*261*). Although the molecular advances of the past few decades have given us a tremendous boost in understanding the mechanisms underlying cancer development, we are still at the beginning of unraveling the full potential of the interactions between tumor cells and their microenvironment (*10*). However, it is precisely these individual cellular interactions that lead to the highly heterogeneous disease manifestations and the failure of systematic treatments(*83*). An essential element for the development of tailored therapies and personalized approaches is the establishment of reliable preclinical models that accurately resemble the characteristics of a real tumor. In fact, the wrong experimental model can disrupt the phenomenon being investigated. (*261*)

A major burden in the management of oncological conditions is resistance to therapy and disease recurrence, which is mainly due to the immense heterogeneities that characterize breast cancers (*262*). While predictive models such as MammaPrint or Oncotype DX can be used to estimate response to chemotherapy in individual cases (*133*), there is still a lack of reliable tumor models that reflect the primary tumor as accurately as possible. Such tumor models could be used to estimate which patients will benefit most from which treatment, while also providing a robust framework for studying tumor-TME interactions or invasive and metastatic processes.

To bring us one step further towards precision medicine, and thus, highly personalized care, we generated PDMs consisting not only of tumor cells but also of TME components of the corresponding primary breast tumor with different histopathological features. The PDMs can be used for various subsequent investigations as early as 2 days after sample receipt and can find various applications, including their use in co-culture models (as described in **Appendix E**) or drug response tests (*5*). We performed an in-depth comparison of a broad repertoire of PDMs and their corresponding native breast tumor tissues and confirmed the physiological relevance of the PDMs.

Of note, as a co-author of the present manuscript, I mainly contributed to the PDM isolation, hematoxylin and eosin (H&E) staining, Movat's staining and immunohistochemistry (IHC) staining (**Appendix F** Fig. 1, Fig. 2, Fig. 3). Therefore, this chapter will primarily focus on these contributions, while only a brief overview

will be given for the protein profiling data, pathway signaling data, and treatment response data.

6.3 Isolation of PDMs from a cohort of patients

In the scope of the present work, we obtained n = 102 residual fresh breast tumor tissue specimens from debulking surgeries conducted at the University Hospital Tübingen. Out of the 102 mammary carcinoma tissue samples, PDMs were successfully isolated in 77 cases (**Appendix F** Fig. 1D). Using image-based analysis, we confirmed the overall high cell viabilities of the PDMs (**Appendix F** Fig. 1A,B). We observed considerable variation in the sizes of the isolated PDMs (**Appendix F** Fig. 1C). However, we found no correlation between the success rate of PDM isolation and specific clinical features of the corresponding primary tumor tissue. PDMs were successfully recovered independently of the HR status, histological subtype, or tumor grade (**Appendix F** Fig. 1E). PDM size and isolation success may be attributed to the inherent biological composition of the primary tumor tissue. Additionally, PDM size may be affected by the composition of the digestion medium. An adapted protocol based on the biological properties of the tumor could be established to produce PDMs with more consistent sizes.

6.4 Histotype-specific pathologic features

Next, we aimed to investigate the resemblance of PDMs to the histopathology of their corresponding primary tumors. Breast cancer, being a highly heterogeneous group of tumors, exhibits significant histologic variability. Factors such as mitotic activity, stromal extent, cellular atypia[1], and pleomorphism[2] contribute to this heterogeneity (*264*). Distinct histologic types of breast cancer possess unique morphologic characteristics, including the formation of nests, clusters, cords, trabeculae, or single file lines by malignant cells (*10*, *265*). To address this, the samples were classified into different histologic types: IDC-NST, DCIS, ILC and LCIS. Subsequently, we performed H&E staining to assess the

1: **Cellular atypia** describes structural abnormalities in cells.

2: **Pleomorphism** describes irregularities in both cellular and/or nuclear shape and size and correlates with tumor aggressiveness and clinical outcomes. It is a fundamental microscopic criterion for the cytologic diagnosis of cancer (*263*).

morphologic features and connective tissue compartments of both PDMs and PTT (**Appendix F** Fig. 2A,B).

A certified pathologist from the University Hospital in Tübingen, conducted a comparative analysis of the PDMs and their corresponding primary tumors. The pathologic evaluation demonstrated that the vast majority of PDMs exhibited histological similarities to breast cancer tissue and their specific histologic subtype. Stromal compartments were identified in more than half of the PDMs. Furthermore, there was concurrence in cellular atypia between PDMs and their corresponding primary tumor tissue. In 20.5% of cases, PDMs and their corresponding primary tumors displayed a similar nuclear grade, while 59% of PDMs exhibited a decrease in nuclear grade by 1. Overall, PDMs showed significant similarity to the histopathologic features of their corresponding primary tumors. (**Appendix F** Fig. 1C)

6.5 PDM's comprise ECM components

The ECM is a sophisticated meshwork of various macromolecules that serves as a structural framework and a reservoir for growth factors. Alterations in the expression of ECM components may result in deregulated matrix remodeling and can contribute to disease progression, including breast cancer. Tumorigenesis and metastasis in mammary carcinomas are often accompanied by an increased ECM-stiffness, e.g., through excessive collagen deposition. (*266*)

Thus, tumor models that comprise the ECM structures of native tumors are highly desired test systems for studying disease and therapy resistance.

To this end, we aimed to visualize connective tissue components in PDMs and the respective primary tumor tissue (PTT) using Movat's staining[3]. Large areas of green staining were observed in PTT, indicating the presence of proteoglycans (PGs) and glycosaminoglycans (GAGs) (stained in cyan blue) as well as collagen fibers (yellow) (**Appendix F** Fig. 2D). Dense collagen networks were predominantly detected near the tumor masses, contributing to tissue stiffening. PDMs, isolated from tumor masses of PTT via mechanical disruption and collagenase I+II digestion, lacked the framing collagen fibers but retained the inner tumor cell mass and its ECM components. PGs/GAGs were found in BC-PDMs when their expression within tumor masses in the PTT

3: **Movat's stain** is a pentachrome staining method that uses a combination of 5 dyes to selectively detect various components of connective tissue, including collagen and proteoglycans, depending on the chemical properties of the dyes on histologic slides (*267*)

was high. While elastic fibers were more abundant in ILCs than in IDC-NSTs, no significant differences in the amount of collagen were found between ILCs and IDC-NSTs. However, ILC PDMs tended to have slightly higher amounts of collagen than IDC-NST PDMs (**Appendix F** Fig. 2E), consistent with the observations in **Appendix E** Fig. 2D,E and with the literature (*268*).

Taken together, Movat's staining allowed the visualization of distinct ECM components in both PDMs and PTT. We identified the presence of the most abundant breast cancer-related ECM proteins in PDMs.

6.6 IHC staining

We then focused on investigating the expression of CKs, CAF markers, immune cell markers, and the potential presence of HRs using IHC staining. Remarkably, our PDM repertoire resembled both HR-positive and TNBC PDMs (**Appendix F** Fig. 3A,B). Since different treatment strategies are required for HR-positive breast cancers and TNBCs, the accurate identification and in vitro maintenance of HR presence or absence is crucial for the development of personalized treatment plans (*130*).

CK expression is an important differentiation marker in precancerous breast lesions. Mammary carcinomas exhibit distinct patterns of CK expression, with luminal subtypes characterized by luminal CKs (CK8/CK18/CK19) as basal subtypes showing basal CKs (CK5/CK6/CK7/CK14). However, some breast tumors display a combination of both CK types. (*269*)

Here, we investigated the expression of CK5, CK6 and CK18 in HR-positive PDMs as well as TNBC PDMs. We observed a highly heterogeneous pattern of CK expression (**Appendix F** Fig. 3C,D). This heterogeneity allowed us to classify HR^+ PDMs into four distinct groups:

1. $CK5^-/CK18^+$ (luminal, differential glandular type)
2. $CK5^+$ (basal type)
3. $CK5/6^+$ (basal, stem cell phenotype)
4. $CK5/6/18^+$ (intermediate glandular phenotype)

We found significantly higher expression of CK18, a marker for luminal breast cancers, in HR-positive PDMs compared to TNBC PDMs. Consistent with previous findings, TNBC PDMs lacked CK18 expression but exhibited a moderate CK5/6 expression.

The absence of CK18 expression, a hallmark of EMT, has been associated with tumor progression and increased cancer cell migration (*270*).

FAPα, a marker for CAFs, was detected in all PDMs to varying degrees, with a significant increase in ILC PDMs, congruent with existing literature (*271*). Furthermore, the presence of M2 macrophages was indicated by the TAM marker CD163 in a small subset of the examined tissues. CD8, a marker for cytotoxic T-cells and PD-L1, an T-cell inhibitory checkpoint marker, were mostly negative with few exceptions. Of note, there was no considerable correlation between the presence of IICs and hormone receptor status (**Appendix F** Fig. 3E,F).

In summary, the PDMs mirrored the HR receptor status of the corresponding PTT and exhibited heterogenous expression of CKs and FAPα. Immune cell markers were sporadically identified.

6.7 Protein profiling analyses

Our next aim was to expand the histological and immunohistochemical PDM characterization by comprehensive protein profiling analyses. To this end, protein expression and the activity of key signal transduction pathways was investigated in PDM and corresponding PTT using the DigiWest® technology[4].

4: The **DigiWest® technology** is a multiplex protein profiling method for the in-depth analysis of the activity of signaling pathways in drug development and biomarker discovery. It enables the analysis of 800 total and phosphorylated proteins per sample in a single run by combining standardized protein separation and western blotting techniques with a multiplexed, bead-based immunoassay platform (*272*).

The profiling panel encompassed cell cycle proteins, from JAK/-STAT, MAPK, RTK, PI3K/AKT, EMT/Cytoskeleton and Wnt signaling pathways. Our data revealed an overall high positive correlation of averaged protein signals in PDMs and their matched PTTs (**Appendix F** Fig. 4A). Additionally, no significant differences were observed in signal pathway activity and the expression of breast cancer-related proteins (**Appendix F** Fig. 4B). However, some proteins showed varying abundance between PDMs and PTTs. For instance, PDMs showed elevated CK5 and CK6 protein levels, possibly due to estrogen deprivation in the culture conditions (*273*, *274*). Furthermore, we identified a reduction in the presence of a specific set of immune cells in PDMs compared to PTTs, regardless of the breast tumor type (**Appendix F** Fig. 4C,D). However, correlation analysis showed a general positive correlation between protein signals in matched PDMs and PTTs (**Appendix F** Fig. 4E,F).

Protein profiling data of PDMs revealed a significant upregulation of oncogenic signaling pathways, particularly PI3K/AKT and

MAPK/RTK, in TNBC PDMs compared to HR-positive PDMs (**Appendix F** Fig. 5E), which is in accordance with the literature (*275*). Notably, increased MAPK pathway activity is associated with high disease relapse in patients diagnosed with TNBC (*276*).

Additionally, we detected an upregulation of proteins associated with cell cycle and metabolism in TNBC PDMs (**Appendix F** Fig. 5F). The observed upregulation of signaling pathways in the TNBC PDMs significantly impacts various key processes in cancer cells, such as proliferation, differentiation, migration, cell growth and survival. Our findings are consistent with previous research in TNBC and highlight that PDMs capture the protein pathway activation characteristics of their corresponding primary tissue.

Furthermore, we sought to investigate the PDM response to four anti-cancer drugs over time: the selective estrogen receptor modulator tamoxifen (TAM), the chemotherapeutics docetaxel (DTX) and paclitaxel (PTX) and the CDK4/6 inhibitor palbociclib (PAB). By assessing the treatment's impact on cell viability, we categorized the PDMs as either "responders" or "non-responders". Of note, among the tested drugs, the highest response was obtained with DTX treatment, with 9 out of 29 PDM models demonstrating a positive response, while TAM displayed the lowest response, with 4 out of 29 PDM models showing increased cell death (**Appendix F** Fig. 6A). Utilizing DigiWest® analysis to explore the proteomic profiles of the "responders" and "non-responders", allowed us to identify defined protein panels that were significantly elevated or decreased in the "responder" vs. the "non-responder" group in response to the respective drug treatment (**Appendix F** Fig. 6B-O). These proteins were clustered into distinct "sensitivity" and "resistance" panels, providing important information about why breast cancers may or may not respond to certain treatments.

Overall, we confirmed that the protein pathway profiles of PDMs are similar to those of the corresponding native tumor and that PDMs mirror the protein expression of PTTs with positive correlation. In line with the literature, an upregulation of specific oncogenic pathways in TNBCs was observed. Furthermore, our data revealed heterogeneous responses of PDMs to different anti-cancer drugs and allowed the identification of defined, previously described and novel protein panels associated with treatment response or resistance.

6.8 Conclusion

We isolated breast cancer PDMs from FPTT of different histologic and molecular subtypes, and by using different histopathological and molecular approaches, we demonstrated that PDMs capture the remarkable heterogeneity observed in breast cancer. The PDMs hold great promise as valuable tools for predicting treatment response, thereby enhancing our ability to tailor therapies to individual patients.

General discussion and conclusion

7

Tumors are complex ecosystems that reside within their compliant tissues. Research over the past decades has provided a massive amount of information about the interactions between malignant cells and the surrounding stromal components, some of which play an ambivalent role in cancer progression. While they can exert tumor-repressive functions in the early stages of cancer, the surrounding cells can be hijacked and rewired during tumor evolution to become "accomplices" rather than "gendarmes". Co-opted by the malignant cells, stromal components secrete multiple factors including cytokines, ILs, proteases, growth factors or (lymph-)angiogenic factors in a way beneficial for the tumor, ultimately promoting cancer cell proliferation and invasion. (*17*)

As the tumor emerges in the lumen of the ducts or lobules, malignant cells come into direct cellular contact with the mammary epithelium, which is considered to play a dual role in the disease course (*250*). Here, we aimed to fill a gap in our current understanding of how breast tumor-adjacent mammary epithelial tissue influences breast cancer growth. To closely mirror the patient's situation, we conducted the experiments using microtumors isolated from fresh primary breast cancer tissues with different molecular and histological properties. We validated the physiological relevance of the PDMs by performing an in-depth comparison with the corresponding primary tumor tissue, using histopathological and protein-based analyses. Our results confirmed that the PDMs closely resemble their native tumor counterparts, thus establishing their relevance in drug testing. We identified altered expression patterns in a defined set of proteins associated with therapy sensitivity and resistance.

To investigate whether tumor-adjacent mammary epithelial tissue (reflected by iPSC-derived MLOs) potentially exerts effects on tumor (PDMs and breast cancer cell line-derived spheroids) progression, we established a 3D floating matrix that allowed for the co-culture of both components in close proximity. The MLOs expressed both, luminal and basal markers while the organoid's functionality was confirmed by milk protein expression in acinar-like structures upon hormonal stimulation. Over a period of 10 days, we observed significant differences in size and invasiveness of PDMs from BCP1 when co-cultured with MLOs compared to the PDMs cultured alone, without the presence of MLOs. A

similar trend was observed in the case of MDA-MB-231 spheroids, a cell line known to be highly invasive (*260*). Furthermore, we detected elevated levels of soluble FN and MMP2, two markers associated with invasion and metastasis in all co-culture setups compared to the respective monocultures of breast cancer spheres or MLOs. The present work substantiates the importance of inter- and intratumoral heterogeneities observed in different breast cancers for tumor growth and invasiveness. We presented a physiologically relevant in vitro system that allows the study of cancer progression and interaction with the TME. Importantly, our results indicate that the tumor-adjacent mammary epithelium has the potential to enhance the progression of advanced human breast tumors.

7.1 iPSCs can be generated from CD34$^+$ HSPCs derived from PBMCs of healthy and diseased donors

A first step towards the establishment of the co-culture system was the generation of high quality iPSCs from HSPCs, multipotent cells associated with the expression of the surface marker CD34. This cell type represents an attractive source for iPSC reprogramming, as it maintains greater genomic stability than terminally differentiated cells (*176*).

The variability between iPSC lines has been widely recognized, which underscores the importance of accurate reporting and standardized quality control procedures. These practices help to reduce variability and ensures the sharing of reproducible results (*277*). Here, we followed the guidelines of iPSC characterization recommended by the European Bank for induced Pluripotent Stem Cells (EBiSC) and examined the iPSC lines for: vector clearance, pluripotency (differentiation potential), expression of markers for human pluripotent stem cells and self-renewal, morphology, cell line identity, mycoplasma contamination and genomic integrity (*235*).

In fact, the emerging putative iPSC colonies must be carefully examined, as previous studies showed that only rare cell clusters were identified as fully reprogrammed iPSCs, while the vast majority of cells remained partially reprogrammed intermediates (*278*). These partially reprogrammed cells are challenging to distinguish from bona fide iPSCs, as they also give rise to densely

packed colonies. However, they appear to have missed certain "milestones" during reprogramming, such as the upregulation of TRA-1-60 or SSEA-4, leaving the intermediates trapped in their incompletely reprogrammed state (*278*). While no single marker alone is sufficient to identify a fully reprogrammed state, studies revealed that expression of TRA-1-60 and DNMT3-β may be an indicator of fully reprogrammed iPSCs (*278*). Using RT-PCR and flow cytometry, we confirmed the expression of DNMT3-β and TRA-1-60 in all of our iPSC lines.

Indeed, reprogramming is a highly organized process involving specific molecular events in a precise sequence within a limited time frame (*278*). Although iPSCs can be generated in a reproducible manner, only a small fraction of transfected/transduced cells attain a fully pluripotent state. This phenomenon may be a consequence of certain "roadblocks" that prevent efficient reprogramming (*279*). Of note, coaxing a mature cell back into a pluripotent state is an exciting paradigm in biology as normal development seems to follow a unidirectional path, which is characterized by a stepwise decrease in cellular pluripotency (*280*). Thus, reprogramming suffers from low efficiencies (0.1%-10% for most somatic cell types (*281*)) and delayed kinetics (*282*). These hallmarks are a significant hindrance to the generation of high quality iPSCs and can be attributed to several cell intrinsic factors (*279*).

One of these roadblocks is **senescence**, a permanent cell cycle arrest that can be induced e.g., by telomere shortening, oxidative stress, DNA damage or oncogenic signaling (*279*). Cells with longer telomeres (such as those found in young donors) exhibit lower expression levels of senescence-related genes and are therefore easier to reprogram (*283*). A critical transcription factor involved in the DNA damage response is p53. When activated by stress factors, such as transfection/transduction during reprogramming, the tumor suppressor protein p53 is activated and can induce apoptosis or senescence to prevent further damage to the system (*284*). In fact, Klf4, one of the OSKM-factors, can either activate or antagonize p53, depending on the cell type and expression level, potentially leading to oncogene-mediated activation of the p53 pathway (*285*). Deletion or depletion of p53 can improve the reprogramming efficiency of human somatic cells (*283*, *285*, *286*). Considering that HSPCs are affected by age-related cellular senescence (*287*) and that the age of our donors ranged from 48 to 86 years, we attempted to overcome the barrier of senescence by introducing mp53DD into the CD34$^+$ cells during

the reprogramming process. mp53DD is a dominant negative mutant of p53 and its transient expression will interfere with the normal activity of the wildtype p53 protein, allowing cells to adopt a pluripotent identity without entering a senescent or apoptotic state (*288*). In contrast to permanent deletion or strong long-term inhibition, mp53DD is diluted out during normal iPSC passaging, making the cells less prone to genomic instability and malignant transformation (*279*).

Another major roadblock to pluripotency is mediated by an unfavorable **stoichiometry of key reprogramming factors** (*279*). In the context of Yamanaka factor-based reprogramming, a balanced, equimolar stoichiometry of OSKM transcription factors was shown to be highly effective in initiating and maintaining pluripotency, and influences the biological and molecular characteristics as well as the epigenetic status of iPSCs (*289*).

Early mechanistic studies have been carried out using viral vectors that express monocistronic reprogramming factors, but monocistronic reprogramming can cause copy number and integration site variation, resulting in inconsistent cell-to-cell stoichiometries. The solution to this problem has been the development of polycistronic expression cassettes, which are capable of the production of multiple proteins from a single transcript. (*290*) However, larger plasmids may hinder successful entry into the cell during transfection due to their higher molecular weight and physical size (*291*). In our studies, we achieved pluripotency with the introduction of 5 episomal vectors with equimolar stoichiometries of reprogramming factors, originally designed in the laboratory of Shin'ya Yamanaka (*286*, *292*). Two of the plasmids contained bicistronic expression cassettes encoding for Sox2/Klf5 and L-Myc/Lin28, respectively. These sequences were linked through a "self-cleaving" F2A peptide, which triggers ribosomal skipping of the linker's C-terminal proline and glycine resulting in a separation between the end of the 2A sequence and the downstream peptide (*293*). To ensure maintenance of high-level transgene expression, all reprogramming factors were under the control CAG promoters.

Transfection efficiency was further enhanced in our system due to oriP/EBNA-1 mediated nuclear import, while retention of the vector DNA allows iPSC generation through one single transfection (*294*). Furthermore, we used non-transforming L-Myc instead of c-Myc since this factor is known to be more specific and potent during iPSC reprogramming (*286*).

In summary, although there are obstacles to the efficient ge-

neration of iPSCs, we have successfully overcome some of them (mp53DD expression / established OSKM stoichiometry). As a result, we obtained a collection of high-quality iPSC clones from three donors, which served as the basis for the subsequent differentiation into different types of organoids. It is worth noting that other factors, including the modulation of specific signaling pathways or the epigenetic state of the source cells, are also barriers to reprogramming (discussed in detail in excellent reviews such as Haridhasapavalan et al., 2020 (*279*)). Thus, additional interventions to address these factors could further improve reprogramming efficiency.

7.2 iPSCs-derived generation of MLOs

While the past few years witnessed the publication of numerous protocols describing the differentiation of iPSC into various types of organoids with a particular focus on brain (*207*, *209*–*211*), intestine (*295*) or kidney (*219*–*221*), less attention has been paid to the development of functional organoids representing mammary tissue. To the best of our knowledge, there is only one peer-reviewed protocol, published by Ying Qu and colleagues, describing the differentiation of iPSCs into MLOs (*230*). In the present work, our goal was to follow the previously published protocol to generate MLOs that could serve as tumor-adjacent mammary epithelial tissue for studying its role in cancer growth and invasiveness. Through a stepwise approach, we successfully developed MLOs that express breast-specific, luminal and basal markers. Of note, we have made a few minor adjustments to our protocol: To increase the efficiency and convenience of mEB generation, we used microwell culture plates, which allow the formation of up to 300 mEBs in a single well, as opposed to the 384-well plates used in the original publication. In addition, we used organoid embedding sheets as a substrate for embedding organoids and breast cancer spheres in Matrigel-collagen droplets, ensuring consistent and reproducible results.

Throughout life, the mammary gland undergoes several steps of growth, morphogenesis, cell diversification or full phenotypic differentiation. Numerous factors contribute to these processes, some of which are also co-opted by breast cancers to remodel the tissue to their own advantage. For instance, pTHrP is essential for the formation of the embryonic mammary gland, as its depletion prevents the embryonic mammary bud to form the neonatal

duct system. During lactation, pTHrP regulates maternal calcium homeostasis through its osteolytic activity. On the other hand, pTHrP also contributes to the pathophysiology of breast cancer. When secreted by metastatic breast cancer cells in the bone, pTHrP contributes to osteolytic bone destruction and further promotes metastasis (*296*). (*297*)

It is therefore not surprising that pTHrP is an essential cell culture supplement for the correct differentiation into MLOs. In the absence of pTHrP, the organoids fail to develop alveolar structures and express mammary-related markers (*230*). While previous studies demonstrated that MCF-7 breast cancer cells can express pTHrP and proliferate in the presence of pTHrP in vitro, indicating a potential autocrine response (*298*), we can exclude the possibility that the increased growth and invasiveness effects, as well as the elevated FN and MMP2 levels we observed, are solely a consequence of the culture media supplemented with the respective growth factors or hormones such as pTHrP. Since the monocultures of MLOs and the respective breast cancer spheres, respectively, had the same media as the co-culture, the effects are likely due to either factors secreted by the MLO or direct cell-to-cell contact between the MLO and the breast cancer sphere.

7.3 Tumor-adjacent mammary epithelial tissue reinforces processes associated with growth and invasion

Our data indicated a significant increase in tumor size and invasiveness of BCP1 PDMs in presence of MLOs compared to the BCP1 PDMs cultured alone. A similar trend was observed when MLOs were co-cultured with MDA-MB-231 spheroids. However, PDMs derived from BCP2, BCP3 as well as the poorly invasive MCF-7 cell-derived spheroids maintained a circular, non-invasive phenotype when cultured alone and remained phenotypically unaffected by the presence of the MLOs.

Interestingly, the proliferative and invasive capacities of the PDMs alone in ECM or in co-culture with MLOs seem to mirror the tumor progression state observed in the native breast tumor tissue. While all BCPs were diagnosed with invasive carcinomas, BCP1 exhibited the highest proliferative capacity, with a tumor size of at least 5 cm and invasion into a minimum of 7 regional lymph

nodes. Thus, among the 3 patient-derived breast cancer tissues analyzed, the tumor from BCP1 was most advanced (**Table 5.1**). PDMs derived from this primary tumor displayed the most aggressive behavior in terms of tumor growth and invasiveness in monoculture, while tumor-adjacent mammary epithelium (MLOs) seemed to push this phenotype even further. The findings are further supported by signal transduction analysis, which revealed elevated levels of proteins associated with cell cycle, MAPK/RTK signaling, and PI3K/AKT/Wnt signaling in BCP1 PDMs (=BC96) (**Appendix F** Fig. 5D). These pathways are closely associated with several critical features of cancer, such as cancer cell survival, angiogenesis, and metastasis (*299*, *300*). However, no conclusions can be drawn with respect to BCP2 and BCP3 as they were not included in the study described in **Appendix F**.

Furthermore, the upregulation of soluble FN and MMPs in presence of the MLOs was most pronounced for BCP1 PDMs. A similar pattern regarding invasiveness, cancer cell growth, and FN and MMP2 levels was observed in co-cultures of MDA-MB-231 spheroids. This TNBC cell line was originally isolated from a metastatic breast adenocarcinoma and is known for its high invasiveness. In contrast, the poorly invasive MCF-7 spheroids did not show that phenotype. (*260*)

Consistent with our observations, previous in vitro and in vivo studies have demonstrated a tumor-promoting effect of normal and/or benign mammary epithelial cells (*250*, *252*). For instance, breast cancer cells co-injected with benign mammary epithelial cells into nude mice exhibited up to a three-fold size increase compared to the tumor cells injected without benign epithelial cells. Surprisingly, even metabolically inert benign mammary epithelial cells were able to promote tumor growth, suggesting that the benign cells engage with tumor cells through direct cell-to-cell contacts, leading to the secretion of auto-stimulatory factors by the cancer cells. Specifically, IL-6 and GM-CSF were found to be significantly elevated in co-cultures with direct physical contact. (*250*) Furthermore, the medium supernatant of benign mammary epithelial cells was found to enhance the clonogenic behavior of breast cancer cells. The investigators detected a subset of cytokines, in particular MCP-1, specific to the conditioned medium (*250*). Whether MCP1, IL6 and GM-CSF are also elevated in our culture setups will be examined in future studies.

Another group cultured MDA-MB-231 cells in conditioned medium derived from normal mammary epithelial cells and observed a significantly increased invasive phenotype in the cancer cells

(*252*). The investigators identified CXCL12/SDF-1 as the major driving force behind this effect. SDF-1 is a chemokine involved in the migration, invasion and metastasis of cancer cells (*301*). SDF-1 was secreted by the normal mammary epithelial cells and bound to its receptor, CXCR4, expressed on the surface of the MDA-MB-231 cancer cells. This, in turn, led to overexpression of uPAR on the surface of the cancer cells, which is known to drive breast cancer cells from a dormant to an aggressive phenotype. (*252*) In fact, SDF-1-CXCR4 interaction leads to the activation of numerous intracellular signaling pathways and downstream effects, associated with cell survival, proliferation, chemotaxis, migration and adhesion (*302*).

Bright field images of our co-cultures suggest direct physical contact between the MLOs and the respective breast cancer spheres, although further analysis is required to confirm this observation (**Appendix E**, Fig. 4C). Thus, the growth and invasion effects mediated by the presence of MLOs could be attributed to both direct cell-to-cell contacts and/or secretion of soluble factors such as SDF-1. It is possible that PDMs from BCP1 and MDA-MB-231 spheroids, but not PDMs from BCP2, BCP3 and MCF-7 spheroids, express CXCR4 on their surface and thus activate the SDF-1-CXCR4 axis in co-culture. In fact, studies have reported negligible expression of CXCR4 on the surface of MCF-7 cells, while MDA-MB-231 cells have been shown to highly express this receptor (*303*). To investigate this further, our next step will involve assessing the SDF-1 levels in the supernatants. Furthermore, it will be crucial to examine the expression of the CXCR4 receptor in the PDMs. It is conceivable that the SDF-1/CXCR4 contributes, at least in part, to the observed increased growth and invasiveness effects in the co-cultures of MLOs and BCP1 PDMs or MDA-MB-231 spheroids.

In summary, previous studies have shown that both normal and benign adjacent breast epithelial cells can exert a tumor-promoting effect. However, it remains to be elucidated whether our MLOs can be considered “normal” or whether they have undergone prelesional alterations. The latter possibility is supported by evidence revealing morphological and phenotypic differences between regions immediately surrounding breast tumors and non-tumor bearing healthy breast tissue. In particular, transcriptome analysis has identified an intermediate state between “healthy” and “tumor” in tissue adjacent to the tumor (*304*). It should be noted that this transformation may take more time and may not be fully established within a 10-day period. To test this, future

experiments could include transcriptome profiling of organoids co-cultured with breast cancer spheres and organoids cultured alone.

The observation that PDMs derived from BCP2 and BCP3, as well as MCF-7 spheroids did not show these pro-invasive effects can be attributed to several aspects: first, BCP3 was diagnosed with a mucinous carcinoma, which is a rare type of mamma carcinoma but associated with low invasion and good clinical outcomes (*305*). Furthermore, among the received tissues, this tissue had the lowest proliferation rate. MCF-7 cells are also known to be less aggressive than MDA-MB-231 cells and are poorly invasive (*260*). BCP2 PDMs were expected to be more invasive, but these PDMs generally contained large parts of ECM within the microtumors (**Appendix E**, Fig. 2E, *black arrow*, Fig. 2D). This finding is consistent with existing literature reporting that ILC has the highest levels of intratumoral collagen (*268*). Furthermore, it has been reported that downregulation of CK18 is associated with tumor progression and significantly correlates with advanced tumor stages and is more frequently observed in ductal than in lobular breast carcinomas (*306*). We observed the lowest CK18 expression in the IDC-NST PDMs from BCP1 and in MDA-MB-231 spheroids - the breast cancer spheres with the most aggressive behavior in our in vitro experiments.

Based on our cumulative observations, it can be concluded that PDMs mimic the characteristics of their corresponding primary tumor with regard to in vitro/ex vivo functionality and behavior. Furthermore, it appears that MLOs have the ability to enhance the progression of tumors with a pre-existing proliferative and/or advanced phenotype.

7.4 Increased secretion of FN and MMP2 from invasive breast cancer spheres in the presence of tumor-adjacent mammary epithelial cells

We sought to examine whether the interaction between tumor-adjacent mammary epithelial tissue and breast cancer spheres could result in an upregulation of factors associated with cancer growth and invasion. Indeed, we identified two soluble factors, FN and MMP2, that were significantly upregulated in all co-cultures,

except of the MCF-7 co-culture. MMP2 plays a key role in ECM degradation, thereby promoting tumor invasion and metastasis (*253*), while FN expression correlates with tumor aggressiveness and poor clinical outcome in patients with invasive breast cancers (*254*).

Consistent with our previous findings, we observed that PDMs derived from BCP1 showed the strongest response to the presence of MLOs. This was evident from two aspects: (i) within the studied cohort, the co-culture of BCP1 PDMs and MLOs showed the most substantial differences in FN and MMP2 concentrations compared to the respective controls (monocultures of BCP1 PDMs and MLOs), and (ii) the levels of FN and MMP2 in the co-culture of BCP1 PDMs and MLOs were higher than those observed in the co-culture involving other breast cancer spheres. Similar to our invasion and growth results, the co-culture with MDA-MB-231 spheroids showed a strong upregulation of FN and MMP2 compared to the levels measured in the respective monocultures. Notably, BCP1 PDMs and MDA-MB-231 cultured alone secreted higher levels of both factors compared to the other samples, supporting our hypothesis that the presence of tumor-adjacent mammary epithelium further accelerates the progression of already advanced, highly aggressive tumors.

Interestingly, PDMs derived from BCP2 and BCP3 seemed to respond to the presence in MLOs in terms of FN and MMP secretion, but no significant changes in invasion were observed in the previous experiments. Although slightly increased, no significant effects were observed in the co-cultures with MCF-7 spheroids. It is conceivable that the effects are initially observed at the molecular level, paving the way for subsequent invasion into the surrounding tissue.

Fibronectin expression in primary breast tumors is of particular interest as it is an indicator of breast cancer progression and strongly correlates with decreased patient survival, regardless of the breast cancer subtype (*307*, *308*). As a tumor expands, it can deposit FN and collagen fibrils, causing an increased tissue stiffness. In early tumor stages, the fibrils are typically aligned parallel to the primary tumor boundary. However, as the tumor mass expands, it exerts physical pressure on the fibrils, causing them to reorient perpendicular to the tumor margin. This rearrangement provides a "pathway" for tumor cell migration. (*307*)

When FN is upregulated under pathological conditions, it activates numerous signaling cascades, including MAPK/ERK and

PI3K/AKT, which promote EMT and invasion, metastasis or resistance to therapy (*309*). Interestingly, fibronectin secretion can also be a consequence of hypoxic conditions, but hypoxia is also a significant driver of EMT (*310*, *311*).

What we identified in our co-culture media supernatants is soluble FN. Soluble FN exhibits a globular conformation and lacks the ability to spontaneously assemble into fibrils without exogenous cues. The compact form of soluble FN needs to be stretched to uncover its hidden FN-FN binding site and allow the assembly of a fibrillar matrix. Stretching can occur by cell-mediated processes involving integrin binding to FN's tripeptide recognition sequence Arg-Gly-Asp (RGD). (*312*)

Notably, since FN assembly is a stepwise process, breast cancer cells may secrete higher levels of soluble FN or contribute to increased FN matrix production through interactions with non-malignant cells. The increased FN content may promote metastatic initiation after extravasation. Indeed, recent studies have shown that breast cancer cells undergoing EMT were able to secrete large amounts of globular FN. (*307*)

It is intriguing to note that both FN and MMP2 are upregulated in the co-cultures, as these two components appear to be intertwined in their roles.

Matrix degradation is a crucial process in the establishment of metastasis, and this process is primarily driven by the activity of proteases, particularly MMPs (*116*). In their function as zinc-dependent endopeptidases, they are able to degrade almost all macromolecules within the ECM (*313*, *314*). The resulting spaces created by the MMP-mediated proteolysis further facilitates cancer cell migration (*116*). Among this family of peptidases, MMP2 plays a prominent role: its increased activity, observed in many oncological conditions, including breast cancer, enables malignant cells to invade their vicinity and spread to distant organs (*315*). MMP2, also referred to as gelatinase A or type IV collagenase, contains three FN type II repeats in its catalytic site (*316*) and can degrade not only type IV collagen, a major component of the basement membrane (*315*, *317*) but also multiple other ECM proteins, including fibronectin (*117*). It was observed that FN is capable of promoting the expression of MMP2 in MCF-7 breast cancer cells (*315*, *318*). Furthermore, various studies have shown that FN can induce MMP2 expression in different types of cancers, including breast cancer (*315*), cervical cancer (*319*) or prostate cancer (*320*). In this context, it was shown that FN changes the

global methylation profile of the MMP2 gene promoter in breast cancer cells (*315*).

Furthermore, a previous study examined the interaction between fibroblasts and head and neck cancer cells and found, that a direct contact between the tumor cells and the fibroblasts was mandatory to especially activate MMP2 secretion. SDF-1 appeard to enhance cancer cell invasion though paracrine-activated CXCR4, which triggered MMP-dependent cell invasion. The authors concluded, that both cell-matrix and cell-cell interactions including autocrine and paracrine signaling play crucial roles in the invasive behavior of cancer cells via MMP2 and MMP9 (*321*).

Although the authors demonstrated this using CAFs, we speculate based on our and previous observations, that the tumor-adjacent mammary epithelium can promote tumor progression via inducing MMP2 and FN upregulation. Another potential player in this scenario might be TGF-β1, which is known to promote tumorigenesis and increase metastasis in a number of different cancers and can promote both MMP2 and FN expression and regulates MMPs activity by regulating the synthesis of TIMPs (*322*, *323*).

Further analysis has to be performed to elucidate whether the upregulated FN and MMP2 levels are a consequence of (i) mutual influence, e.g., upregulation of MMP2 through FN (*315*) or increased FN levels as a result of the MMP2 catalytic activity, (ii) of hypoxic conditions in the co-cultures that promote FN and MMP2 upregulation (*310*), or (iii) upregulation of MMP2 and FN as a result of paracrine signaling, e.g., via SDF-1 or TGF-β secretion from the MLOs (*321*, *322*). Furthermore, it remains to be clarified why all co-culture models show increased FN and MMP2 expression levels in co-culture, but not all show an enhanced effect on growth and invasion.

In general, the establishment of a co-culture system between tumor-adjacent mammary tissue and breast cancer offers opportunities for various further investigations. For example, valuable insights into potentially altered protein expression profiles at the contact site between breast cancer sphere and organoid could be obtained by performing multiplex IF staining on cross-sectioned co-cultures. Markers known to play a critical role in tumor invasion and progression, such as N-cadherin, β-catenin or vimentin, could provide information on activated EMT programs (*324*). In addition, fluorescent labeling of tumor cells prior to co-culture could be used to enhance the discrimination between cancer cells and

organoids, thereby facilitating the tracking of their respective cellular trajectories (*325*). Another approach worth considering is the implementation of DigiWest® analysis, which would allow the examination of potentially altered signaling pathways in tumor-adjacent mammary epithelial tissue and breast cancer spheres cultured alone versus in co-culture (*10*).

7.5 Limitations and future challenges of the organoid technology

Organoids provide many opportunities in various research applications, but as any other model, they face limitations and come across with challenges or drawbacks that need to be addressed in the future. One aspect of organoids that challenges our co-culture system is their heterogeneity (*326*, *327*). As organoid differentiation relies on self-organization and lack embryonic axes, they highly vary in composition, shape and size (*197*, *231*). It was not possible to guide the MLO differentiation in a way that every organoid is consistent in the number and spatial localization of the distinct cell types. Therefore, we could not control whether the tumor was in contact with the part of the organoid expressing either luminal or basal markers. For future experiments, whole mount IF staining could be performed to identify the contact side retrospectively, although it may not be possible to control this aspect in advance.

Furthermore, our floating co-culture system was composed of a defined ratio of mouse sarcoma-derived Matrigel and rat-tail derived collagen. This combination enabled us to generate an ECM that approximates the stiffness of mammary gland tissue (*230*). While Matrigel allows for an efficient cell growth and differentiation, its major drawback is its batch-to-batch variability, its non-human rodent origin and its complex composition, which might affect the reproducibility (*195*). Despite the fact that we used growth-factor reduced (GFR)-Matrigel as alternative to the regular Matrigel, a chemically defined, xenogenic-free synthetic material should be considered in future studies for improved reproducibility and customization according to specific experimental setups (*328*).

Another general, well-known limitation of organoid culture is their maturity. While expression profiles of iPSC-derived organoids resemble in most cases that of fetal tissue, the generation of organoids with a more mature identity would be desirable (*231*,

326). Despite their impressive number of cell types, organoids generally lack an microenvironment and supporting tissue such as an immune component, vascularization or a microbiome (*231*).

Vascularization, for instance, can improve organoid maturation, as it can facilitate epithelial maturation in vivo. The group around Ryuji Morizane recently reported an in vitro method using millifluidic chips, allowing for the expansion of endothelial progenitor cells and generating vascular networks with perfusable lumens surrounded by mural cells. Those organoids contained more mature podocytes and tubular compartments with enhanced cellular polarity and adult gene expression in comparison to the static kidney organoid controls. (*329*)

Another study showed that MLO generation can be facilitated by adding fibroblasts to the culture (*231*). Furthermore, microfluidic organ-on-a-chip approaches can aid to enhance reproducibility (e.g., through geometric control of contact sides or nutrient supply), allow higher throughout readouts and may allow for increased maturity, for instance through electrical (*330*) or mechanical (*331*) stimulation (*326*).

Taken together, iPSC-derived organoids offer a variety of possibilities, especially in the context of autologous systems. While they approximate their native counterparts by expressing tissue-specific markers and functionalities, further research is needed to improve their ability to mimic critical aspects such as the maturation state of the native tissue. Nevertheless, organoids are a powerful tool for the study of cellular processes, striking a balance between avoiding oversimplification (as observed in cell-line based experiments) and irrelevant complexity with limited clinical translation (as seen in animal models).

7.6 PDMs as physiologically relevant cancer models

Conventional cancer models, like cell lines grown in a 2D monolayer, have contributed tremendously to our current knowledge of cancer. However, they exhibit remarkable differences from native tumors and are therefore of very limited use for translational research. The high clonal selection, the lack of a TME, altered cell morphologies and deregulated cell cycles caused by monolayer growth, the lack of 3D cell-cell and cell-ECM communications and the failure to address nutrient, oxygen, or anticancer drug

gradients are only some of many factors that leave therapeutics promising in vitro but turned out to be less effective in vivo. (*261*, *332*)

Cell line-derived spheroids or patient-derived organoids (PDOs) allow for 3D cell-cell and cell-ECM communications. Similar to the in vivo tumor, in which O_2 and nutrient gradients decrease with the distance from a blood vessel, these gradients decrease in in vitro models from the outer cell layer to the inner core of the model (*332*).

While 3D spheroids derived from immortalized cancer cell line are very homogenous in their composition, PDOs are derived form stem cells and therefore provide structural, functional, and molecular similarities to the tissue of origin. They can be expanded and passaged in vitro for long periods of time due to the self-renewal capacity of adult/cancer stem cells, do not suffer from strong selection, and allow for in-depth genetic and phenotypic tumor characterization. Although studies report the combination of PDOs with components of the TME, such as fibroblasts, endothelial cells and immune cells, PDOs do not fully recapitulate the original composition of the primary tumor tissue in terms of ECM, TAMs, TILs, CAFs or tumor endothelial cells. Another limiting factor of current PDO models is the applicability of individualized drug response testing due to the required establishment time of 1-3 months, which impacts the timeframe for obtaining drug test results . (*5*, *333*)

By contrast, animal models overcome some of these limitations but come across with different drawbacks. While patient-derived xenograft (PDX) models recapitulate the human disease better than cell line-derived xenograft models, copy number alternations diverge substantially from their parental tumors during passaging and undergo mouse-specific tumor evolution (*334*). Furthermore, many mouse models are immunocompromised, preventing immune responses. Syngeneic mouse models have an intact immune system, but the experimental outcome can differ dependent on the chosen inbred model background (*335*). Humanized mouse models allow the transplantation of human cells, tissues or immune components, enabling the mouse to acquire e.g. a functional human immune system. However, depending on the specific type of humanized mouse model, a shortened lifespan of the mice due to graft-versus-host disease, an increased risk of EBV-related B-cell lymphoma when injected with large numbers of human-derived cells, or a limited lifespan of human-derived T-cells represent major challenges (*336*).

To address the limitations of the existing tumor models, we isolated PDMs from different types of primary breast tumor tissue and compared the PDMs to the respective primary tumor. We found that the PDMs closely resemble general histological features and tumor-type specific features of IDC-NST and ILC-like growth patterns, cellular pleomorphism and atypia of corresponding primary tumor tissue sections (*10*). Using Movat's staining, we found that the collagen and PGs/GAGs – abundant breast-cancer related ECM proteins – were preserved in the PDMs. This is an important aspect, since increased collagen deposition, as well as fiber orientation, lead to increased ECM stiffness and correlates with a limited treatment response and poor clinical outcomes (*337*). In fact, extensive collagen deposition is the major pathological feature of certain cancers, and tumors with higher invasive potential develop stiffer ECMs (*337*–*339*). Malignant cells interact with their neighboring components by inducing alterations in the ECM, similar to those detected in never-healing wounds (*337*). Furthermore, collagen can enhance exosome (extracellular vesicles of endosomal origin) secretion, which play a critical role in cancer cell survival, growth, invasion and metastasis (*340*). The power of ECM stiffening is further illustrated by the fact that ECM stiffening alone can induce malignant transformation of mammary epithelial cells (*341*, *342*). Thus, while neoplastic cells can influence peri-tumoral collagen formation, the mechanical characteristics of collagen and its microenvironment have a huge impact on cancer cell behavior, too (*337*).

Other important mediators in oncological conditions are PGs and GAGs, ubiquitous structural and functional components of the ECM. PGs transduce signals by binding various molecules such as growth factors, adhesion factors or cytokines to modulate cancer progression. Several studies reported that PGs/GAGs are associated with metabolic reprogramming, angiogenesis, immune surveillance, cell proliferation, distant metastases, and treatment resistance. (*343*)

For instance, lung cancer cells expressing high levels of CD44 have been shown to be stimulated by hyaluronan (a major GAG commonly found around tumor cells in vivo), allowing them to evade cytotoxic T-lymphocyte-mediated killing (*344*). In another study, it was observed that hyaluronan fragments originating from cancer cells can induce dendritic cells to acquire a semi-mature phenotype, which in turn promotes the immune escape of the tumor by triggering T-cell deletion (*345*).

In addition, PGs/GAGs have emerged as regulators of CSC func-

tion and therapy resistance (*346*). For example, the heparan sulfate proteoglycan syndecan-1 (CD138) is known to modulate the growth and differentiation of the mammary progenitor population. Knockdown experiments targeting syndecan-1 in MCF-7 and MDA-MB-231 cells revealed a significant decrease in several stemness-associated features, including ALDH-1 activity and $CD44^+/CD24^-$ phenotype (in MDA-MB-231 cells) (*347*). Thus, ECM components can modulate various biological processes associated with tumorigenesis, cancer progression, therapy resistance and clinical outcomes and are therefore an important feature for reliable cancer models. In conclusion, compared to other cell-based cancer models, our PDMs largely retained key players of the ECM, namely collagen and PGs/GAGs, which are essential modulators of tumor progression and therefore indispensable in cancer modeling.

We furthermore examined the PDMs for expression of CKs, immune cell and CAF-associated markers as well as hormonal receptors. In fact, the expression levels of CKs, essential components of the intermediate filament, provides information about the epithelial cell type, tissue functional state, or tissue growth and differentiation (*269*). TNBC PDMs exhibited a significant down-regulation of CK18, which was found to be associated with tumor progression and metastasis in breast cancer (*270*, *306*). Studies revealed that down-regulation of CK18 occurs more frequently in ductal than in lobular carcinomas, which aligns with our previous findings (BCP1, BCP2 and BCP3, **Appendix E**) and with literature (*306*). However, in the cohort described in **Appendix F**, we found lower CK18 expressions in ILC than in IDC-NST PDMs. Due to the fact that we included a greater number of IDC-NST PDMs compared to ILC PDMs, we speculate that a larger total number of PDMs, and specifically more ILC PDMs, should be considered in our study.

We detected the expression of FAPα, a marker for CAFs, in both ILC and IDC-NST PDMs. The expression was more pronounced in ILCs, which is consistent with the literature (*271*). CAFs are important regulators of disease progression because they are in constant contact with malignant cells and have the ability to remodel the ECM by synthesizing and secreting substantial amounts of collagens (I, II, IV and V), HA and laminin. Simultaneously, they can degrade the ECM by secreting MMPs (*348*). Unlike normal fibroblasts and the myofibroblasts involved in wound healing, CAFs cannot return to a normal phenotype or undergo apoptosis (*349*). The presence of CAFs within PDMs underscores

their heterogeneous, in vivo-like composition.

Of note, the distinction between HR-positive and TNBC is of great importance for the treatment strategy. For example, endocrine therapies such as TAM or aromatase inhibitors, which block the estrogen signaling pathway and inhibit the growth-promoting effects of estrogen on cancer cells, are commonly prescribed to patients diagnosed with early-stage ER-positive breast cancer (*350*). In contrast, the treatment of TNBC is more challenging as it is resistant to many effective therapeutic approaches (*276*). As a result, conventional cytotoxic chemotherapy remains the primary treatment approach for TNBC (*351*).

Using protein based analyses, we identified upregulated PI3K/-AKT and MAPK/RTK signaling profiles in TNBC PDMs, with a broad set of overexpressed proteins that have been linked to tumor progression (*276*, *352*). For example, we detected GSK3β overexpression, which is known to regulate EMT and CSC properties in TNBCs (*353*). Increased eIF4E expression can upregulate proteins, such as cyclin D, angiogenesis factors or fibroblast growth factors, important in the regulation of cell growth and differentiation. Overexpressed eIF4E in TBNC is therefore predicts a worse clinical outcome. (*354*). Another protein overexpressed in our TNBC PDMs is Glut1, which was shown to promote cell proliferation, migration and invasion by regulating EGFR and integrin signaling in TNBCs (*355*). We furthermore challenged the PDMs in drug testing experiments and were able to categorize the PDMs according to a killing response induced by the respective drug and identified protein panels associated with treatment resistance and sensitivity.

Taken together, we confirmed the high correlation between PDM and their corresponding PTT in terms of histo-pathological features, the presence of important stromal components and protein and signaling pathway signatures. We furthermore confirmed that several proteins associated with the PI3K/AKT and MAPK/RTK signaling profiles were significantly upregulated in PDMs from TNBC patients compared to HR-positive PDMs. Cytotoxicity assays with widely used breast cancer drugs allowed us to identify protein panels associated with treatment response and sensitivity. Our data emphasize the value of PDMs as an in vivo-like cancer model that reflects the heterogeneities observed among patient-individual breast cancers and may find application in predicting treatment responses, thus, bringing research one step closer to personalized treatment strategies.

7.7 Conclusion

Much like the unique and ever-changing patterns seen in a kaleidoscope, cancer is a highly diverse spectrum of diseases that evolve and alter their characteristics and interactions as the disease progresses. This inherent complexity makes advanced cancers with high recurrence rates particularly challenging to cure. While the 5-year survival rate for local (non-metastatic) invasive breast cancer is 99%, the survival chances declines drastically to 27% for cases in which the cancer has spread to other parts of the body (*356*). Metastatic relapse can occur over a period of months to decades and involves a multi-step process beginning with dissemination from the primary tumor, intravasation, survival in the circulation, extravasation, and finally metastatic seeding (*357*). Despite tremendous efforts, many drugs fail in clinical trials due to low efficacy or severe side effects. Metastatic tumors are stubbornly resistant to therapy and thus remain the primary concern in achieving a cure for these advanced cases (*357*). Therefore, there is an urgent need for reliable cancer models that allow to study processes associated with invasion and metastasis and to facilitate testing of pre-clinical therapies in an patient-individualized manner. To address this need, we have introduced patient-derived microtumors that retain important characteristics of the primary lesion, which can significantly contribute to a better understanding of cancer physiology and prediction of treatment responses. PDMs hold great promise as a model system for personalized treatment, particularly for patients with aggressive or metastatic breast cancers, where overall survival is poorer. Of note, tumor progression is influenced by many factors, including components of the surrounding stroma and tumor-adjacent cells, which are in direct contact with the growing tumor and potentially play a role in driving tumor progression. In our pursuit of investigating the interactions between breast tumors and the tumor-adjacent mammary epithelium, we have developed a physiologically relevant floating co-culture system that allows us to more precisely study processes associated with tumor growth and invasion. In this way, we hope to contribute to the identification of further mechanisms underlying tumor progression induced by interaction with the TME and to shed more light on the “enemy within”.

8 Outlook

8.1 Expanding the co-culture capabilities: towards other organoid types

Our co-culture setup has the potential to be extended to other cancer types, such as CRC or kidney cancer. Progress has already been made in this direction in the course of this thesis with the successful differentiation of iPSCs into colon and kidney organoids. Notably, we used healthy donor iPSCs (**Appendix D**) to establish the differentiation protocol, but as described in the previous chapters, blood from CRC and renal cancer patients could be reprogrammed into iPSCs as a basis for autologous systems.

Differentiation into kidney organoids involved guiding the iPSCs through several stages, the late primitive streak, the intermediate mesoderm and the metanephric mesoderm, resulting in the formation of pretubular aggregates and renal vesicles, until kidney organoids arose in culture by day 20 (*358*). To initiate this process, single iPSCs were seeded between two layers of GFR-Matrigel to form cavitated iPSC spheroids (**Figure 8.1** A, B left). The cavitated spheroids were further differentiated into tubular organoids by inhibiting glycogen synthase kinase 3-β (GSK3β) for precisely 36 hours and subsequently self-organized into kidney organoids (**Figure 8.1** B, right). The organoids showed expression of E-cadherin (E-Cad), a distal tubule marker, as well as capsule-like structures expressing nephrin (NPHS1) and podocalyxin (PODXL) in podocyte-like cells, while Pax8 indicated the presence of the intermediate mesoderm/metanephric mesenchyme (**Figure 8.1** C, E). Pax8 expression peaked around day 10.

The kidney organoids were then gently detached from their supporting cell layer and embedded in a 3D floating GFR-Matrigel matrix, where their high viability was confirmed (**Figure 8.1** D). In parallel, spheroids were generated from the 786-O kidney cancer cell line and stained with LuminiCell Tracker™ (Merck Millipore) to distinguish them from the organoid. Over a period of 3 days, we observed the growth of the two components towards each other, with the cancer cells attaching to the organoid (**Figure 8.1** F, *black arrow*).

For the differentiation into colon organoids, we followed the protocol of Miguel Crespo and colleagues, which includes a stepwise process leading to the differentiation into definite endoderm (DE), posterior hindgut endoderm and finally into colon organoids (*295*). Successful differentiation into DE was confirmed via flow cytometry by the expression of the endodermal markers CXCR4, c-Kit, Sox17 and FOXA2 at day 4. PDGFR-α, which should not be expressed at this stage, was used as a negative control (**Figure 8.2** A). The cells were then differentiated to the hindgut, confirmed by positive CDX2 expression after 5 days, which is critical to exclude misdirection to the small intestine (**Figure 8.2** B, F). The cells were then treated with colonic medium for an additional 12 days to generate colonic epithelial cells. These cells were cultured in GFR-Matrigel domes (**Figure 8.2** C), resulting in the formation of pseudostratified embryonic gut-like spheroids that progressively self-organized into convoluted colon organoids expressing markers specific to the large intestine (e.g. carbonic anhydrase II (CAII), mucin 2 (MUC2) and mucin 5B (MUC5B)) around day 50 (**Figure 8.2** D, E).

In particular, CRC PDMs and kidney PDMs can be derived from their corresponding primary tumor tissues and combined with colon and kidney organoids, similar to the MLO-PDM co-cultures. While healthy donor iPSCs were used to establish differentiation into colon and kidney organoids, autologous models could be generated by generating iPSCs from the blood of CRC and kidney cancer patients. These co-culture models have potential applications in several areas, such as studying the interaction of cancer with its "native" tissue habitat, exploring microbiome interactions, or conducting toxicity studies.

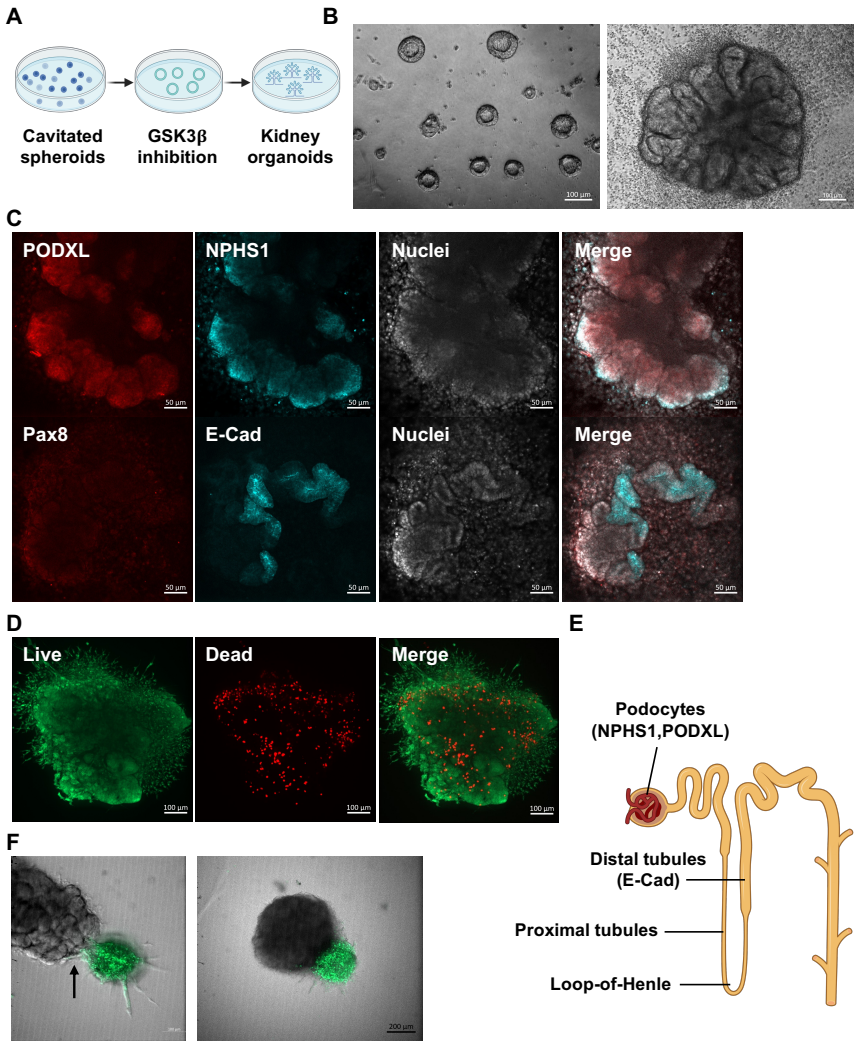

Figure 8.1: iPSC-derived differentiation into kidney organoids A Schematic workflow for the generation of iPSC-derived kidney organoids. Single-cell iPSCs were embedded between two layers of GFR-Matrigel ("Matrigel sandwich") resulting in the formation of cavitated spheroids and subsequently kidney organoids. **B** Bright field images of cavitated spheroids (left) and a fully differentiated organoid (right). Scale bars: 100 µm. **C** IF stainings confirm the expression of podocalyxin (PODXL), nephrin (NPSH1), E-Cadherin (E-CAD), and to a lower extent Pax8. Counterstaining: DAPI. Scale bars: 50 µm. **D** Live-dead staining of kidney organoids after 3 days in floating GFR-Matrigel matrix. **F** Co-culture of kidney organoids (unstained) and 786-O spheroids (stained with LuminiCell Tracker™) after 3 days. **F** Illustration of a human nephron.

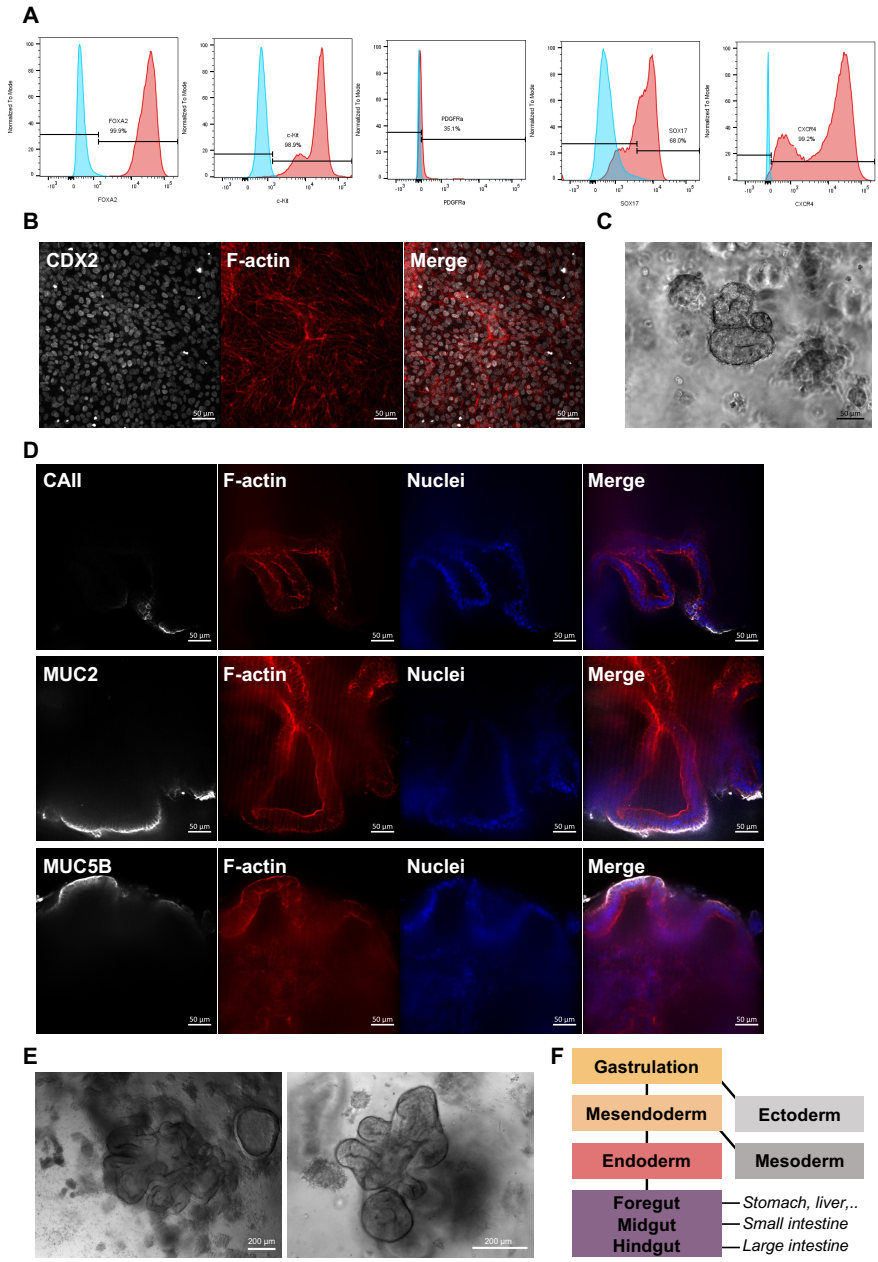

Figure 8.2: iPSC-derived differentiation into colon organoids. A Flow cytometry data confirm the expression of FOXA2, c-Kit, SOX17, CXCR4 and the absence of PDGFRα. Flow cytometry data were acquired using the BD LSR-Fortessa™ Cell Analyzer (BD Biosciences) and analyzed using FlowJo v10 software (FlowJo LLC). **B** IF staining confirms hindgut differentiation by positive CDX2 expression. Counterstaing: Phalloidin. Scale bars: 50 µm. **C** Bright field image of pseudostratified embryonic gut-like spheroid. Scale bar: 50 µm. **D** IF stainings confirm the expression of markers of the large intestine, carbonic anhydrase II (CAII), mucin 2 (MUC2), mucin 5B (MUC5B). Counterstaings: DAPI and Phalloidin. Scale bars: 50 µm. **E** Bright field images of day 50 colon organoids. Scale bars: 200 µm. **F** Schematic overview of the differentiation into the large intestine.

Acknowledgements

Mein herzlicher Dank gilt Prof. Dr. Katja Schenke-Layland und Prof. Dr. Ulrich Rothbauer. Als Gutachter meiner Doktorarbeit habt Ihr mich mit Wissen und Expertise durch meine schöne Zeit als Doktorandin begleitet und seid mir immer eine große Stütze gewesen. Das ist viel wert, vielen Dank. Des Weiteren möchte ich mich bei Prof. Dr. Gabriele Dodt und Prof. Dr. Peter Loskill für Eure Interesse sowie Eure Zeit und Mühe bei der Begutachtung meiner Arbeit ausdrücklich bedanken.

Ein weiterer Dank gilt meinem Arbeitsgruppenleiter Dr. Christian Schmees: Ich danke Dir, dass Du mir dieses wunderbare Projekt ermöglicht hast und mir stets mit größter fachlicher Kompetenz zur Seite gestanden hast. Dein nicht nur umfangreiches, sondern auch stets aktuelles Wissen reicht weit über die Grenzen der Tumorbiologie hinaus und ist eine Bereicherung für jeden, der es in Anspruch nehmen darf. Danke, dass du immer ein offenes Ohr für deine Mitarbeiter*innen hast, für die schönen Gruppenausflüge im Hochseilgarten, im Escape Room oder zu Restaurants wie "Herr Dang" sowie für die vielen netten Gespräche.

Ich danke meinen lieben Kolleginnen und Kollegen für die tolle Zusammenarbeit, die lustigen Gespräche beim Mittagessen oder Kaffeetrinken und die vielen Treffen außerhalb der Arbeit: Sei es eine Radtour im Schönbuch, ein Ausflug nach Wien, eine Bierwanderung im Wald, Besuche auf dem Schokoladenmarkt, Vanilleeis und Espresso an einem warmen Sommertag, eine Erkundungstour durch die Falkensteiner-Höhle oder unser monatliches Treffen. Ich habe in Euch Freunde fürs Leben gefunden und schätze mich deshalb sehr glücklich. Weiterhin danke ich meiner Familie und meinen Freunden außerhalb der Arbeit, die immer für mich da sind.

Declaration

Ich erkläre hiermit, dass ich die zur Promotion eingereichte Arbeit mit dem Titel “Under the Influence of Tumor-adjacent Tissue: A 3D Co-culture Model Combining iPSC-derived Organoids and Patient-derived Microtumors” selbstständig verfasst, nur die angegebenen Quellen und Hilfsmittel benutzt und wörtlich oder inhaltlich übernommene Zitate also solche gekennzeichnet habe. Ich erkläre, dass die Richtlinien zur Sicherung guter wissenschaftlicher Praxis der Universität Tübingen beachtet wurden. Ich versichere an Eides statt, dass diese Angaben wahr sind und dass ich nichts verschwiegen habe. Mir ist bekannt, dass die falsche Angabe einer Versicherung an Eides statt mit Freiheitsstrafe bis zu drei Jahren oder mit Geldstrafe bestraft wird.

Anna-Lena Keller

Bibliography

(*1*) **Keller**, **A.-L.**, Binner, A., Schenke-Layland, K., and Schmees, C. (2022). Establishment of Four Induced Pluripotent Stem Cell Lines from CD34+ Hematopoietic Stem and Progenitor Cells from a Patient Diagnosed with an Invasive Lobular Mammary Carcinoma. *Stem Cell Research* **64**, 102902.

(*2*) **Keller**, **A.-L.**, Greis, D., Eybe, J., Plöger, S., Weiss, M., Koch, A., Brucker, S. Y., Schenke-Layland, K., and Schmees, C. (2022). Generation and Characterization of Three Induced Pluripotent Stem Cells Lines from an 86-Year Old Female Individual Diagnosed with an Invasive Lobular Mammary Carcinoma. *Stem Cell Research*, 102988.

(*3*) **Keller**, **A.-L.**, Binner, A., Breitmeyer, R., Vogel, S., Anderle, N., Rothbauer, U., Schenke-Layland, K., and Schmees, C. (2021). Generation and characterization of the human induced pluripotent stem cell line NMIi010-A from peripheral blood mononuclear cells of a healthy 49–year old male individual. *Stem Cell Research* **54**, 102427.

(*4*) Breitmeyer, R., Vogel, S., Heider, J., Hartmann, S.-M., Wüst, R., **Keller**, **A.-L.**, Binner, A., Fitzgerald, J. C., Fallgatter, A. J., and Volkmer, H. (2023). Regulation of synaptic connectivity in schizophrenia spectrum by mutual neuron-microglia interaction. *Communications Biology* **6**, 472.

(*5*) Anderle, N., Koch, A., Gierke, B., **Keller**, **A.-L.**, Staebler, A., Hartkopf, A., Brucker, S. Y., Pawlak, M., Schenke-Layland, K., and Schmees, C. (2022). A Platform of Patient-Derived Microtumors Identifies Individual Treatment Responses and Therapeutic Vulnerabilities in Ovarian Cancer. *Cancers* **14**, 2895.

(*6*) Walter, B., Canjuga, D., Yüz, S. G., Ghosh, M., Bozko, P., Przystal, J. M., Govindarajan, P., Anderle, N., **Keller**, **A.-L.**, and Tatagiba, M. (2021). Argyrin F Treatment-Induced Vulnerabilities Lead to a Novel Combination Therapy in Experimental Glioma. *Advanced Therapeutics* **4**, 2100078.

(*7*) Przystal, J. M., Becker, H., Canjuga, D., Tsiami, F., Anderle, N., **Keller**, **A.-L.**, Pohl, A., Ries, C. H., Schmittnaegel, M., and Korinetska, N. (2021). Targeting CSF1R alone or in combination with PD1 in experimental glioma. *Cancers* **13**, 2400.

(*8*) Holl, M., Becker, L., **Keller**, **A. L.**, Feuerer, N., Marzi, J., Carvajal Berrio, D. A., Jakubowski, P., Neis, F., Pauluschke-Frohlich, J., Brucker, S. Y., Schenke-Layland, K., Kramer, B., and Weiss, M. (2021). Laparoscopic Peritoneal Wash Cytology-Derived Primary Human Mesothelial Cells for In Vitro Cell Culture and Simulation of Human Peritoneum. *Biomedicines* **9**, 176.

(*9*) Holl, M. et al. (2022). Cell Type-Specific Anti-Adhesion Properties of Peritoneal Cell Treatment with Plasma-Activated Media (PAM). *Biomedicines* **10**, 927.

(*10*) Anderle, N., Schäfer-Ruoff, F., Staebler, A., Kersten, N., Koch, A., Önder, C., **Keller**, **A.-L.**, Liebscher, S., Hartkopf, A., Hahn, M., Templin, M., Brucker, S. Y., Schenke-Layland, K., and Schmees, C. (2023). Breast cancer patient-derived microtumors resemble tumor heterogeneity and enable protein-based stratification and functional validation of individualized drug treatment. *Journal of Experimental & Clinical Cancer Research* **42**, 210.

(*11*) **Keller**, **A.-L.**, Anderle, N., Schrenk, M., Greis, D., Binner, A., Visser, D., Göpfert, J., Koch, A., Weiss, M., and Brucker, S. (2023). Co-cultures of iPSC-derived Mammary-like Organoids and Patient-derived Microtumors Model Invasive Behavior of Breast Cancer ex vivo.

(*12*) Gerlinger, M., McGranahan, N., Dewhurst, S. M., Burrell, R. A., Tomlinson, I., and Swanton, C. (2014). Cancer: evolution within a lifetime. *Annu Rev Genet* **48**, 215–36.

(*13*) Hanahan, D., and Weinberg, R. A. (2000). The hallmarks of cancer. *cell* **100**, 57–70.

(*14*) Heppner, G. H. (1984). Tumor heterogeneity. *Cancer research* **44**, 2259–2265.

(*15*) Dagogo-Jack, I., and Shaw, A. T. (2018). Tumour heterogeneity and resistance to cancer therapies. *Nature reviews Clinical oncology* **15**, 81–94.

(*16*) Koch, L. (2020). Tumour Evolution: From Linear Paths to Branched Trees. *Nat. Res*, S14.

(*17*) Hanahan, D., and Coussens, L. M. (2012). Accessories to the crime: functions of cells recruited to the tumor microenvironment. *Cancer cell* **21**, 309–322.

(*18*) Gambardella, V., Tarazona, N., Cejalvo, J. M., Lombardi, P., Huerta, M., Roselló, S., Fleitas, T., Roda, D., and Cervantes, A. (2020). Personalized medicine: recent progress in cancer therapy. *Cancers* **12**, 1009.

(*19*) Darwin, C., *On the origin of species, 1859*; Routledge: 2004.

(*20*) Vendramin, R., Litchfield, K., and Swanton, C. (2021). Cancer evolution: Darwin and beyond. *The EMBO Journal* **40**, e108389.

(*21*) Druker, B. J., Sawyers, C. L., Kantarjian, H., Resta, D. J., Reese, S. F., Ford, J. M., Capdeville, R., and Talpaz, M. (2001). Activity of a specific inhibitor of the BCR-ABL tyrosine kinase in the blast crisis of chronic myeloid leukemia and acute lymphoblastic leukemia with the Philadelphia chromosome. *New England Journal of Medicine* **344**, 1038–1042.

(*22*) Nowell, P. C. (2007). Discovery of the Philadelphia chromosome: a personal perspective. *The Journal of clinical investigation* **117**, 2033–2035.

(*23*) Greaves, M., and Maley, C. C. (2012). Clonal evolution in cancer. *Nature* **481**, 306–313.

(*24*) Nowell, P. C. (1976). The Clonal Evolution of Tumor Cell Populations: Acquired genetic lability permits stepwise selection of variant sublines and underlies tumor progression. *Science* **194**, 23–28.

(*25*) Lin, L., and Lin, D.-C. (2019). Biological significance of tumor heterogeneity in esophageal squamous cell carcinoma. *Cancers* **11**, 1156.

(*26*) Colangelo, T., Polcaro, G., Muccillo, L., D'Agostino, G., Rosato, V., Ziccardi, P., Lupo, A., Mazzoccoli, G., Sabatino, L., and Colantuoni, V. (2017). Friend or foe?: The tumour microenvironment dilemma in colorectal cancer. *Biochimica et Biophysica Acta (BBA)-Reviews on Cancer* **1867**, 1–18.

(*27*) Kobayashi, S., Boggon, T. J., Dayaram, T., Jänne, P. A., Kocher, O., Meyerson, M., Johnson, B. E., Eck, M. J., Tenen, D. G., and Halmos, B. (2005). EGFR mutation and resistance of non–small-cell lung cancer to gefitinib. *New England Journal of Medicine* **352**, 786–792.

(*28*) Gorre, M. E., Mohammed, M., Ellwood, K., Hsu, N., Paquette, R., Rao, P. N., and Sawyers, C. L. (2001). Clinical resistance to STI-571 cancer therapy caused by BCR-ABL gene mutation or amplification. *Science* **293**, 876–880.

(*29*) Wang, T.-L., Diaz Jr, L. A., Romans, K., Bardelli, A., Saha, S., Galizia, G., Choti, M., Donehower, R., Parmigiani, G., Shih, I.-M., et al. (2004). Digital karyotyping identifies thymidylate synthase amplification as a mechanism of resistance to 5-fluorouracil in metastatic colorectal cancer patients. *Proceedings of the National Academy of Sciences* **101**, 3089–3094.

(*30*) Merlo, L. M., Pepper, J. W., Reid, B. J., and Maley, C. C. (2006). Cancer as an evolutionary and ecological process. *Nature reviews cancer* **6**, 924–935.

(*31*) Campbell, P. J., Yachida, S., Mudie, L. J., Stephens, P. J., Pleasance, E. D., Stebbings, L. A., Morsberger, L. A., Latimer, C., McLaren, S., and Lin, M.-L. (2010). The patterns and dynamics of genomic instability in metastatic pancreatic cancer. *Nature* **467**, 1109–1113.

(*32*) Shah, S. P., Roth, A., Goya, R., Oloumi, A., Ha, G., Zhao, Y., Turashvili, G., Ding, J., Tse, K., and Haffari, G. (2012). The clonal and mutational evolution spectrum of primary triple-negative breast cancers. *Nature* **486**, 395–399.

(*33*) Landau, D. A., Carter, S. L., Stojanov, P., McKenna, A., Stevenson, K., Lawrence, M. S., Sougnez, C., Stewart, C., Sivachenko, A., and Wang, L. (2013). Evolution and impact of subclonal mutations in chronic lymphocytic leukemia. *Cell* **152**, 714–726.

(*34*) Anderson, K., Lutz, C., Van Delft, F. W., Bateman, C. M., Guo, Y., Colman, S. M., Kempski, H., Moorman, A. V., Titley, I., and Swansbury, J. (2011). Genetic variegation of clonal architecture and propagating cells in leukaemia. *Nature* **469**, 356–361.

(*35*) Davis, A., Gao, R., and Navin, N. (2017). Tumor evolution: Linear, branching, neutral or punctuated? *Biochimica et Biophysica Acta (BBA)-Reviews on Cancer* **1867**, 151–161.

(*36*) Azer, E. S., Ebrahimabadi, M. H., Malikić, S., Khardon, R., and Sahinalp, S. C. (2020). Tumor phylogeny topology inference via deep learning. *Iscience* **23**, 101655.

(*37*) Weber, L. L., and El-Kebir, M. (2021). Distinguishing linear and branched evolution given single-cell DNA sequencing data of tumors. *Algorithms for Molecular Biology* **16**, 1–12.

(*38*) Noble, R., Burri, D., Le Sueur, C., Lemant, J., Viossat, Y., Kather, J. N., and Beerenwinkel, N. (2022). Spatial structure governs the mode of tumour evolution. *Nature ecology & evolution* **6**, 207–217.

(*39*) Williams, M. J., Werner, B., Barnes, C. P., Graham, T. A., and Sottoriva, A. (2016). Identification of neutral tumor evolution across cancer types. *Nature genetics* **48**, 238–244.

(*40*) Ling, S., Hu, Z., Yang, Z., Yang, F., Li, Y., Lin, P., Chen, K., Dong, L., Cao, L., and Tao, Y. (2015). Extremely high genetic diversity in a single tumor points to prevalence of non-Darwinian cell evolution. *Proceedings of the National Academy of Sciences* **112**, E6496–E6505.

(*41*) Bakhoum, S. F., and Landau, D. A. (2017). Chromosomal instability as a driver of tumor heterogeneity and evolution. *Cold Spring Harbor perspectives in medicine* **7**, a029611.

(*42*) Gisselsson, D., Pettersson, L., Höglund, M., Heidenblad, M., Gorunova, L., Wiegant, J., Mertens, F., Dal Cin, P., Mitelman, F., and Mandahl, N. (2000). Chromosomal breakage-fusion-bridge events cause genetic intratumor heterogeneity. *Proceedings of the National Academy of Sciences* **97**, 5357–5362.

(*43*) Maura, F., Boyle, E. M., Rustad, E. H., Ashby, C., Kaminetzky, D., Bruno, B., Braunstein, M., Bauer, M., Blaney, P., Wang, Y., et al. In *Seminars in cell & developmental biology*, 2022; Vol. 123, pp 115–123.

(*44*) Notta, F., Chan-Seng-Yue, M., Lemire, M., Li, Y., Wilson, G. W., Connor, A. A., Denroche, R. E., Liang, S.-B., Brown, A. M., and Kim, J. C. (2016). A renewed model of pancreatic cancer evolution based on genomic rearrangement patterns. *Nature* **538**, 378–382.

(*45*) Baca, S. C., Prandi, D., Lawrence, M. S., Mosquera, J. M., Romanel, A., Drier, Y., Park, K., Kitabayashi, N., MacDonald, T. Y., and Ghandi, M. (2013). Punctuated evolution of prostate cancer genomes. *Cell* **153**, 666–677.

(*46*) Gao, R., Davis, A., McDonald, T. O., Sei, E., Shi, X., Wang, Y., Tsai, P.-C., Casasent, A., Waters, J., and Zhang, H. (2016). Punctuated copy number evolution and clonal stasis in triple-negative breast cancer. *Nature genetics* **48**, 1119–1130.

(*47*) Langie, S. A., Koppen, G., Desaulniers, D., Al-Mulla, F., Al-Temaimi, R., Amedei, A., Azqueta, A., Bisson, W. H., Brown, D., Brunborg, G., et al. (2015). Causes of genome instability: the effect of low dose chemical exposures in modern society. *Carcinogenesis* **36**, S61–S88.

(*48*) Ishida, T., Fujihara, N., Nishimura, T., Funabashi, H., Hirota, R., Ikeda, T., and Kuroda, A. (2019). Live-cell imaging of macrophage phagocytosis of asbestos fibers under fluorescence microscopy. *Genes and environment* **41**, 1–11.

(*49*) Gorbunova, V., Seluanov, A., Mao, Z., and Hine, C. (2007). Changes in DNA repair during aging. *Nucleic acids research* **35**, 7466–7474.

(*50*) Burrell, R. A., McGranahan, N., Bartek, J., and Swanton, C. (2013). The causes and consequences of genetic heterogeneity in cancer evolution. *Nature* **501**, 338–345.

(*51*) Dumaz, N., Drougard, C., Sarasin, A., and Daya-Grosjean, L. (1993). Specific UV-induced mutation spectrum in the p53 gene of skin tumors from DNA-repair-deficient xeroderma pigmentosum patients. *Proceedings of the National Academy of Sciences* **90**, 10529–10533.

(*52*) Bonneville, R., Krook, M. A., Kautto, E. A., Miya, J., Wing, M. R., Chen, H.-Z., Reeser, J. W., Yu, L., and Roychowdhury, S. (2017). Landscape of microsatellite instability across 39 cancer types. *JCO precision oncology* **1**, 1–15.

(*53*) Andor, N., Maley, C. C., and Ji, H. P. (2017). Genomic instability in cancer: teetering on the limit of tolerance. *Cancer research* **77**, 2179–2185.

(*54*) Sulaiman, A., McGarry, S., Han, X., Liu, S., and Wang, L. (2019). CSCs in breast cancer—one size does not fit all: Therapeutic advances in targeting heterogeneous epithelial and mesenchymal CSCs. *Cancers* **11**, 1128.

(*55*) Prasetyanti, P. R., and Medema, J. P. (2017). Intra-tumor heterogeneity from a cancer stem cell perspective. *Molecular cancer* **16**, 1–9.

(*56*) Marusyk, A., and Polyak, K. (2010). Tumor heterogeneity: causes and consequences. *Biochimica et Biophysica Acta (BBA)-Reviews on Cancer* **1805**, 105–117.

(*57*) Witt, A., Lee, C., Lee, T., Azzam, D., Wang, B., Caslini, C., Petrocca, F., Grosso, J., Jones, M., and Cohick, E. (2017). Identification of a cancer stem cell-specific function for the histone deacetylases, HDAC1 and HDAC7, in breast and ovarian cancer. *Oncogene* **36**, 1707–1720.

(*58*) Najafi, M., Farhood, B., and Mortezaee, K. (2019). Cancer stem cells (CSCs) in cancer progression and therapy. *Journal of cellular physiology* **234**, 8381–8395.

(*59*) Suster, N. K., and Virant-Klun, I. (2019). Presence and role of stem cells in ovarian cancer. *World journal of stem cells* **11**, 383.

(*60*) Neumeister, V., Agarwal, S., Bordeaux, J., Camp, R. L., and Rimm, D. L. (2010). In situ identification of putative cancer stem cells by multiplexing ALDH1, CD44, and cytokeratin identifies breast cancer patients with poor prognosis. *The American journal of pathology* **176**, 2131–2138.

(*61*) Al-Hajj, M., Wicha, M. S., Benito-Hernandez, A., Morrison, S. J., and Clarke, M. F. (2003). Prospective identification of tumorigenic breast cancer cells. *Proceedings of the National Academy of Sciences* **100**, 3983–3988.

(*62*) Bhola, N. E., Balko, J. M., Dugger, T. C., Kuba, M. G., Sánchez, V., Sanders, M., Stanford, J., Cook, R. S., and Arteaga, C. L. (2013). TGF-β inhibition enhances chemotherapy action against triple-negative breast cancer. *The Journal of clinical investigation* **123**, 1348–1358.

(*63*) Lawson, D. A., Bhakta, N. R., Kessenbrock, K., Prummel, K. D., Yu, Y., Takai, K., Zhou, A., Eyob, H., Balakrishnan, S., and Wang, C.-Y. (2015). Single-cell analysis reveals a stem-cell program in human metastatic breast cancer cells. *Nature* **526**, 131–135.

(*64*) Curley, M. D., Therrien, V. A., Cummings, C. L., Sergent, P. A., Koulouris, C. R., Friel, A. M., Roberts, D. J., Seiden, M. V., Scadden, D. T., and Rueda, B. R. (2009). CD133 expression defines a tumor initiating cell population in primary human ovarian cancer. *Stem cells* **27**, 2875–2883.

(*65*) Wang, L., Zhi, X., Lu, Y., Cong, Y., Fu, Z., Cao, J., Xu, S., Lv, J., and Ruan, H. (2022). Identification of microRNA expression profiles of CD44+ ovarian cancer stem cells. *Archives of Gynecology and Obstetrics* **306**, 461–472.

(*66*) O'Brien, C. A., Pollett, A., Gallinger, S., and Dick, J. E. (2007). A human colon cancer cell capable of initiating tumour growth in immunodeficient mice. *Nature* **445**, 106–110.

(*67*) Haraguchi, N., Ishii, H., Mimori, K., Ohta, K., Uemura, M., Nishimura, J., Hata, T., Takemasa, I., Mizushima, T., and Yamamoto, H. (2013). CD49f-positive cell population efficiently enriches colon cancer-initiating cells. *International journal of oncology* **43**, 425–430.

(*68*) Regan, J. L., Schumacher, D., Staudte, S., Steffen, A., Haybaeck, J., Keilholz, U., Schweiger, C., Golob-Schwarzl, N., Mumberg, D., and Henderson, D. (2017). Non-canonical hedgehog signaling is a positive regulator of the WNT pathway and is required for the survival of colon cancer stem cells. *Cell reports* **21**, 2813–2828.

(*69*) Regan, J. L., Schumacher, D., Staudte, S., Steffen, A., Lesche, R., Toedling, J., Jourdan, T., Haybaeck, J., Golob-Schwarzl, N., and Mumberg, D. (2022). Identification of a neural development gene expression signature in colon cancer stem cells reveals a role for EGR2 in tumorigenesis. *Iscience* **25**, 104498.

(*70*) Singh, S. K., Hawkins, C., Clarke, I. D., Squire, J. A., Bayani, J., Hide, T., Henkelman, R. M., Cusimano, M. D., and Dirks, P. B. (2004). Identification of human brain tumour initiating cells. *nature* **432**, 396–401.

(*71*) Lucki, N. C., Villa, G. R., Vergani, N., Bollong, M. J., Beyer, B. A., Lee, J. W., Anglin, J. L., Spangenberg, S. H., Chin, E. N., and Sharma, A. (2019). A cell type-selective apoptosis-inducing small molecule for the treatment of brain cancer. *Proceedings of the National Academy of Sciences* **116**, 6435–6440.

(*72*) Yang, Z. F., Ho, D. W., Ng, M. N., Lau, C. K., Yu, W. C., Ngai, P., Chu, P. W., Lam, C. T., Poon, R. T., and Fan, S. T. (2008). Significance of CD90+ cancer stem cells in human liver cancer. *Cancer cell* **13**, 153–166.

(*73*) Yang, Z. F., Ngai, P., Ho, D. W., Yu, W. C., Ng, M. N., Lau, C. K., Li, M. L., Tam, K. H., Lam, C. T., and Poon, R. T. (2008). Identification of local and circulating cancer stem cells in human liver cancer. *Hepatology* **47**, 919–928.

(*74*) Terris, B., Cavard, C., and Perret, C. (2010). EpCAM, a new marker for cancer stem cells in hepatocellular carcinoma. *Journal of hepatology* **52**, 280–281.

(*75*) Li, C., Heidt, D. G., Dalerba, P., Burant, C. F., Zhang, L., Adsay, V., Wicha, M., Clarke, M. F., and Simeone, D. M. (2007). Identification of pancreatic cancer stem cells. *Cancer research* **67**, 1030–1037.

(*76*) Abel, E. V., Kim, E. J., Wu, J., Hynes, M., Bednar, F., Proctor, E., Wang, L., Dziubinski, M. L., and Simeone, D. M. (2014). The Notch pathway is important in maintaining the cancer stem cell population in pancreatic cancer. *PloS one* **9**, e91983.

(*77*) Leon, F., Seshacharyulu, P., Nimmakayala, R. K., Chugh, S., Karmakar, S., Nallasamy, P., Vengoji, R., Rachagani, S., Cox, J. L., and Mallya, K. (2022). Reduction in O-glycome induces differentially glycosylated CD44 to promote stemness and metastasis in pancreatic cancer. *Oncogene* **41**, 57–71.

(*78*) Kim, W.-T., and Ryu, C. J. (2017). Cancer stem cell surface markers on normal stem cells. *BMB reports* **50**, 285.

(*79*) Zhen, X., Choi, H. S., Kim, J.-H., Kim, S.-L., Liu, R., Ko, Y.-C., Yun, B.-S., and Lee, D.-S. (2020). Caudatin isolated from Cynanchum auriculatum inhibits breast cancer stem cell formation via a GR/YAP signaling. *Biomolecules* **10**, 925.

(*80*) Lu, R., Fan, C., Shangguan, W., Liu, Y., Li, Y., Shang, Y., Yin, D., Zhang, S., Huang, Q., and Li, X. (2017). Neurons generated from carcinoma stem cells support cancer progression. *Signal transduction and targeted therapy* **2**, 1–10.

(*81*) Pan, Y., Hysinger, J. D., Barron, T., Schindler, N. F., Cobb, O., Guo, X., Yalçın, B., Anastasaki, C., Mulinyawe, S. B., and Ponnuswami, A. (2021). NF1 mutation drives neuronal activity-dependent initiation of optic glioma. *Nature* **594**, 277–282.

(*82*) Varga, J., and Greten, F. R. (2017). Cell plasticity in epithelial homeostasis and tumorigenesis. *Nature cell biology* **19**, 1133–1141.

(*83*) Lüönd, F., Tiede, S., and Christofori, G. (2021). Breast cancer as an example of tumour heterogeneity and tumour cell plasticity during malignant progression. *British journal of cancer* **125**, 164–175.

(*84*) Hanahan, D., and Weinberg, R. A. (2011). Hallmarks of cancer: the next generation. *cell* **144**, 646–674.

(*85*) Hanahan, D. (2022). Hallmarks of cancer: new dimensions. *Cancer discovery* **12**, 31–46.

(*86*) Wang, M., Zhao, J., Zhang, L., Wei, F., Lian, Y., Wu, Y., Gong, Z., Zhang, S., Zhou, J., and Cao, K. (2017). Role of tumor microenvironment in tumorigenesis. *Journal of Cancer* **8**, 761.

(*87*) Wei, R., Liu, S., Zhang, S., Min, L., and Zhu, S. (2020). Cellular and extracellular components in tumor microenvironment and their application in early diagnosis of cancers. *Analytical Cellular Pathology* **2020**.

(*88*) Anderson, N. M., and Simon, M. C. (2020). The tumor microenvironment. *Current Biology* **30**, R921–R925.

(*89*) Abbasi, S., Sinha, S., Labit, E., Rosin, N. L., Yoon, G., Rahmani, W., Jaffer, A., Sharma, N., Hagner, A., and Shah, P. (2020). Distinct regulatory programs control the latent regenerative potential of dermal fibroblasts during wound healing. *Cell stem cell* **27**, 396–412. e6.

(*90*) Dvorak, H. F. (2015). Tumors: wounds that do not heal—redux. *Cancer immunology research* **3**, 1–11.

(*91*) Ding, X., Ji, J., Jiang, J., Cai, Q., Wang, C., Shi, M., Yu, Y., Zhu, Z., and Zhang, J. (2018). HGF-mediated crosstalk between cancer-associated fibroblasts and MET-unamplified gastric cancer cells activates coordinated tumorigenesis and metastasis. *Cell death & disease* **9**, 867.

(*92*) Quante, M., Tu, S. P., Tomita, H., Gonda, T., Wang, S. S., Takashi, S., Baik, G. H., Shibata, W., DiPrete, B., and Betz, K. S. (2011). Bone marrow-derived myofibroblasts contribute to the mesenchymal stem cell niche and promote tumor growth. *Cancer cell* **19**, 257–272.

(*93*) Belhabib, I., Zaghdoudi, S., Lac, C., Bousquet, C., and Jean, C. (2021). Extracellular matrices and cancer-associated fibroblasts: targets for cancer diagnosis and therapy? *Cancers* **13**, 3466.

(*94*) Balkwill, F. R., Capasso, M., and Hagemann, T. (2012). The tumor microenvironment at a glance. *Journal of cell science* **125**, 5591–5596.

(*95*) Crawford, Y., Kasman, I., Yu, L., Zhong, C., Wu, X., Modrusan, Z., Kaminker, J., and Ferrara, N. (2009). PDGF-C mediates the angiogenic and tumorigenic properties of fibroblasts associated with tumors refractory to anti-VEGF treatment. *Cancer cell* **15**, 21–34.

(*96*) Kim, D. J., Dunleavey, J. M., Xiao, L., Ollila, D. W., Troester, M. A., Otey, C. A., Li, W., Barker, T. H., and Dudley, A. C. (2018). Suppression of TGFβ-mediated conversion of endothelial cells and fibroblasts into cancer associated (myo) fibroblasts via HDAC inhibition. *British Journal of Cancer* **118**, 1359–1368.

(*97*) Rattigan, Y. I., Patel, B. B., Ackerstaff, E., Sukenick, G., Koutcher, J. A., Glod, J. W., and Banerjee, D. (2012). Lactate is a mediator of metabolic cooperation between stromal carcinoma associated fibroblasts and glycolytic tumor cells in the tumor microenvironment. *Experimental cell research* **318**, 326–335.

(*98*) Guido, C., Whitaker-Menezes, D., Capparelli, C., Balliet, R., Lin, Z., Pestell, R. G., Howell, A., Aquila, S., Andò, S., and Martinez-Outschoorn, U. (2012). Metabolic reprogramming of cancer-associated fibroblasts by TGF-β drives tumor growth: connecting TGF-β signaling with "Warburg-like" cancer metabolism and L-lactate production. *Cell cycle* **11**, 3019–3035.

(*99*) Hayes, C., Donohoe, C. L., Davern, M., and Donlon, N. E. (2021). The oncogenic and clinical implications of lactate induced immunosuppression in the tumour microenvironment. *Cancer Letters* **500**, 75–86.

(*100*) Quinn, W. J., Jiao, J., TeSlaa, T., Stadanlick, J., Wang, Z., Wang, L., Akimova, T., Angelin, A., Schäfer, P. M., Cully, M. D., et al. (2020). Lactate limits T cell proliferation via the NAD (H) redox state. *Cell reports* **33**.

(*101*) Jin, L., Fuchs, A., Schnitt, S. J., Yao, Y., Joseph, A., Lamszus, K., Park, M., Goldberg, I. D., and Rosen, E. M. (1997). Expression of scatter factor and c-met receptor in benign and malignant breast tissue. *Cancer* **79**, 749–760.

(*102*) Jedeszko, C., Victor, B. C., Podgorski, I., and Sloane, B. F. (2009). Fibroblast hepatocyte growth factor promotes invasion of human mammary ductal carcinoma in situ. *Cancer research* **69**, 9148–9155.

(*103*) Giraudo, E., Inoue, M., and Hanahan, D. (2004). An amino-bisphosphonate targets MMP-9–expressing macrophages and angiogenesis to impair cervical carcinogenesis. *The Journal of clinical investigation* **114**, 623–633.

(*104*) Lin, E. Y., Li, J.-f., Bricard, G., Wang, W., Deng, Y., Sellers, R., Porcelli, S. A., and Pollard, J. W. (2007). Vascular endothelial growth factor restores delayed tumor progression in tumors depleted of macrophages. *Molecular oncology* **1**, 288–302.

(*105*) Ishikawa, F., Ushida, K., Mori, K., and Shibanuma, M. (2015). Loss of anchorage primarily induces non-apoptotic cell death in a human mammary epithelial cell line under atypical focal adhesion kinase signaling. *Cell death & disease* **6**, e1619–e1619.

(*106*) Chen, Q., Zhang, X. H.-F., and Massagué, J. (2011). Macrophage binding to receptor VCAM-1 transmits survival signals in breast cancer cells that invade the lungs. *Cancer cell* **20**, 538–549.

(*107*) Liu, R., Yang, F., Yin, J.-Y., Liu, Y.-Z., Zhang, W., and Zhou, H.-H. (2021). Influence of tumor immune infiltration on immune checkpoint inhibitor therapeutic efficacy: a computational retrospective study. *Frontiers in immunology* **12**, 685370.

(*108*) Schumacher, T. N., and Thommen, D. S. (2022). Tertiary lymphoid structures in cancer. *Science* **375**, eabf9419.

(*109*) Lohr, M., Edlund, K., Botling, J., Hammad, S., Hellwig, B., Othman, A., Berglund, A., Lambe, M., Holmberg, L., Ekman, S., et al. (2013). The prognostic relevance of tumour-infiltrating plasma cells and immunoglobulin kappa C indicates an important role of the humoral immune response in non-small cell lung cancer. *Cancer letters* **333**, 222–228.

(*110*) Tuomela, K., Mukherjee, D., Ambrose, A. R., Harikrishnan, A., Mole, H., Hurlstone, A., Önfelt, B., Honeychurch, J., and Davis, D. M. (2022). Radiotherapy transiently reduces the sensitivity of cancer cells to lymphocyte cytotoxicity. *Proceedings of the National Academy of Sciences* **119**, e2111900119.

(*111*) Napoli, C., Giordano, A., Casamassimi, A., Pentimalli, F., Ignarro, L. J., and De Nigris, F. (2011). Directed in vivo angiogenesis assay and the study of systemic neoangiogenesis in cancer. *International journal of cancer* **128**, 1505–1508.

(*112*) de Jong, J. M., Wang, P., Oomkens, M., and Baron, W. (2020). Remodeling of the interstitial extracellular matrix in white matter multiple sclerosis lesions: Implications for remyelination (failure). *Journal of Neuroscience Research* **98**, 1370–1397.

(*113*) Theocharis, A. D., Skandalis, S. S., Gialeli, C., and Karamanos, N. K. (2016). Extracellular matrix structure. *Advanced drug delivery reviews* **97**, 4–27.

(*114*) Frantz, C., Stewart, K. M., and Weaver, V. M. (2010). The extracellular matrix at a glance. *Journal of cell science* **123**, 4195–4200.

(*115*) Elgundi, Z., Papanicolaou, M., Major, G., Cox, T. R., Melrose, J., Whitelock, J. M., and Farrugia, B. L. (2020). Cancer metastasis: the role of the extracellular matrix and the heparan sulfate proteoglycan perlecan. *Frontiers in oncology* **9**, 1482.

(*116*) Jiang, H., and Li, H. (2021). Prognostic values of tumoral MMP2 and MMP9 overexpression in breast cancer: A systematic review and meta-analysis. *BMC cancer* **21**, 1–13.

(*117*) OKADA, Y., MORODOMI, T., ENGHILD, J. J., SUZUKI, K., YASUI, A., NAKANISHI, I., SALVESEN, G., and NAGASE, H. (1990). Matrix metalloproteinase 2 from human rheumatoid synovial fibroblasts: purification and activation of the precursor and enzymic properties. *European Journal of Biochemistry* **194**, 721–730.

(*118*) Giaquinto, A. N., Sung, H., Miller, K. D., Kramer, J. L., Newman, L. A., Minihan, A., Jemal, A., and Siegel, R. L. (2022). Breast cancer statistics, 2022. *CA: A Cancer Journal for Clinicians* **72**, 524–541.

(*119*) World Cancer Research Fund International Worldwide cancer data `https://www.wcrf.org/cancer-trends/worldwide-cancer-data/` (accessed July 3, 2023).

(*120*) Harbeck, N., Penault-Llorca, F., Cortes, J., Gnant, M., Houssami, N., Poortmans, P., Ruddy, K., Tsang, J., and Cardoso, F. (2019). Breast cancer. *Nat Rev Dis Primers* **5**, 66.

(*121*) Gram, I. T., Park, S.-Y., Maskarinec, G., Wilkens, L. R., Haiman, C. A., and Le Marchand, L. (2019). Smoking and breast cancer risk by race/ethnicity and oestrogen and progesterone receptor status: the Multiethnic Cohort (MEC) study. *International journal of epidemiology* **48**, 501–511.

(*122*) MacMahon, B., Cole, P., Lin, T., Lowe, C., Mirra, A., Ravnihar, B., Salber, E., Valaoras, V., and Yuasa, S. (1970). Age at first birth and breast cancer risk. *Bulletin of the world health organization* **43**, 209.

(*123*) Lambe, M., Hsieh, C.-c., Chan, H.-w., Ekbom, A., Trichopoulos, D., and Adami, H.-O. (1996). Parity, age at first and last birth, and risk of breast cancer: a population-based study in Sweden. *Breast cancer research and treatment* **38**, 305–311.

(*124*) Ursin, G., Bernstein, L., Wang, Y., Lord, S. J., Deapen, D., Liff, J. M., Norman, S. A., Weiss, L. K., Daling, J. R., and Marchbanks, P. A. (2004). Reproductive factors and risk of breast carcinoma in a study of white and African-American women. *Cancer* **101**, 353–362.

(*125*) Britt, K., Ashworth, A., and Smalley, M. (2007). Pregnancy and the risk of breast cancer. *Endocrine-related cancer* **14**, 907–933.

(*126*) Siwko, S. K., Dong, J., Lewis, M. T., Liu, H., Hilsenbeck, S. G., and Li, Y. (2008). Evidence that an early pregnancy causes a persistent decrease in the number of functional mammary epithelial stem cells—implications for pregnancy-induced protection against breast cancer. *Stem Cells* **26**, 3205–3209.

(*127*) Brewer, H. R., Jones, M. E., Schoemaker, M. J., Ashworth, A., and Swerdlow, A. J. (2017). Family history and risk of breast cancer: an analysis accounting for family structure. *Breast cancer research and treatment* **165**, 193–200.

(*128*) Huen, M. S., Sy, S. M., and Chen, J. (2010). BRCA1 and its toolbox for the maintenance of genome integrity. *Nature reviews Molecular cell biology* **11**, 138–148.

(*129*) Weigelt, B., Geyer, F. C., and Reis-Filho, J. S. (2010). Histological types of breast cancer: how special are they? *Molecular oncology* **4**, 192–208.

(*130*) Weigelt, B., and Reis-Filho, J. S. (2009). Histological and molecular types of breast cancer: is there a unifying taxonomy? *Nature reviews Clinical oncology* **6**, 718–730.

(*131*) Brandão, M., Pondé, N., and Piccart-Gebhart, M. (2019). Mammaprint™: a comprehensive review. *Future oncology* **15**, 207–224.

(*132*) Slodkowska, E. A., and Ross, J. S. (2009). MammaPrint™ 70-gene signature: another milestone in personalized medical care for breast cancer patients. *Expert review of molecular diagnostics* **9**, 417–422.

(*133*) Yao, K., Tong, C.-Y., and Cheng, C. (2022). A framework to predict the applicability of Oncotype DX, MammaPrint, and E2F4 gene signatures for improving breast cancer prognostic prediction. *Scientific Reports* **12**, 2211.

(*134*) Vuong, D., Simpson, P. T., Green, B., Cummings, M. C., and Lakhani, S. R. (2014). Molecular classification of breast cancer. *Virchows Archiv* **465**, 1–14.

(*135*) Tsang, J., and Tse, G. M. (2020). Molecular classification of breast cancer. *Advances in anatomic pathology* **27**, 27–35.

(*136*) Hollande, F., and Merino, D., *Metastatic Progression and Tumour Heterogeneity*; MDPI-Multidisciplinary Digital Publishing Institute: 2020.

(*137*) Roy, A. L., and Conroy, R. S. (2018). Toward mapping the human body at a cellular resolution. *Molecular biology of the cell* **29**, 1779–1785.

(*138*) Börner, K., Teichmann, S. A., Quardokus, E. M., Gee, J. C., Browne, K., Osumi-Sutherland, D., Herr, B. W., Bueckle, A., Paul, H., and Haniffa, M. (2021). Anatomical structures, cell types and biomarkers of the Human Reference Atlas. *Nature cell biology* **23**, 1117–1128.

(*139*) Roy, A. L., and Conroy, R. S. (2018). Toward mapping the human body at a cellular resolution. *Molecular biology of the cell* **29**, 1779–1785.

(*140*) Popovic, M., Azpiroz, F., and Chuva de Sousa Lopes, S. M. (2021). Engineered models of the human embryo. *Nature Biotechnology* **39**, 918–920.

(*141*) Wamaitha, S. E., and Niakan, K. K. (2018). Human pre-gastrulation development. *Current topics in developmental biology* **128**, 295–338.

(*142*) Telpalo-Carpio, S., Aguilar-Yañez, J., Gonzalez-Garza, M., Cruz-Vega, D., and Moreno-Cuevas, J. E. (2013). iPS cells generation: an overview of techniques and methods. *Journal of Stem Cells & Regenerative Medicine* **9**, 2.

(*143*) Sozen, B., Jorgensen, V., Weatherbee, B. A., Chen, S., Zhu, M., and Zernicka-Goetz, M. (2021). Reconstructing aspects of human embryogenesis with pluripotent stem cells. *Nature communications* **12**, 5550.

(*144*) Alarcon, V. B., and Marikawa, Y. (2022). Trophectoderm formation: regulation of morphogenesis and gene expressions by RHO, ROCK, cell polarity, and HIPPO signaling. *Reproduction* **164**, R75–R86.

(*145*) Mitiku, N., and Baker, J. C. (2007). Genomic analysis of gastrulation and organogenesis in the mouse. *Developmental cell* **13**, 897–907.

(*146*) Dzhoyashvili, N. A., Shen, S., and Rochev, Y. A. (2015). Natural and Synthetic Materials for Self-Renewal, Long-Term Maintenance, and Differentiation of Induced Pluripotent Stem Cells. *Advanced Healthcare Materials* **4**, 2342–2359.

(*147*) Thomson, J. A., Itskovitz-Eldor, J., Shapiro, S. S., Waknitz, M. A., Swiergiel, J. J., Marshall, V. S., and Jones, J. M. (1998). Embryonic stem cell lines derived from human blastocysts. *science* **282**, 1145–1147.

(*148*) Young, R. A. (2011). Control of the embryonic stem cell state. *Cell* **144**, 940–954.

(*149*) Clark, A. T., Brivanlou, A., Fu, J., Kato, K., Mathews, D., Niakan, K. K., Rivron, N., Saitou, M., Surani, A., Tang, F., et al. (2021). Human embryo research, stem cell-derived embryo models and in vitro gametogenesis: Considerations leading to the revised ISSCR guidelines. *Stem Cell Reports* **16**, 1416–1424.

(*150*) Takahashi, K., and Yamanaka, S. (2006). Induction of pluripotent stem cells from mouse embryonic and adult fibroblast cultures by defined factors. *cell* **126**, 663–676.

(*151*) Takahashi, K., Tanabe, K., Ohnuki, M., Narita, M., Ichisaka, T., Tomoda, K., and Yamanaka, S. (2007). Induction of pluripotent stem cells from adult human fibroblasts by defined factors. *cell* **131**, 861–872.

(*152*) Durnaoglu, S., Genc, S., Genc, K., et al. (2011). Patient-specific pluripotent stem cells in neurological diseases. *Stem Cells International* **2011**.

(*153*) Guenther, M. G., Frampton, G. M., Soldner, F., Hockemeyer, D., Mitalipova, M., Jaenisch, R., and Young, R. A. (2010). Chromatin structure and gene expression programs of human embryonic and induced pluripotent stem cells. *Cell stem cell* **7**, 249–257.

(*154*) Ray, A., Joshi, J. M., Sundaravadivelu, P. K., Raina, K., Lenka, N., Kaveeshwar, V., and Thummer, R. P. (2021). An overview on promising somatic cell sources utilized for the efficient generation of induced pluripotent stem cells. *Stem Cell Reviews and Reports* **17**, 1954–1974.

(*155*) Dahlke, J., Schott, J. W., Vollmer Barbosa, P., Klatt, D., Selich, A., Lachmann, N., Morgan, M., Moritz, T., and Schambach, A. (2021). Efficient genetic safety switches for future application of ipsc-derived cell transplants. *Journal of Personalized Medicine* **11**, 565.

(*156*) Ortuño-Costela, M. d. C., Cerrada, V., García-López, M., and Gallardo, M. E. (2019). The challenge of bringing iPSCs to the patient. *International journal of molecular sciences* **20**, 6305.

(*157*) Zhang, R., Zhang, L.-h., and Xie, X. (2013). iPSCs and small molecules: a reciprocal effort towards better approaches for drug discovery. *Acta Pharmacologica Sinica* **34**, 765–776.

(*158*) Burnight, E. R., Gupta, M., Wiley, L. A., Anfinson, K. R., Tran, A., Triboulet, R., Hoffmann, J. M., Klaahsen, D. L., Andorf, J. L., and Jiao, C. (2017). Using CRISPR-Cas9 to generate gene-corrected autologous iPSCs for the treatment of inherited retinal degeneration. *Molecular Therapy* **25**, 1999–2013.

(*159*) Mandai, M., Watanabe, A., Kurimoto, Y., Hirami, Y., Morinaga, C., Daimon, T., Fujihara, M., Akimaru, H., Sakai, N., and Shibata, Y. (2017). Autologous induced stem-cell–derived retinal cells for macular degeneration. *New England Journal of Medicine* **376**, 1038–1046.

(*160*) Yoshida, S., Kato, T. M., Sato, Y., Umekage, M., Ichisaka, T., Tsukahara, M., Takasu, N., and Yamanaka, S. (2023). A clinical-grade HLA haplobank of human induced pluripotent stem cells matching approximately 40% of the Japanese population. *Med* **4**, 51–66. e10.

(*161*) Mack, A. A., Kroboth, S., Rajesh, D., and Wang, W. B. (2011). Generation of induced pluripotent stem cells from CD34+ cells across blood drawn from multiple donors with non-integrating episomal vectors. *PloS one* **6**, e27956.

(*162*) Aasen, T., Raya, A., Barrero, M. J., Garreta, E., Consiglio, A., Gonzalez, F., Vassena, R., Bilić, J., Pekarik, V., and Tiscornia, G. (2008). Efficient and rapid generation of induced pluripotent stem cells from human keratinocytes. *Nature biotechnology* **26**, 1276–1284.

(*163*) Seki, T., Yuasa, S., Oda, M., Egashira, T., Yae, K., Kusumoto, D., Nakata, H., Tohyama, S., Hashimoto, H., and Kodaira, M. (2010). Generation of induced pluripotent stem cells from human terminally differentiated circulating T cells. *Cell stem cell* **7**, 11–14.

(*164*) Bueno, C., Sardina, J. L., Di Stefano, B., Romero-Moya, D., Muñoz-López, A., Ariza, L., Chillón, M. C., Balanzategui, A., Castaño, J., and Herreros, A. (2016). Reprogramming human B cells into induced pluripotent stem cells and its enhancement by C/EBPα. *Leukemia* **30**, 674–682.

(*165*) Zapata-Linares, N., Rodriguez, S., Mazo, M., Abizanda, G., Andreu, E. J., Barajas, M., Prosper, F., and Rodriguez-Madoz, J. R. (2016). Generation and characterization of human iPSC line generated from mesenchymal stem cells derived from adipose tissue. *Stem Cell Research* **16**, 20–23.

(*166*) Yan, X., Qin, H., Qu, C., Tuan, R. S., Shi, S., and Huang, G. T.-J. (2010). iPS cells reprogrammed from human mesenchymal-like stem/progenitor cells of dental tissue origin. *Stem cells and development* **19**, 469–480.

(*167*) Zhou, T., Benda, C., Dunzinger, S., Huang, Y., Ho, J. C., Yang, J., Wang, Y., Zhang, Y., Zhuang, Q., and Li, Y. (2012). Generation of human induced pluripotent stem cells from urine samples. *Nature protocols* **7**, 2080–2089.

(*168*) Xue, Y., Cai, X., Wang, L., Liao, B., Zhang, H., Shan, Y., Chen, Q., Zhou, T., Li, X., and Hou, J. (2013). Generating a non-integrating human induced pluripotent stem cell bank from urine-derived cells. *PloS one* **8**, e70573.

(*169*) Liu, H., Ye, Z., Kim, Y., Sharkis, S., and Jang, Y.-Y. (2010). Generation of endoderm-derived human induced pluripotent stem cells from primary hepatocytes. *Hepatology* **51**, 1810–1819.

(*170*) Petzendorfer, E., and Guillot, P. V. (2021). Induced pluripotent stem cells derived from amniotic fluid stem cells. *Cell Sources for iPSCs*, 1–13.

(*171*) Yamanaka, S. (2012). Induced pluripotent stem cells: past, present, and future. *Cell stem cell* **10**, 678–684.

(*172*) Chou, B.-K., Mali, P., Huang, X., Ye, Z., Dowey, S. N., Resar, L., Zou, C., Zhang, Y. A., Tong, J., and Cheng, L. (2011). Efficient human iPS cell derivation by a non-integrating plasmid from blood cells with unique epigenetic and gene expression signatures. *Cell research* **21**, 518–529.

(*173*) Chen, H., Schürch, C. M., Noble, K., Kim, K., Krutzik, P. O., O'Donnell, E., Vander Tuig, J., Nolan, G. P., and McIlwain, D. R. (2020). Functional comparison of PBMCs isolated by cell preparation tubes (CPT) vs. lymphoprep tubes. *BMC immunology* **21**, 1–13.

(*174*) Loh, Y.-H., Hartung, O., Li, H., Guo, C., Sahalie, J. M., Manos, P. D., Urbach, A., Heffner, G. C., Grskovic, M., and Vigneault, F. (2010). Reprogramming of T cells from human peripheral blood. *Cell stem cell* **7**, 15–19.

(*175*) Serwold, T., Hochedlinger, K., Swindle, J., Hedgpeth, J., Jaenisch, R., and Weissman, I. L. (2010). T-cell receptor-driven lymphomagenesis in mice derived from a reprogrammed T cell. *Proceedings of the National Academy of Sciences* **107**, 18939–18943.

(*176*) Merling, R. K., Sweeney, C. L., Choi, U., De Ravin, S. S., Myers, T. G., Otaizo-Carrasquero, F., Pan, J., Linton, G., Chen, L., Koontz, S., et al. (2013). Transgene-free iPSCs generated from small volume peripheral blood nonmobilized CD34+ cells. *Blood, The Journal of the American Society of Hematology* **121**, e98–e107.

(*177*) Al Abbar, A., Ngai, S. C., Nograles, N., Alhaji, S. Y., and Abdullah, S. (2020). Induced pluripotent stem cells: Reprogramming platforms and applications in cell replacement therapy. *BioResearch Open Access* **9**, 121–136.

(*178*) Cherkashova, E., Leonov, G., Namestnikova, D., Solov'eva, A., Gubskii, I., Bukharova, T., Gubskii, L., Goldstein, D., and Yarygin, K. (2020). Methods of generation of induced pluripotent stem cells and their application for the therapy of central nervous system diseases. *Bulletin of Experimental Biology and Medicine* **168**, 566–573.

(*179*) Wang, A. Y. L., and Loh, C. Y. Y. (2019). Episomal induced pluripotent stem cells: Functional and potential therapeutic applications. *Cell Transplantation* **28**, 112S–131S.

(*180*) Warren, L., Manos, P. D., Ahfeldt, T., Loh, Y.-H., Li, H., Lau, F., Ebina, W., Mandal, P. K., Smith, Z. D., and Meissner, A. (2010). Highly efficient reprogramming to pluripotency and directed differentiation of human cells with synthetic modified mRNA. *Cell stem cell* **7**, 618–630.

(*181*) Anokye-Danso, F., Trivedi, C. M., Juhr, D., Gupta, M., Cui, Z., Tian, Y., Zhang, Y., Yang, W., Gruber, P. J., and Epstein, J. A. (2011). Highly efficient miRNA-mediated reprogramming of mouse and human somatic cells to pluripotency. *Cell stem cell* **8**, 376–388.

(*182*) Woltjen, K., Michael, I. P., Mohseni, P., Desai, R., Mileikovsky, M., Hämäläinen, R., Cowling, R., Wang, W., Liu, P., and Gertsenstein, M. (2009). piggyBac transposition reprograms fibroblasts to induced pluripotent stem cells. *nature* **458**, 766–770.

(*183*) Davis, R. P., Nemes, C., Varga, E., Freund, C., Kosmidis, G., Gkatzis, K., de Jong, D., Szuhai, K., Dinnyés, A., and Mummery, C. L. (2013). Generation of induced pluripotent stem cells from human foetal fibroblasts using the Sleeping Beauty transposon gene delivery system. *Differentiation* **86**, 30–37.

(*184*) Kim, D., Kim, C.-H., Moon, J.-I., Chung, Y.-G., Chang, M.-Y., Han, B.-S., Ko, S., Yang, E., Cha, K. Y., and Lanza, R. (2009). Generation of human induced pluripotent stem cells by direct delivery of reprogramming proteins. *Cell stem cell* **4**, 472.

(*185*) Jia, F., Wilson, K. D., Sun, N., Gupta, D. M., Huang, M., Li, Z., Panetta, N. J., Chen, Z. Y., Robbins, R. C., and Kay, M. A. (2010). A nonviral minicircle vector for deriving human iPS cells. *Nature methods* **7**, 197–199.

(*186*) Blanchard, J. W., Xie, J., El-Mecharrafie, N., Gross, S., Lee, S., Lerner, R. A., and Baldwin, K. K. (2017). Replacing reprogramming factors with antibodies selected from combinatorial antibody libraries. *Nature biotechnology* **35**, 960–968.

(*187*) Fusaki, N., Ban, H., Nishiyama, A., Saeki, K., and Hasegawa, M. (2009). Efficient induction of transgene-free human pluripotent stem cells using a vector based on Sendai virus, an RNA virus that does not integrate into the host genome. *Proceedings of the Japan Academy, Series B* **85**, 348–362.

(*188*) Fink, K. D., Rossignol, J., Lu, M., Lévêque, X., Hulse, T. D., Crane, A. T., Nerriere-Daguin, V., Wyse, R. D., Starski, P. A., and Schloop, M. T. (2014). Survival and differentiation of adenovirus-generated induced pluripotent stem cells transplanted into the rat striatum. *Cell transplantation* **23**, 1407–1423.

(*189*) Okita, K., Matsumura, Y., Sato, Y., Okada, A., Morizane, A., Okamoto, S., Hong, H., Nakagawa, M., Tanabe, K., and Tezuka, K.-i. (2011). A more efficient method to generate integration-free human iPS cells. *Nature methods* **8**, 409–412.

(*190*) Van Craenenbroeck, K., Vanhoenacker, P., and Haegeman, G. (2000). Episomal vectors for gene expression in mammalian cells. *European journal of biochemistry* **267**, 5665–5678.

(*191*) Coppotelli, G., Mughal, N., Callegari, S., Sompallae, R., Caja, L., Luijsterburg, M. S., Dantuma, N. P., Moustakas, A., and Masucci, M. G. (2013). The Epstein–Barr virus nuclear antigen-1 reprograms transcription by mimicry of high mobility group A proteins. *Nucleic acids research* **41**, 2950–2962.

(*192*) Dye, N. A., Popović, M., Iyer, K. V., Fuhrmann, J. F., Piscitello-Gómez, R., Eaton, S., and Jülicher, F. (2021). Self-organized patterning of cell morphology via mechanosensitive feedback. *Elife* **10**, e57964.

(*193*) Silva-Pedrosa, R., Salgado, A. J., and Ferreira, P. E. (2023). Revolutionizing disease modeling: the emergence of organoids in cellular systems. *Cells* **12**, 930.

(*194*) de Souza, N. (2018). Organoids. *Nature Methods* **15**, 23–23.

(*195*) Rossi, G., Manfrin, A., and Lutolf, M. P. (2018). Progress and potential in organoid research. *Nature Reviews Genetics* **19**, 671–687.

(*196*) Clevers, H. (2016). Modeling development and disease with organoids. *Cell* **165**, 1586–1597.

(*197*) Lancaster, M. A., and Knoblich, J. A. (2014). Organogenesis in a dish: modeling development and disease using organoid technologies. *Science* **345**, 1247125.

(*198*) Werner, S., Vu, H. T.-K., and Rink, J. C. (2017). Self-organization in development, regeneration and organoids. *Current opinion in cell biology* **44**, 102–109.

(*199*) Drost, J., and Clevers, H. (2017). Translational applications of adult stem cell-derived organoids. *Development* **144**, 968–975.

(*200*) Sato, T., Vries, R. G., Snippert, H. J., Van De Wetering, M., Barker, N., Stange, D. E., Van Es, J. H., Abo, A., Kujala, P., and Peters, P. J. (2009). Single Lgr5 stem cells build crypt-villus structures in vitro without a mesenchymal niche. *Nature* **459**, 262–265.

(*201*) Huch, M., Gehart, H., Van Boxtel, R., Hamer, K., Blokzijl, F., Verstegen, M. M., Ellis, E., Van Wenum, M., Fuchs, S. A., and de Ligt, J. (2015). Long-term culture of genome-stable bipotent stem cells from adult human liver. *Cell* **160**, 299–312.

(*202*) Boj, S. F., Hwang, C.-I., Baker, L. A., Chio, I. I. C., Engle, D. D., Corbo, V., Jager, M., Ponz-Sarvise, M., Tiriac, H., and Spector, M. S. (2015). Organoid models of human and mouse ductal pancreatic cancer. *Cell* **160**, 324–338.

(*203*) Kessler, M., Hoffmann, K., Brinkmann, V., Thieck, O., Jackisch, S., Toelle, B., Berger, H., Mollenkopf, H.-J., Mangler, M., and Sehouli, J. (2015). The Notch and Wnt pathways regulate stemness and differentiation in human fallopian tube organoids. *Nature communications* **6**, 8989.

(*204*) Chua, C. W., Shibata, M., Lei, M., Toivanen, R., Barlow, L. J., Bergren, S. K., Badani, K. K., McKiernan, J. M., Benson, M. C., and Hibshoosh, H. (2014). Single luminal epithelial progenitors can generate prostate organoids in culture. *Nature cell biology* **16**, 951–961.

(*205*) Bartfeld, S., Bayram, T., van de Wetering, M., Huch, M., Begthel, H., Kujala, P., Vries, R., Peters, P. J., and Clevers, H. (2015). In vitro expansion of human gastric epithelial stem cells and their responses to bacterial infection. *Gastroenterology* **148**, 126–136. e6.

(*206*) Turhan, A. G., Hwang, J. W., Chaker, D., Tasteyre, A., Latsis, T., Griscelli, F., Desterke, C., and Bennaceur-Griscelli, A. (2021). iPSC-Derived Organoids as Therapeutic Models in Regenerative Medicine and Oncology. *Frontiers in Medicine*, 1838.

(*207*) Lancaster, M. A., Renner, M., Martin, C.-A., Wenzel, D., Bicknell, L. S., Hurles, M. E., Homfray, T., Penninger, J. M., Jackson, A. P., and Knoblich, J. A. (2013). Cerebral organoids model human brain development and microcephaly. *Nature* **501**, 373–379.

(*208*) Li, F., Zhang, P., Wu, S., Yuan, L., and Liu, Z. (2021). Advance in human epithelial-derived organoids research. *Molecular Pharmaceutics* **18**, 3931–3950.

(*209*) Gabriel, E., and Gopalakrishnan, J. (2017). Generation of iPSC-derived human brain organoids to model early neurodevelopmental disorders. *JoVE (Journal of Visualized Experiments)*, e55372.

(*210*) Sun, G., Chiuppesi, F., Chen, X., Wang, C., Tian, E., Nguyen, J., Kha, M., Trinh, D., Zhang, H., and Marchetto, M. C. (2020). Modeling human cytomegalovirus-induced microcephaly in human iPSC-derived brain organoids. *Cell Reports Medicine* **1**, 100002.

(*211*) Kim, J., Lee, S., Lee, J., Park, J.-C., Kim, K. H., Ko, J. M., Park, S.-H., Kim, S.-K., Mook-Jung, I., and Lee, J. Y. (2022). Neurotoxicity of phenylalanine on human iPSC-derived cerebral organoids. *Molecular Genetics and Metabolism* **136**, 132–144.

(*212*) Guo, Y., Wang, P., Ma, J. H., Cui, Z., Yu, Q., Liu, S., Xue, Y., Zhu, D., Cao, J., and Li, Z. (2019). Modeling retinitis pigmentosa: retinal organoids generated from the iPSCs of a patient with the USH2A mutation show early developmental abnormalities. *Frontiers in Cellular Neuroscience* **13**, 361.

(*213*) Lane, A., Jovanovic, K., Shortall, C., Ottaviani, D., Panes, A. B., Schwarz, N., Guarascio, R., Hayes, M. J., Palfi, A., and Chadderton, N. (2020). Modeling and rescue of RP2 retinitis pigmentosa using iPSC-derived retinal organoids. *Stem Cell Reports* **15**, 67–79.

(*214*) Norrie, J. L., Nityanandam, A., Lai, K., Chen, X., Wilson, M., Stewart, E., Griffiths, L., Jin, H., Wu, G., and Orr, B. (2021). Retinoblastoma from human stem cell-derived retinal organoids. *Nature Communications* **12**, 4535.

(*215*) Spence, J. R., Mayhew, C. N., Rankin, S. A., Kuhar, M. F., Vallance, J. E., Tolle, K., Hoskins, E. E., Kalinichenko, V. V., Wells, S. I., and Zorn, A. M. (2011). Directed differentiation of human pluripotent stem cells into intestinal tissue in vitro. *Nature* **470**, 105–109.

(*216*) Tsai, Y.-H., Nattiv, R., Dedhia, P. H., Nagy, M. S., Chin, A. M., Thomson, M., Klein, O. D., and Spence, J. R. (2017). In vitro patterning of pluripotent stem cell-derived intestine recapitulates in vivo human development. *Development* **144**, 1045–1055.

(*217*) Workman, M. J., Mahe, M. M., Trisno, S., Poling, H. M., Watson, C. L., Sundaram, N., Chang, C.-F., Schiesser, J., Aubert, P., and Stanley, E. G. (2017). Engineered human pluripotent-stem-cell-derived intestinal tissues with a functional enteric nervous system. *Nature medicine* **23**, 49–59.

(*218*) Zhang, R.-R., Koido, M., Tadokoro, T., Ouchi, R., Matsuno, T., Ueno, Y., Sekine, K., Takebe, T., and Taniguchi, H. (2018). Human iPSC-derived posterior gut progenitors are expandable and capable of forming gut and liver organoids. *Stem Cell Reports* **10**, 780–793.

(*219*) Taguchi, A., Kaku, Y., Ohmori, T., Sharmin, S., Ogawa, M., Sasaki, H., and Nishinakamura, R. (2014). Redefining the in vivo origin of metanephric nephron progenitors enables generation of complex kidney structures from pluripotent stem cells. *Cell stem cell* **14**, 53–67.

(*220*) Morizane, R., Lam, A. Q., Freedman, B. S., Kishi, S., Valerius, M. T., and Bonventre, J. V. (2015). Nephron organoids derived from human pluripotent stem cells model kidney development and injury. *Nature biotechnology* **33**, 1193–1200.

(*221*) Takasato, M., Er, P. X., Chiu, H. S., Maier, B., Baillie, G. J., Ferguson, C., Parton, R. G., Wolvetang, E. J., Roost, M. S., and Chuva de Sousa Lopes, S. M. (2015). Kidney organoids from human iPS cells contain multiple lineages and model human nephrogenesis. *Nature* **526**, 564–568.

(*222*) Takebe, T., Sekine, K., Enomura, M., Koike, H., Kimura, M., Ogaeri, T., Zhang, R.-R., Ueno, Y., Zheng, Y.-W., and Koike, N. (2013). Vascularized and functional human liver from an iPSC-derived organ bud transplant. *Nature* **499**, 481–484.

(*223*) Sampaziotis, F., Cardoso de Brito, M., Madrigal, P., Bertero, A., Saeb-Parsy, K., Soares, F. A., Schrumpf, E., Melum, E., Karlsen, T. H., and Bradley, J. A. (2015). Cholangiocytes derived from human induced pluripotent stem cells for disease modeling and drug validation. *Nature biotechnology* **33**, 845–852.

(*224*) Takebe, T., Sekine, K., Kimura, M., Yoshizawa, E., Ayano, S., Koido, M., Funayama, S., Nakanishi, N., Hisai, T., and Kobayashi, T. (2017). Massive and reproducible production of liver buds entirely from human pluripotent stem cells. *Cell reports* **21**, 2661–2670.

(*225*) Ang, L. T., Tan, A. K. Y., Autio, M. I., Goh, S. H., Choo, S. H., Lee, K. L., Tan, J., Pan, B., Lee, J. J. H., and Lum, J. J. (2018). A roadmap for human liver differentiation from pluripotent stem cells. *Cell reports* **22**, 2190–2205.

(*226*) McCracken, K. W., Catá, E. M., Crawford, C. M., Sinagoga, K. L., Schumacher, M., Rockich, B. E., Tsai, Y.-H., Mayhew, C. N., Spence, J. R., and Zavros, Y. (2014). Modelling human development and disease in pluripotent stem-cell-derived gastric organoids. *Nature* **516**, 400–404.

(*227*) McCracken, K. W., Aihara, E., Martin, B., Crawford, C. M., Broda, T., Treguier, J., Zhang, X., Shannon, J. M., Montrose, M. H., and Wells, J. M. (2017). Wnt/β-catenin promotes gastric fundus specification in mice and humans. *Nature* **541**, 182–187.

(*228*) Huang, L., Holtzinger, A., Jagan, I., BeGora, M., Lohse, I., Ngai, N., Nostro, C., Wang, R., Muthuswamy, L. B., and Crawford, H. C. (2015). Ductal pancreatic cancer modeling and drug screening using human pluripotent stem cell–and patient-derived tumor organoids. *Nature medicine* **21**, 1364–1371.

(*229*) Wiedenmann, S., Breunig, M., Merkle, J., von Toerne, C., Georgiev, T., Moussus, M., Schulte, L., Seufferlein, T., Sterr, M., and Lickert, H. (2021). Single-cell-resolved differentiation of human induced pluripotent stem cells into pancreatic duct-like organoids on a microwell chip. *Nature biomedical engineering* **5**, 897–913.

(*230*) Qu, Y., Han, B., Gao, B., Bose, S., Gong, Y., Wawrowsky, K., Giuliano, A. E., Sareen, D., and Cui, X. (2017). Differentiation of human induced pluripotent stem cells to mammary-like organoids. *Stem cell reports* **8**, 205–215.

(*231*) Dai, X., Wang, X., Yang, C., Huang, M., Zhou, Z., Qu, Y., Cui, X., Liu, R., and Chen, C. (2022). Human fibroblasts facilitate the generation of iPSCs-derived mammary-like organoids. *Stem cell research & therapy* **13**, 1–12.

(*232*) **Keller**, **A.-L.**, Binner, A., Breitmeyer, R., Vogel, S., Anderle, N., Rothbauer, U., Schenke-Layland, K., and Schmees, C. (2021). Generation and characterization of the human induced pluripotent stem cell line NMIi010-A from peripheral blood mononuclear cells of a healthy 49–year old male individual. *Stem Cell Research* **54**, 102427.

(*233*) Nagasaka, R., Matsumoto, M., Okada, M., Sasaki, H., Kanie, K., Kii, H., Uozumi, T., Kiyota, Y., Honda, H., and Kato, R. (2017). Visualization of morphological categories of colonies for monitoring of effect on induced pluripotent stem cell culture status. *Regenerative Therapy* **6**, 41–51.

(*234*) Liu, L.-P., and Zheng, Y.-W. (2019). Predicting differentiation potential of human pluripotent stem cells: Possibilities and challenges. *World Journal of Stem Cells* **11**, 375.

(*235*) O'Shea, O., Steeg, R., Chapman, C., Mackintosh, P., and Stacey, G. N. (2020). Development and implementation of large-scale quality control for the European bank for induced Pluripotent Stem Cells. *Stem cell research* **45**, 101773.

(*236*) McKinney-Freeman, S. L., Jackson, K. A., Camargo, F. D., Ferrari, G., Mavilio, F., and Goodell, M. A. (2002). Muscle-derived hematopoietic stem cells are hematopoietic in origin. *Proceedings of the National Academy of Sciences* **99**, 1341–1346.

(*237*) Elliott, A. M., Hohenstein Elliott, K. A., and Kammesheidt, A. (2010). High resolution array-CGH characterization of human stem cells using a stem cell focused microarray. *Molecular Biotechnology* **46**, 234–242.

(*238*) Scott, S. A., Cohen, N., Brandt, T., Toruner, G., Desnick, R. J., and Edelmann, L. (2010). Detection of low-level mosaicism and placental mosaicism by oligonucleotide array comparative genomic hybridization. *Genetics in Medicine* **12**, 85–92.

(*239*) Khojasteh, M., Lam, W. L., Ward, R. K., and MacAulay, C. (2005). A stepwise framework for the normalization of array CGH data. *BMC bioinformatics* **6**, 1–15.

(*240*) Wyner, N., Barash, M., and McNevin, D. (2020). Forensic autosomal short tandem repeats and their potential association with phenotype. *Frontiers in genetics* **11**, 884.

(*241*) Fleischer, A., Lorenzo, I. M., Palomino, E., Aasen, T., Gómez, F., Servera, M., Asensio, V. J., Gálvez, V., Izpisúa-Belmonte, J. C., and Bachiller, D. (2018). Generation of two induced pluripotent stem cell (iPSC) lines from p. F508del Cystic Fibrosis patients. *Stem Cell Research* **29**, 1–5.

(*242*) Gudjonsson, T., Adriance, M. C., Sternlicht, M. D., Petersen, O. W., and Bissell, M. J. (2005). Myoepithelial cells: their origin and function in breast morphogenesis and neoplasia. *Journal of mammary gland biology and neoplasia* **10**, 261.

(*243*) Polyak, K., and Hu, M. (2005). Do myoepithelial cells hold the key for breast tumor progression? *Journal of mammary gland biology and neoplasia* **10**, 231–247.

(*244*) Sternlicht, M. D., Kedeshian, P., Shao, Z.-M., Safarians, S., and Barsky, S. H. (1997). The human myoepithelial cell is a natural tumor suppressor. *Clinical cancer research: an official journal of the American Association for Cancer Research* **3**, 1949–1958.

(*245*) Gudjonsson, T., Rønnov-Jessen, L., Villadsen, R., Rank, F., Bissell, M. J., and Petersen, O. W. (2002). Normal and tumor-derived myoepithelial cells differ in their ability to interact with luminal breast epithelial cells for polarity and basement membrane deposition. *Journal of cell science* **115**, 39–50.

(*246*) Pandey, P. R., Saidou, J., and Watabe, K. (2010). Role of myoepithelial cells in breast tumor progression. *Frontiers in bioscience: a journal and virtual library* **15**, 226.

(*247*) Dirat, B., Bochet, L., Dabek, M., Daviaud, D., Dauvillier, S., Majed, B., Wang, Y. Y., Meulle, A., Salles, B., and Le Gonidec, S. (2011). Cancer-associated adipocytes exhibit an activated phenotype and contribute to breast cancer invasion. *Cancer research* **71**, 2455–2465.

(*248*) Pistone Creydt, V., Fletcher, S. J., Giudice, J., Bruzzone, A., Chasseing, N. A., Gonzalez, E. G., Sacca, P. A., and Calvo, J. C. (2013). Human adipose tissue from normal and tumoral breast regulates the behavior of mammary epithelial cells. *Clinical and Translational Oncology* **15**, 124–131.

(*249*) Gantov, M., Pagnotta, P., Lotufo, C., Rindone, G. M., Riera, M. F., Calvo, J. C., and Toneatto, J. (2021). Beige adipocytes contribute to breast cancer progression. *Oncology Reports* **45**, 317–328.

(*250*) Poczobutt, J. M., Tentler, J., Lu, X., Schedin, P. J., and Gutierrez-Hartmann, A. (2010). Benign mammary epithelial cells enhance the transformed phenotype of human breast cancer cells. *Bmc Cancer* **10**, 1–17.

(*251*) Carpenter, P. M., and Nguyen, H. (1998). Mammary epithelium-induced motility of MCF-7 cells. *Anticancer research* **18**, 1063–1068.

(*252*) Serrati, S., Margheri, F., Fibbi, G., Di Cara, G., Minafra, L., Pucci-Minafra, I., Liotta, F., Annunziato, F., Pucci, M., and Del Rosso, M. (2008). Endothelial cells and normal breast epithelial cells enhance invasion of breast carcinoma cells by CXCR-4-dependent up-regulation of urokinase-type plasminogen activator receptor (uPAR, CD87) expression. *The Journal of Pathology: A Journal of the Pathological Society of Great Britain and Ireland* **214**, 545–554.

(*253*) Li, H., Qiu, Z., Li, F., and Wang, C. (2017). The relationship between MMP-2 and MMP-9 expression levels with breast cancer incidence and prognosis. *Oncology letters* **14**, 5865–5870.

(*254*) Bae, Y. K., Kim, A., Kim, M. K., Choi, J. E., Kang, S. H., and Lee, S. J. (2013). Fibronectin expression in carcinoma cells correlates with tumor aggressiveness and poor clinical outcome in patients with invasive breast cancer. *Human pathology* **44**, 2028–2037.

(*255*) Frisch, S. M., and Francis, H. (1994). Disruption of epithelial cell-matrix interactions induces apoptosis. *The Journal of cell biology* **124**, 619–626.

(*256*) Wang, X., Lin, G., Martins-Taylor, K., Zeng, H., and Xu, R.-H. (2009). Inhibition of caspase-mediated anoikis is critical for basic fibroblast growth factor-sustained culture of human pluripotent stem cells. *Journal of Biological Chemistry* **284**, 34054–34064.

(*257*) Schwartz, P. H., Brick, D. J., Stover, A. E., Loring, J. F., and Müller, F.-J. (2008). Differentiation of neural lineage cells from human pluripotent stem cells. *Methods* **45**, 142–158.

(*258*) Paszek, M. J., Zahir, N., Johnson, K. R., Lakins, J. N., Rozenberg, G. I., Gefen, A., Reinhart-King, C. A., Margulies, S. S., Dembo, M., and Boettiger, D. (2005). Tensional homeostasis and the malignant phenotype. *Cancer cell* **8**, 241–254.

(*259*) Dingess, K. A., Gazi, I., van den Toorn, H. W., Mank, M., Stahl, B., Reiding, K. R., and Heck, A. J. (2021). Monitoring human milk β-casein phosphorylation and O-glycosylation over lactation reveals distinct differences between the proteome and endogenous peptidome. *International journal of molecular sciences* **22**, 8140.

(*260*) Kwiatkowska, E., Wojtala, M., Gajewska, A., Soszyński, M., Bartosz, G., and Sadowska-Bartosz, I. (2016). Effect of 3-bromopyruvate acid on the redox equilibrium in non-invasive MCF-7 and invasive MDA-MB-231 breast cancer cells. *Journal of bioenergetics and biomembranes* **48**, 23–32.

(*261*) Clarke, M. A., and Fisher, J. (2020). Executable cancer models: successes and challenges. *Nature Reviews Cancer* **20**, 343–354.

(*262*) Sarhangi, N., Hajjari, S., Heydari, S. F., Ganjizadeh, M., Rouhollah, F., and Hasanzad, M. (2022). Breast cancer in the era of precision medicine. *Molecular Biology Reports* **49**, 10023–10037.

(*263*) Bussolati, G., Marchiò, C., Gaetano, L., Lupo, R., and Sapino, A. (2008). Pleomorphism of the nuclear envelope in breast cancer: a new approach to an old problem. *Journal of cellular and molecular medicine* **12**, 209–218.

(*264*) Makki, J. (2015). Diversity of breast carcinoma: histological subtypes and clinical relevance. *Clinical medicine insights: Pathology* **8**, CPath–S31563.

(*265*) McCart Reed, A. E., Kalinowski, L., Simpson, P. T., and Lakhani, S. R. (2021). Invasive lobular carcinoma of the breast: the increasing importance of this special subtype. *Breast Cancer Research* **23**, 1–16.

(*266*) Patwardhan, S., Mahadik, P., Shetty, O., and Sen, S. (2021). ECM stiffness-tuned exosomes drive breast cancer motility through thrombospondin-1. *Biomaterials* **279**, 121185.

(*267*) Movat, H. Z. (1955). Demonstration of all connective tissue elements in a single section; pentachrome stains. *AMA archives of pathology* **60**, 289–295.

(*268*) Natal, R. d. A., Paiva, G. R., Pelegati, V. B., Marenco, L., Alvarenga, C. A., Vargas, R. F., Derchain, S. F., Sarian, L. O., Franchet, C., Cesar, C. L., et al. (2019). Exploring collagen parameters in pure special types of invasive breast cancer. *Scientific reports* **9**, 1–11.

(*269*) Abd El-Rehim, D. M., Pinder, S. E., Paish, C. E., Bell, J., Blamey, R., Robertson, J. F., Nicholson, R. I., and Ellis, I. O. (2004). Expression of luminal and basal cytokeratins in human breast carcinoma. *The Journal of Pathology: A Journal of the Pathological Society of Great Britain and Ireland* **203**, 661–671.

(*270*) Zajchowski, D. A., Bartholdi, M. F., Gong, Y., Webster, L., Liu, H.-L., Munishkin, A., Beauheim, C., Harvey, S., Ethier, S. P., and Johnson, P. H. (2001). Identification of gene expression profiles that predict the aggressive behavior of breast cancer cells. *Cancer research* **61**, 5168–5178.

(*271*) Park, C. K., Jung, W. H., and Koo, J. S. (2016). Expression of cancer-associated fibroblast-related proteins differs between invasive lobular carcinoma and invasive ductal carcinoma. *Breast cancer research and treatment* **159**, 55–69.

(*272*) Treindl, F., Ruprecht, B., Beiter, Y., Schultz, S., Döttinger, A., Staebler, A., Joos, T. O., Kling, S., Poetz, O., Fehm, T., et al. (2016). A bead-based western for high-throughput cellular signal transduction analyses. *Nature communications* **7**, 12852.

(*273*) Kabos, P., Haughian, J. M., Wang, X., Dye, W. W., Finlayson, C., Elias, A., Horwitz, K. B., and Sartorius, C. A. (2011). Cytokeratin 5 positive cells represent a steroid receptor negative and therapy resistant subpopulation in luminal breast cancers. *Breast cancer research and treatment* **128**, 45–55.

(*274*) Fettig, L., McGinn, O., Finlay-Schultz, J., LaBarbera, D., Nordeen, S., and Sartorius, C. (2017). Cross talk between progesterone receptors and retinoic acid receptors in regulation of cytokeratin 5-positive breast cancer cells. *Oncogene* **36**, 6074–6084.

(*275*) Cossu-Rocca, P., Orrù, S., Muroni, M. R., Sanges, F., Sotgiu, G., Ena, S., Pira, G., Murgia, L., Manca, A., Uras, M. G., et al. (2015). Analysis of PIK3CA mutations and activation pathways in triple negative breast cancer. *PloS one* **10**, e0141763.

(*276*) Eralp, Y., Derin, D., Ozluk, Y., Yavuz, E., Guney, N., Saip, P., Muslumanoglu, M., Igci, A., Kücücük, S., Dincer, M., et al. (2008). MAPK overexpression is associated with anthracycline resistance and increased risk for recurrence in patients with triple-negative breast cancer. *Annals of oncology* **19**, 669–674.

(*277*) Volpato, V., and Webber, C. (2020). Addressing variability in iPSC-derived models of human disease: guidelines to promote reproducibility. *Disease models & mechanisms* **13**, dmm042317.

(*278*) Chan, E. M., Ratanasirintrawoot, S., Park, I.-H., Manos, P. D., Loh, Y.-H., Huo, H., Miller, J. D., Hartung, O., Rho, J., Ince, T. A., et al. (2009). Live cell imaging distinguishes bona fide human iPS cells from partially reprogrammed cells. *Nature biotechnology* **27**, 1033–1037.

(*279*) Haridhasapavalan, K. K., Raina, K., Dey, C., Adhikari, P., and Thummer, R. P. (2020). An insight into reprogramming barriers to iPSC generation. *Stem cell reviews and reports* **16**, 56–81.

(*280*) Epsztejn-Litman, S., Feldman, N., Abu-Remaileh, M., Shufaro, Y., Gerson, A., Ueda, J., Deplus, R., Fuks, F., Shinkai, Y., and Cedar, H. (2008). De novo DNA methylation promoted by G9a prevents reprogramming of embryonically silenced genes. *Nature structural & molecular biology* **15**, 1176–1183.

(*281*) Vidal, S. E., Amlani, B., Chen, T., Tsirigos, A., and Stadtfeld, M. (2014). Combinatorial modulation of signaling pathways reveals cell-type-specific requirements for highly efficient and synchronous iPSC reprogramming. *Stem cell reports* **3**, 574–584.

(*282*) Hayashi, Y., Hsiao, E. C., Sami, S., Lancero, M., Schlieve, C. R., Nguyen, T., Yano, K., Nagahashi, A., Ikeya, M., and Matsumoto, Y. (2016). BMP-SMAD-ID promotes reprogramming to pluripotency by inhibiting p16/INK4A-dependent senescence. *Proceedings of the National Academy of Sciences* **113**, 13057–13062.

(*283*) Utikal, J., Polo, J. M., Stadtfeld, M., Maherali, N., Kulalert, W., Walsh, R. M., Khalil, A., Rheinwald, J. G., and Hochedlinger, K. (2009). Immortalization eliminates a roadblock during cellular reprogramming into iPS cells. *Nature* **460**, 1145–1148.

(*284*) Collado, M., Blasco, M. A., and Serrano, M. (2007). Cellular senescence in cancer and aging. *Cell* **130**, 223–233.

(*285*) Kawamura, T., Suzuki, J., Wang, Y. V., Menendez, S., Morera, L. B., Raya, A., Wahl, G. M., and Belmonte, J. C. I. (2009). Linking the p53 tumour suppressor pathway to somatic cell reprogramming. *Nature* **460**, 1140–1144.

(*286*) Okita, K., Matsumura, Y., Sato, Y., Okada, A., Morizane, A., Okamoto, S., Hong, H., Nakagawa, M., Tanabe, K., Tezuka, K.-i., et al. (2011). A more efficient method to generate integration-free human iPS cells. *Nature methods* **8**, 409–412.

(*287*) Kuranda, K., Vargaftig, J., de la Rochere, P., Dosquet, C., Charron, D., Bardin, F., Tonnelle, C., Bonnet, D., and Goodhardt, M. (2011). Age-related changes in human hematopoietic stem/progenitor cells. *Aging cell* **10**, 542–546.

(*288*) Vdovin, A., Lupatov, A. Y., Kholodenko, I., and Yarygin, K. (2015). Comparison of the efficiency of viral transduction and episomal transfection in human fibroblast reprogramming. *Bulletin of experimental biology and medicine* **160**, 123–128.

(*289*) Papapetrou, E. P., Tomishima, M. J., Chambers, S. M., Mica, Y., Reed, E., Menon, J., Tabar, V., Mo, Q., Studer, L., and Sadelain, M. (2009). Stoichiometric and temporal requirements of Oct4, Sox2, Klf4, and c-Myc expression for efficient human iPSC induction and differentiation. *Proceedings of the National Academy of Sciences* **106**, 12759–12764.

(*290*) Kim, S.-I., Oceguera-Yanez, F., Hirohata, R., Linker, S., Okita, K., Yamada, Y., Yamamoto, T., Yamanaka, S., and Woltjen, K. (2015). KLF4 N-terminal variance modulates induced reprogramming to pluripotency. *Stem Cell Reports* **4**, 727–743.

(*291*) Lesueur, L. L., Mir, L. M., and André, F. M. (2016). Overcoming the specific toxicity of large plasmids electrotransfer in primary cells in vitro. *Molecular Therapy-Nucleic Acids* **5**.

(*292*) Okita, K., Yamakawa, T., Matsumura, Y., Sato, Y., Amano, N., Watanabe, A., Goshima, N., and Yamanaka, S. (2013). An efficient nonviral method to generate integration-free human-induced pluripotent stem cells from cord blood and peripheral blood cells. *Stem cells* **31**, 458–466.

(*293*) Chan, H. Y., Sivakamasundari, Xing, X., Kraus, P., Yap, S. P., Ng, P., Lim, S. L., and Lufkin, T. (2011). Comparison of IRES and F2A-based locus-specific multicistronic expression in stable mouse lines. *PloS one* **6**, e28885.

(*294*) Lakshmipathy, U., and Vemuri, M. C., *Pluripotent Stem Cells: Methods and Protocols*; Springer: 2013.

(*295*) Crespo, M., Vilar, E., Tsai, S.-Y., Chang, K., Amin, S., Srinivasan, T., Zhang, T., Pipalia, N. H., Chen, H. J., Witherspoon, M., et al. (2017). Colonic organoids derived from human induced pluripotent stem cells for modeling colorectal cancer and drug testing. *Nature medicine* **23**, 878–884.

(*296*) Grinman, D. Y., Takyar, F. M., Dann, P., Hens, J. R., Marmol, C., Lee, J., Choi, J., Chodosh, L. A., Sola, M. E. G., and Wysolmerski, J. J. (2022). PTHrP induces STAT5 activation, secretory differentiation and accelerates mammary tumor development. *Breast Cancer Research* **24**, 1–23.

(*297*) Boras-Granic, K., VanHouten, J., Hiremath, M., and Wysolmerski, J. (2011). Parathyroid hormone-related protein is not required for normal ductal or alveolar development in the post-natal mammary gland. *PLoS One* **6**, e27278.

(*298*) Carron, J., Fraser, W., and Gallagher, J. (1997). PTHrP and the PTH/PTHrP receptor are co-expressed in human breast and colon tumours. *British journal of cancer* **76**, 1095–1098.

(*299*) He, Y., Sun, M. M., Zhang, G. G., Yang, J., Chen, K. S., Xu, W. W., and Li, B. (2021). Targeting PI3K/Akt signal transduction for cancer therapy. *Signal transduction and targeted therapy* **6**, 425.

(*300*) Butti, R., Das, S., Gunasekaran, V. P., Yadav, A. S., Kumar, D., and Kundu, G. C. (2018). Receptor tyrosine kinases (RTKs) in breast cancer: signaling, therapeutic implications and challenges. *Molecular cancer* **17**, 1–18.

(*301*) Jamaludin, S., Azimi, I., Davis, F., Peters, A., Gonda, T., Thompson, E., Roberts-Thomson, S., and Monteith, G. (2018). Assessment of CXC ligand 12-mediated calcium signalling and its regulators in basal-like breast cancer cells. *Oncology letters* **15**, 4289–4295.

(*302*) Xu, C., Zhao, H., Chen, H., and Yao, Q. (2015). CXCR4 in breast cancer: oncogenic role and therapeutic targeting. *Drug design, development and therapy* **9**, 4953.

(*303*) Dewan, M., Ahmed, S., Iwasaki, Y., Ohba, K., Toi, M., and Yamamoto, N. (2006). Stromal cell-derived factor-1 and CXCR4 receptor interaction in tumor growth and metastasis of breast cancer. *Biomedicine & pharmacotherapy* **60**, 273–276.

(*304*) Aran, D., Camarda, R., Odegaard, J., Paik, H., Oskotsky, B., Krings, G., Goga, A., Sirota, M., and Butte, A. J. (2017). Comprehensive analysis of normal adjacent to tumor transcriptomes. *Nature communications* **8**, 1077.

(*305*) Zhou, X., Zheng, Z., Li, Y., Zhao, W., Lin, Y., Zhang, J., and Sun, Q. (2021). The clinical features and prognosis of patients with mucinous breast carcinoma compared with those with infiltrating ductal carcinoma: a population-based study. *BMC cancer* **21**, 536.

(*306*) Woelfle, U., Sauter, G., Santjer, S., Brakenhoff, R., and Pantel, K. (2004). Down-regulated expression of cytokeratin 18 promotes progression of human breast cancer. *Clinical cancer research* **10**, 2670–2674.

(*307*) Libring, S., Shinde, A., Chanda, M. K., Nuru, M., George, H., Saleh, A. M., Abdullah, A., Kinzer-Ursem, T. L., Calve, S., Wendt, M. K., et al. (2020). The dynamic relationship of breast cancer cells and fibroblasts in fibronectin accumulation at primary and metastatic tumor sites. *Cancers* **12**, 1270.

(*308*) Shinde, A., Libring, S., Alpsoy, A., Abdullah, A., Schaber, J. A., Solorio, L., and Wendt, M. K. (2018). Autocrine Fibronectin Inhibits Breast Cancer MetastasisAutocrine Fibronectin Limits Metastasis. *Molecular Cancer Research* **16**, 1579–1589.

(*309*) Wang, J. P., and Hielscher, A. (2017). Fibronectin: how its aberrant expression in tumors may improve therapeutic targeting. *Journal of Cancer* **8**, 674.

(*310*) Erler, J. T., Bennewith, K. L., Cox, T. R., Lang, G., Bird, D., Koong, A., Le, Q.-T., and Giaccia, A. J. (2009). Hypoxia-induced lysyl oxidase is a critical mediator of bone marrow cell recruitment to form the premetastatic niche. *Cancer cell* **15**, 35–44.

(*311*) Hapke, R. Y., and Haake, S. M. (2020). Hypoxia-induced epithelial to mesenchymal transition in cancer. *Cancer letters* **487**, 10–20.

(*312*) Ziegler, U., and Stidwill, R. P. (1992). The attachment of nematocytes from the primitive invertebrate Hydra to fibronectin is specific and RDG-dependent. *Experimental cell research* **202**, 281–286.

(*313*) Shiomi, T., and Okada, Y. (2003). MT1-MMP and MMP-7 in invasion and metastasis of human cancers. *Cancer and metastasis reviews* **22**, 145–152.

(*314*) Cabral-Pacheco, G. A., Garza-Veloz, I., Castruita-De la Rosa, C., Ramirez-Acuna, J. M., Perez-Romero, B. A., Guerrero-Rodriguez, J. F., Martinez-Avila, N., and Martinez-Fierro, M. L. (2020). The roles of matrix metalloproteinases and their inhibitors in human diseases. *International journal of molecular sciences* **21**, 9739.

(*315*) Pereira, I. T., Ramos, E. A., Costa, E. T., Camargo, A. A., Manica, G. C., Klassen, L. M., Chequin, A., Braun-Prado, K., de O. Pedrosa, F., Souza, E. M., et al. (2014). Fibronectin affects transient MMP2 gene expression through DNA demethylation changes in non-invasive breast cancer cell lines. *PLoS One* **9**, e105806.

(*316*) Tam, E. M., Moore, T. R., Butler, G. S., and Overall, C. M. (2004). Characterization of the distinct collagen binding, helicase and cleavage mechanisms of matrix metalloproteinase 2 and 14 (gelatinase A and MT1-MMP): the differential roles of the MMP hemopexin c domains and the MMP-2 fibronectin type II modules in collagen triple helicase activities. *Journal of Biological Chemistry* **279**, 43336–43344.

(*317*) Balachander, G. M., Kotcherlakota, R., Nayak, B., Kedaria, D., Rangarajan, A., and Chatterjee, K. (2021). 3D tumor models for breast cancer: Whither we are and what we need. *Acs Biomaterials Science & Engineering* **7**, 3470–3486.

(*318*) Das, S., Banerji, A., Frei, E., and Chatterjee, A. (2008). Rapid expression and activation of MMP-2 and MMP-9 upon exposure of human breast cancer cells (MCF-7) to fibronectin in serum free medium. *Life sciences* **82**, 467–476.

(*319*) Mitra, A., Chakrabarti, J., Banerji, A., Das, S., and Chatterjee, A. (2006). Culture of human cervical cancer cells, SiHa, in the presence of fibronectin activates MMP-2. *Journal of cancer research and clinical oncology* **132**, 505–513.

(*320*) Moroz, A., Delella, F. K., Lacorte, L. M., Deffune, E., and Felisbino, S. L. (2013). Fibronectin induces MMP2 expression in human prostate cancer cells. *Biochemical and biophysical research communications* **430**, 1319–1321.

(*321*) Koontongkaew, S., Amornphimoltham, P., Monthanpisut, P., Saensuk, T., and Leelakriangsak, M. (2012). Fibroblasts and extracellular matrix differently modulate MMP activation by primary and metastatic head and neck cancer cells. *Medical oncology* **29**, 690–703.

(*322*) Munshi, H. G., Wu, Y. I., Mukhopadhyay, S., Ottaviano, A. J., Sassano, A., Koblinski, J. E., Platanias, L. C., and Stack, M. S. (2004). Differential regulation of membrane type 1-matrix metalloproteinase activity by ERK 1/2-and p38 MAPK-modulated tissue inhibitor of metalloproteinases 2 expression controls transforming growth factor-β1-induced pericellular collagenolysis. *Journal of Biological Chemistry* **279**, 39042–39050.

(*323*) Ignotz, R. A., and Massague, J. (1986). Transforming growth factor-beta stimulates the expression of fibronectin and collagen and their incorporation into the extracellular matrix. *Journal of Biological Chemistry* **261**, 4337–4345.

(*324*) Liu, F., Gu, L.-N., Shan, B.-E., Geng, C.-Z., and Sang, M.-X. (2016). Biomarkers for EMT and MET in breast cancer: An update. *Oncology letters* **12**, 4869–4876.

(*325*) Azzarelli, R., Ori, M., Philpott, A., and Simons, B. D. (2021). Three-dimensional model of glioblastoma by co-culturing tumor stem cells with human brain organoids. *Biology Open* **10**, bio056416.

(*326*) Takebe, T., Zhang, B., and Radisic, M. (2017). Synergistic engineering: organoids meet organs-on-a-chip. *Cell stem cell* **21**, 297–300.

(*327*) Liu, C., Oikonomopoulos, A., Sayed, N., and Wu, J. C. (2018). Modeling human diseases with induced pluripotent stem cells: from 2D to 3D and beyond. *Development* **145**, dev156166.

(*328*) Aisenbrey, E. A., and Murphy, W. L. (2020). Synthetic alternatives to Matrigel. *Nature Reviews Materials* **5**, 539–551.

(*329*) Homan, K. A., Gupta, N., Kroll, K. T., Kolesky, D. B., Skylar-Scott, M., Miyoshi, T., Mau, D., Valerius, M. T., Ferrante, T., Bonventre, J. V., et al. (2019). Flow-enhanced vascularization and maturation of kidney organoids in vitro. *Nature methods* **16**, 255–262.

(*330*) Nunes, S. S., Miklas, J. W., Liu, J., Aschar-Sobbi, R., Xiao, Y., Zhang, B., Jiang, J., Massé, S., Gagliardi, M., Hsieh, A., et al. (2013). Biowire: a platform for maturation of human pluripotent stem cell–derived cardiomyocytes. *Nature methods* **10**, 781–787.

(*331*) Huh, D., Matthews, B. D., Mammoto, A., Montoya-Zavala, M., Hsin, H. Y., and Ingber, D. E. (2010). Reconstituting organ-level lung functions on a chip. *Science* **328**, 1662–1668.

(*332*) Boix-Montesinos, P., Soriano-Teruel, P. M., Arminan, A., Orzáez, M., and Vicent, M. J. (2021). The past, present, and future of breast cancer models for nanomedicine development. *Advanced drug delivery reviews* **173**, 306–330.

(*333*) Wensink, G. E., Elias, S. G., Mullenders, J., Koopman, M., Boj, S. F., Kranenburg, O. W., and Roodhart, J. M. (2021). Patient-derived organoids as a predictive biomarker for treatment response in cancer patients. *NPJ precision oncology* **5**, 30.

(*334*) Ben-David, U., Ha, G., Tseng, Y.-Y., Greenwald, N. F., Oh, C., Shih, J., McFarland, J. M., Wong, B., Boehm, J. S., Beroukhim, R., et al. (2017). Patient-derived xenografts undergo mouse-specific tumor evolution. *Nature genetics* **49**, 1567–1575.

(*335*) Bleul, T., Zhuang, X., Hildebrand, A., Lange, C., Böhringer, D., Schlunck, G., Reinhard, T., and Lapp, T. (2021). Different innate immune responses in BALB/c and C57BL/6 strains following corneal transplantation. *Journal of Innate Immunity* **13**, 49–59.

(*336*) Chen, B., Liu, H., Liu, Z., and Yang, F. (2023). Benefits and limitations of humanized mouse models for human red blood cell-related disease research. *Frontiers in Hematology* **1**, 1062705.

(*337*) Franchi, M., Piperigkou, Z., Karamanos, K.-A., Franchi, L., and Masola, V. (2020). Extracellular matrix-mediated breast cancer cells morphological alterations, invasiveness, and microvesicles/exosomes release. *Cells* **9**, 2031.

(*338*) Whatcott, C. J., Diep, C. H., Jiang, P., Watanabe, A., LoBello, J., Sima, C., Hostetter, G., Shepard, H. M., Von Hoff, D. D., and Han, H. (2015). Desmoplasia in primary tumors and metastatic lesions of pancreatic cancerfibrosis in pancreatic metastases. *Clinical cancer research* **21**, 3561–3568.

(*339*) Xu, S., Xu, H., Wang, W., Li, S., Li, H., Li, T., Zhang, W., Yu, X., and Liu, L. (2019). The role of collagen in cancer: from bench to bedside. *Journal of translational medicine* **17**, 1–22.

(*340*) Szvicsek, Z., Oszvald, Á., Szabó, L., Sándor, G. O., Kelemen, A., Soós, A. Á., Pálóczi, K., Harsányi, L., Tölgyes, T., Dede, K., et al. (2019). Extracellular vesicle release from intestinal organoids is modulated by Apc mutation and other colorectal cancer progression factors. *Cellular and Molecular Life Sciences* **76**, 2463–2476.

(*341*) Chaudhuri, O., Koshy, S. T., Branco da Cunha, C., Shin, J.-W., Verbeke, C. S., Allison, K. H., and Mooney, D. J. (2014). Extracellular matrix stiffness and composition jointly regulate the induction of malignant phenotypes in mammary epithelium. *Nature materials* **13**, 970–978.

(*342*) Mao, B.-H., Thi, K. M. N., Tang, M.-J., Kamm, R. D., and Tu, T.-Y. (2023). The interface stiffness and topographic feature dictate interfacial invasiveness of cancer spheroids. *Biofabrication* **15**, 015023.

(*343*) Wei, J., Hu, M., Huang, K., Lin, S., and Du, H. (2020). Roles of proteoglycans and glycosaminoglycans in cancer development and progression. *International journal of molecular sciences* **21**, 5983.

(*344*) Yasuda, M., Tanaka, Y., Fujii, K., and Yasumoto, K. (2001). CD44 stimulation down-regulates Fas expression and Fas-mediated apoptosis of lung cancer cells. *International immunology* **13**, 1309–1319.

(*345*) Kuang, D.-M., Zhao, Q., Xu, J., Yun, J.-P., Wu, C., and Zheng, L. (2008). Tumor-educated tolerogenic dendritic cells induce CD3ε down-regulation and apoptosis of T cells through oxygen-dependent pathways. *The Journal of Immunology* **181**, 3089–3098.

(*346*) Vitale, D., Kumar Katakam, S., Greve, B., Jang, B., Oh, E.-S., Alaniz, L., and Götte, M. (2019). Proteoglycans and glycosaminoglycans as regulators of cancer stem cell function and therapeutic resistance. *The FEBS Journal* **286**, 2870–2882.

(*347*) Ibrahim, S. A., Hassan, H., Vilardo, L., Kumar, S. K., Kumar, A. V., Kelsch, R., Schneider, C., Kiesel, L., Eich, H. T., Zucchi, I., et al. (2013). Syndecan-1 (CD138) modulates triple-negative breast cancer stem cell properties via regulation of LRP-6 and IL-6-mediated STAT3 signaling. *PloS one* **8**, e85737.

(*348*) Hu, D., Li, Z., Zheng, B., Lin, X., Pan, Y., Gong, P., Zhuo, W., Hu, Y., Chen, C., Chen, L., et al. (2022). Cancer-associated fibroblasts in breast cancer: Challenges and opportunities. *Cancer Communications* **42**, 401–434.

(*349*) Xing, F., Saidou, J., and Watabe, K. (2010). Cancer associated fibroblasts (CAFs) in tumor microenvironment. *Frontiers in bioscience: a journal and virtual library* **15**, 166.

(*350*) Gu, G., Dustin, D., and Fuqua, S. A. (2016). Targeted therapy for breast cancer and molecular mechanisms of resistance to treatment. *Current opinion in pharmacology* **31**, 97–103.

(*351*) Lee, J. (2023). Current Treatment Landscape for Early Triple-Negative Breast Cancer (TNBC). *Journal of Clinical Medicine* **12**, 1524.

(*352*) Umemura, S., Yoshida, S., Ohta, Y., Naito, K., Osamura, R. Y., and Tokuda, Y. (2007). Increased phosphorylation of Akt in triple-negative breast cancers. *Cancer science* **98**, 1889–1892.

(*353*) Vijay, G. V., Zhao, N., Den Hollander, P., Toneff, M. J., Joseph, R., Pietila, M., Taube, J. H., Sarkar, T. R., Ramirez-Pena, E., Werden, S. J., et al. (2019). GSK3β regulates epithelial-mesenchymal transition and cancer stem cell properties in triple-negative breast cancer. *Breast Cancer Research* **21**, 1–14.

(*354*) Flowers, A., Chu, Q. D., Panu, L., Meschonat, C., Caldito, G., Lowery-Nordberg, M., and Li, B. D. (2009). Eukaryotic initiation factor 4E overexpression in triple-negative breast cancer predicts a worse outcome. *Surgery* **146**, 220–226.

(*355*) Oh, S., Kim, H., Nam, K., and Shin, I. (2017). Glut1 promotes cell proliferation, migration and invasion by regulating epidermal growth factor receptor and integrin signaling in triple-negative breast cancer cells. *BMB reports* **50**, 132.

(*356*) American Cancer Society Survival Rates for Breast Cancer https://www.cancer.org/cancer/types/breast-cancer/understanding-a-breast-cancer-diagnosis/breast-cancer-survival-rates.html (accessed July 19, 2023).

(*357*) Riggio, A. I., Varley, K. E., and Welm, A. L. (2021). The lingering mysteries of metastatic recurrence in breast cancer. *British journal of cancer* **124**, 13–26.

(*358*) Freedman, B. S., Brooks, C. R., Lam, A. Q., Fu, H., Morizane, R., Agrawal, V., Saad, A. F., Li, M. K., Hughes, M. R., Werff, R. V., et al. (2015). Modelling kidney disease with CRISPR-mutant kidney organoids derived from human pluripotent epiblast spheroids. *Nature communications* **6**, 8715.

Appendix

Additonal information on iPSC lines

A

To access additional information on iPSC lines, including characterization data, ethics or cell culture details, QR codes can be scanned to access the hPSCreg database. As an alternative, the web links listed in the table below can also be used.

QR codes:

Weblinks:

iPSC clone identifier	Weblink	Reference
NMIi010-A	https://hpscreg.eu/cell-line/NMIi010-A	(Keller, Binner et al. 2021)
NMIi011-A	https://hpscreg.eu/cell-line/NMIi011-A	(Keller, Binner et al. 2022)
NMIi011-B	https://hpscreg.eu/cell-line/NMIi011-B	
NMIi011-C	https://hpscreg.eu/cell-line/NMIi011-C	
NMIi011-D	https://hpscreg.eu/cell-line/NMIi011-D	
NMIi012-B	https://hpscreg.eu/cell-line/NMIi012-B	(Keller, Greis et al. 2022)
NMIi012-D	https://hpscreg.eu/cell-line/NMIi012-D	
NMIi012-E	https://hpscreg.eu/cell-line/NMIi012-E	

Stem Cell Research 64 (2022) 102902

Contents lists available at ScienceDirect

Stem Cell Research

journal homepage: www.elsevier.com/locate/scr

Lab Resource: Multiple Cell Lines

Establishment of Four Induced Pluripotent Stem Cell Lines from CD34+ Hematopoietic Stem and Progenitor Cells from a Patient Diagnosed with an Invasive Lobular Mammary Carcinoma

Anna-Lena Keller [a,*], Anna Binner [a], Katja Schenke-Layland [a,b,c], Christian Schmees [a,*]

[a] NMI Natural and Medical Sciences Institute at the University of Tuebingen, Reutlingen, Germany
[b] Institute of Biomedical Engineering, Department for Medical Technologies and Regenerative Medicine, Eberhard Karls University Tuebingen, 72076 Tuebingen, Germany
[c] Cluster of Excellence iFIT (EXC2180) "Image-Guided and Functionally Instructed Tumor Therapies", Eberhard Karls University Tuebingen, Tuebingen 72076, Germany

A B S T R A C T

CD34+ cells were isolated from peripheral blood of a breast cancer patient. By the introduction of five integration-free episomal vectors, the CD34+ cells were successfully reprogrammed and resulted in four iPSC clones. Flow Cytometry, reverse transcriptase PCR and immunocytochemistry confirm a robust expression of pluripotency factors and the concomitant loss of exogenous reprogramming plasmids. The maintenance of genomic integrity was confirmed by array-based comparative genomic hybridization and iPSCs harbored the capacity to differentiate into all three germ layers. Here, we present the generation and characterization of four iPSC lines that will find application in the field of breast cancer research.

Resource Table:

Unique stem cell lines identifier	NMIi011-A NMIi011-B NMIi011-C NMIi011-D
Alternative names of stem cell lines	B1.4 (NMIi011-A) B1.6 (NMIi011-B) B1.7 (NMIi011-C) B1.10 (NMIi011-D)
Institution	NMI Natural and Medical Sciences Institute at the University of Tuebingen, Markwiesenstrasse 55, 72,770 Reutlingen
Contact information of distributor	Dr. Christian Schmees (christian.schmees@nmi.de)
Type of cell lines	Induced pluripotent stem cells (iPSCs)
Origin	Human Age: 77 Sex: female Ethnicity if known: n/a
Cell Source	CD34+ hematopoietic stem and progenitor cells isolated from peripheral blood mononuclear cells (PBMCs)
Clonality	Clonal
Method of reprogramming	Episomal reprogramming
Genetic Modification	No
Type of Genetic Modification	No genetic modification
Evidence of the reprogramming transgene loss	RT-PCR
Associated disease	Breast cancer (invasive lobular carcinoma)
Gene/locus	No mutation or genetic variation detectable
Date archived/stock date	11.03.2021 (date of generation)
Cell line repository/bank	NMIi011-A: https://hpscreg.eu/user/cellline/edit/NMIi011-A NMIi011-B: https://hpscreg.eu/user/cellline/edit/NMIi011-B NMIi011-C: https://hpscreg.eu/user/cellline/edit/NMIi011-C NMIi011-D: https://hpscreg.eu/user/cellline/edit/NMIi011-D
Ethical approval	*Ethics Committee at the Medical Faculty of the Eberhard Karls University and at the University Hospital Tübingen* *Chairmenship:* *Prof. Dr. med. Karl Jaschonek (Chairman)* *Prof. Dr. med. Dr. phil. Urban Wiesing (1st Vice Chairman)* *Prof. Dr. med. Dieter Luft (2nd Vice Chairman)* *Members:* *Prof. Dr. med. Berthold Drexler* *Prof. Dr. med. Jürgen Honegger* *Prof. Dr. med. dent. Bernd Koos* *Prof. Dr. phil. Dipl. Psych. Stefan Klingberg* *Prof. Dr. med. Holger Lerche* *Prof. Dr. rer. nat. Peter Martus*

(continued on next column)

(continued)

(continued on next page)

* Corresponding authors.

https://doi.org/10.1016/j.scr.2022.102902
Received 22 July 2022; Received in revised form 1 August 2022; Accepted 22 August 2022
Available online 26 August 2022

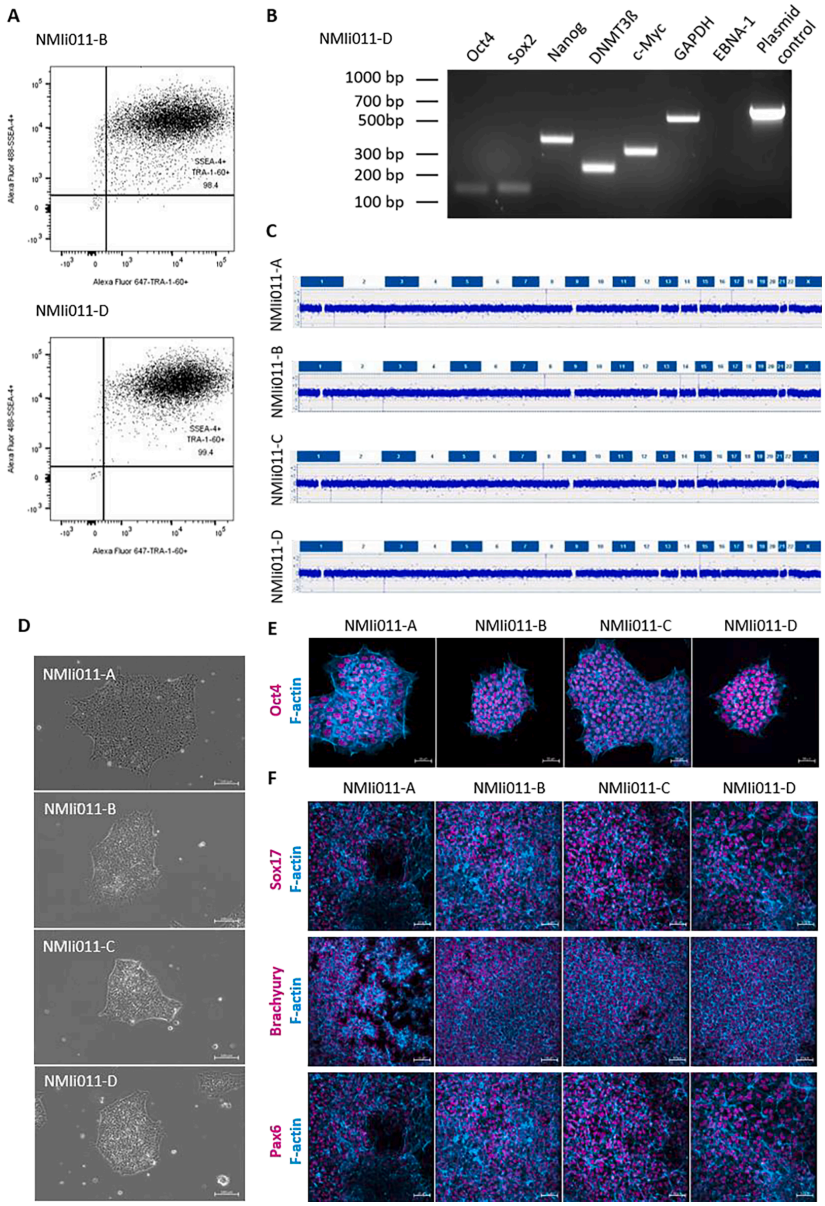

Fig. 1. Characterization overview of the four iPSC lines.

(*continued*)

Prof. Dr. med. Klaus Mörike
Prof. Dr. med. Christian F. Poets
Ulrike Röllecke
Prof. Dr. iur. Dr. h. c. Georg Sandberger

Approval number:
888/2019BO2

1. Resource utility

Besides being known to be one of the leading causes of death among women worldwide, breast cancer is associated with early recurrence and diagnosis at young age. The targeted differentiation of iPSCs into mammary-like organoids will be used as a disease modelling tool and might open new paths towards a better understanding of breast cancer.

Table 1
Characterization and validation.

Classification	Test	Result	Data
Morphology	Bright field microscopy	Normal iPSC morphology	Fig. 1 panel D
Phenotype	Qualitative analysis (Immunofluorescence staining)	Expression of the pluripotency markers OCT4, SOX2, NANOG, SSEA4 and TRA-1-81 shown by immunofluorescence staining	Fig. 1 panel E
	Quantitative analysis	Double positive expression of the pluripotency surface markers SSEA4 and TRA-1-60	Fig. 1 panel A
	(Flow cytometry)		Supplementary Fig. 1 panel A
Genotype	Array-based comparative genomic hybridization (array-CGH)	46XX, Resolution: 5–10 Mb	Fig. 1 panel C
Identity	Short tandem repeat (STR) analysis	DNA profiling performed 17 sites tested, 100 % match	Submitted in archive with journal
Mutation analysis (IF APPLICABLE)	Sequencing	n/a	n/a
	Southern Blot OR WGS	n/a	n/a
Microbiology and virology	Mycoplasma	Negative mycoplasma testing confirmed by PCR	Supplementary Fig. 1 panel C
Differentiation potential	Directed differentiation	Differentiation potential into all three germ layers confirmed by directed differentiation and subsequent immunofluorescence staining. Endoderm: SOX17, FOXA2 Mesoderm: Brachyury, Nestin Ectoderm: PAX6, NCAM	Fig. 1 panel F
Donor screening (OPTIONAL)	HIV 1 + 2 Hepatitis B, Hepatitis C	n/a	n/a
Genotype additional info (OPTIONAL)	Blood group genotyping	n/a	n/a
	HLA tissue typing	n/a	n/a

2. Resource details

Despite the growing knowledge in the field of oncology and improved treatment options, breast cancer remains one of the most frequently diagnosed neoplasms in women while the mortality rate associated with this disease remains alarmingly high (Valdés-Mora et al., 2021). For the treatment of this complex disease, the principle "one size does not fit all" applies very well due to the wide heterogeneity in receptor statuses and the cellular composition of breast cancers (Naik et al., 2020). Therefore, it is a pressing task to improve the understanding of underlying molecular features of breast cancer and its ability to spread to other tissues. iPSCs harbour the capacity to differentiate into organoid structures which hold great promises in clinical translatability and disease modelling (Qu et al., 2017). We have previously reported the generation of an iPSC line from peripheral blood of a healthy individual (Keller et al., 2021 Jul). Here, we show the successful generation and characterization of four iPSC lines derived from CD34+ cells isolated from PBMCs of a patient diagnosed with an invasive lobular mammary carcinoma. After CD34+ cell isolation and further expansion for 7 days, the progenitor cells were transfected via electroporation with 5 episomal plasmids encoding for Oct4, Sox2, Klf4, L-Myc, mp53DD and EBNA1, respectively (Okita et al., 2011 May). The cells were cultured for 18–21 days on Matrigel®-coated plates in ReproTeSR™ medium until first iPSC colonies arose which displayed a typical round-shaped phenotype with densely packed colony cores and prominent cell nuclei (Fig. 1 D). After iPSC expansion, a profound analysis of multiple iPSC characteristics was performed. We first confirmed the absence of potential mycoplasma contaminations by analysing the cell culture supernatants of all four iPSC lines by PCR (Supplementary Fig. 1 C). Secondly, the iPSCs were investigated for single nucleotide polymorphism and genetic aberrations by array-CGH which revealed genomic integrity in all four clones (Fig. 1 C). Array-CGH does not detect balanced chromosome rearrangements. Next, short tandem repeat (STR) analysis identified a 100 % allele match between the four different iPSC clones (data submitted in archive with journal). Furthermore, expression of the pluripotency markers Oct4 (Fig. 1 E), Sox2, Nanog, SSEA4 and TRA-1-81 (data not shown) was confirmed by immunofluorescence staining. For quantitative analysis of pluripotency marker expression, the surface markers SSEA4 and TRA-1-60 were analysed by flow cytometry and showed a robust co-expression in all iPSC lines (Fig. 1 A, Supplementary Fig. 1 A). To prove silencing of exogenously introduced plasmids together with endogenous expression of pluripotency markers, reverse transcriptase PCR (RT-PCR) was performed (Fig. 1 B). To this end, RNA was isolated and complementary DNA (cDNA) was synthesized with reverse transcriptase. PCR confirmed the endogenous expression of the pluripotency markers Oct4, Sox2, Nanog, DNMT3β, c-Myc and the house-keeping gene GAPDH. Exogenously introduced plasmids were silenced as shown by the absence of EBNA1 expression. Reprogramming vectors were used as a positive control. One major characteristics of pluripotent stem cells is their capacity to differentiate into all the three germ layers. The commitment to the three lineages upon in vitro directed differentiation was confirmed by immunofluorescence staining. Endodermal differentiation was proven by the expression of the transcription factors SOX17 and FOXA2 while mesodermal commitment was shown by a positive Brachyury and Nestin staining. Differentiation into the ectodermal lineage was visualized by PAX6 and CD56/NCAM expression (Exemplary images for SOX17, Brachyury and PAX6 are depicted in Fig. 1 F. Remaining stainings are not shown). Taken together, we present four well-characterized iPSC lines generated from CD34+ cells from a breast cancer patient that will be used for tissue and disease modelling in the field of breast cancer research.

3. Materials and methods

3.1. Reprogramming of CD34+ cells into iPSCs

For reprogramming of CD34+ cells into iPSCs, the CD34+ progenitor kit (STEMCELL Technologies) was used according to the manufacturer's manual. In short, CD34+ cells were isolated from PBMCs by positive selection and expanded for 7 days prior to electroporation with the *P*3 primary cell 4D-Nucleofector™ kit (Lonza). For transfection, Epi5 episomal reprogramming vectors (ThermoFisher Scientific) were introduced into the cells. Cells were transferred to a Matrigel®(Corning)-

Table 2
Reagents details. *RRID Requirement for antibodies*: use http://antibodyregistry.org/ to retrieve RRID for antibodies and include ID in table as shown in examples.

	Antibodies used for immunocytochemistry/flow-cytometry			
	Antibody	**Dilution**	**Company Cat #**	**RRID**
Pluripotency and cell surface markers	anti-human OCT4	1: 200	Cell Signaling Technology, Cat# 2750	RRID: AB_823583
	anti-human NANOG (D73G4)	1: 200	Cell Signaling Technology, Cat# 4903	RRID: AB_10559205
	anti-human SOX2 (D6D9)	1:400	Cell Signaling Technology, Cat# 3579	RRID: AB_2195767
	anti-human SSEA4 (MC813)	1:500	Cell Signaling Technology, Cat# 4755	RRID:AB_126425
	Alexa Fluor® 488 anti-human SSEA4 (MC-813-70)	1:30	BioLegend, Cat# 330,411	RRID: AB_1089199
	anti-human TRA-1-81	1:1000	Cell Signaling Technology, Cat# 4745	RRID: AB_2119060
	Alexa Fluor® 647 anti-human TRA-1-60-R	1:30	BioLegend, Cat# 330,605	RRID: AB_1227813
Differentiation markers	anti-human SOX17 (D1T8M)	1:1000	Cell Signaling Technology, Cat# 81,778	RRID: AB_2650582
	anti-human FOXA2 (ERP4466)	1:250	Abcam, Cat# ab108422	RRID: AB_11157157
	anti-human Brachyury (ERP18113)	1:1000	Abcam, Cat# ab209665	RRID: AB_2750925
	anti-human Nestin (10C2)	1:100	STEMCELL Technologies, Cat# 60091AD.1	RRID: AB_2650581
	anti-human PAX6 (EPR15858)	1:350	Abcam, Cat# ab195045	RRID: AB_2750924
	anti-human NCAM/CD56 (HCD56)	1:100	STEMCELL Technologies, Cat# 60021AD.1	RRID: AB_2891082
Nuclear marker	Hoechst 33,258	1:250	ThermoFisher Scientific, Cat# H3569	RRID: AB_2651133
F-actin markers	Phalloidin CruzFluor™ 594 conjugate	1:1000	Santa Cruz Biotechnnology, Cat# sc-363795	
	Phalloidin-tetramethylrhodamine conjugate	1:1000	Santa Cruz Biotechnnology, Cat# sc-362065	
Secondary antibodies	anti-rabbit Alexa Fluor® 488	1:1000	Abcam, Cat# ab150073	RRID:AB_2636877
	Cy5-AffiniPure Goat anti-Rabbit	1:1000	Jackson ImmunoResearch Labs Cat# 111-175-144	RRID:AB_2338013
	Cy5-AffiniPure Goat anti-Mouse	1:1000	Jackson ImmunoResearch Labs Cat# 115-175-146	RRID:AB_2338713
	Primers			
	Target	**Size of band**	**Forward/Reverse primer (5′-3′)**	
Episomal plasmids (RT-PCR)	EBNA1	666 bp	ATCGTCAAAGCTGCACACAG/CCCAGGAGTCCCAGTCA	
Pluripotency marker (endogenous) (RT-PCR)	OCT4	144 bp	GACAGGGGGAGGGGAGGAGCTAGG/ CTTCCCTCCAACCAGTTGCCCCAAAC	
Pluripotency marker (endogenous) (RT-PCR)	NANOG	391 bp	CAGCCCCGATTCTTCCACCAGTCCC/ CGGAAGATTCCCAGTCGGGTTCACC	
Pluripotency marker (endogenous) (RT-PCR)	SOX2	151 bp	GGGAAATGGGAGGGGTGCAAAAGAGG/ TTGCGTGAGTGTGGATGGGATTGGTG	
Pluripotency marker (endogenous) (RT-PCR)	DNMT3β	242 bp	TGCTGCTCACAGGGCCCGATACTTC/ TCCTTTCGAGCTCAGTGCACCACAAAAC	
Pluripotency marker (endogenous) (RT-PCR)	c-Myc	328 bp	GCGTCCTGGGAAGGGAGATCCGGAGC/ TTGAGGGGCATCGTCGCGGGAGGCTG	
House-keeping gene (RT-PCR)	GAPDH	572 bp	TCACCATCTTCCAGGAGCG/CTGCTTCACCACCTTCTTGA	

coated plate and cultivated in ReproTeSR™ medium until first iPSC colonies arose. The colonies were manually picked and further expanded by using mTeSR™ Plus. iPSCs were passaged with Gentle Cell Dissociation Reagent (STEMCELL Technologies) and cultured at 37 °C, 5 % CO_2 and 20 % O_2. iPSC colonies were cryopreserved with CryoStor CS10® freezing medium (STEMCELL Technologies) and kept in liquid N_2 for long time storage. iPSC characterization is summarized in Fig. 1 and Table 1.

3.2. Directed differentiation

One major hallmark of PSCs is their capacity to give rise to the three germ layers. To prove this ability, all four iPSC lines were differentiated into the endoderm, the mesoderm and the ectoderm using the STEMDIFF™ Trilineage differentiation kit (STEMCELL Technologies) according to the manufacturers' instructions. In brief, single cell iPSCs were plated on Matrigel®-coated cell culture plates and incubated with mTeSR1™ overnight. The starting cell number varied among the germ layers. Then, mTeSR1™ was replaced by the appropriate differentiation media. For endodermal and the mesodermal differentiation, media were replaced daily until day 5 while the ectoderm differentiation medium was refreshed daily until day 7. After 5 and 7 days, respectively, cells were ready for immunofluorescence staining (Table 2).

3.3. Immunocytochemistry

iPSCs at passage 8 were fixed with 4 % PFA in 1xPBS for 15 min at room temperature (RT) and washed 3 times with 1xPBS. For blocking and permeabilization, iPSCs were incubated for 2 h at RT with 0.1 % Triton X-100 and 2 % BSA in 1xPBS. iPSCs were decorated with the primary antibodies diluted in blocking and permeabilization solution overnight at 4 °C. Secondary antibodies and counter staining were applied to the cells for 45 min at RT.

3.4. Mycoplasma test

To test for potential mycoplasma contamination, 100 µL of cell culture supernatants at passage 4 were collected and analysed by PCR using the Venor®*GeM* Classic Kit (Minerva Biolabs) according to the manufacturer's protocol.

3.5. Chromosomal integrity

Array-CGH was performed at passage 11 at the Clinical Genetics, Olgahospital Stuttgart, Germany to confirm genetic stability.

3.6. RT-PCr

To confirm the endogenous expression of pluripotency markers and the absence of episomal vectors, RT-PCR was performed at passage 3–13. Therefore, total RNA from 2 × 10^6 cells was isolated using the RNeasy Mini Kit (Qiagen). DNA was degraded for 30 min at 37 °C with the RQ1 Kit (Promega). cDNA synthesis was performed with MuLV reverse transcriptase (New England Biolabs) for 60 min at 42 °C. The PCR products were visualized on a 2 % agarose gel (Table 2).

3.7. Flow cytometry

iPSCs at passage 10 were dissociated into single cells by Accutase™ (STEMCELL Technologies) and stained with conjugated antibodies for 30 min at 4 °C in the dark (Table 2). Flow Cytometry data were acquired at the FACSFortessa platform (BD Biosciences) and analysed with the FlowJo V10 software (FlowJo, LCC).

3.8. STR analysis

Isolation of genomic DNA from all four iPSC lines and subsequent STR analysis was performed by the Institute of Pathology at the Katharinenhospital Stuttgart, Germany.

Declaration of Competing Interest

The authors declare that they have no known competing financial interests or personal relationships that could have appeared to influence the work reported in this paper.

Acknowledgements

We thank Dr. Hans-Jürgen Pander and Dr. Eveline Fiedler from the Institute of Clinical Genetics at the Olgahospital Stuttgart, Dr. Dieter Techel from the Institute of Pathology at the Katharinenhospital Stuttgart and Prof. Dr. Martin Weiss from the Department of Women's Healthy at the University of Tuebingen, Germany for their valuable feedback and excellent technical support. This work received financial support from the State Ministry of Baden-Wuerttemberg for Economic Affairs, Labour and Housing Construction (Grant No. 3-4332.62-HSG/84)

Appendix A. Supplementary data

Supplementary data to this article can be found online at https://doi.org/10.1016/j.scr.2022.102902.

References

Keller, A.L., Binner, A., Breitmeyer, R., Vogel, S., Anderle, N., Rothbauer, U., Schenke-Layland, K., Schmees, C., 2021 Jul. Generation and characterization of the human induced pluripotent stem cell line NMIi010-A from peripheral blood mononuclear cells of a healthy 49-year old male individual. Stem Cell Res. 54, 102427 https://doi.org/10.1016/j.scr.2021.102427. Epub 2021 Jun 11 PMID: 34139596.

Naik, N., Madani, A., Esteva, A., et al., 2020. Deep learning-enabled breast cancer hormonal receptor status determination from base-level H&E stains. Nat. Commun. 11, 5727. https://doi.org/10.1038/s41467-020-19334-3.

Okita, K., Matsumura, Y., Sato, Y., Okada, A., Morizane, A., Okamoto, S., Hong, H., Nakagawa, M., Tanabe, K., Tezuka, K., Shibata, T., Kunisada, T., Takahashi, M., Takahashi, J., Saji, H., Yamanaka, S., 2011 May. A more efficient method to generate integration-free human iPS cells. Nat. Methods 8 (5), 409–412. https://doi.org/10.1038/nmeth.1591. Epub 2011 Apr 3 PMID: 21460823.

Qu, Y., Han, B., Gao, B., Bose, S., Gong, Y., Wawrowsky, K., Giuliano, A.E., Sareen, D., Cui, X., 2017. Differentiation of Human Induced Pluripotent Stem Cells to Mammary-like Organoids. Stem Cell Rep. 8 (2), 205–215.

Valdés-Mora, F., Salomon, R., Gloss, B.S., Law, A.M.K., Venhuizen, J., Castillo, L., Murphy, K.J., Magenau, A., Papanicolaou, M., Rodriguez de la Fuente, L., Roden, D. L., Colino-Sanguino, Y., Kikhtyak, Z., Farbehi, N., Conway, J.R.W., Sikta, N., Oakes, S.R., Cox, T.R., O'Donoghue, S.I., Timpson, P., Ormandy, C.J., Gallego-Ortega, D., 2021. Single-cell transcriptomics reveals involution mimicry during the specification of the basal breast cancer subtype. Cell Rep. 35 (2), 108945.

Stem Cell Research 66 (2023) 102988

Contents lists available at ScienceDirect

Stem Cell Research

journal homepage: www.elsevier.com/locate/scr

Lab Resource: Multiple Cell Lines

Generation and characterization of three induced pluripotent stem cells lines from an 86-year old female individual diagnosed with an invasive lobular mammary carcinoma

Anna-Lena Keller [a,*], Deborah Greis [a], Jana Eybe [a], Sarah Plöger [a], Martin Weiss [a,d], André Koch [d], Sara Y. Brucker [c,d], Katja Schenke-Layland [a,b,c], Christian Schmees [a,*]

[a] NMI – Natural and Medical Sciences Institute at the University of Tuebingen, Reutlingen, Germany
[b] Institute of Biomedical Engineering, Department for Medical Technologies and Regenerative Medicine, Eberhard Karls University Tuebingen, 72076 Tuebingen, Germany
[c] Cluster of Excellence iFIT (EXC2180) "Image-Guided and Functionally Instructed Tumor Therapies", Eberhard Karls University Tuebingen, Tuebingen 72076, Germany
[d] Department of Women's Health, Eberhard Karls University Tuebingen, 72076 Tuebingen, Germany

A B S T R A C T

Invasive lobular carcinoma (ILC) is a distinct type of breast cancer and is accounting up to 10–15 % of all mammary carcinomas showing a pronounced increase in incidence rates over the last two decades. We generated three induced pluripotent stem cell (iPSC) lines from CD34+ progenitor cells isolated from a mammary carcinoma patient diagnosed with ILC. Here, we describe the characterization of the iPSCs by array-based comparative genomic hybridization (array CGH), immunocytochemistry, flow cytometry, reverse transcriptase polymerase chain reaction and directed in vitro differentiation. The iPSC lines will find application in the field of breast cancer research.

Resource Table:

Unique stem cell lines identifier	NMIi012-B NMIi012-D NMIi012-E
Alternative names of stem cell lines	DG2 (NMIi012-B)DG4 (NMIi012-D)DG5 (NMIi012-E)
Institution	NMI Natural and Medical Sciences Institute at the University of Tuebingen, Markwiesenstrasse 55, 72,770 Reutlingen
Contact information of distributor	Dr. Christian Schmees (christian.schmees@nmi.de)Anna-Lena Keller (anna-lena.keller@nmi.de)
Type of cell lines	Induced pluripotent stem cells (iPSCs)
Origin	Human Age: 86 Sex: female Ethnicity if known: n/a
Cell Source	CD34+ hematopoietic stem and progenitor cells isolated from peripheral blood mononuclear cells (PBMCs)
Clonality	Clonal
Method of reprogramming	Episomal reprogramming
Genetic Modification	No
Type of Genetic Modification	No genetic modification
Evidence of the reprogramming transgene loss	Reverse transcriptase polymerase chain reaction (RT-PCR)
Associated disease	Invasive lobular mammary carcinoma (ILC)
Gene/locus	No mutation or genetic variation detectable
Date archived/stock date	19th of November 2021 (date of CD34+ cell reprogramming)
Cell line repository/bank	NMIi012-B: https://hpscreg.eu/cell-line/NMIi012-BNMIi012-D: https://hpscreg.eu/cell-line/NMIi012-DNMIi012-E: https://hpscreg.eu/cell-line/NMIi012-E
Ethical approval	Ethics Committee at the Medical Faculty of the Eberhard Karls University and at the University Hospital Tübingen Chairmenship: *Prof. Dr. med. Karl Jaschonek (Chairman)* *Prof. Dr. med. Dr. phil. Urban Wiesing (1st Vice Chairman)* *Prof. Dr. med. Dieter Luft (2nd Vice Chairman)* Members: *Prof. Dr. med. Berthold Drexler* *Prof. Dr. med. Jürgen Honegger* *Prof. Dr. med. dent. Bernd Koos* *Prof. Dr. phil. Dipl. Psych. Stefan Klingberg*

(continued on next column)

(continued)

(continued on next page)

* Corresponding authors.
E-mail addresses: anna-lena.keller@nmi.de (A.-L. Keller), christian.schmees@nmi.de (C. Schmees).

https://doi.org/10.1016/j.scr.2022.102988
Received 26 October 2022; Received in revised form 30 November 2022; Accepted 1 December 2022
Available online 2 December 2022

Table 1
Characterization and validation.

Classification	Test	Result	Data
Morphology	Bright field microscopy	Normal iPSC morphology	Fig. 1 panel B
Phenotype	Qualitative analysis (Immunofluorescence staining)	Expression of the pluripotency markers: Nanog, TRA-1–81	Fig. 1 panel A
	Quantitative analysis (Flow Cytometry)	Double positive expression of the pluripotency surface markers SSEA4 & TRA-1–60	Fig. 1 panel E
Genotype	Array-based comparative genomic hybridization	46XX, Resolution: 5 – 10 Mb	Fig. 1 panel C
Identity	STR analysis	DNA profiling performed; 17 sites tested, 100 % allele match	Available with the authors
Mutation analysis (IF APPLICABLE)	Sequencing	n/a	n/a
	Southern Blot OR WGS	n/a	n/a
Microbiology and virology	Mycoplasma	Absence of potential mycoplasma contamination confirmed by PCR	Supplementary figure panel B
Differentiation potential	Directed differentiation	Directed differentiation into all three germlayers confirmed by immunofluorescence staining; Endoderm: Sox17, Foxa2 Mesoderm: Brachyury, NCAM Ectoderm: Pax6, Nestin	Fig. 1 panel D
Donor screening (OPTIONAL)	HIV 1 + 2 Hepatitis B, Hepatitis C	n/a	n/a
Genotype additional info (OPTIONAL)	Blood group genotyping	n/a	n/a
	HLA tissue typing	n/a	n/a

(*continued*)

	Prof. Dr. med. Holger Lerche *Prof. Dr. rer. nat. Peter Martus* *Prof. Dr. med. Klaus Mörike* *Prof. Dr. med. Christian F. Poets* *Ulrike Röllecke* *Prof. Dr. iur. Dr. h. c. Georg Sandberger* Approval number: *888/2019BO2*

1. Resource utility

Breast cancer is the leading cause of death among women. After metastasis, the 5-year survival rate declines to only 26 % and metastasized mammary carcinoma are known to be less responsive to chemotherapies. Thus, it is a pressing task to better understand the early features of breast cancer progression. The herein described iPSC lines will be differentiated into organoids of the mammary gland and subsequently used as healthy tissue scaffold for patient-derived microtumors in an autologous manner to study cancer invasion (see Table 1).

2. Resource details

The risk factors that contribute to the evolution of breast cancer are manifold and range from the underlying genetic background, the exposure of exogenous hormones and physical inactivity to an increased alcohol consumption (Cheng et al., 2020). Despite years of intensive laboratory and clinical research, the incidences for breast cancer worldwide rise steadily. Moreover, drug resistance and cancer relapse represent an enormous burden leaving breast cancer as one of the major causes of death among women. Breast cancer can be classified into different categories. ILC is a frequent type of mammary carcinoma and holds a distinct clinical behaviour and morphology compared to the non-specific type (NST) (McCart Reed et al., 2021). Since ILC is generally low grade, this type of cancer is normally associated with a good prognosis. However, ILCs are highly metastatic and thus, ILC is known to have a worse overall long-term outcome compared to NST (Metzger-Filho et al., 2019). Therefore, it remains a pressing task to better understand the mechanisms that lead to metastasis and tumor progression. Here, we describe the generation and characterization of three iPSC lines from a blood sample of a breast cancer patient diagnosed with ILC that will find application in the field of breast cancer research. CD34+ hematopoietic stem and progenitor cells were isolated from peripheral blood mononuclear cells (PBMCs) obtained from a female, treatment-naïve breast cancer patient (Mack et al., 2011). After initial isolation, CD34+ cells were expanded for 7 days in StemSpan™ CD34+ Expansion medium. Electroporation was performed to transfect the cells with episomal vectors that deliver five reprogramming factors: Oct4, Sox2, L-Myc, Klf4, Lin28, mp53DD and EBNA1 (Okita et al., 2013). First iPSC colonies appeared after 18 days. The colonies were manually picked and further expanded in mTeSR™ Plus medium on Matrigel®-coated cell culture plates. The iPSC colonies showed a typical iPSC-like structure exhibiting a circular phenotype consisting of closely packed, small cells (Fig. 1B). After a few passages, a profound characterization of the iPSC clones was undertaken. First, supernatants were collected and analysed for potential mycoplasma contamination, the absence of which, however, was confirmed by PCR (supplementary figure B). Next, we investigated the iPSCs for their expression of pluripotency markers. We confirmed a positive expression of Sox2 and TRA-1–81 (Fig. 1A) via immunofluorescence (IF) staining as well as SSEA4 and TRA-1–60 by flow cytometry (Fig. 1E). Reverse transcriptase PCR was performed to confirm that iPSCs endogenously express the pluripotency markers Sox2, Oct4, Nanog, DNMT3β, c-Myc as well as the housekeeping gene GAPDH with concomitant loss of exogenously introduced reprogramming vectors shown by the absence of EBNA1. The episomal vector expressing EBNA1 served as a positive control (Fig. 1F; supplementary figure A). Array CGH was performed to detect potential gains or losses in chromosomal material. However, genomic integrity was confirmed in all three iPSC clones (Fig. 1C). Notably, array CGH does not sense balanced chromosomal translocations or mosaicism. Moreover, iPSC identity was proven by short-tandem repeat (STR) analysis, which confirmed a 100 % allele match within the clones. Finally, the iPSCs were tested for their potential to differentiate into all three germ layers via directed in vitro differentiation. IF staining was used to detect Sox17 (endodermal marker), Brachyury (mesodermal marker) and Pax6 (ectodermal marker) (Fig. 1D). In summary, these three stem cell lines represent a well-characterized tool and will find application in the field of breast cancer research.

3. Materials and methods

3.1. Reprogramming of CD34+ cells into iPSCs

For the reprogramming of CD34+ hematopoietic stem and progenitor cells into iPSCs, the CD34+ Progenitor Reprogramming Kit

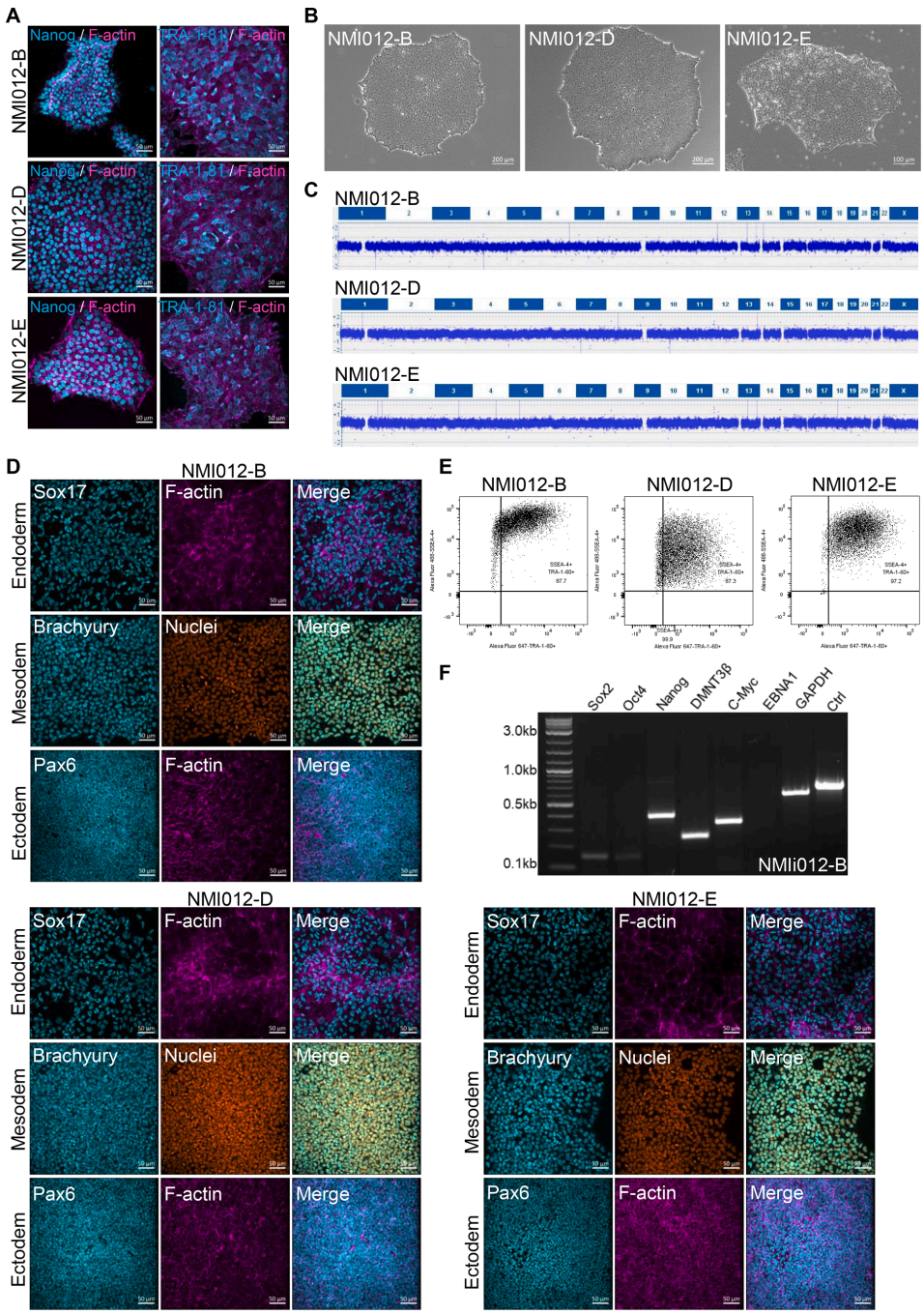

Figure 1: Characterization overview of three iPSC clones generated from a breast cancer patient.

Fig. 1. Characterization overview of three iPSC clones generated from a breast cancer patient.

Table 2
Reagents details.

	Antibodies used for immunocytochemistry/flow-cytometry			
	Antibody	Dilution	Company Cat #	RRID
Pluripotency markers	anti-human OCT4	1: 200	Cell Signaling Technology, Cat# 2750	RRID: AB_823583
	anti-human NANOG (D73G4)	1: 200	Cell Signaling Technology, Cat# 4903	RRID: AB_10559205
	anti-human SOX2 (D6D9)	1:400	Cell Signaling Technology, Cat# 3579	RRID: AB_2195767
	anti-human SSEA4 (MC813)	1:500	Cell Signaling Technology, Cat# 4755	RRID:AB_126425
	Alexa Fluor® 488 anti-human SSEA4 (MC-813–70)	1:30	BioLegend, Cat# 330,411	RRID: AB_1089199
	anti-human TRA-1–81	1:1000	Cell Signaling Technology, Cat# 4745	RRID: AB_2119060
	Alexa Fluor® 647 anti-human TRA-1–60-R	1:30	BioLegend, Cat# 330,605	RRID: AB_1227813
Differentiation markers	anti-human SOX17 (D1T8M)	1:1000	Cell Signaling Technology, Cat# 81,778	RRID: AB_2650582
	anti-human FOXA2 (ERP4466)	1:250	Abcam, Cat# ab108422	RRID: AB_11157157
	anti-human Brachyury (ERP18113)	1:1000	Abcam, Cat# ab209665	RRID: AB_2750925
	anti-human NCAM/CD5 (HCD56)	1:100	STEMCELL Technologies, Cat# 60021AD.1	RRID: AB_2891082
	anti-human PAX6 (EPR15858)	1:350	Abcam, Cat# ab195045	RRID: AB_2750924
	anti-human Nestin (10C2)	1:100	STEMCELL Technologies, Cat# 60091AD.1	RRID: AB_2650581
Nuclear marker	Hoechst 33,258	1:250	ThermoFisher Scientific, Cat# H3569	RRID: AB_2651133
F-actin marker	Phalloidin-tetramethylrhodamine conjugate	1:1000	Santa Cruz Biotechnnology, Cat# sc-362065	
Secondary antibodies	anti-rabbit Alexa Fluor® 488	1:1000	Abcam, Cat# ab150073	RRID:AB_2636877
	Cy5-AffiniPure Goat anti-Rabbit	1:1000	Jackson ImmunoResearch Labs Cat# 111–175-144	RRID:AB_2338013
	Cy5-AffiniPure Goat anti-Mouse	1:1000	Jackson ImmunoResearch Labs Cat# 115–175-146	RRID:AB_2338713
	Primers			
	Target	Size of band	Forward/Reverse primer (5′-3′)	
Episomal plasmids (RT-PCR)	EBNA1	666 bp	ATCGTCAAAGCTGCACACAG/CCCAGGAGTCCCAGTCA	
Pluripotency marker (endogenous) (RT-PCR)	OCT4	144 bp	GACAGGGGGAGGGGAGGAGCTAGG/ CTTCCCTCCAACCAGTTGCCCCAAAC	
Pluripotency marker (endogenous) (RT-PCR)	NANOG	391 bp	CAGCCCCGATTCTTCCACCAGTCCC/ CGGAAGATTCCCAGTCGGGTTCACC	
Pluripotency marker (endogenous) (RT-PCR)	SOX2	151 bp	GGGAAATGGGAGGGGTGCAAAAGAGG/ TTGCGTGAGTGTGGATGGGATTGGTG	
Pluripotency marker (endogenous) (RT-PCR)	DNMT3β	242 bp	TGCTGCTCACAGGGCCCGATACTTC/ TCCTTTCGAGCTCAGTGCACCACAAAAC	
Pluripotency marker (endogenous) (RT-PCR)	c-Myc	328 bp	GCGTCCTGGGAAGGGAGATCCGGAGC/ TTGAGGGGCATCGTCGCGGGAGGCTG	
House-keeping (RT-PCR)	GAPDH	572 bp	TCACCATCTTCCAGGAGCG/CTGCTTCACCACCTTCTTGA	

(STEMCELL Technologies™) was carried out according to the provided technical manual. In brief, CD34+ hematopoietic stem and progenitor cells were isolated from PBMCs and were expanded for 7 days. On day 8, Epi5™ reprogramming vectors (ThermoFisher Scientific) were introduced into the CD34+ cells via electroporation using the P3 Primary Cell 4D-Nucleofector™ X Kit L (Lonza). The transfected cells were seeded on a Matrigel®-coated (Corning®) cell culture plate and maintained for 2 days in CD34+ expansion medium. Then, the medium was changed to ReproTeSR™ (STEMCELL Technologies™) medium until first iPSC colonies appeared. Single colonies were manually transferred to Matrigel®-coated wells and expaneded in mTeSR™ Plus medium. The iPSCs were passaged with Gentle Cell Dissociation Medium (STEMCELL Technologies™) and cryopreserved with CryoStor® CS10 (STEMCELL Technologies) in liquid nitrogen. Cells were kept at 37 °C, 5 % CO_2, 20 % O_2.

3.2. Test for potential mycoplasma contamination

To monitor potential mycoplasma contaminations, 100 µL cell culture supernatant at were collected from each iPSC clone at passage 3 and investigated via PCR by using the Venor®*GeM* Classic Kit (Minerva Biolabs®) according to the manufacturer's instructions.

3.3. Immunofluorescence staining

iPSCs at passage 6 were washed with PBS prior to fixation with 4 % PFA in 1xPBS for 15 min at room temperature (RT). The fixation solution was removed and cells were washed 3 times with 1xPBS. Next, cells were incubated in blocking and permeabilization buffer composed of 2 % goat serum and 0.1 % Triton X-100 (Carl Roth®) in 1x PBS for 2 h at RT. In an overnight step at 4 °C, the cells were decorated with primary antibodies in blocking and permeabilization solution. On the next day, iPSCs were washed 3 times with 1xPBS and incubated with the secondary antibody solution composed of secondary antibody, DAPI (nuclear stain) and Phalloidin (F-actin stain) in blocking and permeabilization buffer for 45 min at RT. The images were taken with a Zeiss Spinning Disc Confocal Microscope.

3.4. Flow cytometry

The iPSCs at passage 3–6 were dissociated with Accutase™ (STEMCELL Techologies™) and washed with staining buffer (10 % FCS in 1xPBS). The single-cell suspension was stained with conjugated antibodies for 30 min at 4 °C in the dark. Data acquisition was performed

with the FACSFortessa platform (BD Biosciences) and the collected data were analysed with the FlowJo V10 software (FlowJo, LCC).

3.5. Directed differentiation into the three germ layers

To test iPSCs for their potential to differentiate into all three germ layers, the STEMdiff™ Trilineage Differentiation Assay Kit (STEMCELL Techonologies™) was used according to the provided technical manual. Prior to iPSC-differentiation, iPSCs were cultured in mTeSR1™ medium (STEMCELL Technologies™). iPSCs were dissociated with Accutase™ (STEMCELL Techonologies™) and single cells were seeded on Matrigel®-coated cell culture plates in defined cell numbers. The cells were maintained in endodermal and mesodermal induction medium for 5 days and in ectodermal induction medium for 7 days. Medium exchange was performed daily.

3.6. RT-PCr

RT-PCR from RNA for quantitative expression analysis was performed at passage 3–13. Total RNA from 2×10^6 cells was isolated using the RNeasy Mini Kit (Qiagen). DNA was degraded for 30 min at 37 °C with the RQ1 Kit (Promega). cDNA synthesis was performed with MuLV reverse transcriptase (New England Biolabs) for 60 min at 42 °C. The PCR products were visualized on a 2 % agarose gel (Table 2).

3.7. Genomic stability

Genomic integrity at passages 10–14 was confirmed via array CGH at the Clinical Genetics, Olgahospital, Stuttgart, Germany.

3.8. STR-analysis

STR-analysis was carried out at the Institute of Pathology at the Katharinenhospital Stuttgart, Germany.

Declaration of Competing Interest

The authors declare that they have no known competing financial interests or personal relationships that could have appeared to influence the work reported in this paper.

Acknowledgements

We thank Dr. Hans-Jürgen Pander and Dr. Eveline Fiedler from the Institute of Clinical Genetics at the Olgahospital Stuttgart, Dr. Dieter Techel from the Institute of Pathology at the Katharinenhospital Stuttgart and Prof. Dr. Martin Weiss from the Department of Women's Healthy at the University of Tuebingen, Germany for their valuable feedback and excellent technical support. This work received financial support from the State Ministry of Baden-Wuerttemberg for Economic Affairs, Labour and Housing Construction (Grant No. 3-4332.62-HSG/84)

Appendix A. Supplementary data

Supplementary data to this article can be found online at https://doi.org/10.1016/j.scr.2022.102988.

References

Cheng, H.G., Gonzalez-Reymundez, A., Li, I., Pathak, A., Pathak, D.R., de los Campos, G., Vazquez, A.I., Sang, Q.-X., 2020. Breast cancer survival and the expression of genes related to alcohol drinking. PLos One 15 (2), e0228957.

Mack, A.A., Kroboth, S., Rajesh, D., Wang, W.B., Borlongan, C.V., 2011. Generation of induced pluripotent stem cells from CD34+ cells across blood drawn from multiple donors with non-integrating episomal vectors. PLoS One 6 (11), e27956.

McCart Reed, A.E., Kalinowski, L., Simpson, P.T., Lakhani, S.R., 2021. Invasive lobular carcinoma of the breast: the increasing importance of this special subtype. Breast Cancer Res. 23 (1), 1–16.

Metzger-Filho, O., Ferreira, A. R., Jeselsohn, R., Barry, W. T., Dillon, D. A., Brock, J. E., Vaz-Luis, I., Hughes, M. E., Winer, E. P., & Lin, N. U. (2019). Mixed invasive ductal and lobular carcinoma of the breast: prognosis and the importance of histologic grade. The oncologist, 24(7), e441-e449.

Okita, K., Yamakawa, T., Matsumura, Y., Sato, Y., Amano, N., Watanabe, A., Goshima, N., Yamanaka, S., 2013. An efficient nonviral method to generate integration-free human-induced pluripotent stem cells from cord blood and peripheral blood cells. Stem cells 31 (3), 458–466.

Stem Cell Research 54 (2021) 102427

Contents lists available at ScienceDirect

Stem Cell Research

journal homepage: www.elsevier.com/locate/scr

Lab Resource: Single Cell Line

Generation and characterization of the human induced pluripotent stem cell line NMIi010-A from peripheral blood mononuclear cells of a healthy 49–year old male individual

Anna-Lena Keller [a,*], Anna Binner [a], Ricarda Breitmeyer [a], Sabrina Vogel [a], Nicole Anderle [a], Ulrich Rothbauer [a,b], Katja Schenke-Layland [a,c,d,e], Christian Schmees [a,*]

[a] NMI Natural and Medical Sciences Institute at the University of Tuebingen, Reutlingen, Germany
[b] Pharmaceutical Biotechnology, University of Tuebingen, Tuebingen, Germany
[c] Department of Biomedical Engineering, Eberhard Karls University Tübingen, Germany
[d] Cluster of Excellence iFIT (EXC2180) "Image-Guided and Functionally Instructed Tumor Therapies", University of Tuebingen, Tuebingen, Germany
[e] Department of Medicine/Cardiology, Cardiovascular Research Laboratories, David Geffen School of Medicine at UCLA, Los Angeles, CA, USA

A B S T R A C T

Peripheral-blood derived CD34$^+$ hematopoietic stem and progenitor cells were isolated from a 49-year old male donor and were successfully reprogrammed into human induced pluripotent stem cells (hiPSCs) using integration-free episomal vectors. The hiPSC line exhibited a typical stem cell-like morphology and endogenously expressed several pluripotency markers by concomitant loss of exogenous reprogramming vectors. Genomic integrity was confirmed by microarray-based comparative genomic hybridization (array CGH). Further analysis affirmed the ability of this hiPSC line to differentiate into all three germ layers. Thus, the reported cell line may serve as a healthy control for disease modeling.

1. Resource table

Unique stem cell line identifier	NMIi010-A
Alternative name(s) of stem cell line	AH.2
Institution	NMI Natural and Medical Sciences Institute at the University of Tuebingen, Markwiesenstrasse 55, 72,770 Reutlingen
Contact information of distributor	Dr. Christian Schmees; christian.schmees@nmi.de M.Sc. Anna-Lena Keller; anna-lena.keller@nmi.de
Type of cell line	iPSC
Origin	Human
Additional origin info required for human ESC or iPSC	Age: 49 Sex: male Ethnicity if known: caucasian
Cell Source	Peripheral-blood derived CD34$^+$ hematopoietic stem and progenitor cells
Clonality	Clonal
Associated disease	None
Gene/locus	*n/a*
Date archived/stock date	23.05.2020 (date of generation)
Cell line repository/bank	https://hpscreg.eu/user/cellline/edit/NMIi010-A
Ethical approval	Ethics Committee at the Medical Faculty of the Eberhard Karls University and at the University Hospital Tübingen Chairmenship: Prof. Dr. med. Karl Jaschonek (Chairman) Prof. Dr. med. Dr. phil. Urban Wiesing (1st Vice Chairman) Prof. Dr. med. Dieter Luft (2nd Vice Chairman) Members: Prof. Dr. med. Berthold Drexler Prof. Dr. med. Jürgen Honegger Prof. Dr. med. dent. Bernd Koos Prof. Dr. phil. Dipl. Psych. Stefan Klingberg Prof. Dr. med. Holger Lerche Prof. Dr. rer. nat. Peter Martus Prof. Dr. med. Klaus Mörike Prof. Dr. med. Christian F. Poets Ulrike Röllecke Prof. Dr. iur. Dr. h. c. Georg Sandberger Approval number: 888/2019BO2

* Corresponding author.
E-mail addresses: anna-lena.keller@nmi.de (A.-L. Keller), christian.schmees@nmi.de (C. Schmees).

https://doi.org/10.1016/j.scr.2021.102427
Received 17 May 2021; Received in revised form 7 June 2021; Accepted 9 June 2021
Available online 11 June 2021

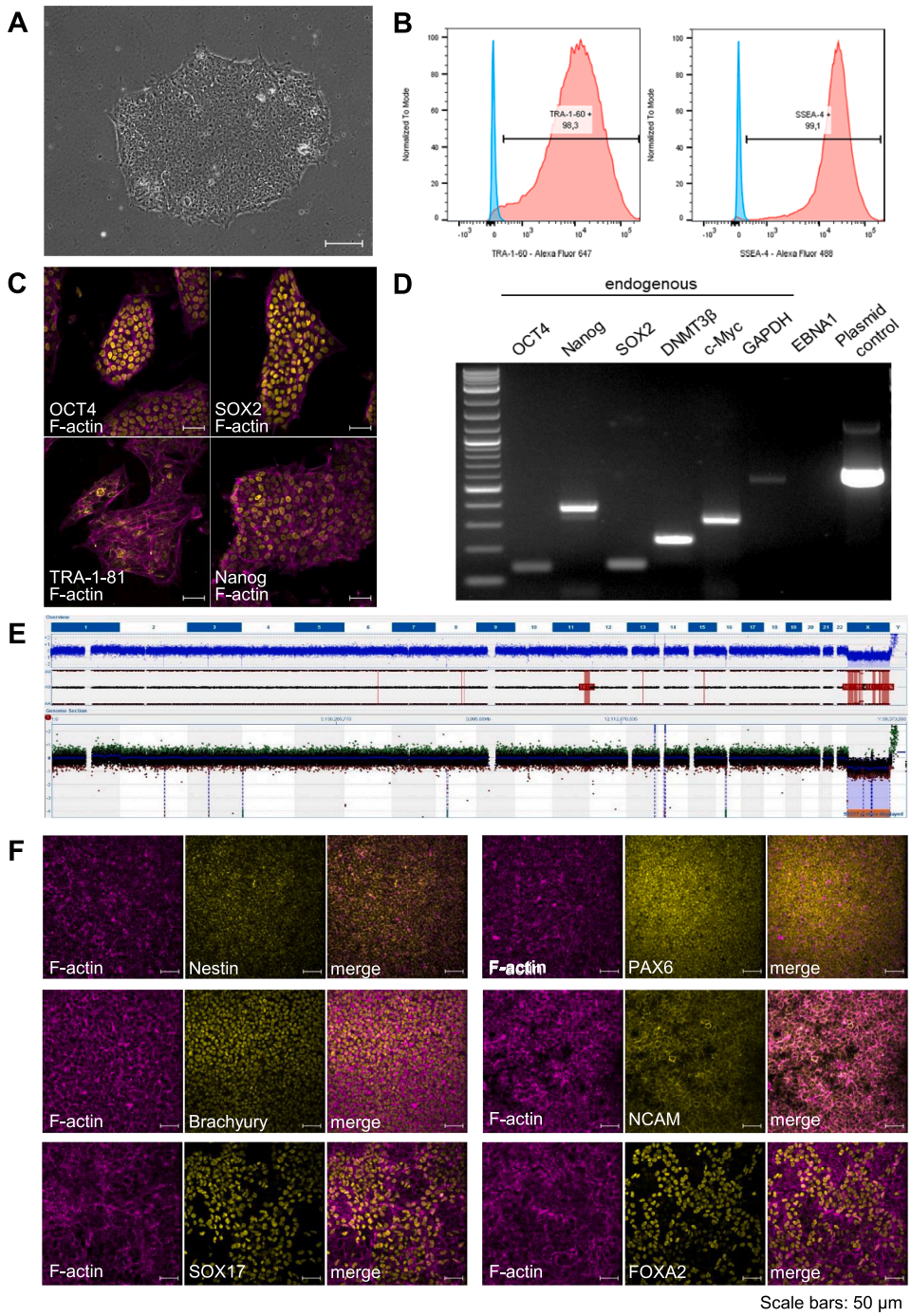

Fig. 1. Characterization of the hiPSC line NMIi010-A.

2. Resource utility

A major hallmark of hiPSCs is their differentiation potential into manifold cell types and tissues. Thus, hiPSCs hold great promise as in-vitro model for disease modelling. Here, we present the generation of a hiPSC line from a healthy donor, which functions as a control in future investigations of disease modeling in tumor biology.

3. Resource details

The successful reversion of terminally differentiated cells back into a pluripotent state was a profound scientific milestone of the recent years. Since then, robust and efficient protocols have been established describing the reprogramming of human somatic cells into hiPSCs by the ectopic and transient expression of defined reprogramming factors (Takahashi et al., 2007). The most frequently utilized source material for reprogramming experiments are dermal fibroblasts due to their uncomplicated cultivation, expansion and cryopreservation characteristics in respect of viability and nutrient conditions (Takahashi et al., 2007; Yu et al., 2007). However, skin biopsies remain invasive surgical interventions and the subsequent isolation of fibroblasts is relatively labor-intense. Plus, skin fibroblasts suffer from exposure to environmental risk factors such as ultraviolet radiation leading to the accumulation of point mutations. Value can be found in alternative, more accessible cell sources less prone to genetic alterations such as blood-derived $CD34^+$ hematopoietic stem and progenitor cells (Zhang, 2013). These cells are constantly replenished in the bone marrow, maintain genomic integrity, lack V(D)J recombination and can be obtained by blood sampling, i.e. *via* a minimal invasive procedure.(Mack et al., 2011; Chou et al., 2011) In this study, we isolated $CD34^+$ cells from peripheral blood mononuclear cells (PBMCs) of a healthy male individual. The cells were expanded prior to electroporation with five non-integrative episomal plasmids overexpressing OCT4, SOX2, KLF4, L-Myc, LIN28, mp53DD and EBNA1. After 21 days in culture, first hiPSC-like colonies were manually picked and expanded in mTesR + medium on matrigel-coated cell culture plates. Medium exchange was performed on a daily base. The cells were passaged by detachment using gentle cell dissociation reagent (GCDR). The hiPSC colonies exhibited a typical hiPSC-like morphology with tightly packed colonies and prominent nuclei (Fig. 1A). After a few passages, a comprehensive characterization of the hiPSC line was performed. First, absence of mycoplasma contamination was proven by PCR at passage 3 (Supplementary Fig. 1A). Secondly, we observed the consistent expression of the pluripotency markers OCT4, SOX2, TRA-1-81 and Nanog via immunofluorescence staining (Fig. 1C) and flow cytometry (Fig. 1B), respectively, at passage 5. Thirdly, at passage 18, array CGH analysis confirmed the integrity of the genome without aberrations (Fig. 1E). Alterations in chromosome structure, mosaicism, polyploidy and translocations or inversions cannot be detected by array CGH. Fourthly, short tandem repeat (STR) analysis identified a 100% allele match between hiPSCs and parental PBMCs. Fifthly, reverse transcriptase polymerase chain reaction (RT-PCR) was performed at passage 4 to examine the endogenous expression of pluripotency factors. The housekeeping gene GAPDH served as PCR control. Exogenously introduced genes were silenced shown by the absence of EBNA1 expression. Reprogramming vectors were used as positive control (Fig. 1D). Finally, the differentiation potential of NMIi010-A into all three germ layers was confirmed by immunofluorescence staining. Endodermal differentiation was proven by SOX17 and FOXA2 expression after five-day incubation with endodermal medium. Brachyury and NCAM expression indicated a successful mesodermal differentiation after a cultivation duration of five days with mesodermal medium while ectodermal differentiation was shown by PAX6 and Nestin expression after seven days in ectodermal differentiation medium (Fig. 1F). Taken together, following successful reprogramming of $CD34^+$ cells from a healthy individual into hiPSCs, this cell line represents a valid healthy control in upcoming studies in our lab focused on disease modelling in tumor biology.

Table 1
Characterization and validation.

Classification	Test	Result	Data
Morphology	Photography	Normal iPSC morphology	Fig. 1A
Phenotype	Qualitative analysis	Positive immunofluorescence staining of the pluripotency markers: OCT4, SOX2, TRA-1–81 and Nanog.	Fig. 1C
	Quantitative analysis (Flow Cytometry)	Percentage of TRA-1-60 positive cells: 98.3%. Percentage of SSEA-4 positive cells: 99.1%	Fig. 1B
Genotype	Array comparative genomic hybridization (array CGH)	46XY, Resolution: 5–10 Mb	Fig. 1E
Identity		DNA profiling performed	
	STR analysis	17 sites tested, 100% match	submitted in archive with journal
Mutation analysis	Sequencing	*n/a*	*n/a*
	Southern Blot OR WGS	*n/a*	*n/a*
Microbiology and virology	Mycoplasma	Negative mycoplasma testing confirmed by PCR.	Supplementary Fig. 1A
Differentiation potential	Directed differentiation	Differentiation into all three germlayers shown by immunofluorescence staining. Endoderm: FOXA, SOX17. Mesoderm: Brachyury, NCAM. Ectoderm: PAX6, Nestin.	Fig. 1F
Donor screening	HIV 1 + 2, Hepatitis B, Hepatitis C	*n/a*	*n/a*
Genotype additional info	Blood group genotyping	*n/a*	*n/a*
	HLA tissue typing	*n/a*	*n/a*

4. Materials and methods

4.1. Reprogramming of $CD34^+$ hematopoietic stem and progenitor cells into hiPSCs

PBMCs were isolated from 50 mL donor blood using SepMate isolation tubes (STEMCELL Technologies). Next, $CD34^+$ cells were obtained by positive selection with the CD34 MicroBead Kit (Miltenyi Biotec). The cells were cultivated and expanded for 7 days in StemPro 34 SFM medium (ThermoFisher Scientific) supplemented with GlutaMAX-I (ThermoFisher Scientific), 100 ng/mL recombinant human SCF, 50 ng/mL recombinant human IL-3 and 25 ng/mL recombinant human GM-CSF (all from PeproTech). 1×10^6 expanded $CD34^+$ cells were electroporated with Epi5 Episomal reprogramming vectors (ThermoFisher Scientific) using the P2 Primary Cell Kit (Lonza) with the Nucleofector 4D system (Lonza). The electroporation settings indicated for human $CD34^+$ cells was chosen. Transfected cells were cultured on matrigel (1:50; Corning) and incubated overnight at 37 °C in complete StemPro 34 SFM medium. On the next day, N2B27 medium was prepared according to the Epi5 Episomal iPSC reprogramming Kit user manual and added to the cells. Medium was replenished daily until day 9 post-electroporation. Cells were further cultivated in mTeSR + medium

Table 2
Reagents details.

	Antibodies used for immunocytochemistry/flow-cytometry			
	Antibody	Dilution	Company Cat #	RRID
Pluripotency and Cell Surface Markers	Alexa Fluor(R) 488 anti-human SSEA-4 antibody	1:30	BioLegend Cat# 330,411	RRID: AB_1089199
	Alexa Fluor(R) 647 anti-human TRA-1-60-R antibody	1:30	BioLegend Cat# 330,605	RRID: AB_1227813
	OCT4 Antibody	1:200	Cell Signaling Technology Cat# 2750	RRID:AB_823583
	Nanog (D73G4) XP Rabbit Antibody	1:200	Cell Signaling Technology Cat# 4903	RRID: AB_10559205
	Mouse Anti-Human TRA-1-81 Monoclonal Antibody, Unconjugated, Clone TRA-1-81	1:1000	Cell Signaling Technology Cat# 4745	RRID: AB_2119060
	SSEA-4 (MC813) Mouse Antibody	1:500	Cell Signaling Technology Cat# 4755	RRID:AB_126425
	SOX2 (D6D9) XP Rabbit mAb antibody	1:400	Cell Signaling Technology Cat# 3579	RRID: AB_2195767
Differentiation markers	Anti-Human CD56 (NCAM) Antibody	1:100	Stemcell Technologies Cat#60021	RRID: AB_2891082
	Rabbit anti-SOX17	1:1000	Cell Signaling Technology Cat# 81778,	RRID: AB_2650582
	FOXA2 antibody [EPR4466]	1:250	Abcam Cat# ab108422	RRID: AB_11157157
	anti-human Brachyury/bry	1:1000	Abcam Cat# ab209665	RRID: AB_2750925
Nuclear Marker	NucBlue™ Fixed Cell ReadyProbes™ Reagent (DAPI)	1 drop in 500 µL	Invitrogen Cat#R37606	RRID: AB_2891083
Actin Markers	Phalloidin CruzFluor 488 Conjugated antibody	1:2000	Santa Cruz Biotechnology Cat# sc-363791	RRID: AB_2631056
Secondary antibodies	Cy5-AffiniPure Goat Anti-Rabbit IgG	1:1000	Jackson ImmunoResearch Labs Cat# 111-175-144	RRID: AB_2338013
	Cy5-AffiniPure Goat Anti-Mouse IgG	1:1000	Jackson ImmunoResearch Labs Cat# 115-175-146	RRID: AB_2338713
	Primers			
	Target	Size of band	Forward/Reverse primer (5′-3′)	
Episomal Plasmids (RT-PCR)	EBNA1	666 bp	ATCGTCAAAGCTGCACACAG/CCCAGGAGTCCCAGTCA	
Pluripotency Marker (RT-PCR)	OCT4	144 bp	GACAGGGGGAGGGGAGGAGCTAGG/ CTTCCCTCCAACCAGTTGCCCCAAAC	
Pluripotency Marker (RT-PCR)	NANOG	391 bp	CAGCCCCGATTCTTCCACCAGTCCC/ CGGAAGATTCCCAGTCGGGTTCACC	
Pluripotency Marker (RT-PCR)	SOX2	151 bp	GGGAAATGGGAGGGGTGCAAAAGAGG/ TTGCGTGAGTGTGGATGGGATTGGTG	
Pluripotency Marker (RT-PCR)	DNMT3β	242 bp	TGCTGCTCACAGGGCCCGATACTTC/ TCCTTTCGAGCTCAGTGCACCACAAAAC	
Pluripotency Marker (RT-PCR)	c-Myc	328 bp	GCGTCCTGGGAAGGGAGATCCGGAGC/ TTGAGGGGCATCGTCGCGGGAGGCTG	
House-Keeping Gene (RT-PCR)	GAPDH	572 bp	TCACCATCTTCCAGGAGCG/CTGCTTCACCACCTTCTTGA	

(STEMCELL Technologies). Upon appearance of hiPSC-like colonies, the cells were manually picked and expanded in mTeSR + medium. Cells were passaged by using GCDR (STEMCELL Technologies) every 4–6 days and kept at 37 °C, 5%CO_2, 20% O_2. Characterization is summarized in Fig. 1 and Table 1.

4.2. Chromosomal integrity

2 × 10^6 hiPSCs at passage 18 were examined for single nucleotide polymorphism and chromosomal copy number variants by array CGH at the Institute of Clincal Genetics at the Olgahospital Stuttgart, Germany.

4.3. Immunocytochemistry

HiPSCs were fixed in 4% paraformaldehyde (Sigma-Aldrich) for 15 min at room temperature (RT) and washed prior to blocking and permeabilization with 0.1% Triton X-100 and 2% BSA in 1X PBS for 2 h at RT. Primary antibodies were incubated overnight at 4 °C (Table 2). Secondary antibodies and Phalloidin were applied for 45 min at RT (Table 2).

4.4. Flow cytometry

HiPSCs were dissociated using Accutase (STEMCELL Technologies) and stained for 30 min at 4 °C with conjugated antibodies (Table 2). Data were acquired at the FACSFortessa platform (BD Biosciences) and analyzed using FlowJo V10 software (FlowJo, LCC).

4.5. RT-Pcr

Total RNA of 2 × 10^6 cells was extracted using RNeasy Mini Kit (Qiagen). DNA was degraded at 37 °C for 30 min (RQ1 Kit, Promega). Complementary DNA synthesis was performed at 42 °C for 60 min using MuLV reverse transcriptase (New England Biolabs). RT-PCR products were separated on a 2% agarose gel (Table 2).

4.6. STR analysis

Genomic DNA was isolated from PBMCs and hiPSCs (DNeasy Blood & Tissue Kit, Qiagen). STR analysis was performed by the Institute of Pathology at the Katharinenhospital Stuttgart, Germany.

4.7. Trilineage differentiation potential

Differentiation of iPSCs into endoderm, mesoderm and ectoderm was carried out according to the STEMdiff™ Trilineage Differentiation Kit protocol (STEMCELL Technologies). Cells were analyzed by immunofluorescence staining of lineage specific markers (Table 2).

4.8. Mycoplasma test

100 μL of cell culture supernatant were collected and analyzed for potential mycoplasma contamination by PCR. Mycoplasma test was performed using the Venor®GeM Classic Kit (Minerva Biolabs) according to the manufacturer's instruction.

Declaration of Competing Interest

The authors declare that they have no known competing financial interests or personal relationships that could have appeared to influence the work reported in this paper.

Acknowledgements

We thank Dr. Hans-Jürgen Pander and Dr. Eveline Fiedler from the Institute of Clinical Genetics at the Olgahospital Stuttgart, Dr. Dieter Techel from the Institute of Pathology at the Katharinenhospital Stuttgart and Prof. Dr. Martin Weiss from the Department of Women's Healthy at the University of Tuebingen, Germany for their valuable feedback and excellent technical support. This work received financial support from the State Ministry of Baden-Wuerttemberg for Economic Affairs, Labour and Housing Construction (Grant No. 3-4332.62-HSG/84).

Appendix A. Supplementary data

Supplementary data to this article can be found online at https://doi.org/10.1016/j.scr.2021.102427.

References

Takahashi, K., Tanabe, K., Ohnuki, M., Narita, M., Ichisaka, T., Tomoda, K., Yamanaka, S., 2007. Induction of pluripotent stem cells from adult human fibroblasts by defined factors. Cell 131 (5), 861–872. https://doi.org/10.1016/j.cell.2007.11.019. PMID: 18035408.

Yu, J., Vodyanik, M.A., Smuga-Otto, K., Antosiewicz-Bourget, J., Frane, J.L., Tian, S., Nie, J., Jonsdottir, G.A., Ruotti, V., Stewart, R., Slukvin, I.I., Thomson, J.A., 2007. Induced pluripotent stem cell lines derived from human somatic cells. Science. 318 (5858), 1917–1920. https://doi.org/10.1126/science.1151526. Epub 2007 Nov 20 PMID: 18029452.

Zhang XB. Cellular reprogramming of human peripheral blood cells. Genomics Proteomics Bioinformatics. 2013 Oct;11(5):264-74. doi: 10.1016/j.gpb.2013.09.001. Epub 2013 Sep 21. PMID: 24060839; PMCID: PMC4357833.

Mack AA, Kroboth S, Rajesh D, Wang WB. Generation of induced pluripotent stem cells from CD34+ cells across blood drawn from multiple donors with non-integrating episomal vectors. PLoS One. 2011;6(11):e27956. doi: 10.1371/journal.pone.0027956. Epub 2011 Nov 22. PMID: 22132178; PMCID: PMC3222670.

Chou BK, Mali P, Huang X, Ye Z, Dowey SN, Resar LM, Zou C, Zhang YA, Tong J, Cheng L. Efficient human iPS cell derivation by a non-integrating plasmid from blood cells with unique epigenetic and gene expression signatures. Cell Res. 2011 Mar;21(3):518-29. doi: 10.1038/cr.2011.12. Epub 2011 Jan 18. PMID: 21243013; PMCID: PMC3193421.

Publication 4 | E

Co-cultures of iPSC-derived Mammary-like Organoids and Patient-derived Microtumors Model Invasive Behavior of Breast Cancer Ex Vivo

Anna-Lena Keller[1,*], Nicole Anderle[1], Monika Schrenk[1], Deborah Greis[1], Anna Binner[1], Dmitri Visser[1], Jens Göpfert[1], André Koch[2], Martin Weiss[1,2], Sara Y. Brucker[2,3], Katja Schenke-Layland[1,3,4], Christian Schmees[1,*]

1. NMI – Natural and Medical Sciences Institute at the University of Tuebingen, Reutlingen, Germany
2. Department of Women's Health, Eberhard Karls University Tuebingen, Tuebingen, Germany
3. Cluster of Excellence iFIT (EXC2180) "Image-Guided and Functionally Instructed Tumor Therapies", Eberhard Karls University Tuebingen, Tuebingen, Germany
4. Institute of Biomedical Engineering, Dept. for Medical Technologies and Regenerative Medicine, Eberhard Karls University Tübingen, 72076 Tübingen, Germany

*Please address correspondence to: anna-lena.keller@nmi.de, christian.schmees@nmi.de

1. Abstract

Background

The tumor-adjacent mammary epithelium can play a pivotal role in tumor growth and progression. We investigated the invasive behavior of patient-derived microtumors and breast cancer cell line-derived spheroids in co-culture with induced pluripotent stem cell-derived mammary-like organoids in an autologous and allogenic manner. This co-culture systems enables a better understanding of the tumor-promoting function of the tumor-adjacent mammary epithelium in different types of breast cancers.

Methods

Using three-dimensional co-culture settings of induced pluripotent stem cell-derived mammary-like organoids and patient-derived microtumors or cancer cell line-derived spheroids, we investigated tumor growth and invasiveness of the cancers by using imaging-based analysis. Levels of Fibronectin and Metalloproteinase-2 in co-cultures and respective mono-cultures were measured using multiplexed Luminex assay.

Results

We observed significant increases in growth and invasiveness of invasive ductal carcinoma of no special type patient-derived microtumors in co-culture with induced pluripotent stem cell-derived mammary-like organoids. We identified upregulations of the prognostic markers Fibronectin and

Metalloproteinase-2 in all co-cultures compared to respective mono-cultures of mammary-like organoids, patient-derived microtumors and cell line-derived spheroids.

Conclusions

These findings indicate a tumor-promoting role of the tumor-adjacent mammary epithelium probably dependent on the tumor composition and tumor stage. Our results highlight the importance of breast tumor models that closely resemble the heterogenous composition of primary breast tumors.

2. Keywords

Breast cancer, patient-derived microtumors, induced pluripotent stem cells, epithelium, mammary-like organoids, co-culture, extracellular matrix, Metalloproteinase-2, Fibronectin

3. Background

Despite decades of intensive laboratory and clinical research in the field of tumorbiology, the mortality rate among women worldwide associated with breast cancer remains alarmingly high [1]. Although early detection correlates with a promising clinical outcome, the 5-year survival rate of metastasized breast cancer declines to only 26% [2]. One major hurdle in finding suitable treatment options is breast cancers' exceptionally high inter- and intratumoral heterogeneity [3]. Not only variations in cell-intrinsic hallmarks such as the (epi-) genetic profile, the transcriptome and proteome, cancer stemness or proliferation capacities but also the highly dynamic tumor microenvironment (TME) define breast cancer as a spectrum of pathogenic entities that differ in receptor stages and histological properties [3]. Furthermore, the TME is not just a silent bystander but plays an active role in tumor progression. It consists of tissue resident and recruited cells such as immune cells, blood vessels, fibroblasts as well as the extracellular matrix (ECM) and reciprocally exchanges secreted vesicles and soluble factors with the malignant cells [4, 5]. Cancer cells need a constant adaptation to the stochastic and dynamic alterations of its near surrounding and progressively remodel the TME in their own favor. The ECM plays a key role in this process. It represents a pleiotropic scaffold of manifold proteins and serves as an orchestrated regulator of tissue integrity and homeostasis [6]. Once hijacked by the neoplastic cells, the balanced processes of ECM synthesis and degradation can be unhinged. Matrix metalloproteinases (MMPs) can degrade ECM components such as collagen, proteoglycans, fibronectin (FN) or laminin which, in turn, releases growth factors and cytokines bound within the matrix [7]. These events, eventually, push cancer cells towards proliferation and invasion [8, 9]. Another fuel that drives cancer growth are tumor-neighboring cells. During oncogenic

transformation, tumor-adjacent mammary epithelial cells stand in direct contact to the cancer cells and are known to exert an ambivalent role in tumorigenesis: In early disease stages, they might have a tumor suppressive function but during cancer progression, they might take over a tumor-promoting role and reinforce tumorigenicity and invasion [10, 11]. Previous investigators highlighted the important role of the mammary epithelium in tumorigenesis, but most of the previous work was performed with immortalized cell lines or in two-dimensional culture setups, which does not recapitulate tissue architecture and complexity [12-14]. In the present study, we introduce a three-dimensional (3D) co-culture system of patient-derived breast microtumors or cell line-derived spheroids (hereafter summarized as “breast cancer spheres”) and mammary-like organoids (MLOs), which allows to investigate the influence of the mammary epithelium on tumor growth, invasion, and metastasis-related processes in an autologous and allogenic manner. We recently generated induced pluripotent stem cells (iPSCs) from peripheral blood of two breast cancer patients (BCP) diagnosed with invasive lobular carcinomas [15, 16]. Here, we differentiated those iPSCs into functional MLOs expressing luminal and basal markers of the mammary epithelium. Additonally, we describe the isolation of breast cancer patient-derived microtumors (PDMs) – small tumor fragments isolated from residual fresh primary breast tumor tissue that reflect the heterogeneous nature of tumors [17-20]. The co-culture of breast cancer spheres and MLOs led to a significant upregulation of two crucial prognostic markers, FN and Metalloproteinase-2 (MMP2), known to be associated with invasive and metastatic tumor phenotypes and a poor prognosis for breast cancer patients [21, 22]. Furthermore, we observed a significant increase in tumor growth and invasion of invasive ductal carcinoma of the no special type (IDC-NST) upon co-culture with MLOs. Our data emphasize the potential importance of the tumor-adjacent mammary epithelium on tumor growth, invasion and processes associated with metastatic progression.

4. Material and Methods

4.1 Human specimen

In the scope of the publicly funded PRIMO (personalized medicine for tailored cancer therapies) project, residual primary breast tumor tissue specimens were obtained post-operatively and after completion of histopathological examination from the Department for Women’s Health at the University Hospital, Tuebingen. The research project was approved by the ethics committee of the medical faculty of the University Hospital Tuebingen, Germany (project number 788/2018BO2 and 888/2019BO2). Written informed consent was obtained from all participants prior to surgery.

4.2 Isolation and cultivation of PDMs

Isolation and cultivation of PDMs was performed as previously described [17-20]. In brief, primary tumor tissue (PTT) was mechanically dissected with a scalpel and a forceps into 1-2 mm fragments. Then, the tumor tissue was digested overnight at 37°C with a Liberase™ DH (Roche, Switzerland) enzyme mixture while shaking at 100 rpm. The residual tissue contained the microtumors. The PDMS were cultured for up to 3 weeks or cryopreserved in CryoStor® CS10 (STEMCELL Technologies, Canada) in liquid nitrogen for long-term storage.

4.3 Live and dead staining

To assess cell viability, samples were incubated for 30 – 60 min at 37°C with live-dead-staining solution. Appropriate cell cultivation medium was supplemented with 2 µM Calcein-AM™ live cell stain (Invitrogen™) and 5 µM SYTOX™ Orange Nucleic Acid Stain for dead cells (Invitrogen™). 1 µg/mL Hoechst 33258 (Invitrogen™, Thermo Fisher Scientific) was added to visualize Nuclei. Fluorescence images were taken with a spinning disc confocal Cell Observer Z1 microscope (Carl Zeiss GmBH) using FITC, TRITC and DAPI filter channels. 3D projections of confocal z-stacks were generated using the ZEN software version 2.6 (Zeiss). Viability analysis was performed with the Microscopy Image Analysis Software Imaris 9.0 (Oxford Instruments). 3D masks for the TRITC and DAPI channels were created, thresholds were adjusted, and the intensity sum for each channel was measured. The percentages of viable and dead cells were calculated form the total cell count.

4.4 Whole mount immunofluorescence (IF) staining

The samples were fixed in 4% PFA (Carl Roth, Germany) for 30 minutes at ambient temperature and subsequently washed 3 times with 1xDPBS (Gibco™, Thermo Fisher Scientific). The cells were permeabilized and blocked with blocking solution consisting of 5% goat serum (MP Biomedicals, USA) or donkey serum (Merck, Germany) and 0.1% Triton™ X-100 (Carl Roth, Germany) in 1xDPBS overnight at 4°C. Primary antibodies were diluted in fresh blocking solution and incubated with the samples at 4°C overnight while gentle shaking. Used primary antibodies: CK18 (abcam, UK; #ab133263), CK14 (abcam; #ab7800), CK8 (abcam; #ab53280), β-casein (abcam; #ab47972), p63 (abcam; #ab124762), EpCAM (Life Technologies, #14-9326-82), Ki67 (Cell Signaling Technology, USA; #9449) and AP2γ (abcam; # ab218107). Secondary antibodies, Hoechst 33258 (Invitrogen™, Thermo Fisher Scientific) and Phalloidin-tetramethylrhodamine conjugate (Santa Cruz Biotechnology, USA) were diluted in fresh blocking solution and incubated with the samples at 4°C overnight. Used secondary antibodies: anti-rabbit Cy5 (Jackson ImmunoResearch, USA; #111-175-144), anti-mouse Cy5 (Jackson ImmunoResearch; #115-175-

146), anti-rabbit 488 (abcam; #ab150073). Confocal fluorescence images were acquired using a spinning disc microscope (Cell Observer SD, Carl Zeiss GmBH, Germany). Brightfield images were recorded with an AxioVert A1 microscope (Carl Zeiss GmBH).

4.5 Histology

The samples were fixed with 4% ROTI® Histofix (Carl Roth, Germany) for 1 h, washed with 1xPDBS and dehydrated in ethanol series (2 x 15 min in 50% ethanol, 2 x 15 min in 70% ethanol). All steps were performed at ambient temperature. The samples were embedded in Epredia™ Richard-Allan Scientific™ HistoGel™ (Fisher Scientific, USA). Paraffin infiltration was performed with a HistoCore PEARL (Leica Biosystems, Germany) tissue processor overnight. The processed tissue was sliced into 3 µm sections using a semi-automated microtome (Leica). The sections were baked in a 55°C heat cabinet for 60 min and subsequently dehydrated in descending alcohol series. Hematoxylin-eosin (H&E) staining was included to identify nucleic and cytoplasmic regions. Immunohistochemistry (IHC) was performed with an Autostainer Link 48 (Agilent, USA). Finally, the sections were mounted with CV Mount (Leica Biosystems) mounting medium. Slide images were taken with a ZEISS Axioscan 7 microscope slide scanner (Carl Zeiss GmBH).

4.6 iPSC culture

CD34+ hematopoietic stem and progenitor cells were isolated from peripheral blood mononuclear cells (PBMCs) from two patients diagnosed with an invasive lobular carcinoma and reprogrammed into iPSCs with non-integrative episomal vectors (Thermo Fisher Scientific, USA). The iPSCs were characterized comprehensively as recently described [15, 16]. For the co-culture with BCP 1 PDMs, BCP 3 PDMs and MDA-MB-231 spheroids, MLOs derived from the cell line NMIi011-A were used (here referred to as “MLO 1”) [16]. NMIi012-B derived MLOs (here named “MLO 2”) were used for the co-culture with BCP 2 PDMs and MCF-7 spheroids [15]. Notably, NMIi012-B iPSCs were generated from PBMCs of BCP 2. Therefore, the co-cultures of MLO 2 and BCP 2 were autologous, while the other co-cultures were allogenic. For iPSC maintenance, cells were feeder-independently cultured on 6-well cell culture plates coated with hESC-qualified Matrigel® (Corning, USA) in chemically defined mTeSR™ Plus (STEMCELL Technologies, Canada). The enzyme-free Gentle Cell Dissociation Reagent (STEMCELL Technologies) was used for passaging. For long time storage, iPSCs were resuspended in CryoStor® CS10 (STEMCELL Technologies) and kept at -150°C. The herein used iPSCs were obtained from BCP 4 (PDMs not included in this study) as well as from BCP 2 (PDMs included in this study).

4.7 MLO differentiation

Differentiation into MLOs was performed as described before [23, 24] with the following adaptions. iPSC maintenance medium was switched to mTeSR™ 1 medium (STEMCELL Techologies) 2 – 3 days prior to differentiation start. iPSCs were lifted by Accuatse™ (STEMCELL Technologies), resuspended in MammoCult™ human medium (STEMCELL Technologies), supplemented with 4 µg/mL heparin (STEMCELL Technologies), 0.48 µg/mL hydrocortisone (STEMCELL Technologies) and 10 µM Y-27632 (STEMCELL Technologies). The cells were plated onto an AggreWell™800 plate (STEMCELL Technologies) with 900,000 cells per microwell and centrifuged for 3 min at 100 g. On the next day, medium exchange with complete MammoCult™ human medium was performed. From now on, the medium was changed every second day until day 10. For the generation of control embryoid bodies (EB), iPSC spheroids were maintained in mTeSR™ 1 for 10 days. Mammary embryoid bodies (mEBs) were embedded into a mixed Matrigel® (2.5 mg/mL) / Collagen I (1 mg/mL) (Sigma-Aldrich, USA) gel on cold Organoid Embedding Sheets (STEMCELL Technologies). After solidification at 37°C, 5% CO2 and 20% O2 for 30 min, gel-droplets were rinsed off the Organoid Embedding Sheets and cultured in complete EpiCult™-B human medium (STEMCELL Technologies) supplemented with 100 ng/mL parathyroid hormone-related protein (PTHrP) (PeproTech, USA) for 5 days. Medium exchange was performed after 3 days. At day 5, medium was changed to branch and alveolar induction medium composed of complete EpiCult™-B human medium supplemented with 1 µg/mL hydrocortisone, 10 µg/mL insulin (Sigma-Aldrich), 50 ng/mL HGF (PeproTech) and 50 ng/mL FGF-10 (PeproTech) for 20 days. To induce milk protein expression, the medium was replaced with prolactogenic medium consisting of 10 µg/mL prolactin (PeproTech), 1 µg/mL hydrocortisone, 10 µg/mL insulin and 10% FCS (Gibco™, Thermo Fisher Scientific) in complete EpiCult™-B human medium until day 40.

4.8 Cancer-spheroid generation

MDA-MB-231 (ATCC, USA) and MCF-7 (ATCC) cells were maintained in DMEM/F-12 medium (Gibco™, Thermo Fisher Scientific) supplemented with 10% FBS (Gibco™, Thermo Fisher Scientific), 1% Penicillin-Streptomycin (Gibco™, Thermo Fisher Scientific) and 1x L-Glutamine (Gibco™, Thermo Fisher Scientific). For spheroid generation, cells were detached with Trypsin-EDTA (0.25%) (Gibco™, Thermo Fisher Scientific) and counted. 500 cells per well were plated on a U-bottom 96 well plate pre-coated with Anti-Adherence Rinsing Solution (STEMCELL Technologies). The plate was spun for 3 min at 100 g and incubated at 37°C, 5% CO2 overnight. After 3 days, spheroids were used for further investigations.

4.9 Culturing of PDMs / spheroids in ECM droplets

For the co-culture of PDMs / cancer cell line-derived spheroids and MLOs, one single mEB (day-10) and one single PDM or spheroid were injected together at the center of a liquid 25µL Matrigel® (2.5 mg/mL) - collagen I (1 mg/mL) droplet on cold Organoid Embedding Sheets using a 10 µL pipette. The gel droplets were solidified at 37°C, 5% CO2 and 20% O2 for 30 min and subsequently incubated in complete EpiCult™-B human medium supplemented with 100 ng/mL PTHrP for the first 5 days. Then, the medium was switched to EpiCult™-B human medium supplemented with 1 µg/mL hydrocortisone, 10 µg/mL insulin, 50 ng/mL HGF and 50 ng/mL FGF10 for another 5 days as described before (“Mammary-like organoid differentiation”).

4.10 Co-culture set-up

Organoid embedding sheets were placed on ice and 25 µL of the liquid Matrigel® (2.5 mg/mL) / Collagen I (1 mg/mL) mixture was added to each mold. One single mEB and one single PDM or cancer cell line spheroid were gently placed in close proximity to each other at the center of each liquid droplet using a 10 µL pipette. The Organoid Embedding Sheets were placed at 37°C, 5% CO2 and 20% O2 for 30 min until solidification. The droplets were rinsed off and further cultured in complete EpiCult™-B human medium supplemented with 100 ng/mL PTHrP for 5 days and subsequently in EpiCult™-B human medium supplemented with 1 µg/mL hydrocortisone, 10 µg/mL insulin, 50 ng/mL HGF and 50 ng/mL FGF10 for another 5 days as described before (“Mammary-like organoid differentiation”).

4.11 Luminex assay

Levels of FN and MMP2 were determined as part of a custom-made 13-plex multiplexed Luminex assay (order number LXSAHM-13, R&D Systems, Minneapolis, MN, USA). Samples were diluted 1:2 for analysis and were processed according to the kit manufacturer's instructions. All measurements were done in singlets. The instrument settings specified in the kit instructions were used for the analyses, and the analysis was performed on a FlexMap® 3D analysis system (Luminex, Austin, TX, USA, operated under Luminex xPONENT® software version 4.2,). The data was exported and the concentrations of the samples were back-calculated with the Bio-Plex® Manager data analysis software (Version 6.2, Biorad, Hercules, CA, USA). FN and MMP2 values were normalized to the blanks, which consisted only of medium and Matrigel®-collagen gel without cells.

4.12 Statistical Analysis

Statistical analysis was performed with the scientific 2D graphing and statistics software GraphPad Prism version 9.3.1. Unless stated otherwise, 2way ANOVA using Tukey's multiple comparison test with **** $p<0.0001$, *** $p<0.001$, ** $p<0.01$ * $p<0.05$ was used for all statistical analyses.

4.13 Invasion assay

To investigate the degree of invasiveness, brightfield images of the different tumor types were examined using the image-processing program ImageJ. The maximum value of 1 represents an ideal circle, while the minimum value of 0 describes that the object under investigation is not circular at all. The reciprocal value (1/Circularity) was then formed from the measured circularity values, which indicates the degree of invasiveness.

5. Results

5.1 iPSC-derived mammary-like organoids harbor characteristics of the human mammary gland

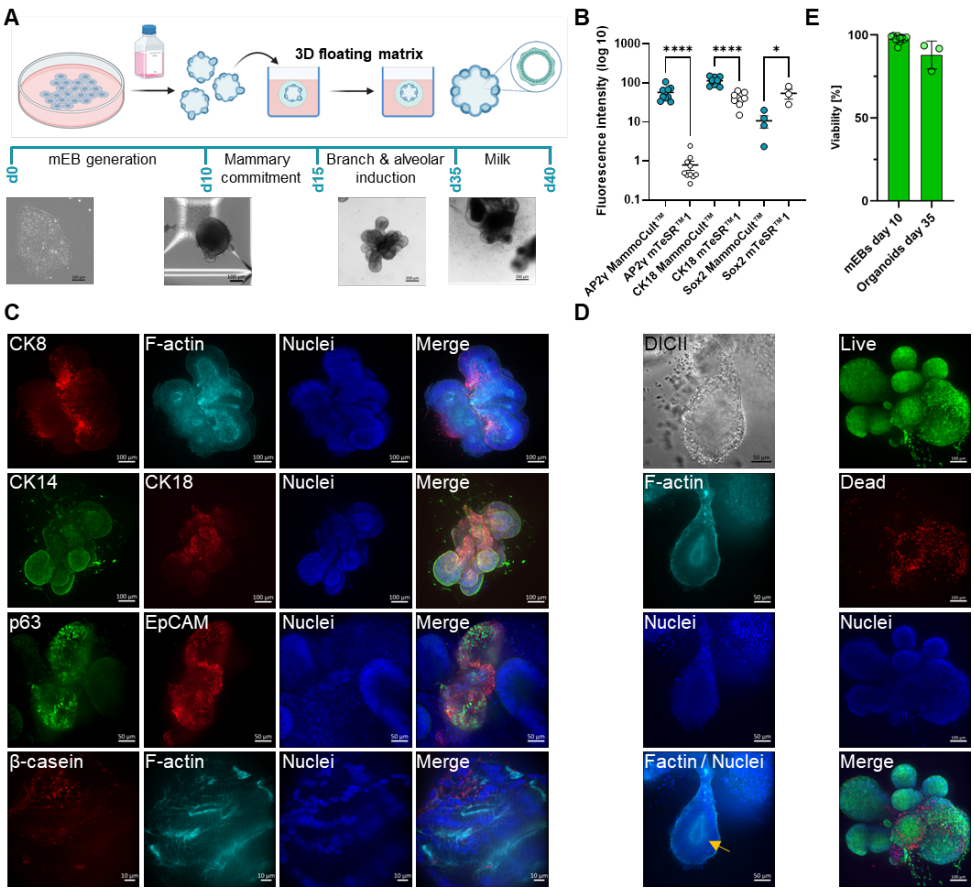

Figure 1: iPSC-derived MLOs share common characteristics with the human mammary gland. A) *Schematic overview of the iPSC-derived differentiation into MLOs based on previously described protocols [23, 24]. For a period of 10 days, solid iPSC spheres are cultured in low-attachment plates in either complete MammoCult™ human medium for the differentiation into mEBs of the non-neural ectodermal lineage or in mTeSR™ iPSC maintenance medium for the generation of control EBs. mEBs and EBs were further cultured in a Matrigel®-collagen matrix droplet in differently supplemented media until day 35. At day 35, MLOs were incubated in prolactogenic medium for 5 days to induce milk protein expression. Created with BioRender.* ***B)*** *AP2γ (n=10), CK18 (n=10) and Sox2 (n=4, MammoCult™ and n=3, mTeSR1™) expression of day-10 mEBs and EBs. **** p<0.0001, *** p<0.001, ** p<0.01 * p<0.05, One-way ANOVA using Tukey's multiple comparison test.* ***C)*** *Whole mount IF staining of day-20 MLOs indicate the expression of CK8, p63, EpCAM, CK14 and CK18. At day 35, MLOs were incubated in prolactogenic medium resulting in the expression of the milk protein β-casein in gland-like structures.* ***D)*** *Formation of acinar structures with hollow lumen (yellow arrow) during differentiation into MLOs.* ***E)*** *Viability assay for day-10 mEBs (n=10) and day-35 MLOs (n=3) via parallel staining of Calcein-AM™, SYTOX™ Orange and Hoechst. Data were acquired with the microscopy analysis software Imaris 9.0*

based on 2D projections of confocal images (representative image of day-35 MLO: lower panel). Error bars: standard deviation (SD).

iPSC-derived organoids represent 3D, self-organizing cellular assemblies, which recapitulate organ-like features and thus, find application in disease modeling and precision oncology [25]. For the generation of a co-culture platform consisting of tumor-adjacent mammary gland tissue and breast cancer spheres in an autologous and allogenic manner, we first aimed at differentiating iPSC into MLOs expressing luminal and basal markers of the mammary epithelium. Our differentiation protocol comprises two steps and is based on previously described protocols [23, 24]. In a first step, solid iPSC spheres were directed into the non-neural ectodermal lineage for a period of 10 days by the incubation in serum-free culture medium optimized for culturing human breast tissue, as schematically illustrated in **Figure 1**A. The non-neural ectodermal iPSC spheres are referred to as “mammary embryoid bodies” (mEBs). As a control for the up- or downregulation of differentiation- and pluripotency markers, we concomitantly kept iPSC spheres in regular stem cell maintenance medium resulting in normal embryoid bodies (EBs). We examined the mEBs and EBs for their expression of CK18 and AP2γ, crucial markers associated with the mammary epithelium and mammary gland differentiation, and of the pluripotency transcription factor Sox2. In line with a successful differentiation, our data revealed a significant upregulation of AP2γ and CK18 in mEBs compared to EBs. Contrary, Sox2 expression was maintained in EBs but downregulated in mEBs (**Figure 1**B). The second stage of the protocol comprises the generation of a 3D floating system, consisting of day-10 mEBs that are cultured in the center of floating Matrigel®-collagen droplets. The matrix approximately recapitulated the stiffness of a normal mammary gland of about 170 Pa [23, 26]. Since our overall aim comprises the co-culture of MLOs and PDMs or cancer cell line-derived spheroids, we intended to combine our breast cancer spheres with mEBs at the beginning of stage 2 of the differentiation protocol and to monitor the co-culture for 10 days. Therefore, we sought to ensure that day-20 MLOs express markers associated with the mammary epithelium. Whole mount IF staining revealed that day-20 MLOs were positive for the luminal epithelial markers CK8, CK18 and EpCAM and for the basal epithelial markers CK14 and p63 (**Figure 1**C). As a proof for functionality, day-35 MLOs were incubated for another 5 days in prolactogenic medium and stained positive for the expression of the milk protein β-casein in gland-like structures (**Figure 1**C, lower panel). Furthermore, day-20 MLOs formed acinar-like structures with hollow lumen (yellow arrow) as shown by parallel staining of F-actin and Nuclei (**Figure 1**D). To confirm that our organoids are viable prior to embedding in Matrigel®-collagen matrices and during the downstream differentiation, we performed a viability test of day-10 mEBs and day-35 MLOs via parallel staining with Calcein-AM™ (viable cells), SYTOX™ Orange (dead cells) and Hoechst nucleic acid stain. Both the mEBs and the MLOs exhibited a

mean viability of at least 88% ± 6.9 (**Figure 1**E). Representative 2D projections of confocal 3D images illustrated the high overall viability of day-35 MLOs (**Figure 1**E, lower panel). Taken together, we demonstrated the successful iPSC-derived differentiation into MLOs, which express markers of the mammary epithelium and harbor phenotypical and functional properties of the human mammary gland such as the formation of acinar structures or β-casein expression.

5.2 Generation of viable, heterogenous patient-derived microtumors from histologically different types of primary breast cancers

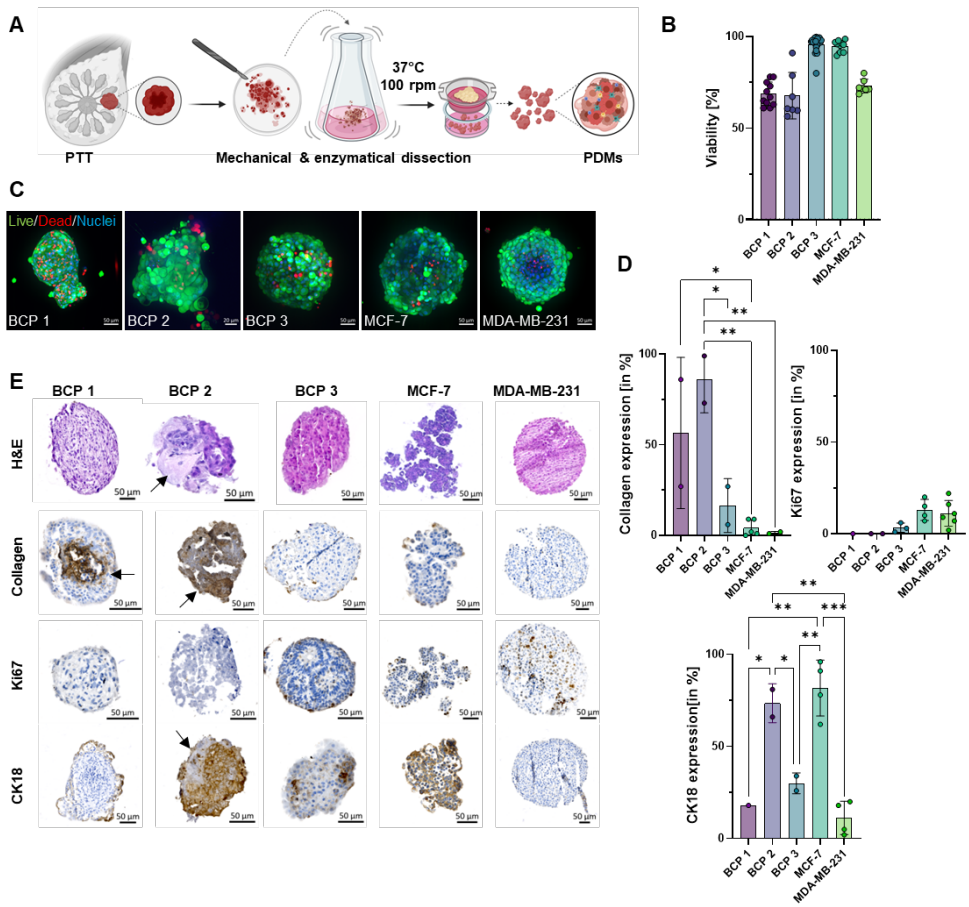

Figure 2: Vital, heterogenous PDMs can be isolated from PPT. A) *Schematic overview of the isolation of PDMs from PTT (created with BioRender). Residual fresh tumor tissue was collected after completion of pathological examination in culture medium at the day of surgery and processed at the same day. Tumor specimens were mechanically minced into 1-2 mm tissue pieces and subsequently enzymatically digested overnight. PDMs were retained by the filtration of the digested tissue through a 40 µm mesh and maintained in suspension culture for a maximum of 3 weeks or cryopreserved in liquid nitrogen until further use.* ***B)*** *Viability data were semi-quantitatively acquired with the microscopy*

image analysis software Imaris 9.0 based on confocal image stacks of the live-dead cell stained PDMs and cell line-derived spheroids, respectively. Mean viability in percent: BCP 1 (n=11): 69%, BCP 2 (n=7): 67%, BCP 3 (n=20): 96%, MCF-7 (n=10): 95%, MDA-MB-231 (n=7): 73%. ***C)*** *Representative 2D projections of 3D confocal images of the breast cancer PDMs and cell line-derived spheres.* ***D)*** *Percentages of DAB+ cells stained for collagen, Ki67 and CK18 expression based on IHC stainings. Statistics: **** p<0.0001, *** p<0.001, ** p<0.01, * p<0.05, One-way ANOVA using Tukey's multiple comparison test. Error bars: SD.* ***E)*** *Representative images of 3 µm slices of the breast cancer PDMs and cell line-derived spheres stained with H&E (upper panel). Lower panel: Representative images of the IHC DAB+ staining for collagen, Ki67 and CK18. Black arrows indicate non-cellular, stromal regions within the BCP 2 PDMs.*

Breast cancer is a heterogenous malignant lesion of viable origin and can be classified according to molecular and morphological features. To better understand breast cancer's invasive properties and interaction with the TME, it is crucial to use cancer models that reflect this diverse nature of breast carcinomas. We previously introduced the isolation of ovarian and brain microtumors from primary tumor tissue (PTT) and described the heterogenous nature of PDMs and their functionality in compound testing [17-19]. Here, we transferred this knowledge to breast cancer lesions and isolated breast microtumors from primary breast tumor tissue. To this end, residual tumor specimen from n = 3 treatment-naïve patients diagnosed with histologically different breast cancers were obtained after completion of histopathological examination. Anonymized clinicopathological data including histopathological and clinical staging of respective tumors are summarized in **Table 1**. The PTT was mechanically dissected into 1 – 2 mm fragments and enzymatically digested overnight (**Figure 2**A). The residual cell aggregates represented the PDMs, which typically showed an average diameter of 120 µm. The total number of isolated PDMs from individual tumor specimens ranged from 200 to 4500, depending on the size and biological composition of the PTT. To compare cellular composition and viability of PDMs with widely used breast cancer model systems we generated cancer spheroids from MCF-7 and MDA-MB-231 cell lines. Image-based analysis revealed a mean PDM viability from 82% (range: 68 - 95%), which resembled the mean viability of cell line-derived spheroids of 84% (range: 73% - 95%) (**Figure 2**B). Representative images of the life-dead cell staining indicated the high overall viability of PDMs and cell line spheroids (**Figure 2**C). To determine the proliferation activity of PDMs and cell line-derived spheroids in suspension culture, we stained the cancer models for Ki67, a commonly used proliferation marker. For the PDM models studied, low levels of Ki67 expression were observed (range: 0% - 3%), while the spheroids derived from the cancer cell lines showed a higher mean proliferative activity of 11% in suspension culture (**Figure 2**D). Furthermore, we assessed the expression of primary tumor tissue resident ECM components such as collagen in isolated PDM models compared to spheroids derived from cell lines. Our data revealed a significant difference of the collagen amount in BCP 1 and BCP 2 compared to BCP 3 confirming the heterogenous inter- and intratumoral heterogeneity of individual breast tumors. In contrast to cell line-derived spheroids, PDMs contained substantial amounts of extracellular matrix (ECM) components (**Figure 2**D,E, black arrows). CK18 acts as a breast cancer prognostic marker due to

its frequent downregulation during epithelial-mesenchymal-transition (EMT) [27]. We observed that CK18 expression was significantly reduced in PDMs from BCP 1 compared to BCP2. As expected, spheroids derived from highly metastatic MDA-MB-231 cells expressed significantly lower levels of CK18 compared to spheroids derived from non-metastatic MCF-7 cells (**Figure 2**D,E) [27]. Representative images of immunohistochemistry (IHC) stainings reflected the distribution of the investigated markers. Hematoxylin and eosin (H&E) staining indicated the heterogenous cellular morphology and cell density of the different breast cancer spheres (**Figure 2**E).

Table 1: Overview of the anonymized patient cohort.

Patient	Age	Histology	ER	PR	HER2	T	N	M	L	V	Pn	Ki67
BCP 1	48	IDC-NST	+	+	-	3	3a	0	1	0	0	21%
BCP 2	86	ILC	+	+	-	3	1a	0	0	0	1	10%
BCP 3	71	Mucinous	+	+	-	2	0	0	0	0	0	5-10%

BCP 1 was diagnosed with an invasive ductal carcinoma of the no special type (IDC-NST), BCP 2 developed an invasive lobular carcinoma (ILC) and BCP 3 was diagnosed with a mucinous ductal carcinoma. All tumors were primary tumors and derived from treatment-naïve patients. TNM-classification identifies the size of the tumor (T), regional lymph node involvement (N) and the presence of distant metastases (M). T2: 2-5 cm; T3: > 5cm. N0: no regional lymph node spread. N1: invasion to 1-3 lymph nodes. N3: invasion to 7+ lymph nodes. L, V, and Pn indicate the invasion to the lymphatic pathways (L), venous (V) and perineural (Pn) invasion, respectively. Ki67 values indicate the respective cancer proliferation rate.

5.3 Invasive behavior of breast cancer PDMs in the presence of extracellular matrix

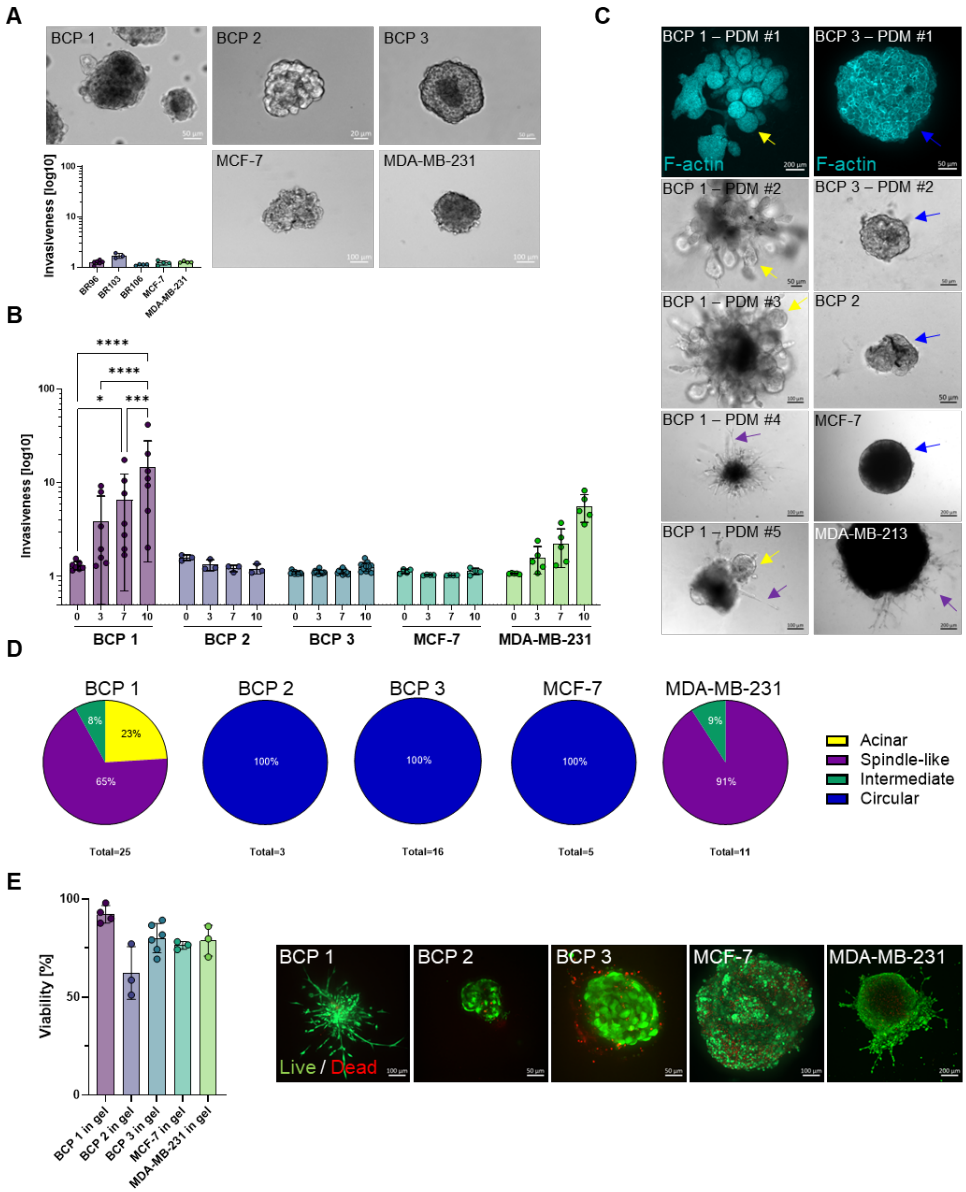

Figure 3: IDC-NST PDMs show invasive phenotypes in a 3D floating ECM system. A) *Representative brightfield images of breast cancer spheres maintained in suspension culture in the absence of ECM. PDMs and cancer cell line-derived spheroids display a non-invasive phenotype in suspension culture, in the absence of ECM. BCP 1: n=7, BCP*

2: n=3, BCP 3, MCF-7 and MDA-MB-231: n=4. ***B)*** *Image-based invasiveness analysis of PDMs and cell line spheroids at day 0, day 3, day 7 and day 10 in the 3D floating ECM system with BCP 1: n=7, BCP 2: n=3, BCP 3: n=12, MCF-7: n=4, MDA-MB-231: n=5.* ***C)*** *Representative brightfield images of the breast cancer spheres in ECM display the formation of different phenotypes with the following classifications: acinar (yellow arrow), spindle-like (purple arrow), intermediate and circular (blue arrow). F-actin staining of one exemplary BCP 1 PDM with the acinar phenotype and of one exemplary BCP 3 PDM with the circular phenotype describe the 3D structure of the breast cancer spheres (upper panel).* ***D)*** *Part-of-whole diagrams indicate the percentages of breast cancer spheres exhibiting acinar, spindle-like, intermediate (acinar and spindle-like) and circular phenotypes. BCP 1: n=25, BCP 2: n=3, BCP 3: n=16, MCF-7: n=5, MDA-MB-231: n=11.* ***E)*** *Image based viability analysis of the breast cancer spheres after 10 days in ECM with BCP 1: n=4, BCP 2: n= 3, BCP 3: n=6, MCF-7 & MDA-MB-231: n=3. Percentage of dead cells was calculated from the total cell number. Right panel: Representative 2D projections of 3D confocal images of live-dead-stained PDMs in ECM after 10 days. Statistical tests: 2way ANOVA using Tukey's multiple comparison test. **** p<0.0001, *** p<0.001, ** p<0.01. *p <0.05. Error bars: SD*

In vivo, solid tumors are under the dynamic influence of connective tissue and the ECM, which play a dual role in tissue homeostasis and pathogenesis. After the isolation of PDMs from primary tumor tissue, we aimed at investigating the influence of the ECM on PDMs and cancer cell line spheroids with respect to morphology and invasive behavior. First, the breast cancer spheres were cultured in suspension in absence of ECM for at least 10 days. Representative brightfield images displayed compact, circular, and thus, non-invasive phenotypes among all breast cancer models (**Figure 3**A). Next, breast cancer sphere singlets were individually embedded in the center of liquid Matrigel®-collagen matrix droplets recapitulating the normal mammary gland stiffness. We monitored the phenotypes of the PDMs and spheroids in the floating 3D system over a period of 10 days. Our data revealed a >10-fold increase in the invasiveness of BCP 1 over this experimental time (1.3 ± 0.12 at day 0, to 14.7 ± 12.29 at day 10) (**Figure 3**B). As expected, spheroids generated from the highly metastatic MDA-MB-231 cell line also showed an increase in invasive behavior, although less pronounced compared to BCP-1 PDMs. In contrast, PDMs from BCP 2 and BCP 3 as well as spheroids derived from non-metastatic MCF7 cells maintained a circular, non-invasive phenotype in ECM. Based on their morphology, we classified the observed phenotypes into four groups: acinar structures (yellow arrows), spindle-like protrusions (purple arrows), intermediate structures showing both acinar and spindle-like properties as well as circular morphologies (blue arrows) (**Figure 3**C). 65% of the highly invasive BCP 1 PDMs showed the spindle-like phenotype, while 23% formed acinar protrusions. 8% of BCP 1 PDMs were in an intermediate state at day 10. In contrast, MDA-MB-231 spheroids lacked the formation of prominent acinar phenotypes, however, 9% showed the formation of intermediate structures, while the majority of 91% developed a spindle-like morphology (**Figure 3**D). To exclude the possibility, that the maintenance of circular phenotypes in the non-invasive breast cancer models is caused by different extent of cell death among tested models, we assessed their viability after 10 days in the 3D floating ECM system. Results confirmed a mean cell viability of at least 50% and no significant difference between tested models (**Figure 3**E). Taken together, our results show that

399 the presence of ECM can lead to a pronounced invasive phenotype in patient-derived IDC-NST
400 microtumors.

5.4 Co-culture of invasive PDMs and early MLOs potentiates the development of a metastatic tumor phenotype

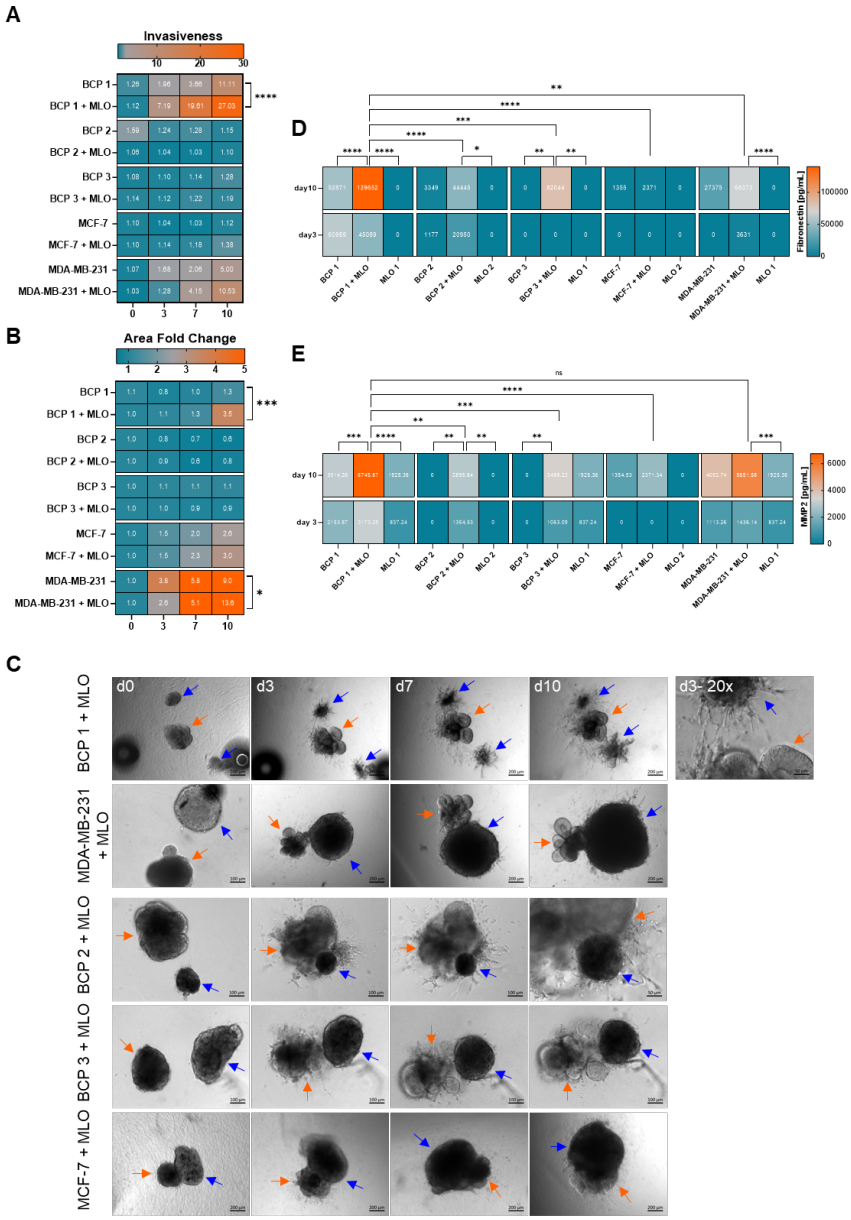

Figure 4: Tumor-adjacent MLOs promote growth and invasiveness of IDC-NST microtumors and support the upregulation of soluble MMP2 and FN. A) *Invasion assay of breast cancer sphere co-cultures and respective mono-*

cultures for a period of 10 days. ***B)*** *Measurement of the area of breast cancer spheres in presence or absence of MLOs for a period of 10 days. For both assays: BCP 1: n=7, BCP 1 + MLO: n=5, BCP2: n=3, BCP 2 + MLO: n=4, BCP 3: n=12, BCP 3 + MLO: n=8, MCF-7: n=4, MCF-7 + MLO: n=2, MDA-MB-231: n=5, MDA-MB-231 + MLO: n=2.* ***C)*** *Representative bright field images of the co-cultures at day 0 (co-culture start), day 3, day 7 and day 10. Red arrows: MLOs. Blue arrows: Breast cancer spheres. BCP 1 d3 – 20x: 20x magnification indicates the spindle-like phenotype of a BCP 1 PDM growing towards the MLO.* ***D), E)*** *Measurement of soluble FN and MMP2 (in pg/mL) from supernatants of the co-cultures and monocultures of breast cancer spheres and MLOs via Luminex assay. Supernatants were collected at day 3 and day 10. For each condition, 3 replicates were measured. Statistics (day 10): **** p<0.0001, *** p<0.001, ** p<0.01, * p<0.05 2way ANOVA using Šidák multiple comparison test. Displayed are median values.*

Breast tumor-adjacent cell populations, such as mammary epithelial cells, might exert a tumor-promoting function during the complex process of cancer progression. We attempted to extend our current knowledge about the potential tumor-promoting function of mammary gland organoids on breast cancer growth and invasion by generating a 3D co-culture system which closely resembles the characteristics and heterogeneity of (cancerous) human breast tissue. To this end, we combined MLOs with breast cancer spheres and monitored growth and invasiveness of the respective cancer models over a period of 10 days. A single organoid and a single breast cancer sphere were placed in close proximity to each other in the center of a liquid Matrigel® collagen droplet, resulting in a 3D floating co-culture system. Representative brightfield images of the co-cultures at different time points are shown (**Figure 4**C). Within the first 3 days, cancer spheres (blue arrows) and MLOs (red arrows) moved towards each other and formed a compact two-component structure. For BCP 1 PDMs, which showed the highest degree of invasiveness in previous experiments with ECM (see above), we observed a directed invasion of the PDMs towards the MLO at day 3 (Figure 4C, d3 - 20x). In fact, the presence of MLOs potentiated the invasive properties of the BCP 1 PDMs in the co-culture setup (**Figure 4**A). In support of this observation, a similar but less pronounced trend could be observed for MDA-MB-231 spheroids in co-culture with MLOs. For BCP 2, BCP 3 and MCF-7, which did not show invasive behavior in previous experiments, there was no significant difference in invasiveness between the breast cancer spheres in co-culture with or in the absence of MLOs. Next, we investigated whether the presence of MLOs influences the growth of breast cancer spheres in addition to its impact on morphology and invasion. To this end, we examined the area fold change of PDMs and cell line spheroids in co-culture or cultured alone. We detected a significant increase in size for both the highly invasive BCP 1 PDMs as well as MDA-MB-231 spheroids co-cultured with MLOs but not for the non-invasive BCP 2 and BCP 3 PDMs and MCF7 spheroids (**Figure 4**B). In a next step, we analyzed differences in the secretion of previously described metastasis-related markers (FN and MMP2) among the different cultures. We found that soluble FN and MMP2 were significantly elevated in all co-cultures of BCP 1, 2, 3 and MDA-MB-231 but not MCF7 at day 10 compared to mono-cultured MLOs and breast cancer spheres (**Figure 4**D, E). Within this cohort, the co-culture of BCP 1 PDMs + MLOs expressed the highest levels of invasion-markers of which FN (mean:

444 47.6 ± 12.9 pg/mL) differed significantly compared to BCP 2, 3, MCF-7 and MDA-MB-231 (**Figure**
445 **4**D). Taken together, our data show that tumor-adjacent breast tissue supports tumor growth and
446 invasiveness of invasive in ductal breast carcinoma microtumors and might play a crucial role in
447 activating the metastasis-related markers MMP2 and FN in breast cancer.

448 6. Discussion

449 The immediate environment of developing tumors is a critical determinant for the fate of the
450 neoplastic lesion, and thus disease progression in the patient. Within this framework, current
451 research has been focused in particular on the interaction between cancer cells and stromal
452 components such as fibroblasts, adipocytes or immune cells [28-30]. However, tumor-adjacent
453 epithelial cells are presumably the first point of interaction for mammary epithelial carcinomas
454 during tumorigenesis and thus, play a decisive role in cancer progression [14].

455 Here, we introduce a 3D co-culture system which allows for the investigation of breast tumor
456 growth, invasion, and metastasis-related processes under the dynamic influence of tumor-
457 adjacent mammary epithelium in an autologous and allogenic manner. Our model system reflects
458 the intra- and intertumoral heterogeneity of individual breast cancer lesions by using patient-
459 derived microtumors (PDMs) of different malignant stages and histological properties. Our
460 approach successfully distinguished invasive from non-invasive breast cancer phenotypes using
461 a combination of morphology and protein secretion analysis. Interestingly, secretion of both FN
462 and MMP, which are discussed as prognostic markers for breast cancer, was significantly up-
463 regulated following co-culture of invasive breast cancer spheres with iPSC-derived organoids of
464 the mammary epithelium.

465 The role of mammary epithelial and myoepithelial cells in tumorigenesis has been controversy
466 discussed. Previous studies have shown that both, the healthy mammary epithelium and the
467 myoepithelium take over a dual role in tumor progression: On the one hand, they can act as
468 "gendarmes" and keep the malignant cells in check. In vivo and in vitro studies reported inhibitory
469 effects of myoepithelial cells on tumor growth and invasion by acting as natural tumor suppressors
470 [31-33]. Furthermore, studies described a breast tumor growth-inhibiting effect of normal
471 mammary epithelial cells. This phenomenon was observed with immortalized breast cancer cell
472 lines and primary cancer cells from reduction mastectomy in combination with immortalized normal
473 epithelial mammary cell lines or primary cells obtained from reduction mammoplasty [34-36]. On
474 the other hand, non-tumorigenic (myo-) epithelial cells can become “accomplices” and support
475 tumor growth. Tumor-associated myoepithelial cells undergo alterations and overexpress
476 oncogenic chemokines such as SDF-1, which supports tumor growth and invasion [37].

Furthermore, it was shown that the tumor-associated myoepithelium supports the invasive progression of ductal carcinomas in situ (DCIS) to IDC via TGF-β signaling [38]. Studies revealed that conditioned medium from immortalized mammary epithelial cells increases MCF-7 motility [13] and that the non-tumorigenic mammary epithelium can promote breast cancer cell proliferation via MCP-1 secretion [14]. It was demonstrated that non-cancerous mammary epithelial cells induce malignant cells to secrete cytokines such as IL-6 and GM-SCF via direct cell-cell contacts [11]. Furthermore, co-injection of mammary benign epithelial cells and breast cancer cells in nude mice xenograft assays led to a three-fold increase in tumor size [11].

Our results are partially in agreement with the tumor-supportive effects caused by the tumor-adjacent mammary epithelium. BCP 1 PDMs displayed a highly invasive phenotype, exceeding the invasive characteristics of MDA-MB-231 spheroids analyzed in parallel. This invasive phenotype was even further potentiated under the influence of co-cultured MLOs. At the same time, these effects could not be observed in spheroids derived from the non-metastatic MCF-7 cell line and in PDMs from BCP 2 and BCP 3. Unlike primary cancer cells or immortalized cells lines, PDMs are not composed of a homogenous culture of neoplastic cells but consist of diverse cell types and stromal components reflecting the heterogeneous nature and composition of primary patient tumors [17-20]. The tumor specimens used in our study can be listed according to their malignant progression in descending order: BCP 1 was diagnosed with a stage III IDC-NST. According to the TNM malignancy classification system, the tumor was identified as T3N3aM0 tumor, indicating a primary tumor size > 5 cm and an involvement of 7+ regional lymph nodes [39]. Moreover, the tumor invaded the lymphatic pathway, while perineural and venous invasion could not be observed (L1V0pN0). Compared to the primary tumors of BCP 2 and 3, the IDC-NST lesion showed the highest Ki67+ proliferation rate of 21%. BCP 2 developed a stage III invasive lobular carcinoma (ILC) with a T3N1aM0 classification. Like BCP 1, the tumor has grown to a size of over 5 cm but invaded to 1-3 regional lymph nodes. Invasion to the lymphatic and venous pathways were not detected, but instead, the tumor showed perineural invasion. BCP 3 was diagnosed with a stage II ductal mucinous carcinoma of the special type with 2 cm – 5 cm in size. The tumor did not spread to the regional lymph nodes (T2N0M0) and did not invade to the lymphatic, venous and perineural system (L0V0pN0). Both, BCP 2 and BCP 3 showed a lower Ki67 score than BCP 1.

Furthermore, we included two immortalized breast cancer cell lines, MCF-7 and MDA-MB-231 to compare the in vitro behavior of PDMs with cell line-derived spheroids with different invasive behavior. MCF-7 is a non-invasive cell line, while MDA-MB-231 shows invasive behavior in vitro [27, 40]. Our results indicate that the malignant severity of the primary tumor is reflected in the

phenotypic behavior of corresponding microtumors in vitro: BCP 1 PDMs developed an invasive phenotype in ECM, which was further increased upon co-culture with MLOs. However, BCP 2 did not show invasive phenotypes in our model when cultured separately in ECM or co-cultured with MLOs, despite its invasive potential in vivo. This deviation could be explained by the fact, that BCP 2 PDMs intratumorally contained large areas of internal ECM and displayed comparably low viability after isolation from the primary tumor and after 10 days in ECM. This might have attenuated the invasive potential of the microtumors. Still, a significant increase in secretion of pro-metastatic factors FN and MMP2 was also observed for this PDM model.

In line with our expectations, BCP 3 PDMs showed a non-invasive phenotype in our analyses. Mucinous breast carcinomas are rare, but are associated with a good clinical prognosis due to their low metastatic rates [41] [42]. The non-invasive behavior in vitro could be due to the fact that the mucus surrounding the tumor provides a mechanical barrier that attenuates cancer invasion [43].

Furthermore, we investigated the supernatants of the PDM/spheroid and MLO mono- and co-cultures and observed that MMP2 was upregulated in all co-culture systems except for MCF7 cells. Activated MMP2 can lead to the degradation of ECM components including the basement membrane, allowing the tumor to invade the surrounding tissue and distant organs in diverse malignant neoplasms and is associated with a poor patient survival [44-47]. Except for MCF7, which did not show a significant up-regulation of MMP2 levels, we observed elevated MMP2 concentrations particularly in the co-cultures of breast cancer spheres and MLOs compared to the respective mono-cultures, which might indicate that the combination of non-cancerous and malignant tissue favors processes associated with invasion and metastasis. One key player in this process could be SDF-1, which is known to be secreted by the tumor-adjacent mammary epithelial cells and to promote breast cancer invasion, motility, and metastasis via the SDF-1/CXCR4 axis and subsequent activation of MMP2 [12, 48, 49]. In addition, we observed highly increased concentrations of soluble FN in the co-cultures compared to the respective mono-cultures of breast cancer spheres and MLOs, again with the exception of MCF7. FN was shown to be associated with migration and invasion of different types of cancers [50, 51] and stimulated cancer cell growth through the upregulation of several inflammatory factors [52]. Elevated FN expression is associated with an invasive and metastatic breast cancer phenotype since FN contributes to EMT-like morphological changes in breast cancer cells [53]. It is conceivable that increased MMP2 expression leads to FN degradation and thus, to elevated concentration of soluble FN [54]. Other studies have shown that increased FN leads to the upregulation of MMP2 [55-57]. Interestingly, FN and MMP2 were upregulated in all co-cultures tested in our study, including those whose

invasive and growth potential was not promoted by MLO co-culture. However, the concentrations of FN and MMP2 were much higher in the co-cultures with BCP 1 PDMs compared to the other co-cultures. Due to the fact that the primary tumor of BCP 1 was in a more advanced tumor stage than the primary tumor of BCP 2 and 3, we postulate that the tumor needs to reach a certain threshold with regard to invasive and proliferative capacity before metastatic behavior with secretion of respective mediators is triggered. The precise regulation of this mechanism needs to be deciphered in further studies. These studies will also address whether direct cell-cell-contacts between breast cancer spheres and MLOs are required for initiation of the observed tumor-promoting processes. Furthermore, one obstacle to overcome in the following years is the fact that iPSC-derived organoids do not reflect the mature identity of an adult organ but rather remain in an immature, embryonic-like stage [24]. As the vast majority of human malignancies, breast cancer included, are age-associated diseases, more mature organoid structures to study the interaction with patient-derived neoplastic material would be of great value but are not yet available [58]. Taken together, our data confirm previous observations on a tumor-promoting effect of tumor-adjacent mammary gland tissue and highlight the importance of intra- and intertumoral heterogeneity of different models. Furthermore, our data indicate that the invasive and proliferative potential of the primary tumors are reflected in the in vitro behavior of the respective microtumors. Therefore, we see the future of breast cancer research in the use of patient-derived models including breast microtumors rather than in cancer cell line-derived spheroids to obtain more precise information about tumor progression and metastasis-associated processes and to better understand the complex behavior of individual breast carcinomas. We hope that this future understanding helps to develop more efficient therapies for individual breast lesions.

7. Conclusion

Overall, this study extends our knowledge of the influence of the tumor-adjacent mammary epithelium on tumor growth, invasiveness and metastasis-related processes. We show that the tumor-adjacent mammary epithelium promotes growth and invasion of microtumors from a patient diagnosed with IDC-NST and assume that the mammary gland tissue serves as a “breast cancer promoting catalyst” especially when the tumor has already reached a certain threshold in terms of cancer stage and proliferation capacity. Our model identified the upregulation of FN and MMP2, two cancer-related prognostic markers for metastatic transformation, when non-cancerous, tumor-adjacent mammary epithelium is present. Thus, we highlight the important role of tumor-adjacent mammary epithelium in cancer progression and emphasize the importance of the use of breast cancer models that reflect the heterogenous nature of primary breast lesions.

8. List of abbreviations

BCP	Breast cancer patient
PDMs	Patient-derived microtumors
iPSCs	Induced pluripotent stem cells
MLOs	Mammary-like organoids
mEBs	Mammary embryoid bodies
EBs	Embryoid bodies
FN	Fibronectin
MMP	Metalloproteinase
EMT	Epithelial-mesenchymal transition
TME	Tumor microenvironment
DCIS	Ductal carcinoma in situ
IDC-NST	Invasive ductal carcinoma of no special type
ILC	Invasive lobular carcinoma
PTT	Primary tumor tissue
PBMCs	Peripheral blood mononuclear cells

9. Declarations

Ethics approval and consent to participate

The research project was approved by the ethics committee of the medical faculty of the University Hospital Tuebingen, Germany (project number 788/2018BO2 and 888/2019BO2). Written informed consent was obtained from all participants prior to surgery.

Consent for publication

All authors give their consent for publication.

Availability of data and materials

The data that support the findings of this study are available upon reasonable request and after signature of an MTA from the corresponding authors.

Competing interests

No potential competing interests were disclosed.

Funding

This work received financial support from the Ministry of Baden-Wuerttemberg for Eco-nomic Affairs, Labor and Tourism (grant 3-4332.62-HSG/84).

595 **Author contributions**

596 Conceptualization and design of the study: A-L.K., C.S. and K.S-L.; data collection, data analysis,
597 investigation and interpretation, A-L.K., N.A., D.G., A.B., D.V., M.S., J.G., A.K., M.W., S.B., and
598 C.S.; writing—original draft, A.K. and C.S.; writing—review and editing, A-L.K., N.A., M.S., D.G.,
599 A.B., D.V., M.W., A.K., S.B. and K.S-L.; visualization: A-L.K. and C.S.; supervision: C.S.; project
600 administration: A-L.K., C.S. and A.K. All authors have read and agreed to the published version
601 of the manuscript.

602 **Acknowledgements**

603 We gratefully acknowledge the Department of Women's Health, Women's
604 University Hospital, Tuebingen University Hospital for excellent support, helpful discussions and
605 providing fresh tumor tissue biopsies and corresponding FFPE material. We thank all patients and
606 healthy volunteers for participating in our study.

607 ## 10. References

608 1. Cheng HG, Gonzalez-Reymundez A, Li I, Pathak A, Pathak DR, de Los Campos G, Vazquez AI: **Breast**
609 **cancer survival and the expression of genes related to alcohol drinking**. *Plos one* 2020,
610 **15**(2):e0228957.
611 2. Malmgren JA, Calip GS, Atwood MK, Mayer M, Kaplan HG: **Metastatic breast cancer survival**
612 **improvement restricted by regional disparity: surveillance, epidemiology, and end results and**
613 **institutional analysis: 1990 to 2011**. *Cancer* 2020, **126**(2):390-399.
614 3. Lüönd F, Tiede S, Christofori G: **Breast cancer as an example of tumour heterogeneity and tumour**
615 **cell plasticity during malignant progression**. *British journal of cancer* 2021, **125**(2):164-175.
616 4. Anderson NM, Simon MC: **The tumor microenvironment**. *Current Biology* 2020, **30**(16):R921-
617 R925.
618 5. Truffi M, Sorrentino L, Corsi F: **Fibroblasts in the tumor microenvironment**. *Tumor*
619 *Microenvironment* 2020:15-29.
620 6. Oskarsson T: **Extracellular matrix components in breast cancer progression and metastasis**.
621 *Breast* 2013, **22 Suppl 2**:S66-72.
622 7. Konopka JA, DeBaun MR, Chang W, Dragoo JL: **The intracellular effect of relaxin on female**
623 **anterior cruciate ligament cells**. *The American Journal of Sports Medicine* 2016, **44**(9):2384-2392.
624 8. Reunanen N, Kähäri V: **Matrix metalloproteinases in cancer cell invasion**. In: *Madame Curie*
625 *Bioscience Database [Internet].* edn.: Landes Bioscience; 2013.
626 9. Jiang Y, Zhang H, Wang J, Liu Y, Luo T, Hua H: **Targeting extracellular matrix stiffness and**
627 **mechanotransducers to improve cancer therapy**. *Journal of Hematology & Oncology* 2022,
628 **15**(1):1-15.
629 10. Jo SH, Heo WH, Son HY, Quan M, Hong BS, Kim JH, Lee HB, Han W, Park Y, Lee DS *et al*: **S100A8/A9**
630 **mediate the reprograming of normal mammary epithelial cells induced by dynamic cell-cell**
631 **interactions with adjacent breast cancer cells**. *Sci Rep* 2021, **11**(1):1337.
632 11. Poczobutt JM, Tentler J, Lu X, Schedin PJ, Gutierrez-Hartmann A: **Benign mammary epithelial cells**
633 **enhance the transformed phenotype of human breast cancer cells**. *Bmc Cancer* 2010, **10**(1):1-17.
634 12. Serrati S, Margheri F, Fibbi G, Di Cara G, Minafra L, Pucci-Minafra I, Liotta F, Annunziato F, Pucci
635 M, Del Rosso M: **Endothelial cells and normal breast epithelial cells enhance invasion of breast**

carcinoma cells by CXCR-4-dependent up-regulation of urokinase-type plasminogen activator receptor (uPAR, CD87) expression. *The Journal of Pathology: A Journal of the Pathological Society of Great Britain and Ireland* 2008, **214**(5):545-554.

13. Carpenter PM, Nguyen H: **Mammary epithelium-induced motility of MCF-7 cells**. *Anticancer research* 1998, **18**(2A):1063-1068.
14. Riverso M, Kortenkamp A, Silva E: **Non-tumorigenic epithelial cells secrete MCP-1 and other cytokines that promote cell division in breast cancer cells by activating ERα via PI3K/Akt/mTOR signaling**. *The international journal of biochemistry & cell biology* 2014, **53**:281-294.
15. Keller A-L, Greis D, Eybe J, Plöger S, Weiss M, Koch A, Brucker SY, Schenke-Layland K, Schmees C: **Generation and Characterization of Three Induced Pluripotent Stem Cells Lines from an 86-Year Old Female Individual Diagnosed with an Invasive Lobular Mammary Carcinoma**. *Stem Cell Research* 2022:102988.
16. Keller A-L, Binner A, Schenke-Layland K, Schmees C: **Establishment of Four Induced Pluripotent Stem Cell Lines from CD34+ Hematopoietic Stem and Progenitor Cells from a Patient Diagnosed with an Invasive Lobular Mammary Carcinoma**. *Stem Cell Research* 2022, **64**:102902.
17. Anderle N, Koch A, Gierke B, Keller A-L, Staebler A, Hartkopf A, Brucker SY, Pawlak M, Schenke-Layland K, Schmees C: **A Platform of Patient-Derived Microtumors Identifies Individual Treatment Responses and Therapeutic Vulnerabilities in Ovarian Cancer**. *Cancers* 2022, **14**(12):2895.
18. Walter B, Canjuga D, Yüz SG, Ghosh M, Bozko P, Przystal JM, Govindarajan P, Anderle N, Keller AL, Tatagiba M: **Argyrin F Treatment-Induced Vulnerabilities Lead to a Novel Combination Therapy in Experimental Glioma**. *Advanced Therapeutics* 2021, **4**(9):2100078.
19. Przystal JM, Becker H, Canjuga D, Tsiami F, Anderle N, Keller A-L, Pohl A, Ries CH, Schmittnaegel M, Korinetska N: **Targeting CSF1R alone or in combination with PD1 in experimental glioma**. *Cancers* 2021, **13**(10):2400.
20. Erne E, Anderle N, Schmees C, Stenzl A: **Patientenabgeleitete Mikrotumoren**. *Die Urologie* 2022:1-6.
21. Bae YK, Kim A, Kim MK, Choi JE, Kang SH, Lee SJ: **Fibronectin expression in carcinoma cells correlates with tumor aggressiveness and poor clinical outcome in patients with invasive breast cancer**. *Human pathology* 2013, **44**(10):2028-2037.
22. Talvensaari-Mattila A, Pääkkö P, Turpeenniemi-Hujanen T: **Matrix metalloproteinase-2 (MMP-2) is associated with survival in breast carcinoma**. *British journal of cancer* 2003, **89**(7):1270-1275.
23. Qu Y, Han B, Gao B, Bose S, Gong Y, Wawrowsky K, Giuliano AE, Sareen D, Cui X: **Differentiation of human induced pluripotent stem cells to mammary-like organoids**. *Stem cell reports* 2017, **8**(2):205-215.
24. Dai X, Wang X, Yang C, Huang M, Zhou Z, Qu Y, Cui X, Liu R, Chen C: **Human fibroblasts facilitate the generation of iPSCs-derived mammary-like organoids**. *Stem cell research & therapy* 2022, **13**(1):1-12.
25. Clevers H: **Modeling development and disease with organoids**. *Cell* 2016, **165**(7):1586-1597.
26. Paszek MJ, Zahir N, Johnson KR, Lakins JN, Rozenberg GI, Gefen A, Reinhart-King CA, Margulies SS, Dembo M, Boettiger D: **Tensional homeostasis and the malignant phenotype**. *Cancer cell* 2005, **8**(3):241-254.
27. Shi R, Liu L, Wang F, He Y, Niu Y, Wang C, Zhang X, Zhang X, Zhang H, Chen M: **Downregulation of cytokeratin 18 induces cellular partial EMT and stemness through increasing EpCAM expression in breast cancer**. *Cellular Signalling* 2020, **76**:109810.
28. Becker LM, O'Connell JT, Vo AP, Cain MP, Tampe D, Bizarro L, Sugimoto H, McGow AK, Asara JM, Lovisa S: **Epigenetic reprogramming of cancer-associated fibroblasts deregulates glucose metabolism and facilitates progression of breast cancer**. *Cell reports* 2020, **31**(9):107701.

29. Wu Q, Li J, Li Z, Sun S, Zhu S, Wang L, Wu J, Yuan J, Zhang Y, Sun S: **Exosomes from the tumour-adipocyte interplay stimulate beige/brown differentiation and reprogram metabolism in stromal adipocytes to promote tumour progression**. *Journal of Experimental & Clinical Cancer Research* 2019, **38**(1):1-20.
30. Qi M, Xia Y, Wu Y, Zhang Z, Wang X, Lu L, Dai C, Song Y, Xu K, Ji W: **Lin28B-high breast cancer cells promote immune suppression in the lung pre-metastatic niche via exosomes and support cancer progression**. *Nature communications* 2022, **13**(1):1-18.
31. Sternlicht MD, Kedeshian P, Shao Z-M, Safarians S, Barsky SH: **The human myoepithelial cell is a natural tumor suppressor**. *Clinical cancer research: an official journal of the American Association for Cancer Research* 1997, **3**(11):1949-1958.
32. Hu M, Yao J, Carroll DK, Weremowicz S, Chen H, Carrasco D, Richardson A, Violette S, Nikolskaya T, Nikolsky Y: **Regulation of in situ to invasive breast carcinoma transition**. *Cancer cell* 2008, **13**(5):394-406.
33. Barsky SH, Karlin NJ: **Myoepithelial cells: autocrine and paracrine suppressors of breast cancer progression**. *Journal of mammary gland biology and neoplasia* 2005, **10**(3):249-260.
34. Spink BC, Cole RW, Katz BH, Gierthy JF, Bradley LM, Spink DC: **Inhibition of MCF-7 breast cancer cell proliferation by MCF-10A breast epithelial cells in coculture**. *Cell biology international* 2006, **30**(3):227-238.
35. Toillon R-A, Chopin V, Jouy N, Fauquette W, Boilly B, Bourhis XL: **Normal breast epithelial cells induce p53-dependent apoptosis and p53-independent cell cycle arrest of breast cancer cells**. *Breast cancer research and treatment* 2002, **71**(3):269-280.
36. Bourhis XDL, Berthois Y, Millot G, Degeorges A, Sylvi M, Martin PM, Calvo F: **Effect of stromal and epithelial cells derived from normal and tumorous breast tissue on the proliferation of human breast cancer cell lines in co-culture**. *International journal of cancer* 1997, **71**(1):42-48.
37. Allinen M, Beroukhim R, Cai L, Brennan C, Lahti-Domenici J, Huang H, Porter D, Hu M, Chin L, Richardson A: **Molecular characterization of the tumor microenvironment in breast cancer**. *Cancer cell* 2004, **6**(1):17-32.
38. Lo P-K, Zhang Y, Yao Y, Wolfson B, Yu J, Han S-Y, Duru N, Zhou Q: **Tumor-associated myoepithelial cells promote the invasive progression of ductal carcinoma in situ through activation of TGFβ signaling**. *Journal of Biological Chemistry* 2017, **292**(27):11466-11484.
39. Rosen RD, Sapra A: **TNM classification**. In: *StatPearls [Internet]*. edn.: StatPearls Publishing; 2021.
40. Gayan S, Teli A, Dey T: **Inherent aggressive character of invasive and non-invasive cells dictates the in vitro migration pattern of multicellular spheroid**. *Scientific reports* 2017, **7**(1):1-11.
41. Lacroix-Triki M, Suarez PH, MacKay A, Lambros MB, Natrajan R, Savage K, Geyer FC, Weigelt B, Ashworth A, Reis-Filho JS: **Mucinous carcinoma of the breast is genomically distinct from invasive ductal carcinomas of no special type**. *The Journal of pathology* 2010, **222**(3):282-298.
42. Dumitru A, Procop A, Iliesiu A, Tampa M, Mitrache L, Costache M, Sajin M, Lazaroiu A, Cirstoiu M: **Mucinous breast cancer: a review study of 5 year experience from a hospital-based series of cases**. *Maedica* 2015, **10**(1):14.
43. Roux P, Knight S, Cohen M, Classe JM, Mazouni C, Chauvet M-P, Reyal F, Colombo P-E, Jouve E, Chopin N: **Tubular and mucinous breast cancer: results of a cohort of 917 patients**. *Tumori Journal* 2019, **105**(1):55-62.
44. Zeng Z-S, Cohen AM, Guillem JG: **Loss of basement membrane type IV collagen is associated with increased expression of metalloproteinases 2 and 9 (MMP-2 and MMP-9) during human colorectal tumorigenesis**. *Carcinogenesis* 1999, **20**(5):749-755.
45. Li H-c, Cao D-c, Liu Y, Hou Y-f, Wu J, Lu J-s, Di G-h, Liu G, Li F-m, Ou Z-l: **Prognostic value of matrix metalloproteinases (MMP-2 and MMP-9) in patients with lymph node-negative breast carcinoma**. *Breast cancer research and treatment* 2004, **88**(1):75-85.

46. Li H, Qiu Z, Li F, Wang C: **The relationship between MMP-2 and MMP-9 expression levels with breast cancer incidence and prognosis**. *Oncology letters* 2017, **14**(5):5865-5870.
47. Jäälinojä J, Herva R, Korpela M, Höyhtyä M, Turpeenniemi-Hujanen T: **Matrix metalloproteinase 2 (MMP-2) immunoreactive protein is associated with poor grade and survival in brain neoplasms**. *Journal of neuro-oncology* 2000, **46**(1):81-90.
48. Muller A, Homey B, Soto H, Ge N, Catron D, Buchanan M, McClanahan T, Murphy E, Yuan W, Wagner S: **et al.(2001). Involvement of chemokine receptors in breast cancer metastasis**. *Nature*, **410**:6824.
49. Zhang R, Pan X, Huang Z, Weber GF, Zhang G: **Osteopontin enhances the expression and activity of MMP-2 via the SDF-1/CXCR4 axis in hepatocellular carcinoma cell lines**. *PLoS One* 2011, **6**(8):e23831.
50. Jia D, Yan M, Wang X, Hao X, Liang L, Liu L, Kong H, He X, Li J, Yao M: **Research article Development of a highly metastatic model that reveals a crucial role of fibronectin in lung cancer cell migration and invasion**. 2010.
51. Waalkes S, Atschekzei F, Kramer MW, Hennenlotter J, Vetter G, Becker JU, Stenzl A, Merseburger AS, Schrader AJ, Kuczyk MA: **Fibronectin 1 mRNA expression correlates with advanced disease in renal cancer**. *BMC cancer* 2010, **10**(1):1-6.
52. Zheng M, Jones DM, Horzempa C, Prasad A, McKeown-Longo PJ: **The first type III domain of fibronectin is associated with the expression of cytokines within the lung tumor microenvironment**. *Journal of cancer* 2011, **2**:478.
53. Li CL, Yang D, Cao X, Wang F, Hong DY, Wang J, Shen XC, Chen Y: **Fibronectin induces epithelial-mesenchymal transition in human breast cancer MCF-7 cells via activation of calpain**. *Oncology letters* 2017, **13**(5):3889-3895.
54. Steffensen B, Chen Z, Pal S, Mikhailova M, Su J, Wang Y, Xu X: **Fragmentation of fibronectin by inherent autolytic and matrix metalloproteinase activities**. *Matrix Biology* 2011, **30**(1):34-42.
55. Pereira IT, Ramos EA, Costa ET, Camargo AA, Manica GC, Klassen LM, Chequin A, Braun-Prado K, de O. Pedrosa F, Souza EM: **Fibronectin affects transient MMP2 gene expression through DNA demethylation changes in non-invasive breast cancer cell lines**. *PLoS One* 2014, **9**(9):e105806.
56. Moroz A, Delella FK, Lacorte LM, Deffune E, Felisbino SL: **Fibronectin induces MMP2 expression in human prostate cancer cells**. *Biochemical and biophysical research communications* 2013, **430**(4):1319-1321.
57. Das S, Banerji A, Frei E, Chatterjee A: **Rapid expression and activation of MMP-2 and MMP-9 upon exposure of human breast cancer cells (MCF-7) to fibronectin in serum free medium**. *Life sciences* 2008, **82**(9-10):467-476.
58. Benz CC: **Impact of aging on the biology of breast cancer**. *Critical reviews in oncology/hematology* 2008, **66**(1):65-74.

Publication 5 | F

Breast Cancer Patient-derived Microtumors Resemble Tumor Heterogeneity and Enable Protein-based Stratification and Functional Validation of Individualized Drug Treatment

Nicole Anderle[1*], Felix Schäfer-Ruoff[1], Annette Staebler[2], Nicolas Kersten[3,4], André Koch[5], Cansu Önder[5], Anna-Lena Keller[1], Simone Liebscher[6], Andreas Hartkopf[5,7], Markus Hahn[5], Markus Templin[1], Sara Y. Brucker[5,8], Katja Schenke-Layland[1,6,8], Christian Schmees[1*]

[1]NMI Natural and Medical Sciences Institute at the University of Tuebingen, 72770 Reutlingen, Germany

[2]Institute of Pathology and Neuropathology, Eberhard Karl's University Tuebingen,72076 Tuebingen, Germany

[3]Interfaculty Institute for Bioinformatics and Medical Informatics (IBMI), University of Tuebingen, 72076 Tuebingen, Germany

[4]FZI Research Center for Information Technology, 76131 Karlsruhe, Germany

[5]Department of Women's Health, University Women's Hospital, Eberhard Karl's University Tuebingen, 72076 Tuebingen, Germany

[6]Institute of Biomedical Engineering, Department for Medical technologies and Regenerative Medicine, Eberhard Karl's University Tuebingen, 72076 Tuebingen, Germany

[7]Department of Gynecology and Obstetrics, University Hospital of Ulm, 89081 Ulm, Germany

[8]Cluster of Excellence iFIT (EXC2180)"Image-Guided and Functionally Instructed Tumor Therapies", Eberhard Karl's University Tuebingen, 72076 Tuebingen, Germany

*Email: nicole.anderle@nmi.de; christian.schmees@nmi.de

1. Abstract

Despite tremendous progress in deciphering breast cancer at the genomic level, the pronounced heterogeneity remains a major obstacle to the advancement of novel and more effective treatment approaches. Frequent treatment failure and the development of treatment resistance highlight the need for patient-derived tumor models that reflect the individual tumors of breast cancer patients and allow a comprehensive analyses and parallel functional validation of individualized and therapeutically targetable vulnerabilities in protein signal transduction pathways. Here, we introduce the generation and application of breast cancer patient-derived 3D microtumors (BC-PDMs). Residual fresh tumor tissue specimens were collected from n=102 patients diagnosed with breast cancer and subjected to BC-PDMs isolation. BC-PDMs retained histopathological characteristics, and extracellular matrix (ECM) components together with key protein signaling pathway signatures of the corresponding primary tumor tissue. Accordingly, BC-PDMs reflect the intertumoral heterogeneity of breast cancer and its key signal transduction properties. DigWest®-based protein expression profiling of identified treatment responder and non-responder BC-PDMs enabled the identification of potential resistance and sensitivity markers of individual drug treatments, including markers previously associated with treatment response and yet undescribed proteins. The combination of individualized drug testing with comprehensive protein profiling analyses of BC-PDMs may provide a valuable complement for personalized treatment stratification and response prediction for breast cancer.

2. Keywords

Preclinical tumor model, tumor heterogeneity, therapy resistance, therapy sensitivity, protein profiling, breast cancer, anti-cancer drug efficacy

3. Background

According to the SEER (The Surveillance, Epidemiology, and End Results - Program) database, breast cancer (BC) remains the most common cancer in women. Despite a 5-year survival rate of 90% (all cancer stages), BC is the 2nd leading cause of cancer death in women. Since 1989, BC mortality rates have been reduced by 43%, primarily through early detection by mammography, improved local treatment, and increasingly effective systemic adjuvant therapies in early stages of cancer (1). Based on the genetic, morphologic, and clinical intertumoral heterogeneity, BC is classified into different subtypes. The WHO distinguishes 19 different histological subtypes including invasive BC, which infiltrate the stroma and surrounding breast tissue, and non-invasive, in-situ carcinomas, which are the preinvasive counterparts. If they arise in the mammary ducts, they are referred to as invasive ductal carcinomas (IDC) or ductal carcinoma in-situ (DCIS). Whereas invasive lobular carcinomas (ILC) and lobular carcinomas in-situ (LCIS) arise from the lobules of the mammary glands (2). The most common invasive subtype is IDC of no special type (NST) showing no distinct architectural features (3). IDC subtypes with defined, distinctive architectural features are less common. Global gene expression analyses have further classified BC into four molecular subtypes with distinct gene expression patterns: the hormone receptor-related luminal-A and luminal B tumors versus the hormone receptor-negative, HER2-enriched and basal-like tumors (4-6). These reflect different phenotypes, disease prognosis, treatment paradigms and responses to therapies (7-11). In clinical practice, BC stratification is performed by the immunohistochemical determination of routine pathologic markers such as estrogen receptor α (ERα), progesterone receptor (PgR) and human epidermal growth factor receptor 2 (HER2), and by semiquantitative evaluation of Ki-67. Besides this intertumoral heterogeneity, enormous diversity of tumor cell profiles is also observed within the same tumor, termed intratumoral heterogeneity (12). Alterations in genome, epigenome/transcriptome, and proteome, in invasive capacity, proliferation, stemness, cell plasticity but also the extrinsic interplay with the tumor microenvironment (13) contribute to the heterogeneity of individual tumor cell subpopulations. This leads to diverse disease manifestations in individual patients and failure of systematic treatment (14). With regard to the TME, we are only at the beginning of our understanding of its interaction with the tumor and how it influences the response to therapy (15, 16). Apparently, different TME gene expression patterns alter BC phenotypes (17, 18). Despite the success of genomic expression analysis in classifying BC according to different gene signatures or revealing gene alterations, a comprehensive understanding of treatment failures due to extensive tumor heterogeneity is still lacking (19, 20). Therefore, more effective therapies need to be developed and the mechanisms of resistance better understood. In particular, a personalized treatment approach based on functional analysis of protein expression data could help to improve treatment efficacy and patient outcome.

Here, we demonstrate the applicability of patient-derived microtumors (PDM) isolated from residual fresh mammary carcinoma tissue samples as an *ex vivo* 3D breast cancer model that not only consists of tumor cells but also of TME and extracellular matrix (ECM) components of the corresponding patient tumor. We successfully generated microtumor samples of different BC subtypes with histopathological features and ECM components corresponding to those of the original primary tumor tissue. Protein profiling of BC-PDMs by DigiWest™ revealed heterogeneous signaling pathway activity similar to the patient´s tumor and reflected the intertumoral heterogeneity of BC. We combined functional drug testing with signaling pathway analyses in BC-PDMs to evaluate therapy responses and identified markers of treatment sensitivity/resistance.

4. Materials and Methods

4.1. Human specimen

Non-processed human breast tumor samples were collected after surgery and completion of pathological examination from patients with primary breast cancer as part of the publicly funded PRIMO project (Personalized medicine for tailored cancer therapies). Written informed consent was obtained from all participants prior to surgery. The research project was approved by the ethics commission at the Medical Faculty Tuebingen (project number #788/2018BO2). Clinical patient data for the above-mentioned samples were submitted in pseudonymized form. A total of n = 102 samples were obtained from consenting participants, who underwent surgery at Center for Women's Health, University Hospital Tuebingen. Inclusion criteria were individuals > 18 years of age who had given informed consent to participate in the project, with unilateral invasive primary and recurrent breast carcinomas regardless of ER-/PgR- and HER2-status, tumor size, nodal-status, and grading. Enrolled patients did not receive neoadjuvant treatment. Patients with distant metastatic disease were excluded.

4.2. Generation of patient-derived microtumors from residual fresh breast tumor tissue

Fresh dissected breast tumor tissues were transported within DMEM/F12 culture media (Gibco) and subsequently processed as previously described (2022) (21). The isolation of patient-derived microtumors was adapted from Kondo et al. (22).

4.3. Viability measurement of BC-PDMs using Calcein-AM live cell and SYTOX™ Orange dead cell stain

Viability of BC-PDMs was assessed by live/dead-cell staining using 6.6 µM Calcein-AM™ (Invitrogen) live cell stain and 5 µM SYTOX™ Orange nucleic acid dead cell stain (Invitrogen). To visualize nuclei 1 µg/mL of Hoechst 33258 (Invitrogen) was added. BC-PDMs were directly picked from the suspension culture and resuspended in staining solution consisting of DMEM/F12 phenol-red free media (Gibco) supplemented with StemPro® hESC supplement (Gibco), 8 ng/ml FGF-basic (STEMCELL Technologies), 0.1 mM 2-mercapto-ethanol (Gibco), 1.8 % BSA (Gibco) and 100 µg/ml primocin (Invivogen). After 30 min of incubation, z-stack images were taken using the Zeiss CellObserver Z1 (Carl Zeiss). Maximum intensity projections of the 3D z-stacks were generating using the ZEN software (Version 2.6). Imaris software (version 8.0) was used to create 3D surface masks for viable and dead cells in the FITC and TRITC channel. For each surface mask, the fluorescent intensity sums and the volume was measured. Fluorescent intensities were normalized to the total (BC-PDMs) volume (μm^3).

4.4. Histology and immunohistochemistry

For histology BC-PDMs were fixed for 1 hour in 4% Roti® Histofix (Carl Roth) at RT and incubated for 5 min in Harris Hematoxylin (Leica Biosystems), shortly washed in dH_2O and dehydrated in an ethanol series (2x 50% ethanol, 2x 70% ethanol, each for 15 min). Using Tissue-Tek® Cryomolds® (Sakura), BC-PDMs were embedded in Richard-Allan Scientific™ HistoGel™ (Thermo Fisher Scientific). Tissue processing was performed using the HistoCore PEARL (Leica Biosystems). After processing, BC-PDMs histogel-blocks were paraffin-embedded for sectioning. Three micrometer sections of FFPE BC-PDMs samples were cut. In contrast, corresponding PTT were snap frozen on dry ice and cut as cryosections (5-7 µm). PTT-cryosections were immersed in ice-cold 4% Roti® Histofix (Carl Roth) for 10 min at 2-4°C and washed afterwards 3x with PBS. Hematoxylin and eosin (H&E) as well as Movat-pentachrome staining was performed on BC-PDMs-FFPE and PTT-cryosections. Immunohistochemical staining of BC-PDMs was performed using the Autostainer Link 48 (Agilent) in combination with the Dako PT Link (Agilent) for antigen-retrieval according to the manufacturer's recommendations. Detailed information of the used antibodies is listed below (Table 1). Stained FFPE/cryosections were imaged with Axio Scan Z1. All primary antibodies were validated in normal, healthy tissues as well as in FFPE and cryosections. DAB and collagen staining (Movat-pentachrome staining) was semi-quantified using ImageJ Fiji software. The color deconvolution plugin was used to separate stains using Ruifrok and Johnston's method for DAB stains (23), and manual deconvolution for collagen stain. The percentage of area positive for DAB/collagen was determined. Percent area fraction was measured as the percentage of pixels in the image or selection to which thresholds were applied.

Table 1. Antibodies for IHC staining.

Antibody	Manufacturer	Product No.	Additional reagents	Usage
rabbit anti-human ERalpha	Abcam	ab16660	Rb Linker Enhancer	1:30
rabbit anti-human HER2/ErbB2	Cell Signaling Technology	4290	Rb Linker Enhancer	1:80
mouse anti-human PgR	Dako	IR068	Ms Linker	R.T.U
rabbit anti-human cytokeratin 5	Abcam	ab64081	Rb Linker Enhancer	1:200
rabbit anti-human cytokeratin 6	Abcam	ab93279	Rb Linker Enhancer	1:50
mouse anti-human cytokeratin 18	Dako	IR618	Ms Linker Enhancer	R.T.U
rabbit anti-human FAPalpha	BioRad	AHP1322	Rb Linker	1:50
rabbit anti-human CD163	Abcam	ab182422	Rb Linker	1:200
mouse anti-human PD-L1	Dako	22C3	Ms Linker Enhancer	1:50
mouse anti-human CD8	Dako	IR623	-	R.T.U

4.5. Multiplex protein profiling via DigiWest

DigiWest was performed as described previously (24). Western blot was carried out using the NuPAGE system (Life Technologies) with a 4-12% Bis-Tris gel and PVDF membranes. Membranes were washed with PBST and proteins were biotinylated by adding 50 µM NHS-PEG12-Biotin in PBST for 1 h. The membranes were washed with PBST and dried overnight. Each protein (Western-Blot) lane was cut into 96 strips of 0.5 mm each. Western Blot-strips were sorted by molecular weight into a 96-well plate (Greiner Bio-One). Proteins were eluted using a 10 µl of elution buffer (8 M Urea, 1% Triton-X100 in 100 mM Tris-HCl pH 9.5). Proteins of each 96-well representing a distinct molecular weight fraction were coupled overnight to Neutravidin-coated MagPlex beads (Luminex) of a distinct color ID. Non-bound binding sites were blocked with 500 µM deactivated NHS-PEG12-Biotin for 1 h. To reconstruct the original Western blot lane, the beads were pooled, with the color IDs representing the molecular weight fraction of the proteins. For antibody incubation 5 µl of the DigiWest bead mixes were added to 50 µl assay buffer (Blocking Reagent for ELISA (Roche) supplemented with 0.2% milk powder, 0.05% Tween-20 and 0.02% sodium azide) in a 96-well plate. In the next step, the assay buffer was discarded, 30 µl of primary antibody solution was added per well to the DigiWest bead mixes and incubated overnight at 15°C on a shaker (for primary antibody list, see SI Materials). Bead mixes were washed 2x with PBST before adding 30 µl secondary antibody (labeled with phycoerythrin – PE) solution. After 1h of incubation at 23°C, the bead mixes were washed 2x in PBST. Read-outs were performed using the Luminex FlexMAP 3D instrument. Protein bands were displayed as peaks by plotting the molecular weight against the corresponding median signal intensity. To integrate peaks an expected molecular weight, a macro-based algorithm created in excel was applied. The local background was subtracted and for each peak the integral of the area was calculated (averaged fluorescent intensities – AFI). The resulting signals were normalized to total protein amount loaded onto the beads, if applicable centered on median of all BC-PDMs/PTT or only BC-PDMs samples. Subsequently, weak protein signals were determined as “lower detection limit minus one.” Further data processing is described in the figures.

4.6. Drug testing in BC-PDMs using CellTox Green™ Cytotoxicity Assay

To assess cell killing effects of different anti-cancer therapies and targeted therapies for breast cancer in BC-PDMs, the real-time CellTox™ Green Cytotoxicity assay (Promega) was performed according to manufacturer’s protocol. After the isolation of BC-PDMs from breast carcinoma specimen, the BC-PDMs were cultured for 1-2 weeks prior efficacy compound testing. The assays were performed according to manufacturer’s protocol. For each treatment, three to five replicates each with n = 15 BC-PDMs were prepared in phenol-red free BC-PDMs culture medium with a total volume of 150 µl. A proprietary cyanine dye binds to DNA in

compromised cells leading to enhanced fluorescent signal. The dye is excluded from viable cells and thereby shows no increase in fluorescence. The fluorescent signal produced by the dye binding to DNA is therefore proportional to cell death. The dye was diluted 1:1000 and signals were measured as relative fluorescent unit (RFU) (485–500 nm Excitation / 520–530 nm Emission) using the Envision Multilabel Plate Reader 2102 and Tecan Spark Multimode Plate Reader. RFU values were background-corrected and treatment to DMSO (H_2O) control fold changes were calculated for each measured time point. Outliers were excluded using Iglewicz and Hoaglin's robust test for multiple outliers applying a recommended Z-score of ≥ 3.5 (25).

4.7. Statistical analysis

Statistical analysis was performed using GraphPad Prism software. Statistical methods are illustrated in the respective figure legends. For Boxplot data, whiskers represent quartiles with minimum and maximum values and the median. Datasets with no normal distribution were analyzed with unpaired, two-tailed Mann-Whitney-U-test, otherwise as indicated. For all analyses, p values < 0.05 were considered statistically significant. Recommended post-hoc tests were applied for multiple comparisons. The certified pathologist was blinded for evaluation of microtumor H&E stainings. Data is analyzed as mean with standard error of the mean (SEM).

5. Results

5.1. BC-PDMs can be isolated from breast tumor tissues of different types with high viability

We previously established a novel 3D platform consisting of patient-derived microtumors (PDM) and tumor infiltrating lymphocytes (TILs) to identify treatment responses and therapeutic vulnerabilities in ovarian cancer and glioblastoma (21, 26, 27). Here, we aimed to extend the PDM isolation method to BC. The study enrolled patients over 18 years of age diagnosed with BC of all molecular subtypes. In total, we obtained n = 102 residual fresh mammary carcinoma tissue samples from debulking surgeries conducted at the University Hospital Tuebingen (Table S1). To analyze the viability of BC-PDMs after the isolation from BC specimen, we combined live-dead cell staining with 3D spinning disc confocal microscopy. As shown in Figure 1A, viable cells were stained with Calcein-AM, dead cells with SYTOX™ Orange and nuclei with Hoechst dye. Comparing the fluorescent intensities of viable and dead cells normalized to the total measured volume (μm^3) in n = 27 BC-PDMs models (Figure 1B), the number of viable cells was significantly higher than that of dead cells (Wilcoxon signed rank test, $p < 0.001$). Within the n = 27 BC-PDMs samples, microtumors had variable sizes, with an average area of 59261 μm^2, a maximum area of 888481 μm^2 and a minimum area of 7003 μm^2 (Figure 1C, Table S2). The overall success rate of BC-PDMs isolation from n = 102 breast carcinomas was > 75%. We were able to isolate more than 100 PDM per sample from 50% of the tissue samples obtained (Figure 1D). In 25.5% of cases, PDM were generated with less than n = 100 PDM per sample, while in the remaining 24.5%, no PDM were recovered from the tissue sample. In total, we successfully established n = 77 BC microtumor samples. Depending on the number of PDM recovered per sample, different downstream analyses could be performed such as immunohistochemistry (IHC), anti-cancer drug efficacy testing and/or protein profiling (see below). To determine whether the success rate of BC-PDMs isolation was related to specific clinical features of the original primary tumor, we correlated the available clinical data of the corresponding tumor samples and the obtained BC-PDMs models (including samples with > 100 isolated PDM) (Figure 1E). The success rate of BC-PDMs isolation appeared to be largely independent of clinical features of the corresponding primary tumor tissue (PTT). BC-PDMs were successfully isolated from breast tumor tissue samples regardless of tumor grade, histological tumor type and hormone receptor status.

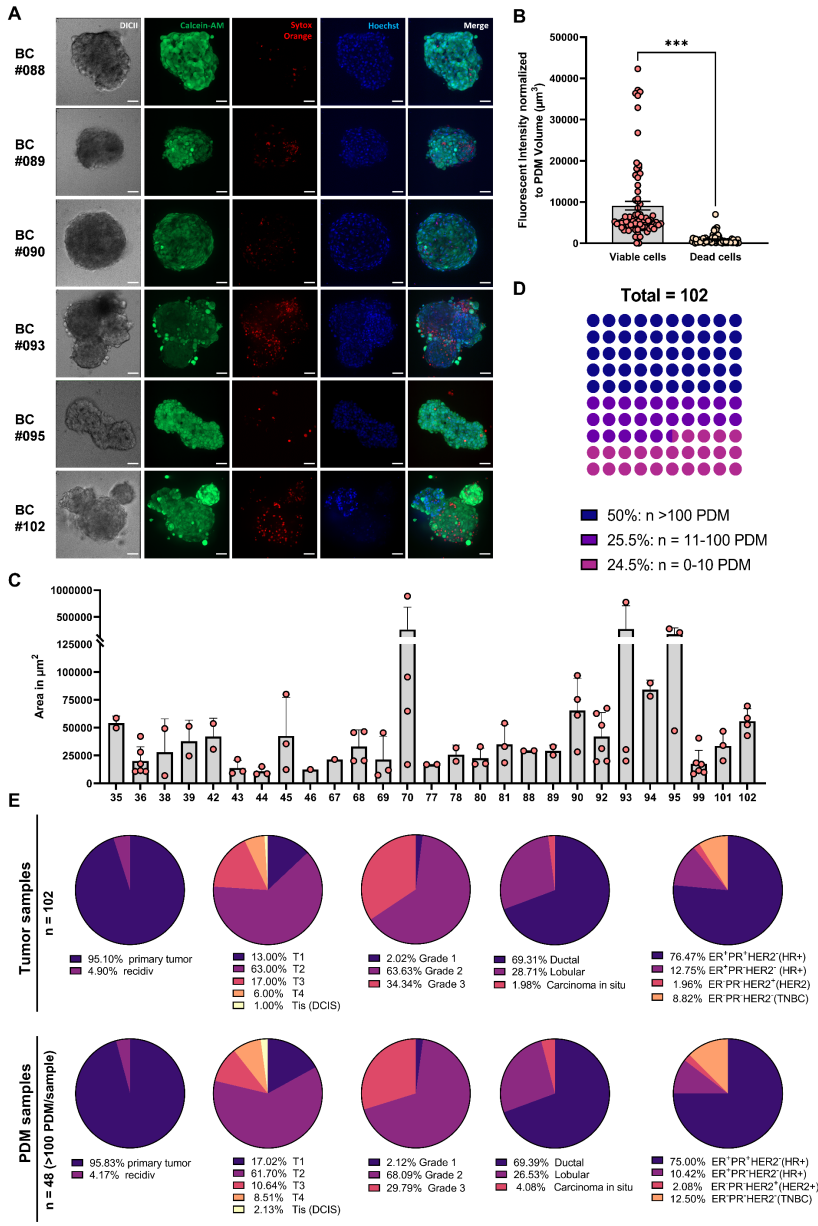

Figure 1. Isolation success of BC-PDMs. (***A***) *Live-dead cell staining of isolated breast cancer (BC) BC-PDMs from representative breast carcinoma tissue samples. BC-PDMs were stained with Calcein-AM (viable cells), SYTOX™ Orange (dead cells) and Hoechst 33258 (nuclei). Scale bars 50 µm.* (***B***) *Quantification of viable and dead cells in n = 27 BC models (on average three BC-PDMs per model) reveals high viability of BC-PDMs. Fluorescent intensities and volumes (µm3) were assessed using the Imaris Software. Wilcoxon paired signed rank test, ***p < 0.001.* (***C***) *Area measurement of BC-PDMs from n = 27 BC models. Data are shown as mean values with SD.* (***D***) *Success rate of microtumor isolation from n = 102 breast carcinomas. 50% of BC BC-PDMs models reached a total number of more than 100 single microtumors.* (***E***) *Correlation of BC-PDMs isolation success rate and clinical characteristics of corresponding breast carcinomas tissue samples.*

5.2. Histotype-specific pathological characteristics of breast tumor tissue are conserved in corresponding BC-PDMs.

Breast carcinomas form a heterogenous group of tumors and show high variability in morphologic features, e.g. degree of pleomorphism, cellular atypia, mitotic activity, or stromal circumference. Yet, there are morphological features characteristic of different histologic sub-types. Among others, tumor cells form nests, clusters, cords, trabeculae, or single file lines ("Indian File") (28) depending on the specific sub-type. Using H&E staining, a certified pathologist compared the histopathological and cytological characteristics of the isolated BC-PDMs and the corresponding PTT. We divided the specimens according to histological classification into invasive ductal carcinomas of no special type (NST) and invasive lobular carcinomas (ILC) with or without in-situ components. Tumor cells of NST-PTT formed irregular invasive nests/clusters, cords, and sheets within the stroma, in some tissues with glandular features (Figure 2A). PTT further displayed distinct ascitic structures filled with tumor cells (#33, #68), tubular structures (#58, #68) with small lumina, papillary structures or no distinct architecture. Similar to corresponding PTT, tumor cells of NST-BC-PDMs formed solid (cohesive), papillary nests with closely spaced cells (BC-PDMs/PTT: #33, #42, #58, #68, #90) and a clear separation from the ECM compartment. In addition, glandular structures were also evident within NST-BC-PDMs (#31 and #45). The histopathologic architecture of ILCs with in-situ sites is more specific than that of IDC. The lobular ascites of in-situ lesions retained their overall structure in PTT and were filled with small, round, monomorphic epithelial cells almost without lumen (e.g. #70, #86). Infiltrating cells within ILCs were dispersed with poor cohesion and grew in slender strands or single files (so called "Indian Files") or concentrically around ducts or lobules (PTT e.g. #25, #70, #86). Tumor cells of ILC-BC-PDMs were mostly discohesive and dissociated in the surrounding stromal tissue (#25, #53, #86, #92, #102), thus resembling primary infiltrating tumor lesions (Figure 2B). This histological feature was also found in NST-BC-PDMs #96. Overall, pathological evaluation of BC-PDMs specimens revealed histological similarity to breast tumor tissue in 90% of cases (n = 39/40) and to histological tumor type (IDC/NST) in 95% of cases (n = 36/38) (Figure 2C). Stromal compartments were present in 57.5% of cases (n = 23/40). In result of comparison of the cytopathology of BC-PDMs and corresponding PTT, similar cellular atypia was found. While some BC-PDMs consisted of small, rather homogenous cells without prominent nucleoli (e.g. #25, #29, #45, #53), other samples exhibited moderate (#31, #33, #58, #96) to strong nuclear pleomorphism (#68, #70, #86, #90, #92, #102) with large, hyperchromatic nuclei and prominent nucleoli. Most BC-PDMs resembled a moderate nuclear grade (n = 21) with moderate hyperchromasia (n = 19). While 20.5% (n = 8/39) of samples had a similar nuclear grade of BC-PDMs and corresponding PTT, the majority (59%) of BC-PDMs had a nuclear

grade decreased by 1 degree (Figure S1A). In summary, BC-PDMs largely resemble the histopathology of the corresponding primary tumor tissue.

5.3. BC-PDMs contain extracellular matrix components of the original tumor tissue

The ECM, representing a complex network of tissue fibers, glycoproteins (e.g. elastin, laminin, fibronectin), proteoglycans (PGs), and glycosaminoglycans (GAGs), not only provides stability and a reservoir for e.g. growth factors, but also plays a role in breast tumorigenesis, invasiveness (29, 30) and therapy response (31). Furthermore, ECM stiffness and density were found to correlate with prognosis in breast cancer (32) (33). To evaluate and compare the ECM within BC-PDMs and corresponding PTT, we used the Movat-pentachrome staining to visualize different components of connective tissue on a single slide (34). In PTT sections, the predominant ECM components were PGs/GAGs (cyan blue) and collagen fibers (yellow), which mostly overlapped (green) (Figure 2D). In all PTT, dense collagen networks were detected in close proximity to the tumor masses due to increased collagen deposition. This leads to the “stiffening” of the tissue (29). The collagen fibers exhibited different morphologies: short and wavy (e.g. PTT #29), thin and linear (e.g. PTT #31) or thick and linear (e.g. #36, #53). Most notable were dense and thick collagen fibers wrapped around tumor masses (e.g. PTT #31, 58), especially in stromal areas adjacent to in-situ lesions (e.g. PTT #36, #86, #102). Tumor borders were either relatively smooth, with collagen fibers drawn at a tangential angle around the tumor (e.g. PTT #86) or oriented perpendicular in the direction of cell invasion (e.g. PTT #58) (Provenzano, 2006 #522). Corresponding BC-PDMs exhibited ECM components to a lesser extent compared to primary tissue. Despite limited enzymatic tissue disruption during BC-PDMs isolation with collagenase I and II, we detected collagen expression (yellow/green) in the corresponding BC-PDMs (e.g. BC-PDMs #29, #36, #58, #53, #70). Compared to tumor masses in the PTT, which are surrounded by thick collagen fibers, the arrangement of collagen in BC-PDMs was less specific. In BC-PDMs, the collagen rather formed a backbone structure for the tumor cells. In general, BC-PDMs appeared like small tumor fragments excised from tumor masses of the corresponding primary tumor tissue and consisted of the inner tumor cell mass with its ECM components, but without the framing collagen fibers. In addition to cross-linked collagen-fibers, PGs/GAGs (cyan blue) were found within tumor masses/islets of the PTT (e.g. #29, #58, #53, #70) and demarcated tumor masses from the stroma as a single layer separated from collagen fibers (e.g. PTT #58, #86, #102). PGs/GAGs were found in BC-PDMs when their expression within tumor masses in corresponding PTT was high (e.g., BC-PDMs #29, 31, #58). Elastic fibers (black) were mostly attached to collagen fibers (e.g. PTT #53, #86, #102) and were more abundant in ILC compared to IDC (NST) tissues. In contrast to other BC-PDMs, the ECM of BC-PDMs #102 exhibited elastic fibers, as in the corresponding primary tumor. Further, mucin (blue/gray) secreted by tumor cells was found in sections of PTT #31

and #86 and in the corresponding BC-PDMs. When comparing the origin of the primary tumor, no striking differences in the amount of collagen were observed between NST-derived and ILC-derived BC-PDMs (Figure 2E). However, ILC-derived BC-PDMs tended to show slightly higher amounts of collagen fibers as previously reported (35). In conclusion, the Movat-pentachrome staining allowed the visualization of different ECM components of the primary tumor within BC-PDMs. Compared to whole tumor masses in tumor tissues, the ECM compartments in BC-PDMs occur to a lesser extent and in slightly different arrangement.

5.4. Immunohistochemical analysis of hormone receptor expression enables distinction of BC-PDMs isolated from hormone receptor positive and TNBC primary tumors.

To further characterize BC-PDMs, we performed immunohistochemistry (IHC) analysis of FFPE-BC-PDMs sections. We examined the expression of hormone receptors, cytokeratins as well as cancer-associated fibroblasts (CAFs) and immune cell markers using DAB staining. To analyze the expression of clinical molecular markers, we stained BC-PDMs sections for ERα, PgR and HER2. BC-PDMs were classified as hormone receptor positive (HR+) or triple negative (TNBC) as determined by pathologic evaluation of the primary tumor (Figure 3A). TNBC is an aggressive type of BC usually with higher grade, higher rate of early recurrence and a worse 5-year prognosis (36-39). It is defined by lacking expression of hormone receptors and HER2. For each tissue sample, the corresponding immunoreactive scores (IRS) and HER2 scores (0-3) were determined (Table S1). ERα and PgR staining of BC-PDMs was consistent with the corresponding clinical classification and was increased in BC-PDMs originating from HR+ PTT (Figure 3B). The level of ERα and PgR expression varied within HR+ BC-PDMs. In contrast, HR expression was strongly reduced in TNBC-PDMs. HER2 was detectable in HR+ BC-PDMs sample #10 and #37. However, HER2 expression in BC-PDMs #37 did not resemble its clinical HER2 score, which was reported to be zero. In conclusion, IHC staining enabled the identification of BC-PDMs isolated from clinical HR+ breast tumors and those isolated from clinical TNBC tumors based on hormone receptor expression.

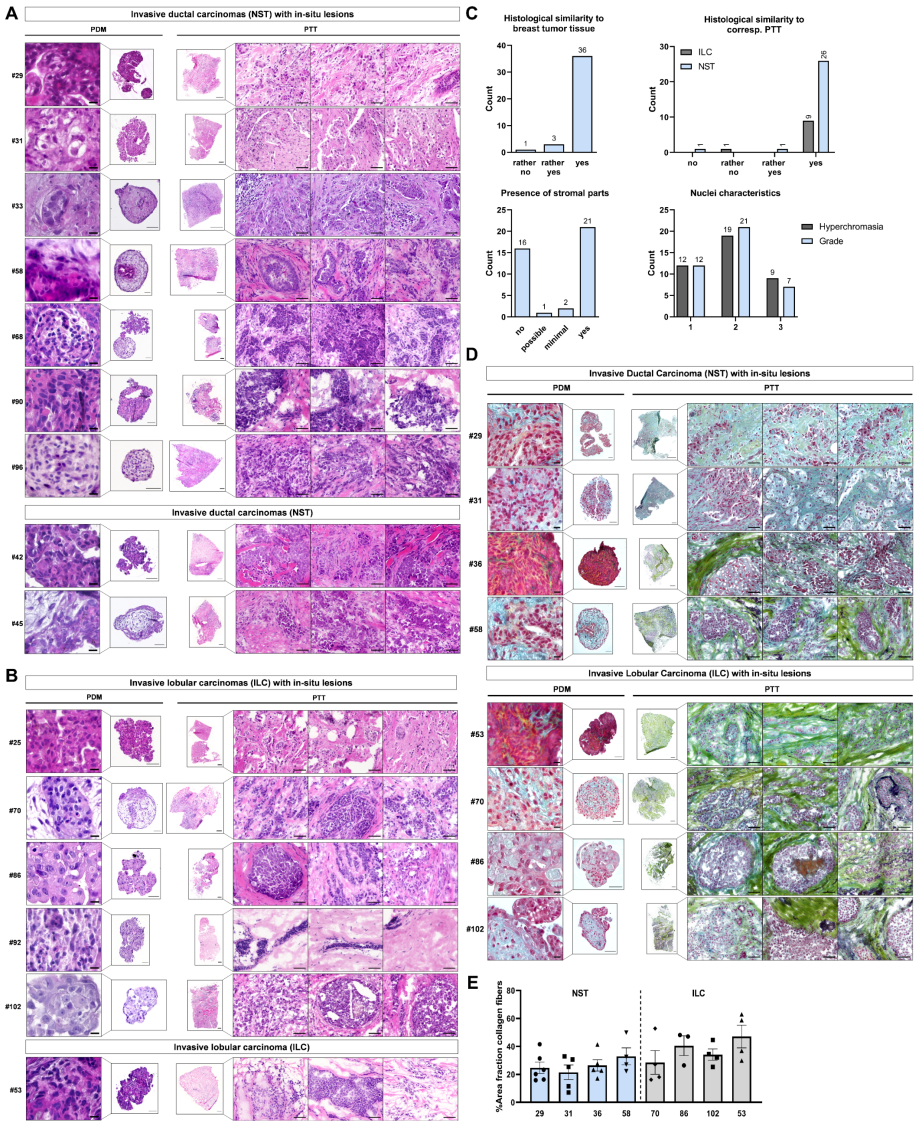

386

Figure 2. Histopathology and cytology of BC-PDMs and corresponding PTT. *H&E staining of BC-PDMs and corresponding primary, (**A**) invasive ductal breast carcinomas (NST) with/without ductal in-situ (DCIS) lesions and (**B**) invasive lobular breast carcinomas (ILC) with/without lobular in-situ (LCIS) lesions. (**C**) Pathological evaluation of BC-PDMs. n =39/40 BC-PDMs resembled histopathology of breast carcinomas, n = 36/39 of the corresponding primary tumor histotype (NST/IDC) and n = 23/40 BC-PDMs displayed stromal parts. Histopathological tumor characteristics of BC-PDMs were assessed such as hyperchromasia and nuclei differentiation (nuclear grade 1: nuclei with little variation in size and shape; grade 3: large nuclei with high variation in size and shape; grade 2: nuclei show features between 1 and 3. (**D**) Pentachrome-movat staining revealed connective tissue compartments in BC-PDMs and PTT e.g. collagen fibers (yellow), PGs/GAGs (cyan blue), collagen/PGs/GAGs-superimposition (green), mucins (blue) and elastin (black). (**E**) Amount of collagen fibers within BC-PDMs. Collagen fibers are measured semi-quantitatively as %-area fraction of a BC-PDMs. RGB images were unmixed by subtractive mixing (color deconvolution) via ImageJ. Ordinary one-way ANOVA, Holm-Šídák's multiple comparisons test, no significant difference of means. Scale bars BC-PDMs: 50 µm/10 µm (zoom); PTT: 500 µm/50 µm (zoom).*

5.5. BC-PDMs display differential expression of luminal and basal cytokeratins

Since cytokeratin (CK) expression is thought to be stable throughout carcinogenesis (40), CKs are studied as differentiation markers in precancerous breast lesions. Breast tissue normally consists of a stratified epithelium with luminal epithelial cells surrounded by a basement membrane composed of myoepithelial cells, both with different CK phenotypes (41, 42). Breast carcinomas are found to express different CKs, such as the luminal subtype expressing luminal epithelial CKs (CK8/CK18/CK19) or the basal subtype expressing basal myoepithelial high molecular weight (HMW) CKs (CK5/CK6/ CK7/CK14) (4, 43, 44). Nevertheless, some breast tumors were shown to express both types of CKs (42, 45). Here, we analyzed CK5, CK6 and CK18 staining of HR+ and TNBC-PDMs. We found highly heterogenous staining of CKs in HR+ and TNBC -PDM. The heterogenous CK expression allowed us to subdivide the BC-PDMs based on CK expression. Thus, we divided HR+ BC-PDMs into four groups based on the evaluated CK expression: $CK5^-/CK18^+$ (luminal, differential glandular phenotype), $CK5^+$ (basal), $CK5/6^+$ (basal, stem cell phenotype) and $CK5/6/18^+$ (intermediate glandular phenotype) (46)(Figure 3C). $CK5^-/CK18^+$-PDM showed significantly higher CK18 expression compared to CK5 (**p = 0.004) or CK6 (**p = 0.005) (Figure 3D). The abundances of CK5 and CK6 were significantly higher in the $CK5^+$ (p = 0.006) and $CK5/6^+$ (p = 0.020) groups compared to the $CK5^-/CK18^+$ group. Some HR+ BC-PDMs were positive for all three CKs. Comparing the CK expression between HR+ BC-PDMs and TNBC -PDM, we found significantly increased CK18 expression (p = 0.006), a marker for luminal carcinomas, in HR+ BC-PDMs (Figure 3D). TNBC BC-PDMs did not show CK18 expression, but moderate expression of CK5/6. This is consistent with the literature (42). As a hallmark of EMT, lack of CK18 expression has been associated with tumor progression (47) as it promotes cancer cell migration (48). Two of the four TNBC -PDM analyzed here showed strong CK5 expression, and BC-PDMs #38 also displayed high CK6 expression. Due to high CK5/6 positivity correlating with poorer prognosis (49), TNBC -PDM #38 was defined as a basal-like subtype of TNBC. Overall, CK5/6 expression was not significantly different among HR+ BC-PDMs (Figure 3D). When comparing ILC and NST BC-PDMs, HMW cytokeratins (CK5/6) were more elevated in ILC BC-PDMs, whereas luminal CK18 was upregulated in NST BC-PDMs (Figure 3E). We next analyzed additional markers such as FAPα, associated with CAFs (cancer-associated fibroblasts), and immune cell markers CD163, CD8 and PD-L1 (Figure 3F). PD-L1, a T cell inhibitory checkpoint marker, and CD8, a marker for cytotoxic T cells, were mostly absent from BC-PDMs except for BC-PDMs #70. $CD8^+$ T cells were detected in BC-PDMs #78. Sporadic expression of CD163 indicating the presence of M2 macrophages was found in BC-PDMs (e.g. #68, #53, #70, #34). In contrast, FAPα was detectable in all stained BC-PDMs, to varying degrees. Among them,

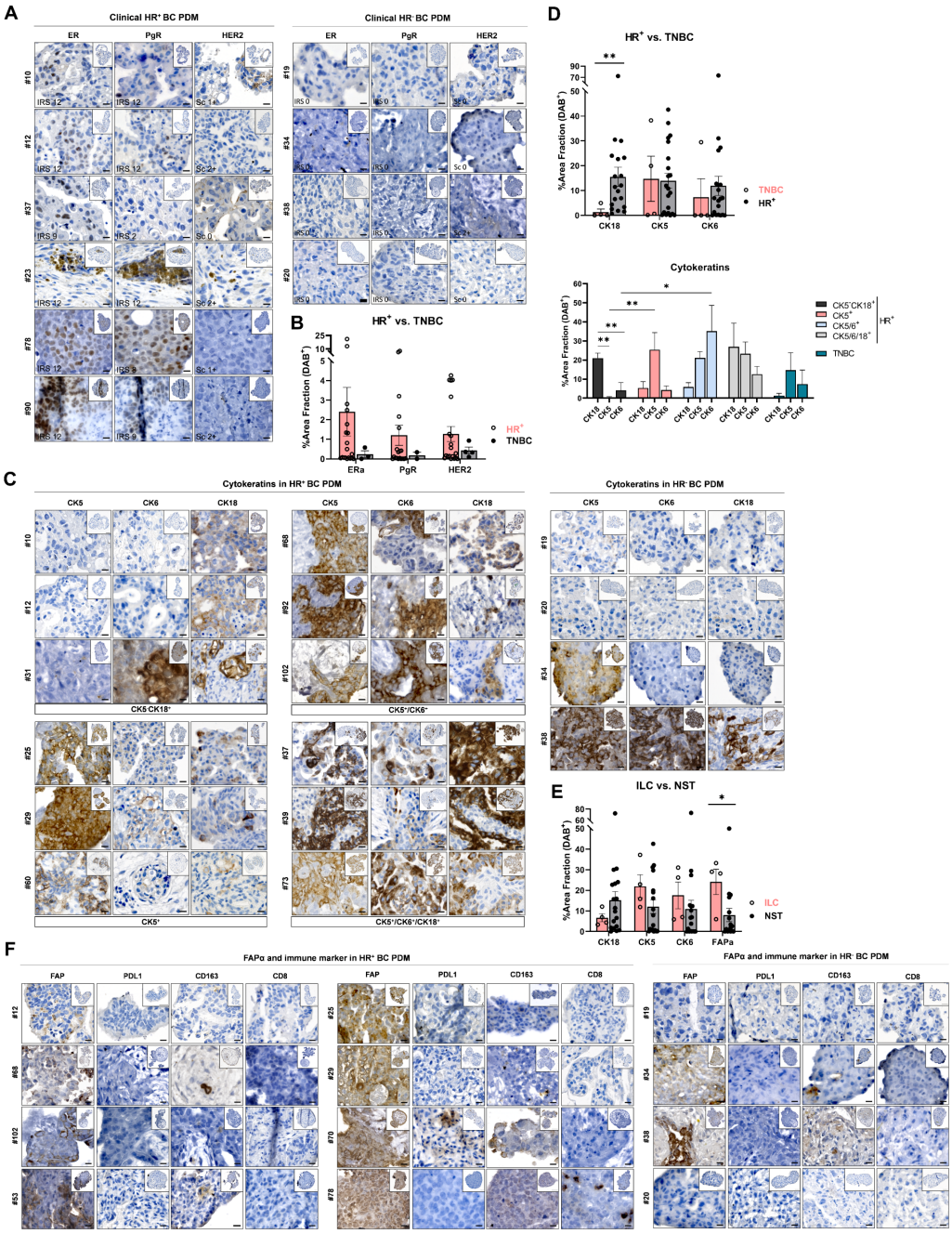
A
Clinical HR+ BC PDM
Clinical HR- BC PDM
ER
PgR
HER2
B
HR+ vs. TNBC
%Area Fraction (DAB+)
ERa
PgR
HER2
HR+
TNBC
C
Cytokeratins in HR+ BC PDM
Cytokeratins in HR- BC PDM
CK5
CK6
CK18
CK5-CK18+
CK5+/CK6-
CK5+
CK5+/CK6+/CK18+
D
HR+ vs. TNBC
%Area Fraction (DAB+)
CK18
CK5
CK6
TNBC
HR+
Cytokeratins
CK5-CK18+
CK5+
CK5/6+
CK5/6/18+
E
ILC vs. NST
FAPa
ILC
NST
F
FAPα and immune marker in HR+ BC PDM
FAPα and immune marker in HR- BC PDM
FAP
PDL1
CD163
CD8

422

423

Figure 3. Immunohistochemical analysis of breast cancer specific and immune cell markers in BC-PDMs. *DAB staining was analyzed semi-quantitatively as %-area fraction of a BC-PDMs. RGB images were unmixed by subtractive mixing (color deconvolution) using ImageJ software. (**A**) Hormone receptor (HR) DAB staining of clinically classified HR+ BC-PDMs vs. TNBC BC-PDMs. Clinically assessed immunoreactive scores (IRS) from primary tumor are indicated. HR+ BC-PDMs were arranged in ascending order of ERα expression (**B**) HR+ BC-PDMs have increased HR expression (ERα, PgR, HER2) compared to TNBC BC-PDMs. (**C**) DAB staining of luminal cytokeratin (CK18) and basal cytokeratins (CK5 and CK6). BC-PDMs were grouped into four groups according to CK staining: $CK5^{-}CK18^{+}$, $CK5^{+}$, $CK5/6^{+}$ and $CK5/6/18^{+}$. (**D**) Significantly elevated expression of luminal CK18 vs. basal CK5/CK6 in HR+ compared to TNBC BC-PDMs. Mann-Whitney U test, **p = 0.006. Differences in CK18, CK5 and CK6 expression in HR+ and TNBC BC-PDMs according to their classification into the previously determined groups. Within group: One-way ANOVA, Holm-Šídák's multiple comparisons test. Different group comparison: Two-way ANOVA, Holm-Šídák's multiple comparisons test. (**E**) Differences in CK and FAPα expression in ILC BC-PDMs vs. NST BC-PDMs. NST-BC-PDMs show higher levels of CK18, while ILC-BC-PDMs show significant higher levels of FAPα. Mann-Whitney U-test, *p = 0.028. Both ILC/NST-BC-PDMs express basal CK5 and 6. (**F**) DAB staining of FAPα and immune markers in BC BC-PDMs grouped into HR+ and TNBC. For HR+ BC-PDMs, BC-PDMs were arranged in ascending order of FAPα expression. Data are mean with SEM. *p < 0.05, **p < 0.01, ***p < 0.001. ERα: estrogen receptor alpha; PgR: progesterone receptor; HER2: HER2/neu-ErbB2 receptor.*

ILC-BC-PDMs showed significantly stronger FAPα staining (Figure 3E, p = 0.028) in accordance with the literature (50). Significant differences between TNBC and HR+ BC-PDMs were not identified. In conclusion, BC-PDMs largely reflect the hormone receptor status of the corresponding tumor tissue and exhibit heterogeneous expression of CKs and FAPα, which are markedly different in HR+ and TNBC and ILC-NST BC-PDMs. In addition, immune cell markers could be identified sporadically in BC-PDMs and independent of hormone receptor status.

5.6. Protein expression and signaling pathway activity of BC-PDMs correlate with corresponding primary tumors

Following histological characterization, we extended the comparison of BC-PDMs with corresponding primary tumor tissues by in-depth quantitative protein profiling analyses. We therefore measured protein expression and activity of key signal transduction pathways in n = 20 matched BC-PDMs-PTT pairs employing the DigiWest® technology (24). In this way, we generated protein profiling datasets covering 142 total and phosphorylated proteins (raw data: Table S3; BC-PDMs-PTT data: Table S4). The analyzed profiling panel comprised proteins from the cell cycle, Jak/STAT, MAPK, RTK, PI3K/Akt, EMT/cytoskeleton and Wnt signaling pathways. Pearson correlation revealed an overall high, positive correlation of averaged protein signals between matched BC-PDMs and PTT with $P_r = 0.856$ ($p < 0.001$; Figure 4A). Furthermore, comparison of signaling pathway activity and expression of breast cancer-related proteins, resulted in no significant differences. Overall, the average protein expression of BC-PDMs resembled that of matched breast cancer tissue (Figure 4B, Table S5). Subsequently, changes in protein abundance were determined between BC-PDMs and PTT pairs. In total, n = 18 analytes displayed significant differences in expression (-log10 (q) > 1.3) and a $\log_2$ fold change of at least |1| (Figure 4C-D). BC-PDMs had increased protein levels of the cytoskeletal protein cytokeratin 5 and 6 (CK5/6), while expression of immune cell markers CD11c, CD16, CD68, CD8 alpha, CD25, PD1 and PD-L1 were decreased. This is consistent with our IHC data, demonstrating that BC-PDMs are small tumor fragments

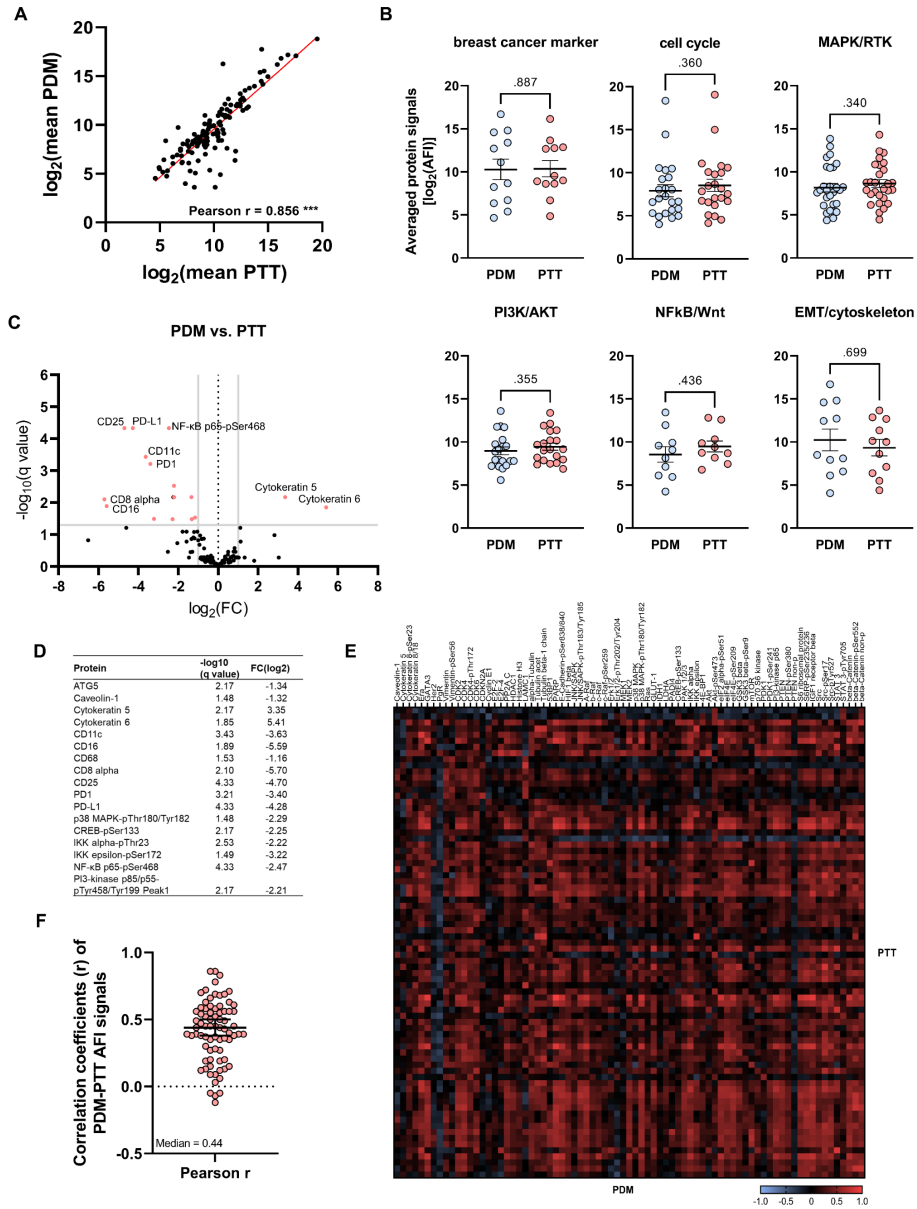

Protein	-log10 (q value)	FC(log2)
ATG5	2.17	-1.34
Caveolin-1	1.48	-1.32
Cytokeratin 5	2.17	3.35
Cytokeratin 6	1.85	5.41
CD11c	3.43	-3.63
CD16	1.89	-5.59
CD68	1.53	-1.16
CD8 alpha	2.10	-5.70
CD25	4.33	-4.70
PD1	3.21	-3.40
PD-L1	4.33	-4.28
p38 MAPK-pThr180/Tyr182	1.48	-2.29
CREB-pSer133	2.17	-2.25
IKK alpha-pThr23	2.53	-2.22
IKK epsilon-pSer172	1.49	-3.22
NF-κB p65-pSer468	4.33	-2.47
PI3-kinase p85/p55-pTyr458/Tyr199 Peak1	2.17	-2.21

Figure 4. Comparison of protein profiles from BC-PDMs and corresponding primary tumor tissue. *N = 20 matched BC-PDMs and PTT-pairs were analyzed. (**A**) X-Y plot of correlated protein means of BC-PDMs and PTT. Protein signals of measured BC-PDMs-PTT samples were correlated using Pearson correlation. DigiWest AFI protein signals were averaged for BC-PDMs/ PTT and log_2 transformed. Each dot represents one protein. Pearson r = 0.856; ***p < 0.001. (**B**) Overall signaling pathway activity in BC-PDMs resembled that of primary BC tumors. Proteins were sorted by pathway affiliation. Shown are AFI protein signals, averaged for BC-PDMs/PTT and log_2 transformed. Mann-Whitney test; p values as indicated. (**C-D**) Differently expressed proteins of matched BC-PDMs-PTT samples. Volcano plot shows proteins with significantly decreased or increased expression in BC-PDMs (red) with an adjusted FDR p-value (-log10 (q)) > 1.3 and a log2 fold change > |1|; multiple t-test with Welch correction; Benjamini, Krieger, and Yekutieli FDR. Exact values are shown in **D**. (**G**) Heatmap of unclustered pearson correlation coefficients (r) shows moderate correlation of AFI protein signals over BC-PDMs and matched PTT samples. (**H**) Pearson correlation coefficients (r) displayed as scatter plot with a median correlation of r = 0.44. Data are mean with SEM. AFI: averaged fluorescent intensities.*

composed of tumor cells, ECM proteins and partially stromal cells of the corresponding tumor tissue, with immune cell infiltrates in a few cases. Other proteins displaying reduced expression in BC-PDMs as compared to matched PTT belong to different signaling pathways. Among them were mainly phospho-proteins of the MAPK pathway (p38 MAPK-pThr180/Tyr163), the PI3K pathway (PI3K p85/p55-pTyr458/199) and the NFkB pathway (NFkB p65-pSer172, IKK alpha-pThr23, IKK epsilon-pSer172). Correlation data of individual proteins showed a general, positive correlation between protein signals of matched BC-PDMs/PTT-pairs (Figure 4E) with a median coefficient of r = 0.44 (Figure 4F). Table S6 lists the proteins whose signal levels correlated significantly with those of the primary tumors. Significant positive correlations were found across all signaling pathways. Among them, ERα protein expression was significantly correlated between BC-PDMs and matched PTT (r = 0.86, ***p < 0.001). ERα is clinically relevant for the classification of breast tumors. In addition to the histological assessment, we demonstrated at the protein level that the protein signaling pathway profiles of BC-PDMs are similar to those of the original tumor tissue across several signaling pathways. Overall, protein expression of PTT is reflected in BC-PDMs with high correlation.

5.7. Cross-comparison of protein profiling data among individual BC-PDMs identifies personalized pathway activation signatures

To classify the BC-PDMs samples based on their individual protein profiles, we analyzed signaling pathway activity of n = 42 BC-PDMs samples using hierarchical cluster linkage (HCL) analysis (Figure 5; Table S7). In addition, samples were assigned according to clinical data as HR+, TNBC or HER2-positive (HER2+) (illustrated in Table S1). Cluster analysis of cell cycle-related proteins resulted in four sample groups with distinct levels of cell cycle regulator expression (Figure 5A). In addition to cluster 1, which included the BC-PDMs sample #38, all HR+ BC-PDMs samples with either weak or mixed expression levels were grouped into cluster 2 (n = 8) and 3 (n = 17). Clusters differed mainly in the expression of transcriptional activators E2F-1, E2F-2, transcriptional repressor E2F-4 and p53. TNBC, HER2+ and the remaining HR+ BC-PDMs samples were grouped into cluster 4 (n = 16) and showed overall increased expression of cell cycle regulatory proteins. HCL of MAPK-RTK pathway proteins distinguished three sample groups separating n = 19 HR+ BC-PDMs with overall decreased protein abundances from n = 19 TNBC-, HER2+- and HR+ BC-PDMs with elevated expression levels (Figure 5B). Notably c-Met, RSK1-pThr573, NF1 and c-Raf were upregulated in the latter group compared with the HR+-only group. When comparing PI3K/Akt pathway activity among individual BC-PDMs models, samples were divided into two groups, too, with one group again consisting of HR+ samples and the other containing all TNBC and HER2+ samples (Figure 5C). Here, BC-PDMs were characterized by enhanced levels of beta-catenin, FoxO3a, Akt-pSer473, CREB, CREB-pSer133, PDK1 and IKKalpha-pThr23.

Next, we visualized the median-centered protein profiling data of BC-PDMs in box-whisker plots. This allowed us to identify individual BC-PDMs samples with increased expression of proteins belonging to cell cycle, MAPK/RTK and/or PI3K/AKT signaling pathways, respectively (Figure 5D). Of interest were BC-PDMs samples with median-centered protein expression $\log_2$ AFI ≥ 1, corresponding to a fold change ≥ 2 (Table S8). Upregulated cell cycle activity was identified in n = 8 BC-PDMs, whereas MAPK/RTK signaling was amplified in n = 11 BC-PDMs with median expression levels ≥ 1. Higher PI3K/Akt pathway activity was present in n = 7 BC-PDMs. Interestingly, all three signaling pathways were concomitantly upregulated in the four BC-PDMs samples #20, #78, #92 and #96. At the same time other BC-PDMs models showed simultaneous downregulation of all analyzed signaling pathways as indicated by $\log_2$ AFI values ≤ -1 (e.g. BC-PDMs #15, #18, #60, #89, #99). Pathway analysis thus allowed the classification of individual BC-PDMs samples based on specific protein expression profiles.

5.8. TNBC-PDMs exhibit increased PI3K/AKT and MAPK/RTK pathway activity

DigiWest-based protein profiling of BC-PDMs also enabled the differentiation of TNBC -PDM from HR+ BC-PDMs samples. TNBCs are known to be characterized by altered oncogenic signaling pathways such as PI3K/Akt and MAPK/Erk (51). Genetic aberrations of upstream regulators, such as activating mutations of PI3K, Ras, b-Raf, loss of function mutations of PTEN, overexpression of EGFR, have been shown to be common in breast cancer and play an important role in its dysregulation (52-57). These changes can cause the development of chemoresistance in TNBC patients (58-60). In line with these findings, we found PI3K/AKT ($p = 0.006$) and MAPK/RTK ($p = 0.032$) pathways significantly upregulated within TNBC -PDM as compared to HR+ BC-PDMs (Figure 5E). Proteins with significantly elevated abundance included AKT ($p = 0.022$), eIF2α-pSer51 ($p = 0.009$), eIF4E ($p = 0.049$), GSK3beta ($p = 0.006$), GSK3beta-pSer9 ($p = 0.007$), PTEN ($p = 0.040$), PTEN non-p ($p = 0.044$), p70S6K ($p = 0.009$), CREB-pSer133 ($p = 0.041$). All these regulators have previously been associated with TNBC. Furthermore, we were able to assign additional proteins with elevated abundance in TNBC -PDM to the MAPK/RTK pathway. Parallel to the PI3K signaling, the MAPK pathway is another driving force in TNBC (61) and correlates with high disease recurrence rates in patients with TNBC (62). We observed significant upregulation for Erk1/2 ($p = 0.022$), MEK2 ($p = 0.002$), Src-pSer17 ($p = 0.012$) and Src-pTyr527 ($p = 0.014$) (Figure 5F). Other signaling pathways (e.g. cell cycle, NFkB-Wnt) did not show a significant distinction in expression between TNBC- and HR+ BC-PDMs. However, we identified upregulation of individual proteins related to the cell cycle: CDK2 ($p = 0.022$),

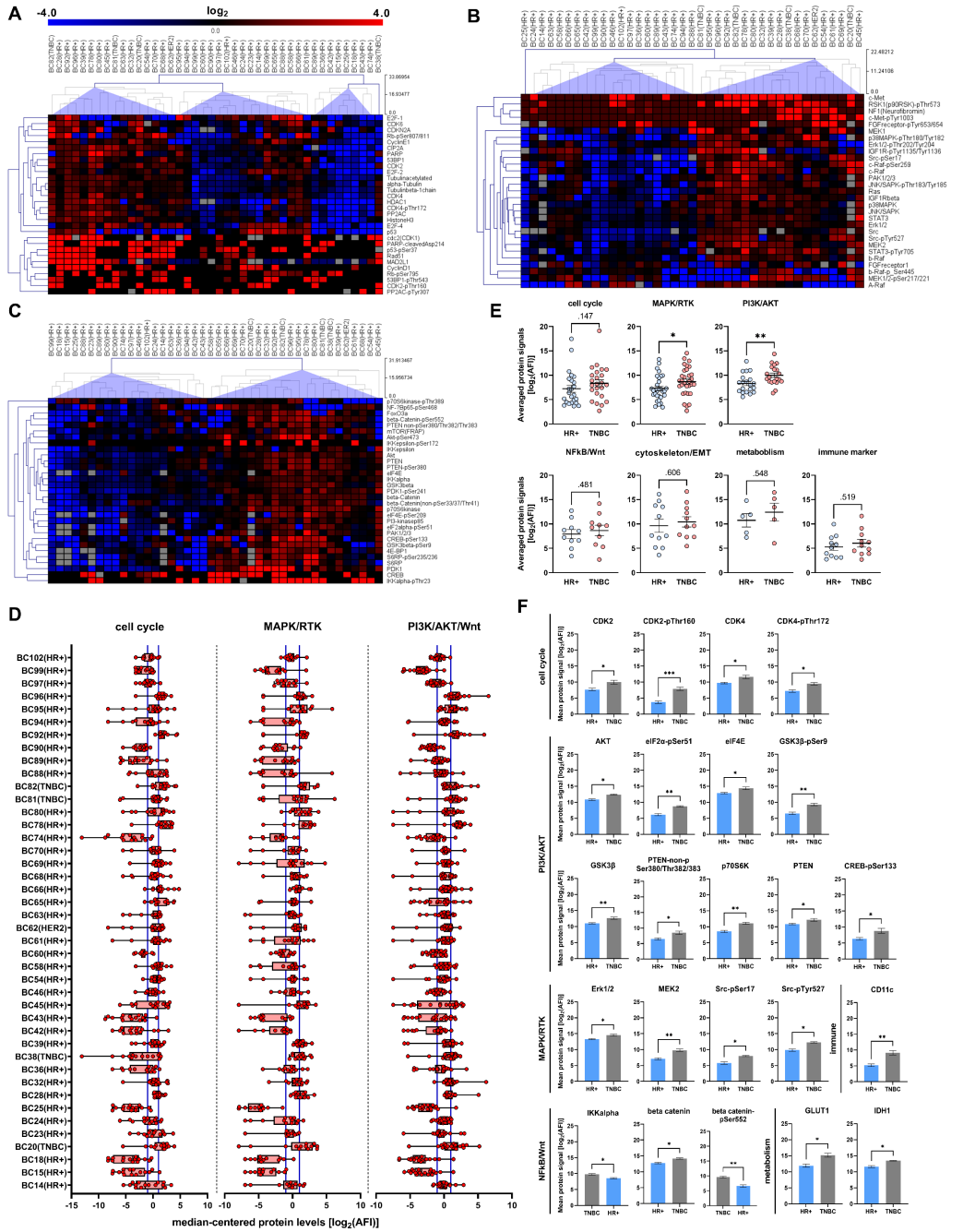
A
-4.0
log2
4.0
B
C
D
cell cycle
MAPK/RTK
PI3K/AKT/Wnt
median-centered protein levels [log2(AFI)]
E
cell cycle
MAPK/RTK
PI3K/AKT
NFkB/Wnt
cytoskeleton/EMT
metabolism
immune marker
Averaged protein signals [log2(AFI)]
HR+
TNBC
F
CDK2
CDK2-pThr160
CDK4
CDK4-pThr172
AKT
eIF2α-pSer51
eIF4E
GSK3β-pSer9
GSK3β
PTEN-non-p Ser380/Thr382/383
p70S6K
PTEN
CREB-pSer133
Erk1/2
MEK2
Src-pSer17
Src-pTyr527
CD11c
IKKalpha
beta catenin
beta catenin-pSer552
GLUT1
IDH1
Mean protein signal [log2(AFI)]
immune
metabolism

Figure 5 DigiWest-based protein pathway profiling of BC BC-PDMs. *Hierarchical cluster linkage analysis (HCL) of median-centered, log_2 transformed AFI protein signals of n = 42 BC BC-PDMs samples, divided into cell cycle, MAPK/RTK and PI3K/Akt pathways. Molecular subtype classifications of BC BC-PDMs samples as indicated. (**A**) HCL of sample and cell cycle-related analytes with complete linkage. Four sample clusters were identified based on differential expression levels. (**B**) HCL of sample and MAPK/RTK-related analytes with average linkage. There are two main sample clusters (excl. BC BC-PDMs #25) that separate samples with high MAPK/PI3K protein expression from those with low expression. (**C**) HCL of sample and PI3K/AKT-related analytes with complete linkage. Two main sample clusters were identified: "high-expression" and "low-expression". (**D**) Differences in signal transduction in BC BC-PDMs samples. Box-whisker plots show median-centered, log2 transformed AFI protein signals of different pathways. Data distribution within samples is illustrated by lines connecting min. and max. values. Each red dot represents a protein. Black lines in box plots indicate the "median" of measured proteins within a sample. Blue lines delineate the values > |1| corresponding to a fold change > 0.5. (**E**) TNBC BC-PDMs showing elevated PI3K/AKT- and MAPK/RTK- pathway activity. The averaged, log2 transformed protein signals are compared between TNBC and HR+ BC-PDMs within different pathways. Mann-Whitney U test, PI3K: p = 0.006, MAPK/RTK: p = 0.032. (**F**) Differentially expressed proteins in TNBC BC-PDMs. Comparison of mean protein expression in TNBC vs. HR+ BC BC-PDMs. Enhanced protein abundances in TNBC BC-PDMs were found for several proteins associated with cell cycle, metabolism, immune system, PI3K/AKT, MAPK/RTK and NFkB pathway. Mann-Whitney U test, *p < 0.05, **p < 0.01, ***p < 0.001. Data are mean with SEM.*

CDK2-pThr160 ($p < 0.001$), CDK4 ($p = 0.025$) and CDK4-pThr172 ($p = 0.019$). While CDK2 hyperactivation is linked to basal-like breast cancer tumors (63), aberrant expression of CDK4 is linked to drug resistance (64). Consistent with increased eIF2α-phosphorylation in TNBC -PDM and the associated upregulation of aerobic glycolysis (65-67), we also found an upregulation of metabolism-related proteins including GLUT1 ($p = 0.029$) and IDH1 ($p = 0.029$). When comparing BC-PDMs derived from NST and ILC tumors, we detected no differences in overall signaling pathway activity (Figure S3A). However, we observed differential expression for individual proteins such as E-Cadherin-pSer838/840, CK8-pSer23 and ERα (Figure S3B). Decreased E-Cadherin levels in ILC-BC-PDMs are in accordance with inactivating *CDH1* (E-Cadherin) mutations that are frequently observed in ILC tumors and disrupt cellular adhesion/epithelial integrity (68, 69). In accordance with G. Ciriello et al. (70), we discovered lower GATA 3 protein levels in ILC tumors. Reduced ERα signal in ILC-BC-PDMs may be explained by decreased GATA3 expression, as it plays a pivotal role in the recruitment of the ER transcription complex (71). In summary, identified overexpressed signaling proteins in TNBC -PDM affect many different cellular processes in cancer cells, including proliferation, differentiation, migration, cell growth and survival. Our results are consistent with previous findings in TNBC and show that BC-PDMs reflect protein signaling pathway activation characteristics of corresponding primary breast tumors.

5.9. Identification of marker panels for individualized responses towards hormone- and chemotherapy using combined cytotoxicity and protein profiling analyses of BC-PDMs

BC-PDMs responses to four anti-cancer drugs were evaluated by a microplate-based cytotoxicity assay. Microtumors derived from different patients were treated with the selective estrogen receptor modulator (SERM) tamoxifen (TAM), the taxane chemotherapeutics docetaxel (DTX) and paclitaxel (PTX), and the CDK4/6 inhibitor palbociclib (PAB). Samples

were not differentiated according to receptor status. Treatment-induced cell death was measured in a time series (24h, 48h and 72h) and compared to the respective vehicle control (Table S9). A significant treatment effect, defined as a significant fold change in cell death between vehicle control and treatment, was considered a response, whereas a nonsignificant effect was considered a non-response or treatment resistance. (Mixed-effects model, Fisher's uncorrected LSD test). This approach allowed to divide the samples into responder (R) and non-responder (Non-R) groups (Figure 6A). BC-PDMs responded heterogeneously to the applied drug treatment. Most frequently they responded to treatment with DTX (9/29). Four samples showed a response to TAM (4/29), six samples to PTX (6/29) and five samples to PAB (5/29). Next, we compared the protein expression profiles (median-centered, log_2 transformed data) of the previously determined responder and non-responder BC-PDMs groups. Using DigiWest® analysis, we generated resistance/sensitivity protein marker panels that clearly distinguished responder from non-responder BC-PDMs (Figure 6). For each treatment, we selected proteins that are associated with therapy response/resistance according to literature and are significantly differentially expressed in responder vs. non-responder BC-PDMs or are involved in therapy-related signaling pathways (Table 2, Figure S4).

In the TAM responder group, we identified a panel of nine proteins with significantly decreased abundances (Figure 6B, Mann Whitney U test, ***$p < 0.001$) and a panel of nine proteins with elevated abundances compared with the non-responder group (Figure 6D, Mann Whitney U test, ***$p < 0.001$). Phosphorylated proteins that were elevated in the treatment-resistant BC-PDMs group (Table 2) included ERα-pSer167, FGFR-pTyr653/654, PI3-kinase p85/p55-

Table 2. Treatment-resistance and -sensitivity panel of BC derived microtumors

	Tamoxifen	Docetaxel	Paclitaxel	Palbociclib
resistance panel	ERα-pSer167 FGFreceptor-pTyr653/654 IGF1Rbeta Src-pSer17 PI3-kinase p85/p55-pTyr458/199 CDK6 Cyclin B1 IKKepsilon-pSer172 beta-Catenin(non-pSer33/37/Thr41)	Caveolin-1 Vimentin-pSer56 CyclinE1 Tau B-Raf-pSer445 IKKε-pSer172 NF-κB p100/p52 Cyp1B1	Caveolin-1 PgR Cytokeratin5 Cytokeratin6 Vimentin-pSer56 MEK1/2-pSer217/221 mTOR(FRAP) IKKα-pThr23	Cytokeratin6 Vimentin-pSer56 CDK6 CyclinE1 Erk1/2-pThr202/Tyr204 FGFRpTyr653/654 eIF4E-pSer209
sensitivity panel	ERα E2F-4 Src-pTyr527 αTubulin Tubulin-ac eIF2α-pSer51 GLUT-1 LDHA PDK1-pSer241	ERα E2F-4 CIP2A Cytokeratin8/18 Tau-pSer202 Erk1/2-pThr202/Tyr204 beta-Catenin-pSer552	GATA3 Cytokeratin8/18 E-Cadherin Tubulin-ac Tubulin beta-1chain cdc2(CDK1) CDK4-pThr172 Cyclin B1 E2F-2 Rb-pSer807/811 NF1(Neurofibromin) c-Met-pTyr1003 beta-Catenin-pSer552	CDK2-pThr160 CyclinD1 ER Her2 c-Raf-pSer259 JNK/SAPK-pThr183/Tyr185 p38MAPK-pThr180/Tyr182 E-Cadherin-pSer838/840

pTyr458/199, and IKKepsilon-pSer172, all of which are directly or indirectly related to TAM resistance according to the literature (72-77). The panel further contained regulators of the cell cycle (CDK6, Cyclin B1) and the Wnt-signaling pathway (non-phosphorylated beta-catenin). Within this panel, CDK6 expression was significantly different in non-responder versus responder BC-PDMs (Figure 6C, Mann-Whitney U test, *p = 0.035). In simple logistic regression analysis, CDK6 was found to negatively affect the likelihood of response to TAM with a 50% decrease in the odds (OR = 0.5, 95% CI 0.21-0.82) (Figure S4B; Table S10; $p < 0.05$ [Wald, LRT]). Proteins found to be relevant for BC-PDMs TAM sensitivity were e.g. ERα, the transcriptional repressor protein E2F-4, the microtubule protein αTubulin and proteins involved in cancer cell metabolism (GLUT1, LDHA and PDK1-pSer241) and stress responses (eIF2A-pSer51).

Using a 7-protein resistance panel, we were able to significantly distinguish DTX non-responder from DTX responder BC-PDMs (Figure 6E, Mann Whitney U-test, ***p < 0.001). This panel included proteins associated with EMT induction (Vimentin-pSer56, NFκB p100/p52 and IKKε-pSer172) or drug metabolism (CYP1B1), which are also known to induce drug resistance to DTX and PTX in cancer cells (78, 79) (Table 2). In addition, higher Caveolin-1, Cyclin E1 and b-Raf-pSer445 protein levels contributed to DTX resistance of BC-PDMs. We found Caveolin-1 (*p = 0.029) and the MAPK-pathway related protein b-Raf-pSer445 (***p < 0.001) to be significantly enriched in non-responder BC-PDMs (Figure 6F, Mann Whitney U-test). Figure 6G shows the protein panel predicting sensitivity of BC-PDMs to DTX treatment (Mann Whitney U-test, *p = 0.017) with increased expression of e.g. ERα, luminal-cell marker (Cytokeratin 8/18), inactive beta-catenin-pSer552 and microtubule associated protein Tau-pSer202 (Table 2). In this panel, we identified Cytokeratin 8/18 (Fig. 6H, Mann Whitney U-test, ***p < 0.001) and Tau-pSer202 (Fig. 6H, Mann Whitney U-test, p = 0.028) to be significantly enriched. By logistic regression analysis, expression of Caveolin-1 and b-Raf-pSer445 was shown to decrease the odds of DTX response of BC-PDMs by 44% (OR = 0.56, 95% CI: 0. 0.32-0.88) and 54% (OR = 0.46, 95% CI: 0.25 to 0.72) and thus contribute to DTX resistance. In contrast, elevated Tau-pSer202 (OR = 1.46, 95% CI: 1.06 to 2.22) and CK8/18 (OR = 1.54, 95% CI: 1.06 to 2.67) levels were significantly associated with DTX treatment response in BC -PDM (Figure S4D; Table S10; $p < 0.05$ [Wald, LRT]).

Paclitaxel treatment resistance of BC-PDMs was determined by a heterogenous panel of 9 proteins enriched in non-responder BC-PDMs (Figure 6I, Mann Whitney U-test, ***p < 0.001). Resistance-associated proteins were Caveolin-1, PgR, mTOR, phosphorylated MEK1/2 (pSer217/221) of the Erk/MAPK signaling pathway, phosphorylated IKKα (pThr23) of the NFκB pathway, the microtubule-associated protein Tau and the basal breast cancer markers Cytokeratin 5, Cytokeratin 6 and Vimentin-pSer56 (Table 2). Moreover, we identified Vimentin-pSer56 to be significantly enriched in the PTX non-responder BC-PDMs (Figure 6J, Mann

606 Whitney U-test, **p = 0.004). Using a 13-protein panel, we could differentiate PTX sensitive
607 from resistant BC-PDMs (Mann Whitney U-test, ***p < 0.001). We discovered several cell
608 cycle-associated proteins (e.g. CDK1, CDK4-pThr172), luminal epithelial cell markers (e.g. E-
609 Cadherin, Cytokeratin 8/18), the microtubule-forming protein Tubulin (acetylated Tubulin,
610 Tubulin beta-chain), the Ras-inhibitor NF1 (Neurofibromin), c-Met-pTyr1003 and beta-Catenin-
611 pSer55, whose expression affected BC-PDMs sensitivity to PTX treatment. Protein
612 abundances differed significantly for GATA3 (Fig. 6L, Mann Whitney U-test, **p = 0.009), NF1
613 (Fig. 6L, Mann Whitney U-test, **p = 0.005) and c-Met-pTyr1003 (Fig. 6L, Mann Whitney U-
614 test, *p = 0.020). The probability of BC-PDMs response to PTX was doubled by increased
615 GATA3 (OR =2.34, 95% CI: 1.24-6.2) and NF1 (OR = 2.15, 95% CI: 1.25-4.5) expression and
616 decreased levels of Vimentin-pSer56 (OR = 0.72, 95% CI: 0.51-0.93) (Figure S4D; Table S10;
617 p < 0.01 [Wald, LRT]). To the best of our knowledge, there are no studies to date that have
618 reported a link between the expression of these proteins and PTX treatment response.

619 For PAB treatment, we identified a resistance panel including proteins previously associated
620 with PAB resistance: CDK6, Cyclin E1 and FGFR. Combined with basal breast cancer markers
621 Cytokeratin 6 and Vimentin, the MAPK-signaling protein Erk1/2- pThr202/Tyr204 and the
622 active mTOR signaling protein eIF4E-pSer209, these proteins could differentiate PAB resistant
623 from PAB sensitive BC-PDMs (Figure 6M, Mann Whitney U-test, ***p < 0.001). In contrast,
624 sensitivity to PAB was predicted by a 8-protein panel (Figure 6N and 6O, Mann Whitney U-
625 test, ***p < 0.001) with increased ERα (**p = 0.003), HER2 (**p = 0.003), CDK2-pThr160 (**p
626 = 0.004), E-Cadherin-pSer838/840 (*p = 0.014), Cyclin D1, c-Raf-p259, JNK/SAPK-
627 pThr183/Tyr185 and p38MAPK-pThr180/Tyr182 signals in responder BC-PDMs. An increase
628 of ERα (OR = 2.15, 95% CI: 1.2-5.91), HER2 (OR = 72.48, 95% CI: 2.36-14948598) and E-
629 Cadherin-pSer838/840 (OR = 1.84, 95% CI: 1.15 to 3.55) by one level more than doubled the
630 odds of BC-PDMs responding to PAB therapy (Figure S4D; Table S10; p < 0.01 [Wald, LRT]).

631 In summary, we identified heterogeneous responses to anti-cancer drug treatment in BC-
632 PDMs. Through comprehensive molecular protein signaling pathway analysis of treatment-
633 responsive and -resistant BC-PDMs, we gained insights into the treatment response
634 mechanisms of breast cancer cells in microtumors, which were shown to resemble
635 histopathological and protein expression profile characteristics of the corresponding primary
636 breast tumor. Our data confirmed several proteins known to play a role in treatment resistance
637 and/or sensitivity, and also identified novel markers that significantly correlate with
638 individualized treatment responses.

639

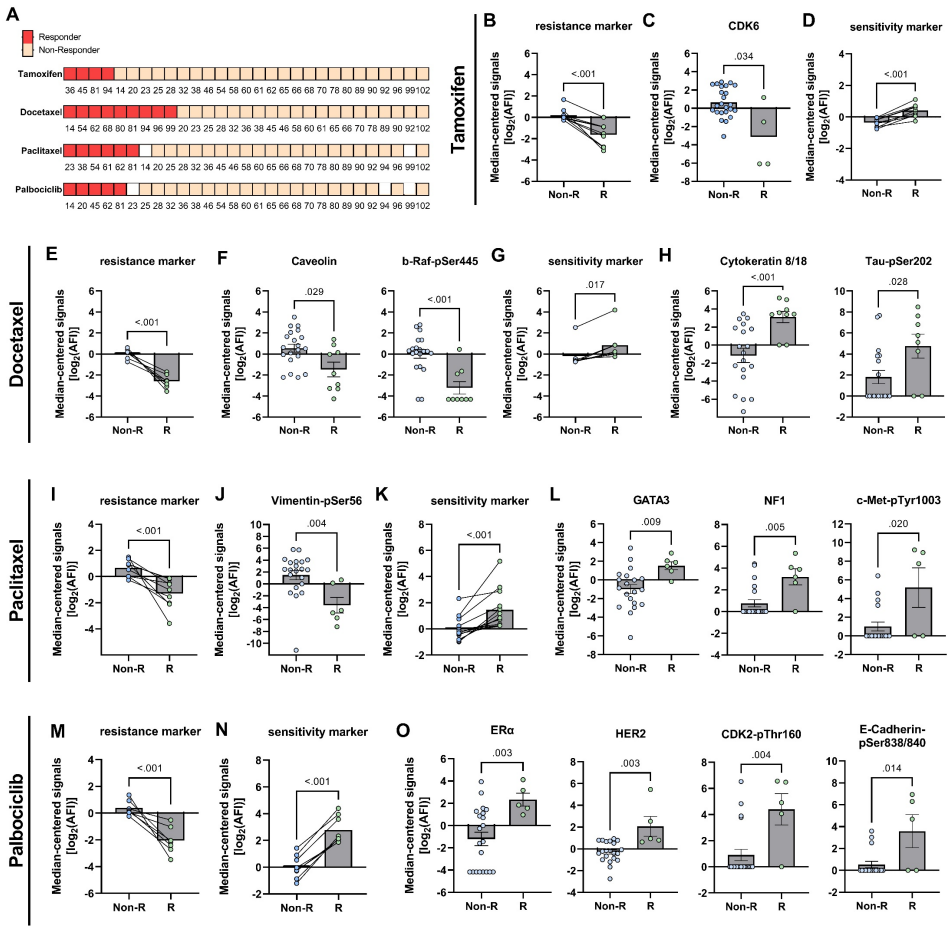

640

Figure 6. Treatment responses analyzed in BC-PDMs and identification of resistance and sensitivity marker panels. (**A**) Treatment response of breast cancer (BC) PDM to anti-cancer drugs. Microtumors were classified as "responder" and non-responder" based on the results of cytotoxicity measurements (Celltox Green™ assay; Promega). Cytotoxicity was determined in a time series (24h, 48h and 72h). Treatment effects were analyzed as fold change of the respective control for each measurement time point using a mixed-effects model (REML) and Fisher's uncorrected LST test. Statistically significant fold changes were defined as "response" and BC-PDMs were accordingly classified as "responders". The numbers indicate BC sample number. (**B-D**) TAM, (**E-H**) DTX, (**I-L**) PTX and (**M-O**) PAB resistance and sensitivity marker panels. Median-centered, log_2-transformed DigiWest AFI protein signals were compared between R and Non-R groups. Each data point within the scatter bar plots represents the same protein in R and Non-R. Lines connect protein data points between Non-R and R. Therapy resistance and sensitivity panels were identified including up to thirteen proteins (for detailed protein list see Table 1.). Comparison of R and Non-R protein "panel" signals by non-parametric, unpaired Mann-Whitney U test. Within these protein panels individual, differentially expressed proteins are depicted (non-parametric, unpaired Mann-Whitney U test). *$p < 0.05$, **$p < 0.01$ and ***$p < 0.001$. Shown are mean with SEM. AFI: average fluorescent intensities; Non-R: non-responder; R: responder; TAM: tamoxifen (100 nM), DTX: docetaxel (5.5 µM), PTX: paclitaxel (4 µM), PAB: Palbociclib (150 nM).

641

6. Discussion

Breast cancer is a highly heterogenous disease with profound morphological, genetic and phenotypical variability resulting in multiple disease manifestations with different response to treatment (14). Gene expression analysis and classical immunohistochemical analysis has enabled the differentiation of BC subtypes and subsequently served to guide treatment selection and patient stratification in BC (4-6). Still, development of treatment resistance remains a major challenge in the management of this malignancy, largely due to the pronounced intra-tumoral heterogeneity that characterizes BC beyond genetic profiles (14). Apart from the intrinsic changes and interactions of tumor cells, also the crosstalk of tumor cells with the complex TME impacts the BC phenotypic manifestation and thus the development of treatment resistance (17, 18). In this study, we successfully generated a repertoire of microtumor samples from different BC subtypes representing disease heterogeneity. We applied previously published protocols for isolating microtumors from primary tumor tissues (21, 26, 27). BC-PDMs recapitulate general histological features and tumor-type specific features of NST (IDC) and ILC like growth patterns, cellular pleomorphism and atypia of the corresponding primary tumor tissue. Using Movat-pentachrome stainings, we found the most abundant BC-related ECM proteins (35, 80), collagen and PGs/GAGs, also present in BC-PDMs. Studies demonstrated that collagen deposition, which increases ECM stiffness, and the density and orientation of collagen fibers affect tumor aggressiveness, invasiveness, therapy responses and correlates with prognosis in BC (81-83). Hence, BC tumor models that comprise ECM structures of native tumors like BC-PDMs represent relevant test systems to investigate disease biology and therapy resistance.

Moreover, our results highlight other features in BC-PDMs characteristic of different BC subtypes as previously described, including hormone-receptor expression in HR+ BC-PDMs compared with TNBC -PDM, increased collagen deposition in ILC-derived BC-PDMs (35), heterogenous expression profiles of luminal (CK18) and basal cell markers (CK5 and CK6) (42) with decreased CK18 expression in TNBC -PDM (47), and high FAPα expression in ILC-BC-PDMs (50). Regarding the CK expression in BC-PDM, we observed similar cellular profiles as described previously by Abd El-Rehim, D.M. et al (42), i.e. the differentiated glandular phenotype ($CK18^+$), the stem cell phenotype ($CK5/6^+$) and an intermediate glandular phenotype ($CK5/6^+$, $CK18^+$) (46). In contrast to this study, we did further differentiate $CK5^+$ BC-PDMs from $CK5^+/CK6^+$ BC-PDMs. According to several reports, 17% of ILCs express basal CKs (84). In our study, ILC-BC-PDMs expressed relatively high levels of CK5/6 compared to NST-BC-PDMs, which is therefore somewhat surprising. In order to provide a more precise statement on this, BC-PDMs established from a larger cohort of ILC samples would need to be evaluated. However, differential protein expression analysis revealed an overall higher expression of CK5 and CK6 in BC-PDMs regardless of breast tumor type compared to primary

tumors. Overexpressed CK5 could be attributable to the culture conditions of BC-PDMs in the form of estrogen deprivation (85, 86).

Compared to frequently employed gene expression analysis of tumor models, our study investigated BC microtumors on the protein level using the DigiWest® method covering 142 total and phosphoproteins. Thereby, breast cancer-related protein expression levels and signaling pathway profiles largely correlated with those of corresponding primary tumors. Hierarchical cluster analysis grouped BC-PDMs according to their classification and molecular protein expression signature. Further, our DigiWest® data confirmed protein signatures of TNBC-PDMs consistent with those in the literature, characterized by upregulated PI3K/Akt and MAPK/RTK signaling (51, 61, 62, 87) with overexpressed proteins associated with integrated stress response (88-91), higher relapse rates, mortality (62, 92, 93), tumor growth and EMT (27, 94-96). When comparing BC-PDMs and primary tumor profiles, we found decreased expression of NFkB signaling pathway proteins NFkB regulates processes of immune and inflammatory responses and is part of the immune defense against transformed cells (97, 98). Because the protein data also showed diminished expression of immune cell markers in BC-PDMs, the attenuated presence of immune cells in microtumors might explain the observed, decreased NFkB-related signals as compared to PTT.

Our study validates the application of BC-PDM for *in vitro* functional drug testing, as demonstrated previously for ovarian cancer and glioblastoma microtumors (21, 26, 27), to functionally complement molecular and histopathological analyses. Protein profiling analysis combined with functional drug testing allowed us to identify phenotypic hallmarks of treatment resistance and sensitivity, as opposed to genetic alterations that may not correlate with clinical benefit (19). As the growth of some types of BC is driven by increased signaling from estrogen and progesterone receptors, hormone therapies have been developed that prevent hormones from binding to these receptors. TAM is a competitive inhibitor of the estrogen receptor known as a selective modulator, while fulvestrant is a selective ER degrader (99). It has been reported that overexpressed CDK6 inhibits fulvestrant-mediated (ER-down regulation-induced) apoptosis and thus induces fulvestrant-resistance (100). Our data implicates that TAM resistance may also be characterized by high CDK6 levels in BC-PDMs illustrating the possibility of resistance mechanisms similar to fulvestrant. Furthermore, it is known that ERα activation through phosphorylation of Ser167 in an estrogen-independent manner and FGFR activation can cause TAM resistance: both proteins were identified within our BC-PDMs TAM resistance panel (72, 76, 101). In line with the clinical application of TAM in HR+ BC (102), increased total ERα levels contribute to TAM sensitivity in BC-PDMs.

The chemotherapeutic agent DTX has shown high activity as an antimicrotubular agent in both neoadjuvant and adjuvant application in advanced and metastatic breast cancer (103). It also

had the strongest effect on BC-PDMs treatment response as compared to other anti-cancer drugs tested. In line with previous studies, BC-PDMs generated from less invasive BC, luminal-like CK8/18 high BC-PDMs with inactive β-catenin signaling and thus lower EMT-transition, and BC-PDMs with high ER expression were sensitive to treatment (104-106). Contrary, we confirmed that high expression of EMT-related and EMT– inducible proteins, high expression of DTX-metabolizing CYP1B1 and increased Caveolin-1 in BC-PDMs predict DTX resistance (78, 79, 107, 108). Surprisingly, we did identify Ser202 phosphorylated Tau to positively and b-Raf-pSer445 to negatively influence DTX sensitivity of BC-PDMs. To date, there are no reports on either protein or their potential impact on response to taxane treatment. However, there are conflicting data on whether the expression of tau correlates with taxane response (109, 110).

As the first taxane compound discovered, PTX has a similar function to DTX as antimicrotubular agent (111). The critical role of the EMT process in PTX resistance, (79), is well represented indicated by the resistance and sensitivity marker panel we identified in BC-PDMs, including EMT-regulator proteins such as Vimentin-pSer56, CK5, CK6, E-Cadherin, CK8/18, IKKα-pThr23, beta-Catenin-pSer55. Contrary to DTX, our results regarding PTX resistance of BC-PDMs indicate that increased total Tau protein levels correlate with treatment resistance. Further studies are warranted to further investigate the importance of Tau protein expression in taxane treatment response of breast cancer. In line with previous *in vitro* studies our data suggest a correlation between high PgR levels and decreased PTX sensitivity (112). Interestingly, we found three proteins being significantly elevated in PTX sensitive BC-PDMs: GATA3, NF1 and c-Met-pTyr1003. So far, these proteins have not been linked to taxane sensitivity, but have generally been associated with breast cancer development (113-116).

In addition to endocrine and chemotherapy, we also tested the CDK4/6 inhibitor palbociclib (PAB). The emergence of several intrinsic and acquired resistance mechanisms has been described preclinically, however without verification in the clinical setting (117). Our comparison of responder and non-responder BC-PDMs protein expression profiles provided intriguing results regarding PAB treatment. We identified several proteins in our BC-PDMs resistance/sensitivity panel to be predictive for PAB response that have been linked to PAB resistance/sensitivity in previous studies, such as CDK6, Cyclin E1, FGFR, Cyclin D1 and ERα (117). Surprisingly, our data also suggest Vimentin, CK6, CDK2-p and HER2 protein expression as novel PAB-treatment response markers. Increased Vimentin and CK6 levels may define a more aggressive and invasive tumor type that is resistant to PAB (49, 118). Our analyses identified phosphorylated CDK2 to contribute to PAB-sensitivity of BC-PDMs, while other studies reported the opposite, as the cyclin E-CDK2 pathway is an important bypass mechanism of the cyclin D1-CDK4/6 axis in acquired PAB-resistance (117). Both CDK4/6-Cyclin D and CDK2-Cyclin E complexes are decisive for the transition of G1- to S-phase and

thus required for cell cycle progression. Further studies are warranted to evaluate this differential response in BC-PDMs.

In summary, we have shown that a salient feature of BC-PDMs, in addition to their histopathological and molecular similarity to the corresponding patient tumor, is the representation of native ECM components that collectively represent the disease heterogeneity of BC. Limitations of this novel patient-derived model system are the restricted number of microtumors available for downstream analyses, the reduced expression of immune cell markers and NFkB signaling proteins, as well as the enhanced expression of CK5 and CK6 as compared to corresponding primary tumor tissue. Further evaluation in additional sample cohorts will be needed to understand the underlying mechanism and to assess the long-term stability of HR-expression in BC-PDMs cultures. Regarding the application of BC-PDMs for assessment of immune cell interaction and immune-oncological treatment responses, we have previously shown functional drug testing of immune checkpoint inhibitors in co-cultures of ovarian cancer and glioblastoma PDM and autologous immune cells (21, 26, 27).

7. Conclusion

Based on comprehensive protein profiling analyses in combination with functional drug testing assays in BC-PDMs our study highlights the potential of identifying patient-tumor specific, differentially expressed proteins to discriminate treatment responders from non-responders and warrants further, confirmatory studies in larger sample cohorts. Specifically, future studies will focus on the comparison of functional drug testing and protein profiling data from BC-PDMs with clinical treatment response in respective patients. As a complement to genomic mutation analysis and standard subtype classification, the combination of individual histopathologic analysis, preclinical drug testing, and parallel protein profiling analyses of BC-PDMs may hold promise for identifying predictive markers of treatment resistance and sensitivity to personalize breast cancer therapies.

8. List of abbreviations

BC	breast cancer
CAFs	cancer-associated fibroblasts
CK	cytokeratin
DAB	3,3′-Diaminobenzidin
DCIS	ductal carcinoma in-situ
DMSO	Dimethyl sulfoxide
DTX	docetaxel
ECM	extracellular matrix

EMT	epithelial-to-mesenchymal transition
ER	estrogen receptor
FAPα	fibroblast-associated protein α
FC	fold change
FFPE	formalin-fixed paraffin-embedded
GAGs	glycosaminoglycans
H&E	hematoxylin and eosin staining
HCL	hierarchical clustering
HER2	human epidermal growth factor receptor 2
HR	hormone receptor
IDC	invasive ductal carcinoma
IHC	immunohistochemistry
ILC	invasive lobular carcinoma
IRS	immunoreactive score
LCIS	lobular carcinoma in-situ
NST	invasive ductal carcinoma of no special type
PAB	palbociclib
PDM	patient-derived microtumors
PgR	progesterone receptor
PGs	proteoglycans
PTT	primary tumor tissue
PTX	paclitaxel
RFU	relative fluorescent units
TAM	tamoxifen
TIL	tumor infiltrating lymphocytes
TME	tumor microenvironment
TNBC	triple-negative breast cancer

9. Declarations

Institutional Review Board Statement: The study was conducted in accordance with the Declaration of Helsinki and approved by the Institutional Review Board (or Ethics Committee) of the University Hospital Tuebingen, Germany (788/2018BO2, November 15th, 2018).

Consent Statement: The use of human samples was approved by the local Ethics Commission at the Medical Faculty Tuebingen under the reference number 788/2018BO2 (15 November 2018). All patients enrolled gave their informed consent to participate in the study prior to surgery.

Data Availability Statement: The data that support the findings of this study are available from the corresponding authors upon reasonable request and after signature of an MTA from the corresponding authors.

Competing interests: A.H. received consulting and speaking fees from AstraZeneca, Amgen, Clovis, Daichii Sankyo, Eisai, ExactScience, Gilead, GSK, Hexal, Lilly, MSD, Novartis, Pfizer, Roche, Pierre-Fabre and Seagen. N.A., F.S-R., N.K, A.K., A.-L.K., B.G., A.S., S.L., M.P., M.H., S.Y.B., K.S-L., M.T. and C.S. declare no competing interest.

Funding: This work received financial support from the Ministry of Baden-Wuerttemberg for Economic Affairs, Labor, and Tourism (grant 3-4332.62-HSG/84).

Author Contributions: Conceptualization and design of the study, C.S., M.T., N.A., A.K., A.H., S.Y.B, and K.S-L.; data collection, data analysis, investigation and interpretation, N.A., F.S-R., S.L., A.K., A.-L.K., A.S., N.K. and C.S.; writing—original draft, N.A. and C.S.; writing—review and editing, N.A., C.S., A.-L.K., K.S-L., A.K., S.Y.B., A.H. and A.S.; visualization, N.A., C.S.; supervision, C.S., S.Y.B., K.S-L.; project administration: N.A., C.S. and A.K. All authors have read and agreed to the published version of the manuscript.

Acknowledgments: We gratefully acknowledge Prof. Dr. Diethelm Wallwiener (Department of Women's Health, University Women's Hospital, Tübingen University Hospital) for his excellent support, helpful discussions and providing fresh tumor tissue biopsies. We thank all patients and healthy volunteers enrolled for giving their informed consent for secondary use of residual tissue, respectively.

10. References

1. Caswell-Jin JL, Plevritis SK, Tian L, Cadham CJ, Xu C, Stout NK, et al. Change in Survival in Metastatic Breast Cancer with Treatment Advances: Meta-Analysis and Systematic Review. JNCI Cancer Spectr. 2018;2(4):pky062.
2. Lakhani SR, Ellis IO, Schnitt S, Tan PH, van de Vijver M. WHO Classification of Tumours of the Breast. 2012.
3. Tavassoli FA. Pathology and genetics of tumours of the breast and female genital organs. World Hhealth Organization Classification of Tumours. 2003.
4. Perou CM, Sørlie T, Eisen MB, Van De Rijn M, Jeffrey SS, Rees CA, et al. Molecular portraits of human breast tumours. Nature. 2000;406(6797):747-52.
5. Sørlie T, Perou CM, Tibshirani R, Aas T, Geisler S, Johnsen H, et al. Gene expression patterns of breast carcinomas distinguish tumor subclasses with clinical implications. Proc Natl Acad Sci U S A. 2001;98(19):10869-74.
6. Sorlie T, Tibshirani R, Parker J, Hastie T, Marron JS, Nobel A, et al. Repeated observation of breast tumor subtypes in independent gene expression data sets. Proc Natl Acad Sci U S A. 2003;100(14):8418-23.
7. Tsang JYS, Tse GM. Molecular Classification of Breast Cancer. Adv Anat Pathol. 2020;27(1):27-35.
8. Carey LA, Dees EC, Sawyer L, Gatti L, Moore DT, Collichio F, et al. The triple negative paradox: primary tumor chemosensitivity of breast cancer subtypes. Clin Cancer Res. 2007;13(8):2329-34.

9. Rouzier R, Perou CM, Symmans WF, Ibrahim N, Cristofanilli M, Anderson K, et al. Breast cancer molecular subtypes respond differently to preoperative chemotherapy. Clinical cancer research. 2005;11(16):5678-85.
10. Martin M, Romero A, Cheang MC, López García-Asenjo JA, García-Saenz JA, Oliva B, et al. Genomic predictors of response to doxorubicin versus docetaxel in primary breast cancer. Breast Cancer Res Treat. 2011;128(1):127-36.
11. Glück S, Ross JS, Royce M, McKenna EF, Jr., Perou CM, Avisar E, et al. TP53 genomics predict higher clinical and pathologic tumor response in operable early-stage breast cancer treated with docetaxel-capecitabine ± trastuzumab. Breast Cancer Res Treat. 2012;132(3):781-91.
12. Koren S, Bentires-Alj M. Breast Tumor Heterogeneity: Source of Fitness, Hurdle for Therapy. Mol Cell. 2015;60(4):537-46.
13. Hong SP, Chan TE, Lombardo Y, Corleone G, Rotmensz N, Bravaccini S, et al. Single-cell transcriptomics reveals multi-step adaptations to endocrine therapy. Nature Communications. 2019;10(1):3840.
14. Lüönd F, Tiede S, Christofori G. Breast cancer as an example of tumour heterogeneity and tumour cell plasticity during malignant progression. Br J Cancer. 2021;125(2):164-75.
15. Heindl A, Sestak I, Naidoo K, Cuzick J, Dowsett M, Yuan Y. Relevance of Spatial Heterogeneity of Immune Infiltration for Predicting Risk of Recurrence After Endocrine Therapy of ER+ Breast Cancer. JNCI: Journal of the National Cancer Institute. 2017;110(2):166-75.
16. Natrajan R, Sailem H, Mardakheh FK, Arias Garcia M, Tape CJ, Dowsett M, et al. Microenvironmental Heterogeneity Parallels Breast Cancer Progression: A Histology-Genomic Integration Analysis. PLoS Med. 2016;13(2):e1001961.
17. Glajcar A, Szpor J, Pacek A, Tyrak KE, Chan F, Streb J, et al. The relationship between breast cancer molecular subtypes and mast cell populations in tumor microenvironment. Virchows Arch. 2017;470(5):505-15.
18. Bareche Y, Buisseret L, Gruosso T, Girard E, Venet D, Dupont F, et al. Unraveling Triple-Negative Breast Cancer Tumor Microenvironment Heterogeneity: Towards an Optimized Treatment Approach. J Natl Cancer Inst. 2020;112(7):708-19.
19. Pezo RC, Chen TW, Berman HK, Mulligan AM, Razak AA, Siu LL, et al. Impact of multi-gene mutational profiling on clinical trial outcomes in metastatic breast cancer. Breast Cancer Res Treat. 2018;168(1):159-68.
20. Pauli C, Hopkins BD, Prandi D, Shaw R, Fedrizzi T, Sboner A, et al. Personalized In Vitro and In Vivo Cancer Models to Guide Precision Medicine. Cancer Discov. 2017;7(5):462-77.
21. Anderle N, Koch A, Gierke B, Keller A-L, Staebler A, Hartkopf A, et al. A Platform of Patient-Derived Microtumors Identifies Individual Treatment Responses and Therapeutic Vulnerabilities in Ovarian Cancer. Cancers (Basel). 2022;14(12):2895.
22. Kondo J, Endo H, Okuyama H, Ishikawa O, Iishi H, Tsujii M, et al. Retaining cell-cell contact enables preparation and culture of spheroids composed of pure primary cancer cells from colorectal cancer. Proc Natl Acad Sci U S A. 2011;108(15):6235-40.
23. Ruifrok AC, Johnston DA. Quantification of histochemical staining by color deconvolution. Anal Quant Cytol Histol. 2001;23(4):291-9.
24. Treindl F, Ruprecht B, Beiter Y, Schultz S, Döttinger A, Staebler A, et al. A bead-based western for high-throughput cellular signal transduction analyses. Nature Communications. 2016;7(1):12852.
25. Iglewicz B, Hoaglin DC. How to detect and handle outliers. Milwaukee, Wis.: Milwaukee, Wis. : ASQC Quality Press; 1993. ix, 87 p. p.
26. Przystal JM, Becker H, Canjuga D, Tsiami F, Anderle N, Keller A-L, et al. Targeting CSF1R Alone or in Combination with PD1 in Experimental Glioma. Cancers (Basel). 2021;13(10):2400.
27. Walter B, Canjuga D, Yüz SG, Ghosh M, Bozko P, Przystal JM, et al. Argyrin F Treatment-Induced Vulnerabilities Lead to a Novel Combination Therapy in Experimental Glioma. Advanced Therapeutics. 2021:2100078.

28. McCart Reed AE, Kalinowski L, Simpson PT, Lakhani SR. Invasive lobular carcinoma of the breast: the increasing importance of this special subtype. Breast Cancer Res. 2021;23(1):6.
29. Lepucki A, Orlińska K, Mielczarek-Palacz A, Kabut J, Olczyk P, Komosińska-Vassev K. The Role of Extracellular Matrix Proteins in Breast Cancer. Journal of Clinical Medicine. 2022;11(5):1250.
30. Klimonda Z, Karwat P, Dobruch-Sobczak K, Piotrzkowska-Wróblewska H, Litniewski J. Breast-lesions characterization using Quantitative Ultrasound features of peritumoral tissue. Sci Rep. 2019;9(1).
31. Henke E, Nandigama R, Ergün S. Extracellular matrix in the tumor microenvironment and its impact on cancer therapy. Frontiers in molecular biosciences. 2020;6:160.
32. Bergamaschi A, Tagliabue E, Sørlie T, Naume B, Triulzi T, Orlandi R, et al. Extracellular matrix signature identifies breast cancer subgroups with different clinical outcome. The Journal of pathology. 2008;214(3):357-67.
33. Riaz M, Sieuwerts AM, Look MP, Timmermans MA, Smid M, Foekens JA, et al. High TWIST1 mRNA expression is associated with poor prognosis in lymph node-negative and estrogen receptor-positive human breast cancer and is co-expressed with stromal as well as ECM related genes. Breast Cancer Res. 2012;14(5):1-15.
34. Movat HZ. Demonstration of all connective tissue elements in a single section; pentachrome stains. AMA Arch Pathol. 1955;60(3):289-95.
35. Natal RdA, Paiva GR, Pelegati VB, Marenco L, Alvarenga CA, Vargas RF, et al. Exploring Collagen Parameters in Pure Special Types of Invasive Breast Cancer. Sci Rep. 2019;9(1):7715.
36. Carey L, Winer E, Viale G, Cameron D, Gianni L. Triple-negative breast cancer: disease entity or title of convenience? Nature Reviews Clinical Oncology. 2010;7(12):683-92.
37. Dent R, Trudeau M, Pritchard KI, Hanna WM, Kahn HK, Sawka CA, et al. Triple-negative breast cancer: clinical features and patterns of recurrence. Clin Cancer Res. 2007;13(15 Pt 1):4429-34.
38. Yin W-J, Lu J-S, Di G-H, Lin Y-P, Zhou L-H, Liu G-Y, et al. Clinicopathological features of the triple-negative tumors in Chinese breast cancer patients. Breast Cancer Res Treat. 2009;115(2):325-33.
39. Dignam JJ, Dukic V, Anderson SJ, Mamounas EP, Wickerham DL, Wolmark N. Hazard of recurrence and adjuvant treatment effects over time in lymph node-negative breast cancer. Breast Cancer Res Treat. 2009;116(3):595-602.
40. Moll R, Franke WW, Schiller DL, Geiger B, Krepler R. The catalog of human cytokeratins: patterns of expression in normal epithelia, tumors and cultured cells. Cell. 1982;31(1):11-24.
41. Taylor-Papadimitriou J, Stampfer M, Bartek J, Lewis A, Boshell M, Lane EB, et al. Keratin expression in human mammary epithelial cells cultured from normal and malignant tissue: relation to in vivo phenotypes and influence of medium. J Cell Sci. 1989;94 (Pt 3):403-13.
42. Abd El-Rehim DM, Pinder SE, Paish CE, Bell J, Blamey R, Robertson JF, et al. Expression of luminal and basal cytokeratins in human breast carcinoma. The Journal of Pathology. 2004;203(2):661-71.
43. Wetzels R, Kuijpers H, Lane EB, Leigh IM, Troyanovsky S, Holland R, et al. Basal cell-specific and hyperproliferation-related keratins in human breast cancer. The American journal of pathology. 1991;138(3):751.
44. Birnbaum D, Bertucci F, Ginestier C, Tagett R, Jacquemier J, Charafe-Jauffret E. Basal and luminal breast cancers: basic or luminous? Int J Oncol. 2004;25(2):249-58.
45. Böcker W, Moll R, Poremba C, Holland R, Van Diest PJ, Dervan P, et al. Common adult stem cells in the human breast give rise to glandular and myoepithelial cell lineages: a new cell biological concept. Lab Invest. 2002;82(6):737-46.
46. Korsching E, Packeisen J, Agelopoulos K, Eisenacher M, Voss R, Isola J, et al. Cytogenetic Alterations and Cytokeratin Expression Patterns in Breast Cancer: Integrating a New Model of Breast Differentiation into Cytogenetic Pathways of Breast Carcinogenesis. Lab Invest. 2002;82(11):1525-33.

47. Woelfle U, Sauter G, Santjer S, Brakenhoff R, Pantel K. Down-Regulated Expression of Cytokeratin 18 Promotes Progression of Human Breast Cancer. Clinical Cancer Research. 2004;10(8):2670-4.
48. Fortier A-M, Asselin E, Cadrin M. Keratin 8 and 18 Loss in Epithelial Cancer Cells Increases Collective Cell Migration and Cisplatin Sensitivity through Claudin1 Up-regulation. J Biol Chem. 2013;288(16):11555-71.
49. Rodríguez-Pinilla SM, Sarrió D, Honrado E, Hardisson D, Calero F, Benitez J, et al. Prognostic significance of basal-like phenotype and fascin expression in node-negative invasive breast carcinomas. Clin Cancer Res. 2006;12(5):1533-9.
50. Park CK, Jung WH, Koo JS. Expression of cancer-associated fibroblast-related proteins differs between invasive lobular carcinoma and invasive ductal carcinoma. Breast Cancer Res Treat. 2016;159(1):55-69.
51. Zhao JJ, Liu Z, Wang L, Shin E, Loda MF, Roberts TM. The oncogenic properties of mutant p110alpha and p110beta phosphatidylinositol 3-kinases in human mammary epithelial cells. Proc Natl Acad Sci U S A. 2005;102(51):18443-8.
52. The Cancer Genome Atlas N. Comprehensive molecular portraits of human breast tumours. Nature. 2012;490(7418):61-70.
53. Liu T, Yacoub R, Taliaferro-Smith LD, Sun S-Y, Graham TR, Dolan R, et al. Combinatorial Effects of Lapatinib and Rapamycin in Triple-Negative Breast Cancer Cells. Mol Cancer Ther. 2011;10(8):1460-9.
54. Cossu-Rocca P, Orrù S, Muroni MR, Sanges F, Sotgiu G, Ena S, et al. Analysis of PIK3CA Mutations and Activation Pathways in Triple Negative Breast Cancer. PLoS One. 2015;10(11):e0141763.
55. Ooms LM, Binge LC, Davies EM, Rahman P, Conway JR, Gurung R, et al. The Inositol Polyphosphate 5-Phosphatase PIPP Regulates AKT1-Dependent Breast Cancer Growth and Metastasis. Cancer Cell. 2015;28(2):155-69.
56. Stephens P, Hunter C, Bignell G, Edkins S, Davies H, Teague J, et al. Lung cancer: intragenic ERBB2 kinase mutations in tumours. Nature. 2004;431(7008):525-6.
57. Lynch TJ, Bell DW, Sordella R, Gurubhagavatula S, Okimoto RA, Brannigan BW, et al. Activating mutations in the epidermal growth factor receptor underlying responsiveness of non-small-cell lung cancer to gefitinib. N Engl J Med. 2004;350(21):2129-39.
58. LoPiccolo J, Blumenthal GM, Bernstein WB, Dennis PA. Targeting the PI3K/Akt/mTOR pathway: effective combinations and clinical considerations. Drug Resist Updat. 2008;11(1-2):32-50.
59. McCubrey JA, Steelman LS, Kempf CR, Chappell WH, Abrams SL, Stivala F, et al. Therapeutic resistance resulting from mutations in Raf/MEK/ERK and PI3K/PTEN/Akt/mTOR signaling pathways. J Cell Physiol. 2011;226(11):2762-81.
60. Steelman LS, Navolanic PM, Sokolosky ML, Taylor JR, Lehmann BD, Chappell WH, et al. Suppression of PTEN function increases breast cancer chemotherapeutic drug resistance while conferring sensitivity to mTOR inhibitors. Oncogene. 2008;27(29):4086-95.
61. Umemura S, Yoshida S, Ohta Y, Naito K, Osamura RY, Tokuda Y. Increased phosphorylation of Akt in triple-negative breast cancers. Cancer Sci. 2007;98(12):1889-92.
62. Eralp Y, Derin D, Ozluk Y, Yavuz E, Guney N, Saip P, et al. MAPK overexpression is associated with anthracycline resistance and increased risk for recurrence in patients with triple-negative breast cancer. Ann Oncol. 2008;19(4):669-74.
63. Sviderskiy VO, Blumenberg L, Gorodetsky E, Karakousi TR, Hirsh N, Alvarez SW, et al. Hyperactive CDK2 Activity in Basal-like Breast Cancer Imposes a Genome Integrity Liability that Can Be Exploited by Targeting DNA Polymerase ε. Mol Cell. 2020;80(4):682-98.e7.
64. Hamilton E, Infante JR. Targeting CDK4/6 in patients with cancer. Cancer Treat Rev. 2016;45:129-38.
65. Warburg O, Wind F, Negelein E. THE METABOLISM OF TUMORS IN THE BODY. J Gen Physiol. 1927;8(6):519-30.

66. Alluri P, Newman LA. Basal-like and triple-negative breast cancers: searching for positives among many negatives. Surg Oncol Clin N Am. 2014;23(3):567-77.
67. Pelicano H, Zhang W, Liu J, Hammoudi N, Dai J, Xu RH, et al. Mitochondrial dysfunction in some triple-negative breast cancer cell lines: role of mTOR pathway and therapeutic potential. Breast Cancer Res. 2014;16(5):434.
68. Vlug E, Ercan C, van der Wall E, van Diest PJ, Derksen PWB. Lobular Breast Cancer: Pathology, Biology, and Options for Clinical Intervention. Arch Immunol Ther Exp (Warsz). 2014;62(1):7-21.
69. Christgen M, Derksen PWB. Lobular breast cancer: molecular basis, mouse and cellular models. Breast Cancer Res. 2015;17(1):16.
70. Ciriello G, Michael, Andrew, Matthew, Suhn, Pastore A, et al. Comprehensive Molecular Portraits of Invasive Lobular Breast Cancer. Cell. 2015;163(2):506-19.
71. Liu Z, Merkurjev D, Yang F, Li W, Oh S, Friedman MJ, et al. Enhancer activation requires trans-recruitment of a mega transcription factor complex. Cell. 2014;159(2):358-73.
72. Campbell RA, Bhat-Nakshatri P, Patel NM, Constantinidou D, Ali S, Nakshatri H. Phosphatidylinositol 3-Kinase/AKT-mediated Activation of Estrogen Receptor α: A NEW MODEL FOR ANTI-ESTROGEN RESISTANCE *. J Biol Chem. 2001;276(13):9817-24.
73. Ghayad SE, Vendrell JA, Larbi SB, Dumontet C, Bieche I, Cohen PA. Endocrine resistance associated with activated ErbB system in breast cancer cells is reversed by inhibiting MAPK or PI3K/Akt signaling pathways. Int J Cancer. 2010;126(2):545-62.
74. Guo JP, Shu SK, Esposito NN, Coppola D, Koomen JM, Cheng JQ. IKKepsilon phosphorylation of estrogen receptor alpha Ser-167 and contribution to tamoxifen resistance in breast cancer. J Biol Chem. 2010;285(6):3676-84.
75. Kastrati I, Joosten SEP, Semina SE, Alejo LH, Brovkovych SD, Stender JD, et al. The NF-κB Pathway Promotes Tamoxifen Tolerance and Disease Recurrence in Estrogen Receptor–Positive Breast Cancers. Mol Cancer Res. 2020;18(7):1018-27.
76. Lv Q, Guan S, Zhu M, Huang H, Wu J, Dai X. FGFR1 Is Associated With Tamoxifen Resistance and Poor Prognosis of ER-Positive Breast Cancers by Suppressing ER Protein Expression. Technol Cancer Res Treat. 2021;20:15330338211004935.
77. Wang W, Nag SA, Zhang R. Targeting the NFκB signaling pathways for breast cancer prevention and therapy. Curr Med Chem. 2015;22(2):264-89.
78. McFadyen MC, McLeod HL, Jackson FC, Melvin WT, Doehmer J, Murray GI. Cytochrome P450 CYP1B1 protein expression: a novel mechanism of anticancer drug resistance. Biochem Pharmacol. 2001;62(2):207-12.
79. Ashrafizadeh M, Mirzaei S, Hashemi F, Zarrabi A, Zabolian A, Saleki H, et al. New insight towards development of paclitaxel and docetaxel resistance in cancer cells: EMT as a novel molecular mechanism and therapeutic possibilities. Biomed Pharmacother. 2021;141:111824.
80. Troup S, Njue C, Kliewer EV, Parisien M, Roskelley C, Chakravarti S, et al. Reduced expression of the small leucine-rich proteoglycans, lumican, and decorin is associated with poor outcome in node-negative invasive breast cancer. Clin Cancer Res. 2003;9(1):207-14.
81. Conklin MW, Eickhoff JC, Riching KM, Pehlke CA, Eliceiri KW, Provenzano PP, et al. Aligned Collagen Is a Prognostic Signature for Survival in Human Breast Carcinoma. The American Journal of Pathology. 2011;178(3):1221-32.
82. Provenzano PP, Inman DR, Eliceiri KW, Knittel JG, Yan L, Rueden CT, et al. Collagen density promotes mammary tumor initiation and progression. BMC Med. 2008;6(1):11.
83. Walsh AJ, Cook RS, Lee JH, Arteaga CL, Skala MC. Collagen density and alignment in responsive and resistant trastuzumab-treated breast cancer xenografts. Journal of biomedical optics. 2015;20(2):026004.
84. Fadare O, Wang SA, Hileeto D. The expression of cytokeratin 5/6 in invasive lobular carcinoma of the breast: evidence of a basal-like subset? Hum Pathol. 2008;39(3):331-6.
85. Kabos P, Haughian JM, Wang X, Dye WW, Finlayson C, Elias A, et al. Cytokeratin 5 positive cells represent a steroid receptor negative and therapy resistant subpopulation in luminal breast cancers. Breast Cancer Res Treat. 2011;128(1):45-55.

86. Fettig LM, McGinn O, Finlay-Schultz J, LaBarbera DV, Nordeen SK, Sartorius CA. Cross talk between progesterone receptors and retinoic acid receptors in regulation of cytokeratin 5-positive breast cancer cells. Oncogene. 2017;36(44):6074-84.
87. Bartholomeusz C, Gonzalez-Angulo AM, Liu P, Hayashi N, Lluch A, Ferrer-Lozano J, et al. High ERK protein expression levels correlate with shorter survival in triple-negative breast cancer patients. Oncologist. 2012;17(6):766-74.
88. Bai X, Ni J, Beretov J, Wasinger VC, Wang S, Zhu Y, et al. Activation of the eIF2α/ATF4 axis drives triple-negative breast cancer radioresistance by promoting glutathione biosynthesis. Redox Biol. 2021;43:101993.
89. Pakos-Zebrucka K, Koryga I, Mnich K, Ljujic M, Samali A, Gorman AM. The integrated stress response. EMBO Rep. 2016;17(10):1374-95.
90. Pouysségur J, Dayan F, Mazure NM. Hypoxia signalling in cancer and approaches to enforce tumour regression. Nature. 2006;441(7092):437-43.
91. Sonenberg N, Hinnebusch AG. Regulation of translation initiation in eukaryotes: mechanisms and biological targets. Cell. 2009;136(4):731-45.
92. Bhat M, Robichaud N, Hulea L, Sonenberg N, Pelletier J, Topisirovic I. Targeting the translation machinery in cancer. Nature Reviews Drug Discovery. 2015;14(4):261-78.
93. Flowers A, Chu QD, Panu L, Meschonat C, Caldito G, Lowery-Nordberg M, et al. Eukaryotic initiation factor 4E overexpression in triple-negative breast cancer predicts a worse outcome. Surgery. 2009;146(2):220-6.
94. McCawley LJ, Li S, Wattenberg EV, Hudson LG. Sustained activation of the mitogen-activated protein kinase pathway. A mechanism underlying receptor tyrosine kinase specificity for matrix metalloproteinase-9 induction and cell migration. J Biol Chem. 1999;274(7):4347-53.
95. Wei Y, Chen YH, Li LY, Lang J, Yeh SP, Shi B, et al. CDK1-dependent phosphorylation of EZH2 suppresses methylation of H3K27 and promotes osteogenic differentiation of human mesenchymal stem cells. Nat Cell Biol. 2011;13(1):87-94.
96. Yang CC, LaBaff A, Wei Y, Nie L, Xia W, Huo L, et al. Phosphorylation of EZH2 at T416 by CDK2 contributes to the malignancy of triple negative breast cancers. Am J Transl Res. 2015;7(6):1009-20.
97. Oeckinghaus A, Ghosh S. The NF-kappaB family of transcription factors and its regulation. Cold Spring Harb Perspect Biol. 2009;1(4):a000034.
98. Chen F, Castranova V. Nuclear Factor-κB, an Unappreciated Tumor Suppressor. Cancer Res. 2007;67(23):11093-8.
99. Nathan MR, Schmid P. A Review of Fulvestrant in Breast Cancer. Oncology and Therapy. 2017;5(1):17-29.
100. Alves CL, Elias D, Lyng M, Bak M, Kirkegaard T, Lykkesfeldt AE, et al. High CDK6 Protects Cells from Fulvestrant-Mediated Apoptosis and is a Predictor of Resistance to Fulvestrant in Estrogen Receptor–Positive Metastatic Breast Cancer. Clinical Cancer Research. 2016;22(22):5514-26.
101. Yamnik RL, Digilova A, Davis DC, Brodt ZN, Murphy CJ, Holz MK. S6 Kinase 1 Regulates Estrogen Receptor α in Control of Breast Cancer Cell Proliferation *. J Biol Chem. 2009;284(10):6361-9.
102. Early Breast Cancer Trialists' Collaborative G. Relevance of breast cancer hormone receptors and other factors to the efficacy of adjuvant tamoxifen: patient-level meta-analysis of randomised trials. The Lancet. 2011;378(9793):771-84.
103. Nowak AK, Wilcken NRC, Stockler MR, Hamilton A, Ghersi D. Systematic review of taxane-containing versus non-taxane-containing regimens for adjuvant and neoadjuvant treatment of early breast cancer. The Lancet Oncology. 2004;5(6):372-80.
104. Kim K, Lu Z, Hay ED. DIRECT EVIDENCE FOR A ROLE OF β-CATENIN/LEF-1 SIGNALING PATHWAY IN INDUCTION OF EMT. Cell Biol Int. 2002;26(5):463-76.
105. Shi R, Liu L, Wang F, He Y, Niu Y, Wang C, et al. Downregulation of cytokeratin 18 induces cellular partial EMT and stemness through increasing EpCAM expression in breast cancer. Cell Signal. 2020;76:109810.

106.Tham Y-L, Gomez LF, Mohsin S, Gutierrez MC, Weiss H, Hilsenbeck SG, et al. Clinical response to neoadjuvant docetaxel predicts improved outcome in patients with large locally advanced breast cancers. Breast Cancer Res Treat. 2005;94(3):279-84.
107.Marín-Aguilera M, Codony-Servat J, Reig Ò, Lozano JJ, Fernández PL, Pereira MV, et al. Epithelial-to-Mesenchymal Transition Mediates Docetaxel Resistance and High Risk of Relapse in Prostate CancerEMT Role in Docetaxel Resistance. Mol Cancer Ther. 2014;13(5):1270-84.
108.Yang C-PH, Galbiati F, Volonté D, Horwitz SB, Lisanti MP. Upregulation of caveolin-1 and caveolae organelles in Taxol-resistant A549 cells. FEBS Lett. 1998;439(3):368-72.
109.Barbolina MV. Dichotomous role of microtubule associated protein tau as a biomarker of response to and a target for increasing efficacy of taxane treatment in cancers of epithelial origin. Pharmacol Res. 2021;168:105585.
110.Pusztai L, Jeong J-H, Gong Y, Ross JS, Kim C, Paik S, et al. Evaluation of Microtubule-Associated Protein-Tau Expression As a Prognostic and Predictive Marker in the NSABP-B 28 Randomized Clinical Trial. J Clin Oncol. 2009;27(26):4287-92.
111.Verweij J, Clavel M, Chevalier B. Paclitaxel (Taxol) and docetaxel (Taxotere): not simply two of a kind. Ann Oncol. 1994;5(6):495-505.
112.Schmidt M, Bremer E, Hasenclever D, Victor A, Gehrmann M, Steiner E, et al. Role of the progesterone receptor for paclitaxel resistance in primary breast cancer. Br J Cancer. 2007;96(2):241-7.
113.Beviglia L, Matsumoto K, Lin C-S, Ziober BL, Kramer RH. Expression of the C-Met/HGF receptor in human breast carcinoma: Correlation with tumor progression. Int J Cancer. 1997;74(3):301-9.
114.Edakuni G, Sasatomi E, Satoh T, Tokunaga O, Miyazaki K. Expression of the hepatocyte growth factor/c-Met pathway is increased at the cancer front in breast carcinoma. Pathol Int. 2001;51(3):172-8.
115.Mehra R, Varambally S, Ding L, Shen R, Sabel MS, Ghosh D, et al. Identification of GATA3 as a Breast Cancer Prognostic Marker by Global Gene Expression Meta-analysis. Cancer Res. 2005;65(24):11259-64.
116.Pearson A, Proszek P, Pascual J, Fribbens C, Shamsher MK, Kingston B, et al. Inactivating NF1 Mutations Are Enriched in Advanced Breast Cancer and Contribute to Endocrine Therapy Resistance. Clinical Cancer Research. 2020;26(3):608-22.
117.Pandey K, An H-J, Kim SK, Lee SA, Kim S, Lim SM, et al. Molecular mechanisms of resistance to CDK4/6 inhibitors in breast cancer: A review. Int J Cancer. 2019;145(5):1179-88.
118.Gravdal K, Halvorsen OJ, Haukaas SA, Akslen LA. A Switch from E-Cadherin to N-Cadherin Expression Indicates Epithelial to Mesenchymal Transition and Is of Strong and Independent Importance for the Progress of Prostate Cancer. Clinical Cancer Research. 2007;13(23):7003-11.